

MYCN Silencing as Therapeutics for Neuroblastoma
using RNA interference

Ruhina Maeshima

Great Ormond Street Institute of Child Health

University College London

A thesis submitted for the degree of Doctor of Philosophy

February 2018

Declaration

I, Ruhina Maeshima declare that the work presented in this thesis is my own. Any contributions from colleagues in the collaboration or diagrams driven from other sources are explicitly referenced in the text.

Abstract

Neuroblastoma (NB) is the most common solid tumour in childhood and accounts for 15% of childhood cancer deaths. It is known that high-risk NB is highly correlated with MYCN amplification. Overexpressed MYCN induces proliferation and cell growth and suppresses apoptosis and differentiation pathways in NB cells. Since RNA interference (RNAi) was first described, many research groups have investigated the application of RNAi with the use of short interfering RNA (siRNA). Our aim is to induce apoptosis and differentiation using RNAi as a novel therapeutic strategy for MYCN-amplified NB. Our hypothesis is that MYCN silencing by anti-MYCN siRNA induces apoptosis and differentiation at the mRNA and protein level. We are encapsulating siRNA with liposome and integrin-receptor targeting peptide to deliver MYCN siRNA into NB cells and optimising cationic and anionic polyethylene glycol (PEG)ylated receptor-targeting nanocomplexes (RTNs). In this project, we also aimed to optimise the methods to store RTNs for a long time in trehalose, which is known as a cryoprotectant. As a result, MYCN was silenced by the siRNA at both the mRNA and protein levels, and the siRNA-mediated MYCN reduction induced downstream effects, such as a neuronal differentiation marker TrkA upregulation and the morphological changes of the cells. The anti-MYCN siRNA delivered using RTNs successfully silenced MYCN mRNA *in vivo* as well. We used an NB cell line with non-functional p53 and resistance toward p53-pathway dependent anti-cancer drugs, probably induced by multiple sessions of chemotherapy and radiotherapy. Therefore, the results are promising for a novel therapy for relapse NB with MYCN amplification. In addition, we successfully demonstrated that trehalose maintains the biophysical properties and the function of RTNs, consisting of either DNA or siRNA at -80 °C. This allows us to make a large amount of RTN for many experiments, store it for the long term, and transport it to a place far from the laboratory.

Acknowledgements

I am truly grateful to Professor Stephen Hart and Dr Andrew Stoker for their supervision, patience, encouragement, intellectual discussions and the freedom to try other approaches. I am also grateful to Professor Stephen Hart and Dr Andrew Stoker for giving me this opportunity to learn the very interesting topic Neuroblastoma at UCL.

I must thank Aris Tagalakis and Ahmad Aldossary, who have been working together, for their friendship, help, encouragement, support and patience, especially; I heartily thank Aris Tagalakis for his supervision: he was my third supervisor. I am grateful to current and previous members in Hart group and Stoker group for their help, kindness and support. Discussions with them were really helpful and encouraged me.

I also thank members of the molecular and cellular immunology laboratory for their kindness and encourage. I thank to Ayad Eddaoudi and Dale Mouldeing for their knowledge, support and kindness. I was not able to complete the flow cytometry work and cell image analysis without their help.

Finally, I would like to thank my parents, who are working harder than anyone, for their financial support, encourage and understanding. To my sisters including my dog, thank you for chatting with me about something different from science and doing something different from science with me when I needed it.

Publications

Tagalakis, AD, Lee, DH, Bienemann, AS, Zhou, H, Munye, MM, Saraiva, L, McCarthy, D, Du, Z, Vink, CA, **Maeshima, R**, White, EA, Gustafsson, K & Hart, SL 2014, 'Multifunctional, self-assembling anionic peptide-lipid nanocomplexes for targeted siRNA delivery', *Biomaterials*, vol. 35, no. 29, pp. 8406-15

Clark, O, Park, I, Di Florio, A, Cichon, AC, Rustin, S, Jugov, R, **Maeshima, R** & Stoker, AW 2015, 'Oxovanadium-based inhibitors can drive redox-sensitive cytotoxicity in neuroblastoma cells and synergise strongly with buthionine sulfoximine', *Cancer Lett.*, vol. 357, no. 1, pp. 316-27

Tagalakis, AD, **Maeshima, R**, Yu-Wai-Man, C, Meng, J, Syed, F, Wu, LP, Aldossary, AM, McCarthy, D, Moghimi, SM & Hart SL 2017, 'Peptide and nucleic acid-directed self-assembly of cationic nanovehicles through giantunilamellar vesicle modification: Targetable nanocomplexes for in vivo nucleic acid delivery', *Acta Biomater.*, vol. 15, no. 51, pp. 351-362

Contents Page

Declaration.....	2
Abstract.....	3
Acknowledgements.....	4
Publications.....	5
Contents Page.....	6
List of Figures.....	12
List of Tables.....	16
Abbreviations.....	17
1. Introduction.....	22
1.1. Neuroblastoma	
1.1.1. Neuroblastoma in clinical presentation.....	23
1.1.2. Classification of Neuroblastoma.....	23
1.1.3. Origin of neuroblastoma.....	26
1.1.4. Familial neuroblastoma.....	26
1.1.5. Sporadic neuroblastoma.....	28
1.2. MYCN	
1.2.1. MYCN and c-Myc.....	31
1.2.2. Functions of MYCN.....	33
1.2.3. Stability and degradation of MYCN.....	36
1.2.4. Transcription of MYCN.....	39
1.2.5. MYCN and target genes.....	41
1.2.5.1. Differentiation.....	43
1.2.5.2. Apoptosis.....	44
1.2.6. Current treatment of neuroblastoma with MYCN amplification.....	46

1.3. Gene Therapy	
1.3.1. RNA interference.....	48
1.3.2. miRNA and siRNA.....	50
1.3.3. Off-target effects of siRNA.....	50
1.4. Receptor-targeting Nanoparticles (RTNs)	
1.4.1. The siRNA delivery by RTNs.....	52
1.4.2. The siRNA for therapeutics for cancers in clinical trials.....	55
1.4.3. Toxicity of lipid-based vectors.....	56
1.4.4. Liposomes.....	58
1.4.5. Peptide.....	60
1.4.6. Long-term storage of RTNs at -80 °C.....	62
1.5. Aim and Hypothesis.....	63
2. Materials and Methods.....	65
2.1. Materials	
2.1.1. Equipment.....	66
2.1.2. Kits and Reagents.....	66
2.1.3. Lipids	68
2.1.3.1. Structure of lipid.....	69
2.1.3.2. Composition of Lipid nanoparticle.....	69
2.1.4. Peptides.....	69
2.1.4.1. Structure of Peptide ME27.....	70
2.1.5. siRNAs.....	70
2.1.6. Taqman Assays (FAM-labelled probes) (Applied Biosystems, Thermo Fisher Scientific).....	71
2.1.7. Primary antibodies for immunoblotting.....	71
2.1.8. Complete culture media.....	72

2.1.9. Recipes.....	72
2.2. Methods	
2.2.1. Cell culture.....	72
2.2.2. Receptor targeting nanocomplexes (RTNs).....	73
2.2.3. Luciferase plasmid DNA transfection.....	75
2.2.4. siRNA transfection.....	76
2.2.5. Biophysical characterisation of RTNs.....	76
2.2.6. Total RNA extraction.....	77
2.2.7. Quantitative real time RT-PCR (qRT-PCR).....	78
2.2.8. Statistical Analysis.....	79
2.2.9. Sub G1 Assay	79
2.2.10. Measurement of neurite length and cell area	80
2.2.11. Proliferation assay.....	80
2.2.12. Cell Viability assay.....	81
2.2.13. Immunoblotting.....	82
2.2.14. Stripping immunoblotting membranes.....	83
2.2.15. Mass Spectrometry analysis for quantitative protein profiling.....	83
2.2.16. Cellular Uptake assay.....	83
2.2.17. Heparin Dissociation assay (siRNA release assay).....	84
2.2.18. Luciferase assay.....	85
2.2.19. Bradford protein assay.....	85
2.2.20. Storage of RTN in trehalose.....	86
2.2.21. Xenografts in mice as a neuroblastoma <i>in vivo</i> model.....	86
2.2.22. RTN transfection <i>in vivo</i>	87
2.2.23. Biodistribution of RTN.....	87
2.2.24. Tumour uptake image in histology.....	88

2.2.25. Caspase-3/7 assay.....	88
3. MYCN silencing and the downstream effects induced by RNAi targeting MYCN.....	89
3.1. Introduction.....	90
3.2. Aims.....	91
3.3. Results	
3.3.1. MYCN and NCYM expression differences among neuroblastoma cell lines at mRNA and protein levels	92
3.3.2. Transfection efficiency in a NB cell line by Lipofectamine RNAiMAX.....	95
3.3.3. Comparison of MYCN silencing efficiency of 3 different siMYCNs.....	98
3.3.4. MYCN silencing at mRNA level by siMYCN in NB cell lines.....	100
3.3.5. TP53, MDM3 and NTRK1 mRNA up/downregulated by MYCN silencing...	104
3.3.6. MYCN silencing and Trk upregulation at protein level.....	109
3.3.7. Differentiation in SK-N-BE(2) by siMYCN.....	111
3.3.8. The sensitivity of NB cell lines toward retinoic acid.....	115
3.3.9. Apoptosis induced by MYCN silencing.....	117
3.3.10. MYCN and NCYM gene silencing by siNCYM and NCYM RNA silencing by siMYCN.....	120
3.3.11. Differentiation in SK-N-BE(2) by siNCYM.....	125
3.3.12. Cell viability (cytotoxicity) assay	129
3.3.13. Suppression of cell proliferation by siMYCN and siNCYM.....	131
3.4. Discussion.....	134
4. MYCN silencing by siRNA delivered using RTNs.....	143
4.1. Introduction.....	144
4.2. Aims.....	145
4.3. Results	
4.3.1. Differences in pDNA transfection efficiency among RTNs.....	146

4.3.2. MYCN silencing efficiency of siMYCN delivered by RTNs <i>in vitro</i>	149
4.3.3. MYCN silencing <i>in vivo</i>	152
4.3.4. Tumour uptake of a cationic PEGylated RTN and the biodistribution <i>in vivo</i>	155
4.3.5. Cellular uptake of DD with cholesterol <i>in vitro</i>	157
4.3.6. MYCN silencing efficiency of DD with cholesterol.....	160
4.3.7. siRNA release assay (heparin dissociation assay).....	162
4.3.8. Differences in cellular uptake efficiency among different conditions of Media change and centrifuge.....	164
4.3.9. MYCN silencing difference with different conditions of media.....	167
4.4. Discussion.....	170
5. Long-term storage of RTNs in trehalose.....	176
5.1. Introduction.....	177
5.2. Aims.....	178
5.3. Results	
5.3.1. Biophysical character and function of the RTNs consisting of DD, ME27 and Luciferase plasmid DNA stored at 4 °C or -80 °C in trehalose.....	179
5.3.2. RTNs in trehalose kept at -80 °C	184
5.3.3. Luciferase silencing by siRNA delivered by RTNs in trehalose stored at 4 °C or -80 °C.....	187
5.3.4. GAPDH silencing by siRNA delivered by RTNs in trehalose stored at 4 or -80°C	191
5.3.5. MYCN silencing by siMYCN delivered with RTNs stored at 4°C or -80°C in trehalose or water	195
5.3.6. Anionic RTNs in 8% trehalose stored at 4°C overnight.....	199
5.4. Discussion.....	203
6. General discussion and conclusion.....	208

7. References.....	214
8. Appendices	
Mass spectrometry analysis	234
Results.....	235
Discussion.....	237
Analysed data.....	239
The raw data of the mass spectrometry data.....	240

List of Figures

Chapter 1.

Fig. 1.1. Neural crest and neuroblastoma (NB).....	27
Fig. 1.2. cMyc and MYCN.....	32
Fig. 1.3. MYCN structure and function.....	35
Fig. 1.4. Regulators of MYCN.....	38
Fig. 1.5. MYCN is upregulated by NCYM RNA-binding protein NonO.....	40
Fig. 1.6. Proteins regulated by MYCN, which control various proteins/pathways.....	42
Fig. 1.7. MYCN-p53-MDM2 relationship in MYCN amplified NB.....	46
Fig. 1.8. RNAi mechanism mediated by siRNA.....	49
Fig. 1.9. Structure of receptor-targeting nanocomplexes.....	53
Fig. 1.10. Mechanism of gene silencing by siRNA delivered by RTNs	54
Fig. 1.11. Integrin receptor family.....	61

Chapter 3.

Fig 3.3.1. Differences in MYCN and NCYM expression levels among cell lines.....	94
Fig.3.3.2.Cellular uptake of SK-N-BE(2) cells.....	97
Fig. 3.3.3. Comparison of MYCN silencing efficiency of 3 different siMYCNs in Kelly cells.....	99
Fig. 3.3.4. Remaining MYCN mRNA in NB cell lines 48 hours after siMYCN transfection quantified using qRT-PCR.....	102
Fig. 3.3.5. TP53, MDM2 and NTRK1 mRNA up/downregulation by siMYCN mediated MYCN reduction in SK-N-BE(2) cells.....	106
Fig. 3.3.6. TP53, MDM2 and NTRK1 mRNA up/downregulation by siMYCN mediated MYCN reduction in Kelly cells.....	107
Fig. 3.3.7. TP53, MDM2 and NTRK1 mRNA up/downregulation by siMYCN mediated MYCN reduction in LAN-5 cells.....	108

Fig. 3.3.8. Immunoblotting of MYCN and Trk following siMYCN transfections.....	110
Fig. 3.3.9. Cell morphology changes after siMYCN transfection.....	113
Fig. 3.3.10. Quantification of neurites after siMYCN transfection of SK-N-BE(2) cells: Fig. 3.3.9.....	114
Fig. 3.3.11. Difference in response towards Retinoic Acid among NB cell lines.....	116
Fig. 3.3.12. Sub G1 assay using PI staining.....	119
Fig. 3.3.13. NCYM RNA expression levels in SK-N-BE(2) and Kelly treated with siMYCN.....	122
Fig. 3.3.14. NCYM/MCYN silencing by siNCYM (anti-NCYM siRNA) in SK-N-BE(2) cells.....	123
Fig. 3.3.15. NTRK1 mRNA expression and MYCN /pan Trk protein expression levels in SK-N-BE(2) treated with siNCYM.....	124
Fig. 3.3.16. Morphology changes of SK-N-BE(2) cells transfected with siNCYM.....	127
Fig. 3.3.17. The neurite length and the number of the neurites per cell area induced by siNCYM at day 2 and day 6.....	128
Fig. 3.3.19. Cell viability (toxicity) assay.....	130
Fig. 3.3.20. Suppression of proliferation by siMYCN and siNCYM in SK-N-BE(2) cells.....	133
Fig. 3.4.1. MYCN protein stability and proteasomal degradation.....	135

Chapter 4.

Fig. 4.3.1. Luciferase pDNA transfection using RTNs.....	148
Fig. 4.3.2. siMYCN transfections using RTNs and the cell viability.....	151
Fig. 4.3.3. MYCN silencing using AT1/ME27/siMYCN <i>in vivo</i>	154
Fig. 4.3.4. Tumour uptake and the biodistribution of the RTN (AT1/ME27/FAM labelled siRNA).....	156

Fig. 4.3.5. Differences in cellular uptake and MFI among DD, DD with 10% and 20% cholesterol.....	158
Fig. 4.3.6. Difference in cellular uptake of RTNs containing DD with 20% and 30% cholesterol at 24 hour time point.....	159
Fig. 4.3.7. siMYCN transfections using RTNs containing DD, DD with 10, 20 and 30% cholesterol.....	161
Fig. 4.3.8. The stability and dissociation property of RTNs containing DD, DD with 20 and 30% cholesterol.....	163
Fig. 4.3.9. Differences in cellular uptake efficiencies among different conditions in media and centrifuge.....	166
Fig. 4.3.10. siMYCN transfections using RTN containing DD with 20% cholesterol in SK-N-BE(2).....	168
Fig. 4.3.11. MYCN silencing by RTN containing DD/ME27/siMYCN.....	169

Chapter 5.

Fig.5.3.1. Biophysical data of RTNs consisting of DD/ME27/Luc DNA in trehalose or water stored at 4 °C or -80 °C.....	182
Fig.5.3.2. Biophysical data and the function of data of RTNs consisting of DD/ME27/Luc DNA in trehalose or water stored at 4 °C or -80 °C.....	183
Fig. 5.3.3. the biophysical characters and the function of RTNs kept at -80 °C.....	186
Fig. 5.3.4. the sizes and zeta potentials of RTNs containing siLuc and the silencing efficiency.....	190
Fig.5.3.5. The biophysical character and the function of RTNs consisting of siGAPDH/siNeg, DD and ME27.....	194
Fig.5.3.6. The biophysical character and the function of RTNs consisting of siMYCN/siNeg, DD and ME27.....	198

Fig. 5.3.7. The biophysical character and the function of RTNs consisting of siMYCN/siNeg, DD and ME27.....	202
Fig. 5.4.1. Structure of trehalose.....	203

List of Tables

Chapter 1.

Table. 1.1. Mutations relevant to neuroblastoma incidence.....	29
Table. 1.2. Correlation of MYCN status and risk in NB.....	30
Table. 1.3. Comparison of siRNA and miRNA.....	51
Table. 1.4. siRNA-based therapeutics in clinical trials	57

Chapter 2.

Table. 2.2.1. Weight ratio of each RTN.....	73
---	----

Abbreviations

°C	Celsius degree
µg	Microgram
µL	Microliter
µM	Micro molar
4-OHT	4-hydroxytomoxifen
Ago2	Argonaute 2
ALK	The anaplastic lymphoma receptor tyrosine kinase
ALP	Alkaline phosphatase
ALT	Alanine aminotransferase
ANOVA	Analysis of variance
AST	Aspartate aminotransferase
AURKA	Aurora A kinase
BARD1	BRCA1-associated RING domain 1
BCA	Bicinchoninic acid
BCL2	B-cell lymphoma 2
BDNF	Brain-derived neurotropic factor
bHLHZip	Basic-region/helix-loop-helix/leucine-zipper
BMI1	B cell-specific Moloney murine leukemia virus integration site 1
BMPs	Bone morphogenetic proteins
BSA	Bovine serum albumin
CDC42	Cell division control protein 42
CDKL5	Cyclin-dependent kinase-like 5
cDNA	Complementary DNA
CML	Chronic myeloid leukaemia
c-Myc	MYC proto-oncogene, bHLH transcription factor
CRISPR/Cas9	Clustered Regularly Interspaced Short Palindromic Repeats and the CRISPR-associated protein 9
CUL7	cullin 7
D	pDNA
dCas9-KRAB	a catalytically-dead Cas9- Krüppel-associated box

DD	DOTMA:DOPE (1:1 molecular ratio)
DDT	Dichlorodiphenyltrichloroethan
DMEM	Dulbecco's modified eagle media
DNA	Deoxyribonucleic acid
Dnmt3a	DNA methylase 3a
DOPE	1,2-dioleoyl-sn-glycero-3- phosphoethanolamine
DOPE- PEG2000	1,2-dioleoyl-sn-glycero- 3-phosphoethanolamine-N- [methoxy(polyethylene glycol)-2000]
DOPG	1,2-dioleoyl-sn-glycero-3-phospho-(1'-rac-glycerol)
DOTMA	1,2-di-O-octadecenyl-3-trimethylammonium propane
DPPE- PEG2000	1,2-dipalmitoyl-sn-glycero-3-phosphoethanolamine -N- [methoxy(polyethylene glycol)-2000]
dsRBP	double-stranded RNA-binding proteins
dsRNA	double-strand RNA
E-box	The enhancer box
ECL	Enhanced chemiluminescence
ECM	The extracellular matrix
EDTA	Ethylenediaminetetraacetic acid
ER α	Estrogen receptor alpha
FACS	Fluorescence-activated cell sorting
FBS	Fetal bovine serum
Fbxw7a	F-box and WD repeat domain-containing 7
Fig.	Figure
GSK3 β	Glycogen synthase kinase 3 β
HATs	Histone acetyl transferase
HDACs	Histone deacetylases
HEPES	4-(2-hydroxyethyl)-1-piperazineethanesulfonic acid
IL-6	Interlukin-6
INF α	Interferon α
K ₁₆	KKKKKKKKKKKKKKKKKK(K ₁₆)
kDa	Kilo Dalton

L	Liposome
L2K	Lipofectamine 2000
lncUSMycN	A long noncoding RNA transcribed from -14 kb upstream from the MYCN transcription start site
M	Molar
MAPK	The mitogen-activated protein kinase
MB	MYC box
MDM2	Mouse double minute 2 homolog
ME27	K ₁₆ RVRRGAC <u>RGD</u> CLG
ME72	K ₁₆ RVRRGA <u>CRGE</u> CLG
MEME	Minimum Essential Medium Eagle
MFI	The mean fluorescence intensity
miRNA	microRNA
Miz-1	Myc-interacting zinc finger protein 1
mM	Millimolar
MOPS	3-(N-morpholino)propanesulfonic acid
mRNA	Messenger RNA
mTOR	Mammalian target of rapamycin
MuLV	Moloney Murine Leukemia Virus
mV	Millivolt
MYCL	MYCL proto-oncogene, bHLH transcription factor
MYCN	MYCN proto-oncogene, bHLH transcription factor
n	The number of samples
n.d.	Non-detectable
NB	Neuroblastoma
NBT-1	NB-associated transcript-1
ncRAN	Noncoding RNA expressed in aggressive NB
NCYM	MYCN opposite strand (MYCNOS), cis-antisense gene of MYCN
NEAA	Non-essential amino acid
ng	Nomogram
NGF	Nerve growth factor

NLRR1	The neuronal-leucine rich repeat-1
nM	Nano molar
nm	Nanometre
NonO	Non-POU domain-containing octamer-binding protein
NSG	NOD-SCID gamma mice
NTRK1	Neurotrophic receptor tyrosine kinase 1
OD	Optical density
P	Peptide
P/S	Penicillin/Streptomycin
p53/TP53	Tumour protein 53
p75NTR	Neurotrophin receptor p75
PATC	protein activator of PKR
PBS	Phosphate-buffered saline
PCR	Polymerase chain reaction
PDI	Polydispersity index
pDNA	Plasmid DNA
PEG	<i>Polyethylene glycol</i>
PHOX2B	Apaired-like homeobox 2b
PI	Propidium iodide
PI3K	Phosphatidylinositol-4,5-bisphosphate 3-kinase
PMSF	Phenylmethanesulfonyl fluoride
PSG	Primary sympathetic ganglia
P-TEFb	positive transcription elongation factor
PVDF	Polyvinylidene difluoride
qRT-PCR	Quantitative real-time PCR
R	siRNA
RA	All- <i>trans</i> retinoic acid
RAP1	RAS-related protein
RISC	the RNAi-induced silencing complex
RLU	Relative luminescence unit
RNA	Ribonucleic acid

RNA pol II	RNA polymerase II holoenzyme
RNAi	RNA interference
RNAiMAX	Lipofectamine RNAiMAX
rpm	Revolutions per minute
RT	Room temperature
RTKs	Receptor tyrosine kinases
RTNs	Receptor-targeting nanocomplexes
S62	Serine 62
SD	Standard deviation
SDS PAGE	Sodium dodecyl sulfate polyacrylamide gel electrophoresis
siGAPDH	Anti-GAPDH siRNA
siLuc	Anti-Luciferase siRNA
siMYCN	Anti-MYCN siRNA
siNCYM	Anti-NCYM siRNA
siNeg	Negative control siRNA
siRNA	Short interfering RNA
SKP2	S-phase kinase-associated protein 2
SP-1	Specificity protein 1
T58	Threonine 58
TAD	Transactivation domain
TFII-H	Transcription factor II Human
TG5	Transglutaminase 5
the EPR effect	The enhanced permeation and retention effect
TIP60	Tat-interactive protein 60 kDa
TLRs	Toll-like receptors
TNF α	Tumour necrosis factor alpha
TRBP	Transactivation response RNA-binding protein
Trks	<i>Tropomyosin receptor kinases</i>
TRRAP	Transformation/Transcription Domain Associated Protein
U	Unit
UT ctrl	Untransfected negative control

CHAPTER 1

Introduction

1. Introduction

1.1. Neuroblastoma

1.1.1. Neuroblastoma in clinical presentation

Neuroblastoma (NB) is one of the most common solid malignant tumours in childhood, and its incidence rate is approximately 6-10 per one million infants (Domingo-Fernandez et al. 2013). Moreover, NB accounts for more than 7% of malignancies and 15% of cancer-related mortality in childhood (Nara et al. 2007; Huang et al. 2011; Maris et al. 2007). The outcomes are widely diverse: more than 90% patients with low-risk NB are cured, while high-risk NB has a poor outcome with less than a 50% survival rate (Whittle et al. 2017).

1.1.2. Classification of Neuroblastoma

There are several classification systems for neuroblastoma used in prior period (Matthay et al. 2016). The international neuroblastoma pathology classification (the Shimada system) was based on morphologic features of neuroblastic tumour, which was established in 1999 (Shimada et al. 1999). This classification distinguishes favourable or unfavourable pathology groups according to the age of patient, the ability of tumour to differentiate and mitosis-karyorrhexis index (MKI): the number of cells undergoing mitosis or karyorrhexis per 5000 cells (low: <100, intermediate: 100-199, high: \geq 200) (Shimada et al. 1999).

- Favourable group: poorly differentiated or differentiating and low or intermediate MKI aged <1.5 years, and differentiating and low MKI aged 1.5-5 years.
- Unfavourable group are: 1) undifferentiated or 2) high MKI tumour aged < 1.5 years, 1) undifferentiated or poorly differentiated or 2) intermediate or high MKI tumour aged 1.5-5 years, and all tumours aged \geq 5 years (Shimada et al. 1999).

International neuroblastoma staging system (INSS) was established in 1988 and revised in 1993 and has been most widely used in reporting studies last 30 years (Matthay et al. 2016). There are six classes in this system: Stage 1, 2A, 2B, 3, 4 and 4S. They are defined as blow:

Stage	Definition
1	Localised tumour with complete gross excision with or without minuscule residual disease. Representative ipsilateral nonadherent lymph nodes negative to tumour microscopically (nodes attached to and removed with the primary tumour may be positive).
2A	Localised tumour with incomplete gross excision; representative ipsilateral nonadherent lymph nodes negative to tumour microscopically.
2B	Localised tumour with incomplete gross excision; representative ipsilateral nonadherent lymph nodes positive to tumour microscopically. Enlarged contralateral regional lymph nodes must be negative microscopically.
3	Unresectable unilateral tumour infiltrating across the midline with or without regional lymph node involvement; or localised unilateral tumour with bilateral extension by infiltration (unresectable) or by lymph node involvement.
4	Any primary tumour with dissemination to distant lymph nodes, bone, bone marrow, liver, skin and/or other organs (except as defined for Stage 4S).
4S	Localised primary tumour (as defined for Stage 1, 2A or 2B), with dissemination limited to skin, liver, and/or bone marrow (limited to infant < 1 year of age)

Taken from Brodeur et al. (1993)

The international neuroblastoma risk group staging system (INRGSS) was established to develop a new clinical staging system for pretreatment NB tumours in 2008. They also established a list of image-defined risk factors (radiographic images). The risk is determined

by the image-defined risk factors, and/or whether tumours are local or metastasis (Matthay et al. 2016). There are 4 classes as blow:

Stage	Definition
L1	Localised tumour not involving vital structure as defined by the list of image-defined risk factors and confined to one body compartment.
L2	Localised tumour with presence of one or more image-defined risk factors.
M	Distant metastatic disease (except MS).
MS	Metastatic disease in children younger than 18 months with metastases confined to skin, liver, and/or one marrow.

Taken from (Monclair et al. 2008)

INSS determines the risk of NB by surgical resection, lymph node involvement and metastatic disease whereas INRGSS uses image study and bone marrow morphology of presurgical disease (Lanzkowsky et al. 2016).

1.1.3. Origin of neuroblastoma

Most (65%) primary NBs are diagnosed in the adrenal medulla and are associated with the sympathetic ganglia (Maris et al. 2007; Maris 2010). It is well-accepted that the origin cells of NB arise from the sympathoadrenal lineage of the neural crest during the development stage (Fig. 1.1.) (Buechner & Einvik 2012; Cheung & Dyer 2013; Marshall et al. 2014). During embryogenesis, the neural crest gives rise to diverse cells, such as enteric neurons, Schwann cells, and adrenal medulla (Pichler & Calin 2014). The rest of the primary tumour cases arise in the chest, neck, and pelvis (Maris 2010; Cheung & Dyer 2013). Patients with bilateral adrenal NBs are rare, which suggests that they may have a predisposing genetic lesion and that two independent genetic lesions in the cells of the left and right sympathoadrenal lineage induce bilateral tumours (Cheung & Dyer 2013).

1.1.4. Familial neuroblastoma

Inherited mutations in the signalling pathways, which are important for the development of the sympathoadrenal lineage, are associated with familial genetic syndromes characterised by predisposition to NB and defects in development (Cheung & Dyer 2013) although familial NB is rare (< 1%-2%) (Mossé et al. 2008). Significant heterogeneity in the clinical presentation of NB is seen even in the same family (Mueller & Matthey 2009). The predisposition mutation first described was a paired-like homeobox 2b (PHOX2B), and the gene encodes a homeodomain transcription factor, which promotes cell-cycle exit and

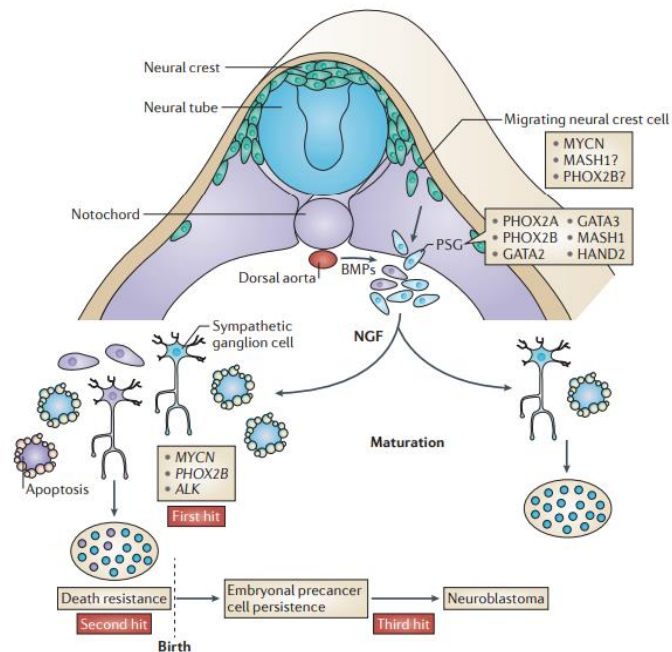


Fig. 1.1. Neural crest and neuroblastoma (NB). Neuroblastoma progenitors migrate from around the neural tube and neural crest to a lateral region to the dorsal aorta and notochord under MYCN and bone morphogenetic protein (BMPs). Blue cells represent normal cells, and purple represents precancer cells. Primary sympathetic ganglia (PSG) are induced by nerve growth factor (NGF) to mature into terminal ganglion cells or to apoptose. The precancer cells obtain death resistance by the mutation on MYCN, PHOX2B or ALK, which leads to NB. Taken from Marshall et al. (2014).

neuronal differentiation (ibid.). Furthermore, PHOX2B plays a crucial role in the development of the neural crest-driven autonomic neurons (ibid.). Therefore, it was hypothesised that a mutation in the differentiation pathway regulated by PHOX2B in the sympathoadrenal lineage of neural crest may contribute to NB tumorigenesis (Cheung & Dyer 2013). However, mutations in PHOX2B can explain only a small subset of familial NB (Mossé et al. 2009).

The most common heritable form of NB is caused by a lesion in the anaplastic lymphoma receptor tyrosine kinase (ALK) gene (Mossé et al. 2009). It was reported that six out of eight

families with three or more affected members had an ALK mutation in the germline cells, while the other two families had PHOX2B mutations (Mueller & Matthey 2009). Knudson's two hit hypothesis explains how cancer is induced from a mutation on a single allele in a germline cell; 'two hits' in the DNA are required for tumorigenesis, and the inherited mutation is 'the first hit' (Payne & Kemp 2005). However, 'the second hit' has not yet been identified, which leads to NB with the inherited ALK mutation (Matthay et al. 2016). Possibilities include a mutation on another ALK allele, amplification of the inherited mutated allele or deletion of the normal allele (Matthay et al. 2016). An ALK mutation is expressed in the developing sympathoadrenal lineage in the neural crest, and it may control the balance of proliferation and differentiation through multiple cellular pathways, such as the mitogen-activated protein kinase (MAPK) and RAS-related protein (RAP1) signal transcription pathways (Motegi et al. 2004, Schonherr et al. 2010). Furthermore, it was reported that PHOX2B regulates ALK gene expression directly (Bachetti et al. 2010). In addition, ALK signalling may be crucial for the proliferation of the sympathoadrenal lineage during development (Reiff et al. 2011).

1.1.5. Sporadic neuroblastoma

In sporadic NB, approximately 6%-10% are caused by somatic ALK-activating mutations and 3%-4% carry a high frequency of ALK gene amplification (Cheung & Dyer 2013). In addition, activating ALK mutations or amplifications are associated with high-risk NB suggesting that ALK is an oncogene in NB. There are several other hallmark genes associated with high-risk NB with a poor outcome, including BARD1, LMO1, and LIN28B (Table 1.1). However, MYCN amplification is the most common genetic lesion (Brodeur & Bagatell 2014). It is known that high-risk NB is strongly associated with MYCN

Table 1.1. Mutations relevant to neuroblastoma incidence. Modified from Domingo-Fernandez et al. (2013).

Chr	Gene	Gene name	Status	Predisposition	Function	References
1p36.31	<i>CHD5</i>	Chromodomain helicase DNA-binding protein	Deletion	Sporadic	Chromatin remodelling and gene transcription	Fujita et al. 2008
1p36.3–p36.2	<i>DFF45</i>	DNA fragmentation factor	Mutation	Sporadic	Apoptosis	Abel et al. 2004
1q23.3	<i>DUSP12</i>	Dual specificity phosphatase 12	SNP	Sporadic	Negatively regulate members of the mitogen-activated protein (MAP) kinase superfamily (MAPK/ERK, SAPK/JNK, p38)	le Nguyen et al. 2011
1p36.3	<i>UBE4B</i>	Ubiquitination factor E4B	Mutation	Sporadic	Ubiquitination	Korona et al. 2003
2p23	<i>ALK</i>	Anaplastic lymphoma receptor tyrosine kinase	Mutation	Hereditary	Genesis and differentiation of the nervous system	Mosse et al. 2008
2q35	<i>BARD1</i>	BRCA1-associated RING domain	SNPs	Sporadic	Interaction with the N-terminal region of BRCA1	Capasso et al. 2009
4p12	<i>PHOX2B</i>	Paired-like homeobox 2B	Germline missense or frameshift	Hereditary Sporadic	Transcription factor	Mosse et al. 2004
5q11.2	<i>DDX4</i>	DEAD box polypeptide 4 isoform	SNP		Alteration of RNA secondary structure	le Nguyen et al. 2011
5q11.2	<i>IL31RA</i>	Interleukin 31 receptor A precursor	SNP		Signalling via activation of STAT-3 and STAT-5	le Nguyen et al. 2011
6p22	<i>FLJ44180</i>	Long intergenic non-protein coding RNA 340	SNP		–	Maris et al. 2008
6p22	<i>FLJ22536</i>	Long intergenic non-protein coding RNA 340	SNP		–	Maris et al. 2008
9p21	<i>CKDNA</i>	Cyclin-dependent kinase inhibitor 2A	Mutation, deletion	Sporadic	Cell-cycle G1 control	Ghiorzo et al. 2006
9p23–p24.3	<i>PTPRD</i>	Protein tyrosine phosphatase, receptor type, D	Microdeletion		Signalling molecules that regulate a variety of cellular processes including cell growth, differentiation, mitotic cycle, and oncogenic transformation	Stallings et al. 2006
11q13	<i>CCND1</i>	Cyclin D1	Amplification, rearrangement		Proto-oncogene, control of cell-cycle/cellular proliferation	Michels et al. 2007
11p11.2	<i>HSD17B12</i>	Hydroxysteroid (17-beta) dehydrogenase 12	SNP		Converts estrone into oestradiol in ovarian tissue	le Nguyen et al. 2011
6q21	<i>LIN28B</i>	Lin-28 homolog B	SNP		RNA-binding protein, negatively regulates let-7 processing	Molenaar et al. 2012
11p15.4	<i>LMO1</i>	LIM domain only 1	SNP, amplification	Sporadic	Cysteine-rich transcriptional regulator	Wang et al. 2011
12q24	<i>PTPN11</i>	Protein tyrosine phosphatase, non-receptor type 11	Mutation	Sporadic	Regulate a variety of cellular processes including cell growth, differentiation, mitotic cycle, and oncogenic	Martinelli et al. 2006
17q11.2	<i>NF1</i>	Neurofibromin 1	Deletion		Negative regulator of the RAS signal transduction pathway	Origone et al. 2003
17q13.1	<i>P53</i>	Tumour protein p53, TP53	Mutation	Sporadic	DNA-binding protein	Carr-Wilkinson et al. 2010
18q21.3	<i>DCC</i>	Netrin 1 receptor	Mutation, deletion	Sporadic	Member of the immunoglobulin superfamily of cell adhesion molecules	Kong et al. 1997
20p11	<i>SLC24A3</i>	Solute carrier family 24	SNP	Sporadic	Plasma membrane sodium/calcium exchangers	Maris et al. 2008

Table 1.2. Correlation of MYCN status and risk in NB High-risk NB is strongly correlated with MYCN amplification. Adapted from Cheung and Dyer (2013).

Risk	MYCN Amplification	Stage	Age at Diagnosis	Overall Survival (%)	Current Treatment Approach
Low-risk	No	4S	< 12 months	> 91 ± 2	Supportive care
	No	Locoregional	≤ 21 years	> 95	Surgery ± Chemotherapy
Intermediate risk	No	4	> 18 months	89 ± 2	Surgery and moderate intensity chemotherapy
High-risk	Yes	Locoregional	≤ 21 years	53 ± 4	Dose-intensive chemotherapy, surgical resection of residual primary tumour, radiation to primary and resistant metastatic sites, myeloablative therapy with autologous stem cell rescue, anti-GD2 immunotherapy and 13- <i>cis</i> -retinoic acid
	Yes	4	< 18 months	29 ± 4	
	Yes or no	4	≥ 18 months and ≤ 21 years	31 ± 1	
	No	4	≥ 12 years	< 10	

amplification, and it has a poor prognosis, whereas tumours with low-risk retain the ability to differentiate and regress spontaneously (Westermarck et al. 2011; Brodeur 2003). MYCN amplification occurs in approximately 20%-25% of the primary tumours of NB (Gustafson & Weiss 2010, Buechner & Einvik 2012; Huang et al. 2011) and is a marker for prognosis, and survival rates, which are low in MYCN-amplified NB (Table 1.2) (Seeger et al. 1985; Gustafson & Weiss 2010).

According to the ‘somatic evolution’ hypothesis, cells with somatic mutations on the proto-oncogenes are subjected to selective pressures such as intercellular competition for resources and immunosurveillance (Crespi & Summers 2005). The surviving cells then display the six ‘hallmark of cancer’:

- self-sufficiency in cell growth
- insensitivity or antigrowth signals

- evasion of apoptosis (via loss or mutation of goalkeeper genes)
- limitless of replication ability
- sustained angiogenesis and
- tissue invasion and metastasis (Crespi & Summers 2005).

1.2. MYCN

1.2.1. MYCN and c-Myc MYCN was first discovered as amplified DNA homology to viral myc (v-myc) in NB cell lines in 1983 (Westermarck et al. 2011, Huang & Weiss 2015). MYCN is a member of the Myc proto-oncogene family that includes c-Myc and MYCL, which are evolutionarily well-conserved transcription factors (Westermarck et al. 2011; Whitfield & Soucek 2012). MYCN is normally located on chromosome 2p24.3 (Schwab et al. 1983; Bell et al. 2010), while c-Myc is on 8q24.21. In addition, c-Myc and MYCN are highly homologous and several domains, such as the DNA-binding domain, are shared between the two proteins (Fig. 1.2a) (Gherardi et al. 2013). MYCN is strictly expressed in certain tissues such as Kidney of the developing embryos in humans and mice but is almost completely absent in adults, while c-Myc is expressed in all proliferative tissues in adults (Westermarck et al. 2011). C-Myc and MYCN are likely to be complementary to each other during embryonic development. The c-Myc expression occurs in many tissues, except neuroepithelium, while MYCN is expressed in all proliferative tissues at high levels (ibid) (Fig. 1.2.b).

Mutations in MYCN in humans and mice are involved with birth defects, and mouse embryos with null MYCN die around E11.5, whereas mice with null c-Myc die around E10.5 (Huang & Weiss 2013). Hence, the role of MYCN in embryonic development seems to be essential. Similarly, MYCN is initially expressed in the entire cells during neural crest development, promoting migration and differentiation (Wakamatsu et al. 1997). Additionally, Olsen et al. (2017) reported that they successfully transformed wild-type neural crest cells to NB by enforced expression of MYCN in mice.



Fig. 1.2. c-Myc and MYCN: a) MYC (c-Myc) and MYCN share the sequence. b) The levels of MYC (c-Myc) and MYCN protein expression in each organ in newborns and adults. Taken from Huang and Weiss (2013).

1.2.2. Functions of MYCN

The protein controls the expression of many genes involved in essential cellular processes, such as proliferation, cell growth, protein synthesis, metabolism, apoptosis, and differentiation (Huang et al. 2011; Feng et al. 2010; Nara et al. 2007; Westermark et al. 2011). MYCN consists of a DNA-binding, basic-region, helix-loop-helix/leucine-zipper (bHLHZip), MYC box (MB), and transactivation domain (TAD) (Fig. 1.3.a). The C-terminus bHLHZip domain heterodimerises with its partner protein, Myc-associated factor X (MAX), to form a transcriptional activator that binds to the enhancer box (E-box) sequence: 5'-CACGTG-3' (Westermark et al. 2011), while c-Myc can also bind non-canonical 5'-CANNTG-3' (Bell et al. 2010).

Recent studies showed that MYC may induce epigenetic changes at target regions by relaxing the nucleosomal barrier, which leads to enhanced transcription (He et al. 2013). MYC recruits transcription co-factors, such as complexes containing transcription domain-associated protein (TRRAP), with either tat-interactive protein 60 kDa (TIP60) or GCN5, which are histone acetyl transferase (HAT), or acetyltransferase, such as p300/CBP (ibid) (Fig. 1.3.B left). HAT or p300/CBP, recruited by MYC via TRRAP, acrylates histone components of target loci. The nucleosomal barrier is then relaxed by acetylation making DNA more accessible and the nucleosome more permissive for transcription (He et al. 2013). It was reported that MYCN binding to GCN5 have similar transcriptional functions in neuronal stem cells (Martinez-Cordenon et al. 2012). Furthermore, it has also been shown that MYC can bind to TATA-binding protein (TBP: a member of the transcriptional pre-initiation complex), which suggests that MYC can recruit RNA Pol II machinery to activate transcription (Fig. 1.3.B, left) (He et al. 2012; Westermark et al. 2011).

Interestingly, P300/CBP, GCN5 and Tip60 all acetylate MYC and acetylated MYC protein is stabilised by prevention of ubiquitin-mediated degradation. Hence HAT is recruited by MYC not only for acetylation of target loci but also for stabilisation of MYC function (He et al. 2013). In addition, it was revealed in neural progenitors that MYC stimulates transcription of GCN5, which gives MYC increased transcriptional activity and the protein stability (Knoepfler et al. 2006).

It was shown that MYCN cannot initiate *de novo* transcription although it is necessary to maintain nucleosome permissiveness for transcription (Knoepfler et al. 2006). In NB, it was found that MYCN was bound to genes which were already transcriptionally activated, and MYCN was also not involved with *de novo* transcription (Cotterman et al. 2008). It is consistent with MYC binding at or near transcription start sites (TSS), and MYC's function to amplify transcription of genes activated transcriptionally (Nie et al. 2012; Lin et al. 2012). Chipumuro et al. (2014) reported that MYCN-driven global transcription amplification in NB was suppressed by cyclin-dependent kinase 7 (CDK7) inhibition without systemic toxicity.

Reversely, the MYC antagonist MAD was shown to recruit a transcription repressor, Sin3, which then binds to histone deacetylases (HDACs), leading to histone deacetylation and silencing of the target loci. In another model, MYCN binds to other transcriptional factors, such as Miz-1 and SP-1, on the initiator element and so repress gene expression (Fig. 1b, right). The MYC/MAX dimer recruits HDACs and DNA methylase 3a (Dnmt3a), which inhibit transcription induced by Miz-1/SP-1 (Westermarck et al. 2011).

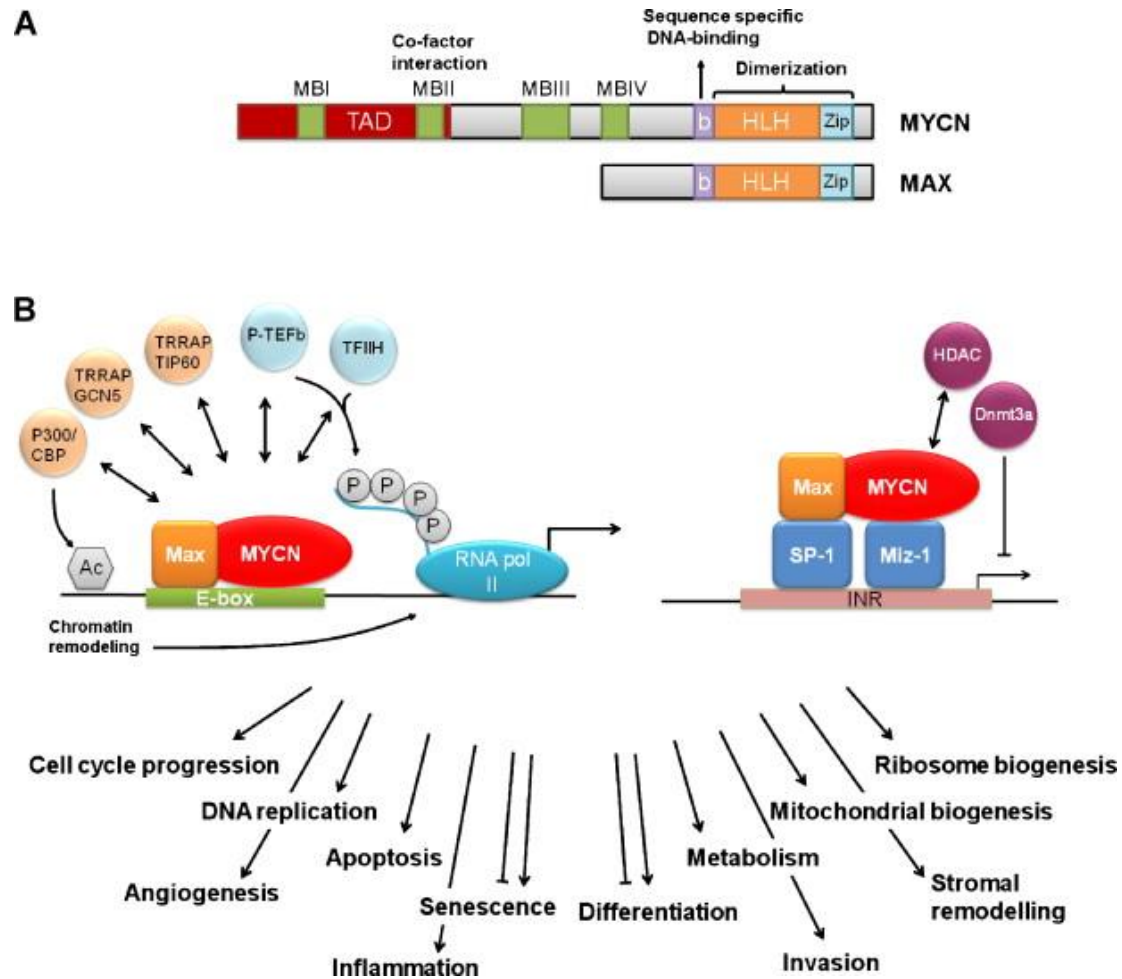


Fig. 1.3. MYCN structure and function A) the structure of MYCN and the partner protein MAX. B) the function of MYCN/MAX. They regulate multiple intracellular processes. Taken from Westermark et al. (2011).

Recently, it was found that MYC transcriptionally amplifies epigenetic modifiers with repressive activities. For instance, it has been shown that MYC stimulates the polycomb repressive complex 2 (PRC2) such as embryonic ectoderm development (Eed), suppressor of zeste 12 (Suz12) and histone methyltransferase enhancer of zeste homolog 2 (EZH2) in embryonic stem cells (He et al. 2013).

Corvetta et al. (2013) reported that a repression complex of MYCN and EZH2 on the promoter of the tumour suppressor gene CLU leads to tumorigenesis in NB. Wang et al. (2012) also showed that high-levels of EZH2, which may be dysregulated by several factors including MYCN, increased the copy number of Ch.7 or loss of tumour suppressor miR-101 located on 1p36 in NB. The loss of miR-101 by co-overexpression of MYC and EZH2 has been found in hepatocellular carcinoma (Wang et al. 2014). In addition, Dardenne et al. (2016) also reported that interaction of overexpressed MYCN and EZH2 induces neuroendocrine prostate cancer. Moreover, MYCN elevates B cell-specific Maloney murine leukaemia virus integration site (BMI1) expression in NB cell lines and NB tumours (Ochiai et al. 2010). It has shown that BMI1 represses tumour suppressor genes such as p53 via stimulation of RING1A/B E3 ligase targeting p53, which leads tumorigenesis.

1.2.3. Stability and degradation of MYCN

Tight control of the MYCN function is essential for modulating cellular mechanisms (Beltran 2014). There are many mechanisms that regulate MYCN, and one such mechanism is to control the MYCN turnover, which is the balance between the cell-cycle rate and MYCN degradation (ibid.). The MYCN protein has a half-life of approximately 20 to 30 minutes in normal cells, while the MAX expression is abundant and consistent in quiescent and proliferation cells (Lu et al. 2003). On the other hand, the protein is extremely stable (about 100 times more than normal) in some amplified NB tumour cell lines which ensures

the cells remain in cell cycles and do not go into the G0 phase (Bonvini et al. 1998; Beltran 2014). The extraordinary stability of the MYCN protein in NB with MYCN amplification may be correlated with co-amplification and co-expression of NCYM (Suenaga et al. 2014) and co-amplified AURKA (Otto et al. 2009).

MYCN protein is degraded by F-box and WD repeat domain-containing 7 (Fbxw7a), ubiquitin ligase, via the ubiquitin-proteasome system (Sjostrom et al. 2005; Gustafson & Weiss 2010). This occurs during the mitotic phase after the cell-cycle kinase cyclin B/CDK1 and glycogen synthase kinase 3 β (GSK3 β) phosphorylate MYCN protein at serine 62 (S62) and threonine 58 (T58), respectively (Sjostrom et al. 2005). Additionally, PP2A dephosphorylates the S62 phosphate in the Pin1-mediated process (Gustafson & Weiss 2010). Because AKT can inactivate GSK3 β , MYCN is stabilised by the PI3K/AKT pathway (Barone et al. 2013; Chesler et al. 2006) (Fig. 1.4.). The AKT/PI3K pathway is activated by receptor tyrosine kinases (RTKs), such as ALK, Trk, and IGF 1R. The RTKs are activated by binding ligands or by mutations, causing continuous activation including activated ALK (Gustafson & Weiss 2010). Furthermore, MYCN is normally located on chromosome 2p24.3 (Schwab et al. 1983; Bell et al. 2010) while ALK is linked to MYCN on chromosome 2p23 (Gustafson & Weiss 2010). There is no evidence to show the direct connection between ALK and MYCN on the transcription level. However, it is likely that activated ALK and other RTKs are involved with the stabilisation of MYCN (Barone et al. 2013, Gustafson & Weiss 2010).

AKT can also activate mammalian target of rapamycin (mTOR) indirectly through several signalling mechanisms. The mTOR forms a complex called mTORC1, and the complex inhibits PP2A by phosphorylation, which contributes to MYCN activation (Gustafson & Weiss 2010). Similarly, Aurora A kinase (AURKA), which is a mitosis kinase and is usually

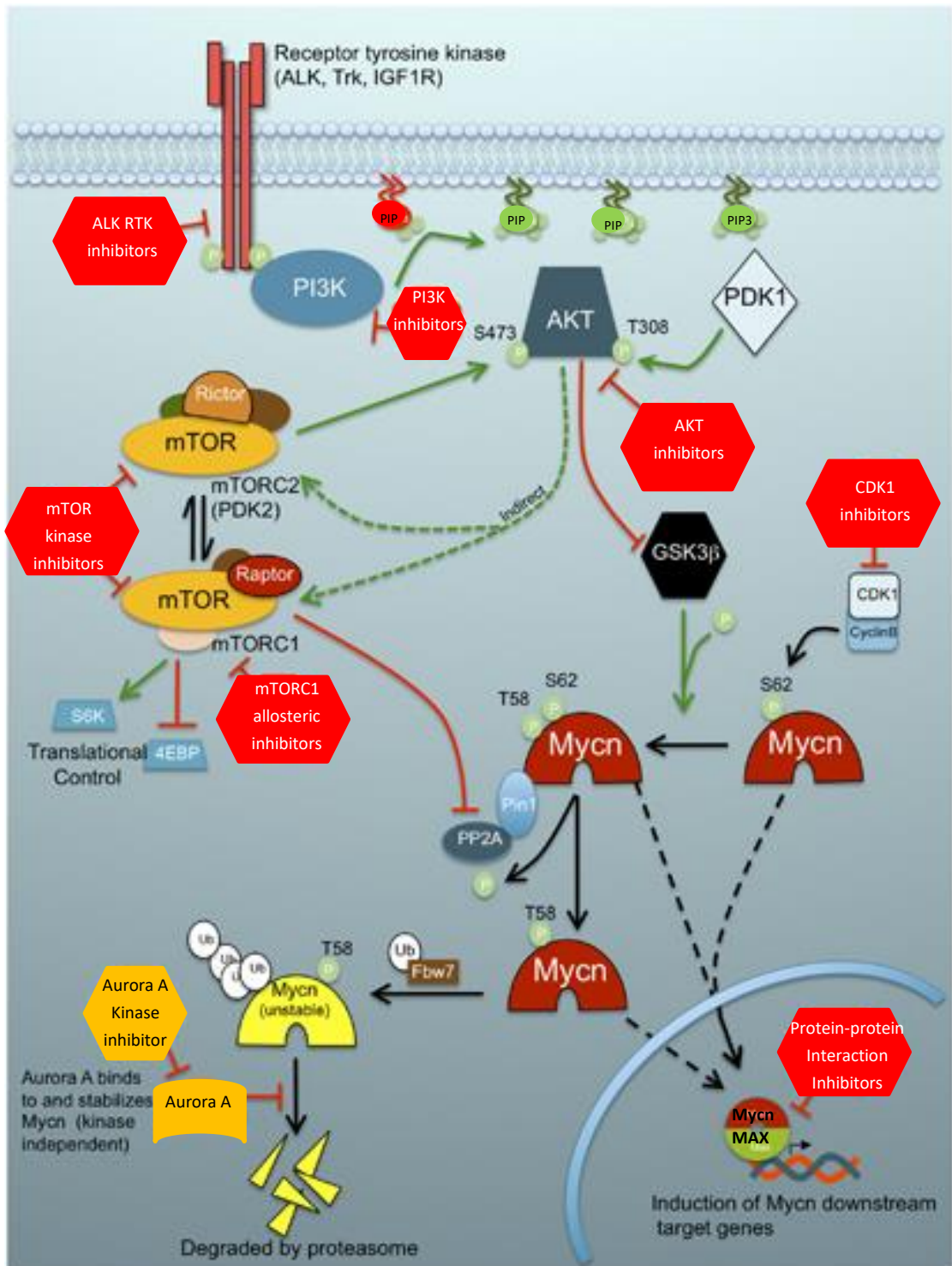


Fig. 1.4. Regulators of MYCN After GSK3 β phosphorylate MYCN, Fbw7 (ubiquitin ligase) degrades the protein via the ubiquitin-proteasome system. However, PI3K/AKT pathway and AURKA stabilise MYCN. Taken from Gustafson & Weiss (2010).

expressed during G1 and mitosis, inhibits Fbxw7-mediated degradation and stabilises MYCN. Overexpression and amplification of AURKA often occurs in MYCN-amplified NB. The two proteins cooperate to promote tumour proliferation and oncogenic activity (Otto et al. 2009). Brockmann et al. (2013) reported that inhibition of AURKA triggers degradation of MYCN in NB. Furthermore, when the MAPK pathway is hyperactivated by activation of H-RAS through an oncogenic RAS mutation and other oncoproteins, the pathway induces MYCN accumulation by accelerating MYCN translation (Kapeli & Hulin 2011).

Suenaga et al. (2014) reported that NCYM, which is the *Cis*-antisense gene of MYCN, is co-expressed and co-amplified with MYCN in some human primary NB and the gene codes a protein which inhibits MYCN phosphorylation by GSK3 β , and so promotes MYCN protein stabilisation (Suenaga et al. 2014). However, Zhao et al. (2016) reported that they could not identify the NCYM protein, with either of the two commercially available anti-NCYM antibodies. In addition, Duffy et al. (2013) stated that GSK3 β inhibitors reduce the MYCN mRNA levels and NB cell viability. The MYCN phosphorylation by GSK3 β can stabilise MYCN (Duffy et al. 2013).

1.2.4. Transcription of MYCN

Even though MYCN has been investigated for decades, the main transcription factors and underlying essential mechanisms for MYCN expression in NB remain poorly understood (Zhao et al. 2016). Despite the findings of transcription factors for MYCN expression in the other cancer cells, such as specificity protein 1 (Sp-1) in cervical cancer (Inge et al. 2002), they are not sufficient for the activation of MYCN transcription in NB (Kramps et al. 2004). Furthermore, Suenaga et al. (2009) reported that the MYCN promoter was activated by the MYCN protein through the direct recruitment to intron 1 on the *MYCN* gene containing two putative E-box sites.

Recently, evidence has shown that noncoding RNA plays a critical role in pathogenesis in NB. Yu et al. (2009), for example, reported that noncoding RNA (ncRNA) expressed in aggressive NB (ncRAN), which is mapped on chromosome 17q25.1, is associated with a poor clinical outcome. Another example is that the loss of lncRNA NB-associated transcript-1 (NBT-1) leads to NB progression via increasing proliferation and suppressing differentiation of neuronal precursors (Pandey et al. 2014).

Importantly, Liu et al. (2016) reported that a long noncoding RNA transcribed from -14 kb upstream from the MYCN transcription start site (lncUSMycN) is overexpressed in NB tissues and cell lines with MYCN amplification, and it upregulates NCYM by activating the

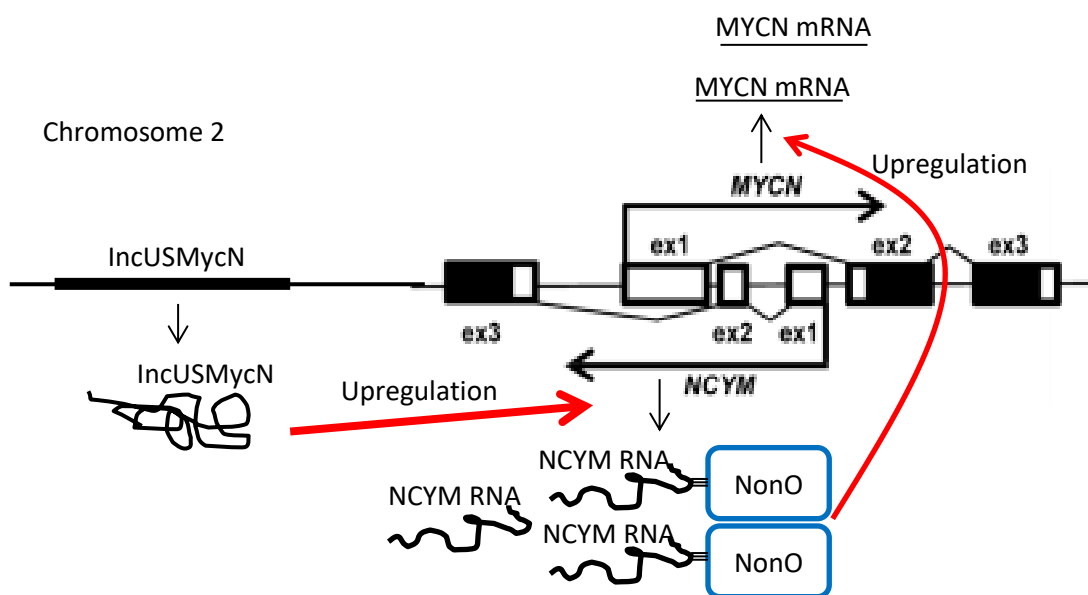


Fig. 1.5. MYCN is upregulated by NCYM RNA-binding protein NonO lncUSMycN upregulates NCYM RNA expression. Modified from Suenaga et al. (2014) and Liu et al. (2016).

transcription of the NCYM gene. The NCYM RNA forms a complex with NonO, RNA-binding protein (Fig. 1.5.), and they upregulate the expression of MYCN mRNA. In addition, Suenaga et al. (2014) mentioned that MYCN activate the NCYM transcription.

1.2.5. MYCN and target genes

Many genes have been identified as downstream targets of MYCN (Fig. 1.6.), but it is still not clear how these genes are regulated directly or indirectly (Valentijn et al. 2012); for example:

- MDM2 (negative regulator of p53, upregulated by MYCN),
- p53 (tumour suppressor, upregulated) (Slack et al. 2005),
- the neuronal-leucine rich repeat-1 (NLRR1: transmembrane protein with unknown function, upregulated),
- S-phase associated kinase 2 (SKP2; a component of the ubiquitin ligase complex, upregulated),
- DKK3/Wnt/ β -catenin pathway (DKK3, suppressing Wnt: downregulated, Wnt/ β -catenin pathway, stimulating expression of target genes: upregulated) (Koppen et al. 2007), and
- PI3K/AKT/mTOR pathway (inducing S6 kinase and eIF4E, initiation factor of eukaryotic translation) (Valentijn et al. 2012; Bell et al. 2010, Beltran 2014).

There are studies published by several groups that MYCN expression at higher levels also triggers not only proliferation and cell growth, but also apoptosis (Gustafson & Weiss 2010). Gustafson and Weiss (2010) pointed out that, if the hypothesis is true, then it contradicts the

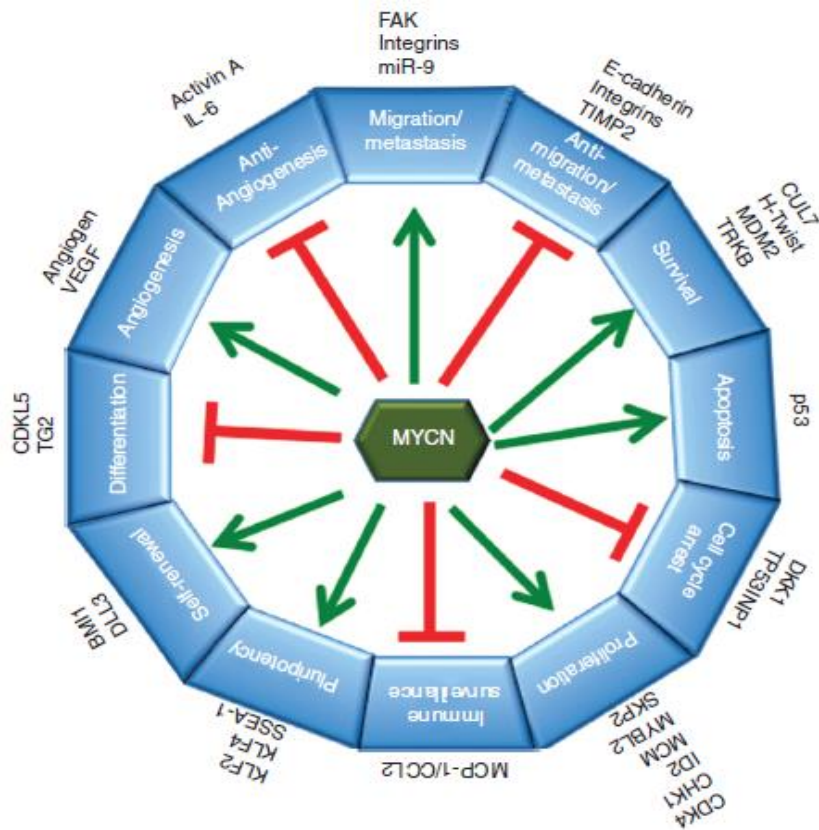


Fig. 1.6. Proteins regulated by MYCN, which control various proteins/pathways
 Taken from Huang and Weiss (2013).

hypothesis that MYCN amplification is strongly correlated with high-risk NB. The inhibition mechanisms of apoptosis as a contributor to MYCN-mediated transformation are complex and poorly understood (Gustafson & Weiss 2010).

Furthermore, many groups have observed the effect of MYCN silencing in MYCN-amplified NB using antisense or RNA interference, and the results are various and appear to depend upon the experimental condition, such as the cell lines. Overall, the reduction of MYCN expression is regarded to induce cell arrest in the G1 phase of the cell cycle, differentiation, and/or apoptosis (Kang et al. 2006; Westermarck et al. 2011; Bell et al. 2010). Conversely, the increase of MYCN expression triggers the re-entry of the quiescent cells into the cell

cycle, which notably shorten the G1 phase and decrease the cell attachment to the extracellular matrix (Bell et al. 2010; Gherardi et al. 2013).

Additionally, high levels of MYCN help the development of NB in terms of proliferation, whereas normal cells can be differentiated. If MYCN is inhibited, then NBs have reduced functions of proliferation and cell growth and eventually cannot survive (Soucek & Evan 2010). Differentiation and apoptosis pathways are important in therapeutics for NB. The details are below.

1.2.5.1. Differentiation

NB is thought to arise originally from the neural crest cells and thereby can self-renew and maintain pluripotency. It is likely that MYCN is associated with the regulation of these stem cell-like properties because c-Myc can be replaced with MYCN in reprogramming fibroblasts into iPS cells (Nakagawa et al. 2010). Hence, MYCN (and c-Myc) promotes 'a stem-like state' because it is likely to block differentiation pathways and induce self-renewal and pluripotency factors (Huang & Weiss 2013). The pluripotency genes KLF2, KLF4, and LIN28B are upregulated by MYCN (Cotterman & Knoepfler 2009). In addition, endosomal and mesodermal differentiation markers (BMP4 and GATA6) are upregulated in MYCN knockout mice (Varlakhanova et al. 2010). Similarly, differentiation proteins, such as cyclin-dependent kinase-like 5 (CDKL5) (Valli et al. 2012) and tissue transglutaminase (TG2) (Liu et al. 2007), are suppressed by MYCN. Valli et al. (2012) mentioned that CDKL5 stops the cell cycle and promotes differentiation after MYCN knockdown.

Similarly, expression of MYCN downregulates cell division control protein 42 (CDC42), a G-protein involved in a cytoskeleton remodelling pathway, and upregulates nm23 (the nucleotide diphosphate kinase, nm23-H1:NME1 and nm23-H2:NME2), which also downregulates CDC42. This interaction inhibits differentiation of MYCN-amplified NB

(Valentijn et al. 2005; Bell et al. 2010). Additionally, MYCN upregulates PAX3, which encodes a transcription factor that is expressed in active progenitor cells during early embryogenesis; the PAX3 expression is subsequently downregulated during neural differentiation (Harris et al. 2002).

Tropomyosin receptor kinase A (TrkA) is a member of the tyrosine receptor kinase family, along with TrkB and TrkC (Westermarck et al. 2011). Moreover, TrkA is a high affinity NGF receptor, while TrkB is a brain-derived neurotropic factor (BDNF), and TrkC is neurotrophin-3 (ibid.). In addition, TrkA is predominantly expressed at a later stage in development, and it is likely that it plays a crucial role in the complete differentiation of sympathetic neurons in normal cells (Dixon & McKinnon 1994). When TrkA is co-expressed with neurotrophin receptor p75NTR, differentiation is enhanced (Ho et al. 2011).

Iraci et al. (2011) reported that TrkA and p75NTR are downregulated by MYCN/SP-1/MIZ-1 repression complex recruiting HDAC1, which affects malignancy of NB by inhibiting the cell response to NGF. Hence, the expression level of TrkA and p75NTR is normally low in aggressive MYCN-amplified NB (Iraci et al. 2011).

1.2.5.2. Apoptosis

The protein p53 is widely known as a proapoptotic protein, but it is rare to find p53 mutations in primary NB tumours (Westermarck et al. 2011; Huang et al. 2011). MYCN upregulates both proliferation and apoptosis (Fulda et al. 2000). Hence, the outcome is dependent upon the status of apoptotic factors cooperating with MYCN, such as BCL2 (the anti-apoptotic protein) (Strasser et al. 1990) or p53 (Chesler et al. 2008). Therefore, MYCN is likely to cooperate with suppressors of p53 signalling, such as miRNA-380-5p (Swarbrick et al. 2010), CUL7 (Kim et al. 2007), BMI1 (Huang et al. 2011), H-Twist (Valsesia-Wittmann et al. 2004), and MDM2 (Slack et al. 2005). Interestingly MDM2, an E3 ubiquitin

ligase, has an important role in the apoptosis pathway in NB by promoting survival by ubiquitination and degradation of p53 (Fig. 1.5.). It is also thought that MDM2 binds the AU-rich elements of the 3'UTR of MYCN mRNA, thereby stabilising the mRNA (Gu et al. 2012). The MYCN can trigger transcription of TP53 and MDM2, and MDM2 is a target of p53-mediated transcription (Slack et al. 2005; Chen et al. 2010).

In contrast, mutations in the p53 pathway are found in NB at relapse, which may occur in response to cytotoxic chemotherapy. Chemotherapy initially has efficacy in the treatment of MYCN-amplified NB, partly because of MYCN-mediated p53 activation (Huang & Weiss 2013). Eventually, these tumours may acquire resistance to the therapy as a result of mutations that inactivate p53 (ibid.). The MYCN and MDM2 upregulate each other, thereby conferring a survival advantage to NB, leading to relapse (ibid.).

Similarly, several groups found that the promoter of apoptotic initiator caspase-8 is methylated (Casciano et al. 2004; Banelli et al. 2005; Lazcoz et al. 2006), and it is likely that it is a mechanism of apoptosis evasion in NB with MYCN amplification. Loss of caspase-8 contributes resistance to tumour necrosis factor-related, apoptosis-inducing, ligand-induced apoptosis in NB cells (Eggert et al. 2001).

Furthermore, prosurvival signalling cascades are constitutively activated in MYCN-amplified NB, while proapoptotic signalling is suppressed. For instance, activation of tropomyosin receptor kinase (TrkB), the same group member as TrkA, is frequently seen in MYCN-amplified NB, while the expression level is low in non-MYCN-amplified NB (Nakagawara et al. 1993). The TrkB activation is associated with resistance to chemotherapy and can upregulate MYCN mRNA. This may imply that TrkB activation is associated with MYCN-amplified NB (Ho et al. 2002; Dewitt et al. 2013).

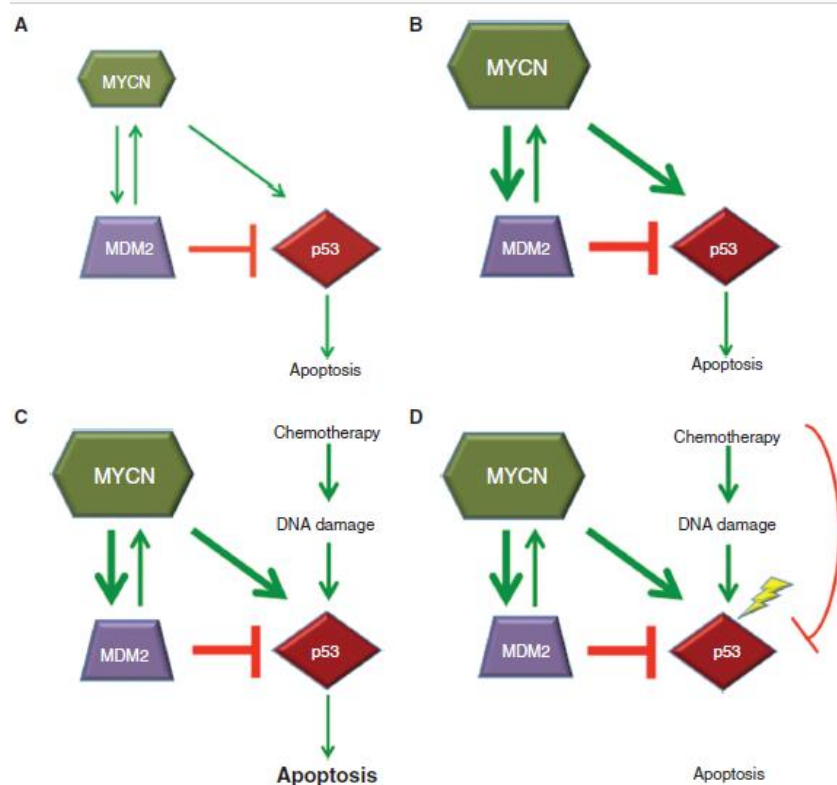


Fig. 1.7. MYCN-p53-MDM2 relationship in MYCN amplified NB. A&B) MYCN upregulates MDM2 and p53, while MDM2 downregulates p53. C) Chemotherapy has efficacy as a p53-dependent apoptosis inducer at the initial stage of the therapy. D) At relapse, p53 or p53 pathways are resistant to chemotherapy due to mutation. Taken from Huang and Weiss (2013).

1.2.6. Current treatment of neuroblastoma with MYCN amplification

Like other cancers, the treatment methods used for NB therapy include surgery, chemotherapy, monoclonal antibody treatment, and radiotherapy (Fig. 1.2.) (Maris et al. 2007; Macmillan Cancer Support website). The NB tumours vary remarkably based upon their stage and biological features (Murphy & Quaglia 2014). Treatment for patients at stage L1 (low-risk) is surgery alone, or surgery and chemotherapy. For patients at stage L2 (intermediate-risk), chemotherapy and surgery are usually necessary, and radiotherapy may be needed as well. There are 4 parts of treatment for patients at stage 4; the first part is

chemotherapy, the second part is surgery to remove the main tumour, followed by radiotherapy to the site of the main tumour. The third is high dose chemotherapy with a stem cell transplant. The final part is maintenance treatment where patients receive 13-*cis* retinoic acid or immunotherapy (Cancer Research UK website).

Localised NB generally has favourable biological features, and surgery alone successfully treats them (Maris et al. 2007). Even MYCN-amplified NB could achieve remission for a long time after surgery alone if it is localised (ibid.). As chemotherapy, 13-*cis*-retinoic acid (RA) has become a standard of therapy in high-risk NB after neuronal differentiation by retinoid was shown *in vitro* (Cheung & Dyer 2013). However, RA resistance can be several NB cells have obtained, which leads to relapse (Clark et al. 2013).

Similarly, anti-GD2 monoclonal antibody has become a standard of care for patients with high-risk NB since 2010. The GD2 is expressed in mature neurons and during foetal development and across NB cells with high density, membrane proximity, and homogeneity. However, the dose is constrained due to the side effects and its efficacy has been observed only in minimal residue disease and has hardly been seen in high-risk NB (Cheung & Dyer 2013). Anti-GD2 monoclonal antibody induces dephosphorylation of protein tyrosine kinase 2 (PTK2), suppresses the PI3K/AKT pathway and triggers apoptosis (Sait & Modak 2017). Sait & Modak (2017) reported that the progression free survival rate for 5 years of high-risk neuroblastoma patients who received anti-GD2 antibody (3F8) alone was 44%, 3F8 combined with intravenous granulocyte-macrophage colony-stimulating factor (GM-CSF) and 13-*cis*-retinoic acid (CRA) was 56%, and 3F8 combined with subcutaneous GM-CSF CRS was 62%.

In short, overexpression of MYCN induces proliferation and cell growth and suppresses apoptosis and differentiation, which contributes to NB tumorigenesis. In addition, there is no

therapy that demonstrates efficacy to cure patients with MYCN-amplified NB. Therefore, MYCN might be a promising target for treatment against high-risk NB, and gene therapy silencing of MYCN by RNA interference (RNAi) can be a novel therapy for NBs.

1.3. Gene Therapy

1.3.1. RNA interference

Fire et al. (1998) first discovered RNAi as double-stranded RNA that enabled gene silencing in the nematode worm *Caenorhabditis elegans*. After that, small interfering RNA (siRNA) was identified as 25-nucleotide antisense RNA in plants by Hamilton and Baulcombe (1999). Then, Elbashir et al. (2001) reported that 21-nt double-stranded RNA mediates RNAi in mammalian cells *in vitro*.

RNAi is a naturally occurring mechanism to regulate genes in most eukaryotic cells and uses a small double-strand RNA (dsRNA) molecule from endogenous or exogenous origin to homology-dependently control gene activity (Aagaad & Rossi 2007; Almeida et al. 2005). In addition, siRNA is 21-22 nt long dsRNA that is two nucleotides longer at its 3' side, allowing it to be recognised by the enzymatic machinery of RNAi that evolutionally induces homology-independent degradation of the target mRNA (*ibid.*). The siRNA is generated by ribonuclease digest of dsRNA in the Dicer integrative complex (Zhang et al. 2004; Videira et al. 2014) (Fig. 1.8.). The siRNA is subsequently integrated into the RNAi-induced silencing complex (RISC) consisting of Argonaute 2 (Ago2), Dicer, and dsRBP. It is known that Dicer has two partners, double-stranded RNA-binding proteins (dsRBP): transactivation response RNA-binding protein (TRBP) and protein activator of PKR (PATC). When Ago2 forms a complex with Dicer and TRBP or PATC, the complex can select the predicted strand, while Ago2 alone uses the guide and passenger RNAs equally (Noland & Doudna 2013).

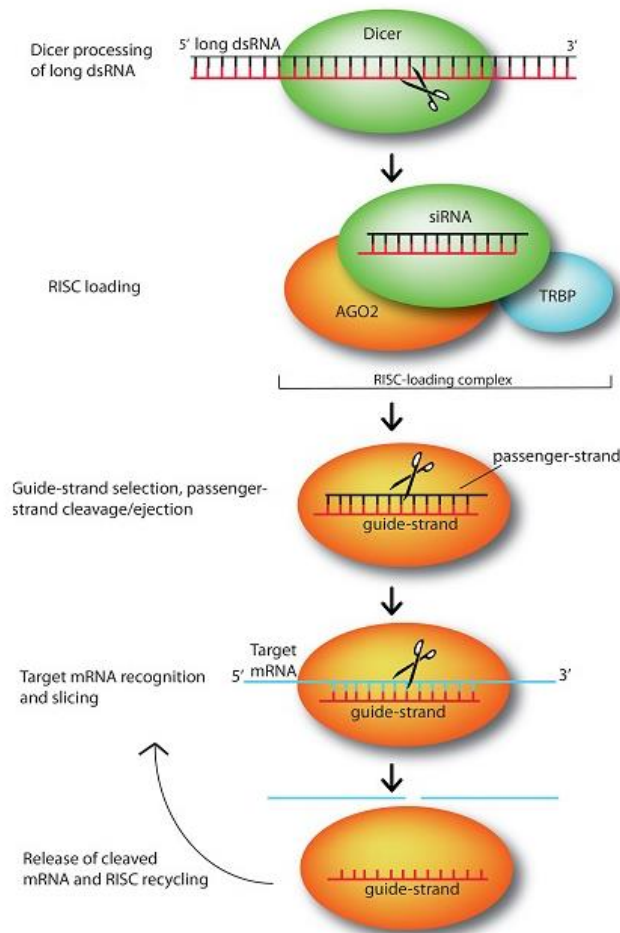


Fig. 1.8. RNAi mechanism mediated by siRNA Taken from Dana et al. (2017)

The RISC complex is activated to recognise homologous mRNA sequences when Dicer cleaves the sense strand (the passenger strand), allowing the remaining antisense strand to become the guide strand within the RISC complex. The RISC comprising the guide siRNA binds the complementary sequence of the target mRNA, allowing the mRNA to be degraded or cleaved (Videira et al. 2014; Singh et al. 2009; Aagaad & Rossi 2007). The RISC comprising the guide siRNA binds mRNA and degrades or cleaves the mRNA again (Whiteheat et al. 2009).

1.3.2. miRNA and siRNA

During the last 20 years, ncRNA including siRNA and microRNA (miRNA) appears to play an important role in regulation of cellular processes (Buechner & Einvik 2012). It is observed that dysregulation of ncRNA is associated with several diseases, including cancer and cardiovascular and developmental disorders (Esteller 2011; Taft et al. 2010). Moreover, miRNA and siRNA have been widely investigated because of the therapeutic potential to regulate target genes and proteins, predisposing diseases including cancers and infections (Lam et al. 2015). The physicochemical properties of siRNA and miRNA are similar, while their functions are distinct (Table 1.3.).

Synthetic single RNAs (miRNA) can inhibit the activity of the endogenous miRNA (miRNA antagonist). In addition, synthetic miRNA can mimic endogenous miRNA functions, which leads to mRNA degradation and gene silencing (miRNA mimic) (Bader et al. 2010). The main difference between siRNA and miRNA for therapeutic purpose is that siRNA targets one mRNA and binds mRNA, whose sequence is fully complementary, while miRNA targets several mRNAs. The sequence is partially complementary to the targeted mRNA (ibid.). Therefore, siRNA more specifically silences the targeted mRNA.

1.3.3. Off-target effects of siRNA

However, siRNA off-target effects have been observed. There are two types of siRNA off-target effects: miRNA-like off-target effects and innate immune response (Jackson & Linsley 2010). In miRNA-like off-target effects, the guide strand of siRNA imperfectly matches the

Table. 1.3. Comparison of siRNA and miRNA Taken from Lam et al.

	siRNA	miRNA
Prior to Dicer processing	Double-stranded RNA that contains 30 to over 100 nucleotides	Precursor miRNA (pre-miRNA) that contains 70–100 nucleotides with interspersed mismatches and hairpin structure
Structure	21–23 nucleotide RNA duplex with 2 nucleotides 3'overhang	19–25 nucleotide RNA duplex with 2 nucleotides 3'overhang
Complementary	Fully complementary to mRNA	Partially complementary to mRNA, typically targeting the 3' untranslated region of mRNA
mRNA target	One	Multiple (could be over 100 at the same time)
Mechanism of gene regulation	Endonucleolytic cleavage of mRNA	Translational repression Degradation of mRNA Endonucleolytic cleavage of mRNA (rare, only when there is a high level of complementary between miRNA and mRNA)
Clinical applications	Therapeutic agent	Drug target Therapeutic agent Diagnostic and biomarker tool

region of 3' UTRs of these transcripts with 5' of the siRNA, which leads to translation arrest or mRNA cleavage (ibid.). It was revealed that siRNA downregulated a set of transcripts which are enriched for transcripts with 3' UTR complementary to the 5' end of the corresponding siRNA guide strand (Jackson et al. 2006; Birmingham et al. 2006). Therefore, the sequence of 5' end of siRNA is important to avoid off-target effect silencing. In addition, it is likely that it is correlated to the siRNA concentration; reducing siRNA concentration minimises the miRNA-like off-target effects (Dharmacon).

Chemically modified siRNA is also available in the market (Dharmacon). Broering et al. (2013) reported that 2'-O-methylation on the siRNA backbone largely abolishes toll-like receptor-mediated activation of the hepatic immune system. It has been shown that 2'-O-deoxy or 2'-fluoro modifications do not have any effect on TLR7/8 activation (Jung et al. 2015).

The other off-target effect is the innate immune response. The siRNA or the vehicles delivering siRNA, such as cationic lipids, are sensed by toll-like receptors (TLRs) expressed by mammalian immune cells, which detect pathogen-associated molecular patterns (Judge & MacLachlan 2008; Schlee et al. 2006). There are several types of TLRs which can detect

RNAs: TLR3, TLR7, and TLR8. They move between the endoplasmic reticulum and intracellular compartments. The TLRs stimulate interferons, tumour necrosis factor alpha (TNF α), and interleukin-6 (IL-6) and reduce gene expression through the recognition of viral infection (Jackson & Linsley 2010). It is likely that siRNA can activate TLR3 signalling, but TLR3 is not a major mechanism of siRNA-activated immune cells (Kariko et al. 2004; Sledz et al. 2003). The siRNA seems to activate TLR7 and TLR8 and to trigger the production of pro-inflammatory cytokines in monocytes and myeloid dendritic cells or the production of interferon α (INF α) in plasmacytoid dendritic cells activated by siRNA (Jackson & Linsley 2010).

The immune response toward siRNAs is dependent upon the cell types due to the selective expression of TLRs (Hornung et al. 2005; Judge et al. 2005; Sioud 2005). Because not all sequences are detected by TLRs, the sequence of siRNA may be important to avoid the off-target effect of the innate immune response as well (Jackson & Linsley 2010). Judge et al. (2005) reported that siRNA or single-stranded RNA containing poly(U) or GU- rich sequence such '-UGUGU-' can activate inflammatory response. They showed U to C substitutions on 2 bases reduces activation of inflammation but it is likely that not all inflammatory sequences have been identified (Jackson & Linsley 2010).

1.4. Receptor-targeting Nanoparticles (RTNs)

1.4.1. The siRNA delivery by RTNs

Due to its negative charge, naked siRNA cannot be taken into negatively charged cell plasma membranes. Xu et al. (2016) mentioned that siRNA delivery using nanoparticles requires: 1) protection of siRNA in the blood and no interaction with proteins in the blood for prolonged circulation, 2) cellular internalisation, and 3) siRNA release to cytoplasm and protection of siRNA from endosomal degradation.

In addition, *in vivo*, there is a size limitation due to the size of the normal endothelial structure; therefore, RTNs should be smaller than 150 nm to pass through the vascular endothelial barrier (Fig. 1.10. Lower). On the other hand, the structure of blood vessels is altered at the inflammation and solid tumour sites; the vasculature and endothelial structure become ‘leaky’. Particles less than 500 nm can cross the wall and have enhanced permeation and retention (called the EPR effect). This effect permits RTNs delivered into the bloodstream to be extravasated into targeted tumour cells (Li & Szoka 2007).

Previous studies on gene and drug delivery have focused on accumulation and penetration via the EPR effects. However, recent studies have revealed that accumulation in the solid tumour does not enhance its therapeutic efficacy (Xu et al. 2016) probably because of the poor gene and drug release (Zhao et al. 2013).

We have developed cationic and anionic receptor-targeting nanocomplexes (RTNs) consisting of lipids, receptor-targeting peptide, and nucleic acid (i.e. plasmid DNA, mRNA, or siRNA) to deliver siRNA into NB cells (Fig. 1.9.). Nanoparticles, consisting of lipids and receptor-targeting peptide, allow siRNA to be delivered into targeted cells.

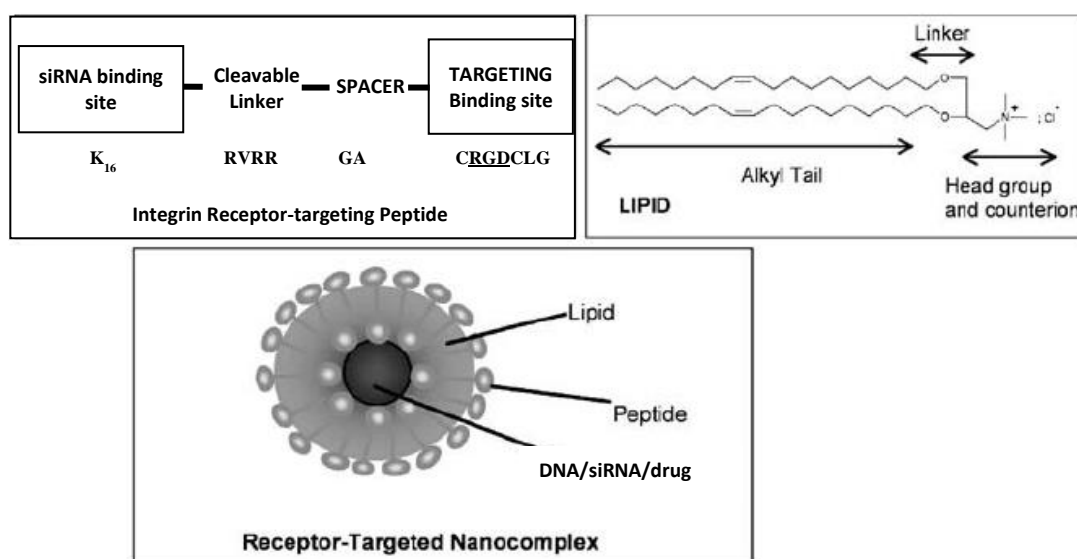


Fig. 1.9. Structure of receptor-targeting nanocomplexes (RTNs) Modified from Hart (2010).

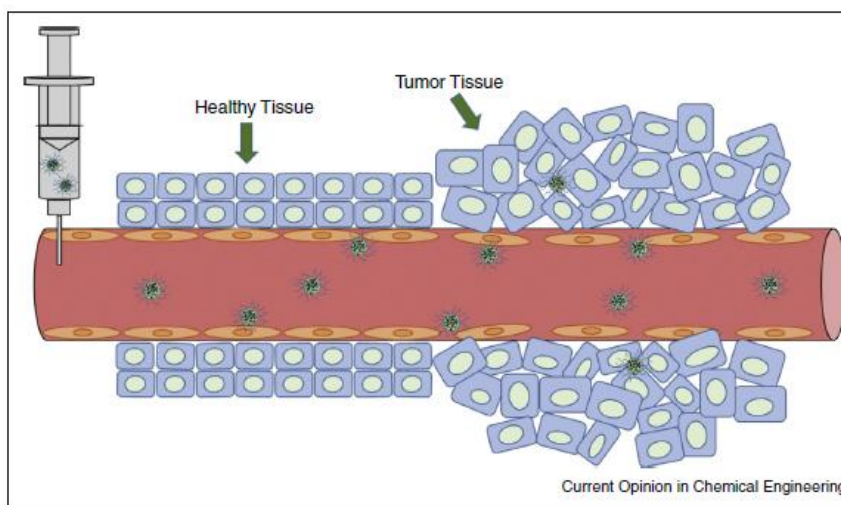
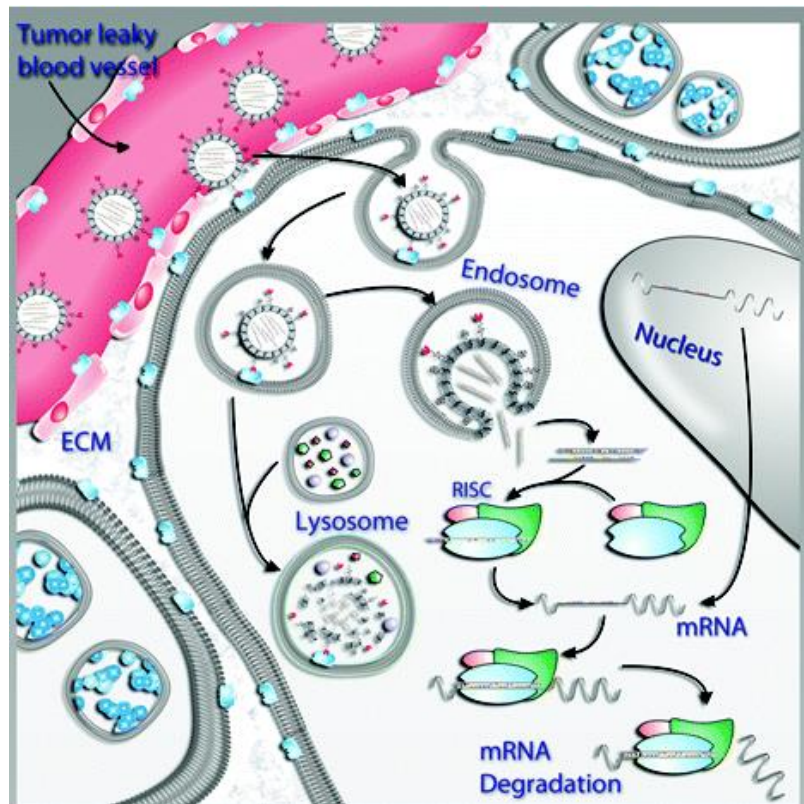

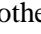




Fig. 1.10. Mechanism of gene silencing by siRNA delivered by RTNs

Upper)  endothelial cell,  RTNs,  siRNA,  overexpressed receptor. Taken from Gomes-Da-Silve et al. (2012). Lower) Healthy blood vessel structure and altered 'leaky' endothelial structure in tumour sites. It allows nanocomplexes to pass through the blood vessel barrier and to be delivered into tumour cells. Taken from Spencer et al. (2015).

Once the targeting peptides of RTNs bind to specific receptors on the targeted cell surface, they are internalised via receptor-mediated endocytosis or clathrin-coated pits. The particles start to be degraded within the endosome and most lipids of the RTNs fuse with the lipid of the endosome. Then, peptide/siRNA complexes are released to the cytoplasm and RNAi by siRNA processes (Hart 2010) (Fig. 1.10. Upper).

Baetlett and Davis (2006) mentioned that the duration of gene silencing by RNAi is dependent upon the doubling time of the cells presumably because the siRNA is diluted. Hence, gene silencing in non-dividing cells lasts for a month or more both *in vitro* and *vivo* (Zuckerman & Davis 2015).

There are several advantages to using non-viral nanoparticles; for instance, a wide variety of formulation can be created. Moreover, RTNs can package any type of nucleic acid and drug and can deliver several nucleic acids and drugs at the same time (Hart 2010).

1.4.2. The siRNA for therapeutics for cancers in clinical trials

Koldehoff et al. (2007) first reported that their research group systemically treated a single patient with chronic myeloid leukaemia (CML) with anti-bcr-abl (a fusion gene found in most CML) siRNA using anionic lipid nanoparticles. As a result, the siRNA remarkably achieved more than 90% gene silencing and induced apoptosis in CML cells; however, after the second dose, the silencing efficiency was not as significant as the first dose, even though the dose was increased (Koldehoff et al. 2007). Numerous studies using siRNA delivered by lipid-based nanocomplexes have been brought to clinical trials. The most advanced study using siRNA encapsulated by lipid nanoparticles is inhibiting transthyretin in transthyretin amyloidosis, and it is now in Phase III (Zuckerman & Davis 2015).

In cancer studies on clinical trials, anti-KRAS siRNA delivered by biodegradable polymer matrix (siG12D LODER) for pancreatic cancer is now in phase II, which is the most advanced siRNA study for cancer (NCT0676259, not yet recruiting). The siG12D LODER is for locally advanced pancreatic cancer and is combined with chemotherapy (Golan et al. 2015). In systemic therapy using liposomes, the most advanced clinical trials are anti-PLK1 siRNA for neuroendocrine tumours (TKM 080301) and adrenocortical carcinoma and anti-PKN3 for advanced or metastasis pancreatic cancer (Atu027) on Phase I/II. Non-targeting lipid nanoparticles (Atu027, consisting of three cationic lipids) were employed and have been completed in 2016 (Lam et al. 2015). Their silencing efficiency was not published. A summary of siRNA-based therapeutics in clinical trials is shown in Table 1.4.

1.4.3. Toxicity of lipid-based vectors

The final goal in gene therapy using RNAi is to achieve efficient gene silencing in the targeted tissues in clinical use without immune activation and toxicity. Currently, viruses, liposomes, and polycationic polythylenimine (PEI)-based nanoparticles are primarily used in therapeutic RNAi (van den Boorn et al. 2011). These three vehicles showed some success; however, there are issues concerning the safety and toxicity in each type of vector. For example, there are many advantages in RNAi using viral vectors, such as long-term silencing by integrating small hairpin RNA (shRNA) cassettes into the genome; however, there are major drawbacks. Viral vehicles may activate complement or coagulation factors (Waeher et al. 2007), and trigger neutralisation of antibody response, which prevents multiple administration. The main issue is the dysregulation of gene expression by insertional mutagenesis and oncogenesis (van den Boorn et al. 2011).

Table. 1.4. siRNA-based therapeutics in clinical trials Modified from Lam et al. (2015) and Zuckerman & Davis (2015).

Name	Indication	siRNA target	Phase	Delivery system	Route of administration	Trial ID
ALN-VSP02	Advanced solid tumour with liver involvement	KSP and VEGF	I, completed	Lipid nanoparticles	Intravenous	NCT01158079 NCT00882180
Atu027	Advanced solid tumour	PKN3	I, completed	Lipid nanoparticles	Intravenous	NCT00938574
Atu027	Pancreatic ductal carcinoma	PKN3	I/II, completed	Lipid nanoparticles	Intravenous	NCT0180638
CALAA-01	Solid tumour	RRM2	I, terminated	Polymer-based targeted nanoparticles	Intravenous	NCT00689065
DCR-MYCN	Solid tumour, multiple myeloma non-Hodgkin's lymphoma	MYC	I, terminated	Lipid nanoparticles (EnCore)	Intravenous	NCT02110563
DCR-MYCN	Hepatocellular carcinoma	MYC	I/II, terminated	Lipid nanoparticles (EnCore)	Intravenous	NCT02314052
siG12D LODER	Advanced pancreatic cancer	Mutated KRAS oncogene	I, completed II, not yet recruiting	Biodegradable polymer-based scaffold	Local implantation	NCT01188785 NCT01676259
siRNA-EphA2-DOPC	Advanced cancer	EphA2	I, recruiting	Natural liposomes	Intravenous	NCT01591356
TKM-080301 (TKM-PLK1)	Primary or secondary liver cancer	PLK1	I, completed	Lipid nanoparticles	Intravenous	NCT01437007
TKM-080301 (TKM-PLK1)	Neuroendocrine tumour and adrenocortical carcinoma	PLK1	I/II, completed	Lipid nanoparticles	Intravenous	NCT01260035

Liposomes seem to be the preferable delivery approach of siRNA; however, there are issues regarding the toxicity. Liposomes also can activate complement or coagulation factors by adsorbing opsonins, which leads to phagocytosis via the mononuclear phagocyte system due to the size and charge. In addition, as mentioned above, cationic lipid nanocomplexes may activate TLR7/8, which triggers the innate immune system response when the nanocomplexes stay in the endosome. Similarly, Kedmi et al. (2010) showed that positively charged lipid-based nanocomplexes significantly increased the levels of liver enzyme alanine aminotransferase (ALT), aspartate aminotransferase (AST), and alkaline phosphatase (ALP), suggesting liver toxicity, and TLR4 was also activated. In a clinical trial of siRNA targeting the Zaire Ebola virus (ZEBOV) RNA polymerase L protein-delivered lipid nanoparticles, a TLR-mediated immune response probably evoked by the nanoparticles was observed in several patients when the dose was escalated (Zatsepin et al. 2016).

The safety and toxicity of lipid-based nanocomplexes have not been investigated sufficiently, while liposomes can be used in broad areas (Winter et al. 2015). Further studies are required for safety in clinical use in the future.

1.4.4. Liposomes

In siRNA delivery, one of the major challenges is developing the methods to carry the nucleic acids to targeted cells efficiently. Liposomes have been widely used for protecting nucleic acids against enzymatic degradation in blood and endosomes/lysosomes (Elsabahyer et al. 2011). Cationic lipids have been traditionally used for siRNA delivery, and lipid nanoparticles consisting of cationic liposomes and PEG are now commonly used in siRNA delivery, while there are anionic liposomes. One of the advantages of using cationic liposomes to carry siRNA is that positively charged RTNs can easily attract the negatively charged plasma membrane, and they achieve high transfection efficiency (Elsabashy et al.

2011). However, cationic RTNs may be sensed by TLRs, as mentioned above, and interact with any cells. Hence, siRNA would be delivered to cells non-specifically. In addition, cationic nanoparticles can interact with negatively charged molecules present in serum *in vivo*. This may shield the positive charge on the surface of the nanoparticles (Elsabahy et al. 2011). The attraction with serum protein in blood could induce premature siRNA release and prompt aggregation (Oliveira et al. 2015).

The use of flexible hydrophilic polymer, such as PEG, can partially solve these problems. Furthermore, PEGylation is commonly employed in nanoparticles for nucleic acid delivery. The PEG forms a protective hydrophilic layer on the cationic RTN surface and changes the surface properties, decreases opsonisation by blood protein, and reduces phagocytosis, called the steric stabilisation effects (Allen et al. 2002, Huang et al. 2008). The PEGylated RNAs can increase circulation time in the blood, which allows RTNs an opportunity to reach target tissues (Hart 2010). On the other hand, PEGylation can prevent RTN cellular uptake (Huang et al. 2010, Mishra et al. 2004) and siRNA endosomal escape. Additionally, PEG might not sufficiently protect siRNA against enzymatic degradation (Oliveira et al. 2015).

Anionic RTNs cannot bind to the negatively charged plasma membrane of cells by themselves due to the repulsion, and only receptor-targeting peptide can make the RTNs bind to cells. That provides the advantages of better targeting specificity and less toxicity and interaction with serum components (Balazs & Godbey 2011; Tagalakis et al. 2014). However, there are also problems; it is difficult to achieve self-assembly between anionic liposomes and negatively charged nucleic acids. In addition, anionic RTNs normally show poor transfection efficiency due to the difficulty in approaching the cell membrane (Tagalakis et al. 2014).

With the flexibility to create new formulations, numerous types of materials have been employed to improve the efficiencies of lipid-based nanocomplexes. One of the common additives is cholesterol. Cholesterol offers an increase in the packing phospholipid molecule, the stability of liposomes, and prevention of aggregation of liposomes (Briuglia et al. 2015), and it protects nucleic acids from enzymatic degradation (Schroeder et al. 2009). Despite the wide use in nanoparticles, the optimal ratio of lipids and cholesterol has not been clearly found (Deniz et al. 2010).

Another example of the flexibility is liposomes designed for cancer. The stability of liposomes by PEGylation is very important in circulation; however, it inhibits the uptake of nanocomplexes in cells (Xu et al. 2016). Xu et al. (2016) reported that they produced PEG linked with copolymers poly(lactic-co-glycolic acid) with acid degradable amide bond, and the PEG was released by the acidity of the tumour when the liposomes approached the tumour tissues. However, uptake of the acidity-sensitive tumour lipid nanocomplexes was not significantly higher compared with normal PEGylated homologous nanocomplexes.

One of the keys for successful siRNA delivery is developing optimised lipids that obtain the balanced stability to protect nucleic acids and the ability to release nucleic acids into the cytoplasm. Further studies are required for clinical use and trials.

1.4.5. Peptide

Receptor-targeting peptides incorporated into lipid nanocomplexes are important to deliver RTNs to specific tissues and prevent unwanted gene silencing (Hart 2010). Peptide ME27 has been used for siRNA delivery to cancer cells in our group. The peptide consists of nucleic acid binding (K_{16}) and integrin-receptor-targeting sites CRGDCLG, connected by a non-cleavable spacer Glycine-Alanine (GA) (Hart 2010) and a cleavable linker RVRR (Grosse et al. 2010).

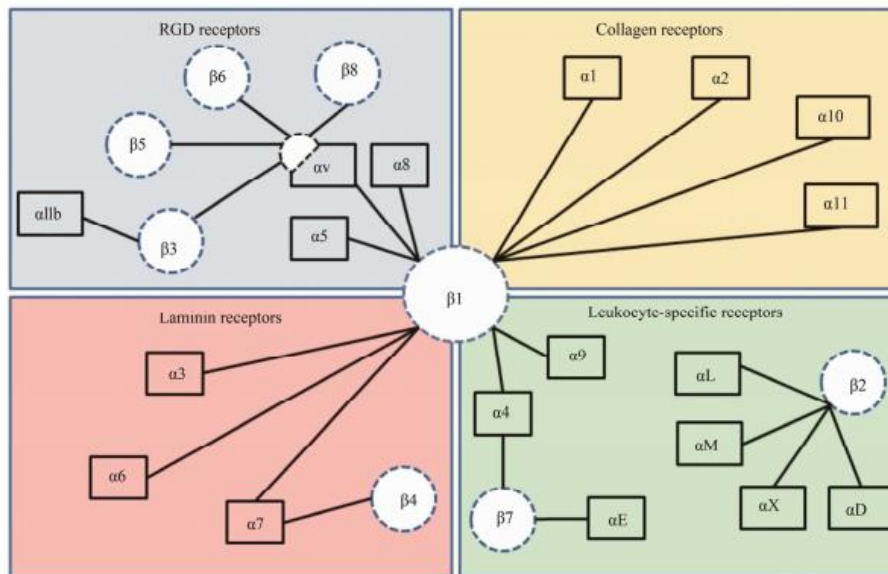


Fig. 1.11. Integrin receptor family Integrin receptors can be classified according to the ligand binding ability; $\alpha v\beta 3$, $\alpha v\beta 5$, $\alpha 5\beta 1$, $\alpha 6\beta 4$, $\alpha 4\beta 1$, and $\alpha v\beta 6$ on the tumour are associated with disease progression. Taken from Goswami (2013).

The spacer prevents interaction between liposomes and siRNA (Hart 2010), while the cleavable linker is degraded by endosomal proteinase furin and cathepsin B and helps siRNA escape from the integrin receptor, and released from PEG moiety (Grosse et al. 2010; Mustapa et al. 2009).

Peptide ME27 targets integrin receptors $\alpha 5\beta 1$, $\alpha v\beta 3$, and $\alpha v\beta 5$ (Fig. 1.11.). The integrin family of cell adhesion receptors is expressed by epithelial cells and expression of $\alpha v\beta 3$, $\alpha v\beta 5$, $\alpha 5\beta 1$, $\alpha 6\beta 4$, $\alpha 4\beta 1$, and $\alpha v\beta 6$ on the tumour is associated with disease progression. Moreover, $\alpha v\beta 3$ and $\alpha 5\beta 1$ expression levels are low or undetectable in normal adult epithelial cells (Desgrosellier & Cheresh 2010). Although integrin promotes epithelial cell adhesion to attach the extracellular matrix (ECM), especially integrin receptor $\alpha v\beta 3$, called the vitronectin receptor, and $\alpha v\beta 5$ binds vitronectin (Harmann et al. 1999) and $\alpha 5\beta 1$ is a fibronectin receptor (Schaffner et al. 2013). Integrin receptors might stimulate migration, proliferation, and survival by activating signalling pathways in tumour cells (ibid.). Young et al. (2013) mentioned that integrin subunits $\alpha 1$, $\alpha 2$, $\alpha 3$, $\alpha 4$, $\alpha 5$, $\alpha 6$, $\alpha 7$, αv , $\beta 1$, $\beta 3$, and $\beta 5$ are expressed in

NB cells. In addition, integrins are associated with survival, proliferation, and migration in NB (Young et al. 2013). Especially $\alpha_5\beta_1$, $\alpha_v\beta_3$, and $\alpha_v\beta_5$ have important role in angiogenesis in tumours (Schaffner et al. 2013). Furthermore, integrin β_1 is critical for receptor-mediated cell migration and invasion in NB cells (Lee et al. 2013).

Other receptors targeted by peptides can be used in siRNA delivery for cancer. Zhu et al. (2013) reported that they targeted the folate receptor, which can be expressed 200-fold more on cancer cells than those on normal cells. The overexpression of the receptor has been observed on several types of cancers, including ovarian cancer, endometrial cancer, and myeloid leukaemia. They delivered anti-MYCIN siRNA using the RTNs in NB in vivo, and successfully silenced more than 50% of MYCIN mRNA. Similarly, several research groups targeted glucose receptors for gene/drug delivery in cancer (Calvalesi & Hargenrother 2013; Li et al. 2014; Venturelli et al. 2016).

1.4.6. Long-term storage of RTNs at -80 °C

We have also aimed to develop optimal methods to store RTNs with the original biophysical characteristics and sufficient transfection/silencing efficiencies to use the same batch of RTNs prepared in large amounts for many experiments and for transport over long distances. Various sugars, such as glucose and sucrose, have been used as cryoprotectants for freezing and lyophilisation (Date et al. 2010; *Anchordoquy* et al. 1997; Patist & Zoerb 2005) and have been reported to stabilise proteins and phospholipids (Crowe et al. 1987). In addition, Tseng et al. (2007a) stated that trehalose enhances DNA transfection efficiency using lipid/DNA nanocomplexes and reduces the cellular cytotoxicity; therefore, trehalose was chosen as a cryoprotectant in our study.

Trehalose is a non-reducing disaccharide and naturally exists in certain cells of plants and insects. It has been studied for more than one hundred years (Ohtake & Wang 2011). It is

widely used in food, cosmetics, and pharmaceutical industries because of its water-retention capability, the ability to increase vegetable cell viability and stabilise lipids, and relatively high glass transition temperature (Patist & Zoerb 2005; Jain & Roy 2009; Richards et al. 2002). It is also known as a cryoprotectant. *Anchordoquy et al. (1997)* reported that trehalose maintains transfection efficiency and biophysical characteristics of freeze-dried lipid/DNA nanocomplexes after re-suspension in water. Similarly, *Ball et al. (2017)* mentioned that trehalose can protect lipid nanocomplexes containing anti-luciferase siRNA and improve the silencing efficiency. *Yadava et al. (2008)* showed that the lyophilisation process did not change siRNA's biological activity packaged by cationic lipid nanocomplexes.

1.5. Aim and Hypothesis

Our hypothesis is that reduction of the MYCN mRNA expression level, mediated by anti-MYCN siRNA (siMYCN) transfection, triggers apoptosis and differentiation in NB cells because MYCN overexpression in MYCN-amplified NB directly or indirectly induces proliferation and cell growth, and suppresses apoptosis and differentiation. Therefore, differentiation and apoptosis induced by MYCN mRNA reduction can be observed in different assays, such as the cell morphology and biological marker of differentiation and apoptosis as downstream effects. In addition, RTNs deliver siMYCN only into targeted NB tumour cells *in vivo* because of the receptor-targeting peptides and the EPR effects. Even though siMYCN was delivered in non-targeted tissues, MYCN is expressed in limited tissues and for a certain period; therefore, serious unwanted silencing would not be caused.

In addition, in the study of long-term storage of RTNs, trehalose can preserve the biophysical characters and the transfection and silencing efficiency of RTNs at -80 °C.

The aims of this study are:

1. To investigate the ability of siMYCN to silence MYCN at both mRNA and protein level and investigate the downstream effects induced by siRNA-mediated MYCN reduction.
2. To attempt MYCN silencing using siMYCN-containing RTNs *in vivo*.
3. To assess the ability of trehalose to maintain the biophysical characteristics and function of RTNs stored at -80 °C.

CHAPTER 2

Materials and Methods

2. Materials and Methods

2.1. Materials

2.1.1. Equipment

Name	Supplier
ABI PRISM 7000 Sequence Detection	Applied Biosystems, Life Technologies
Bio-Rad 96 CFX	Bio-Rad
Canon Rebel XS DS126191 Digital Camera	Canon
CyAn	Beckman Coulter
FACS Calibur	BD Biosciences
FLUOstar Optima	BMG Labtech
Hamamatsu Orca R2 monochrome camera	Hamamatsu Photonics
IVIS Lumina Series III imaging system	PerkinElmer
Leica upright fluorescence	Leica DFC310 FX
NanoDrop ND-1000 Spectrophotometer	Thermo Scientific Scientific
Olympus IX70 microscope	Olympus
Precellys 24 Bead Mill Homogeniser	Bertin Technologies
UVChemi	U V Chemistry Co
Zeiss Axiovert 135 live imaging scope	Zeiss
Zetasizer Nano ZS	Malvern

2.1.2. Kits and Reagents

Name	Supplier
0.05% Trypsin-EDTA	Gibco, Thermo Fisher Scientific
10x PCR buffer	Applied Biosystems, Thermo Fisher Scientific
1M HEPES solution	Fisher Scientific
20x NuPAGE MOPS SDS buffer	Invitrogen, Thermo Fisher Scientific
5x Bradford protein assay reagent	Bio-Rad
5x Reporter Lysis buffer	Promega

Bio-Rad ECL Western Blotting Substrate	Bio-Rad
BlockIt (Alexa Fluor 555)	Invitrogen, Thermo Fisher Scientific
Bovine Serum Albumin (BSA)	Sigma-Aldrich
Cell Counting Kit-8	Sigma-Aldrich
CellTiter 96 Aqueous One Solution Cell Proliferation Assay	Promega
D-(+)-trehalose dihydrate	Sigma-Aldrich
DMEM+GlutaMAX (Dulbecco's modified eagle media)	Gibco, Thermo Fisher Scientific
dNTPs	Thermo scientific, Thermo Fisher Scientific
Foetal Bovine Serum (FBS)	Sigma-Aldrich
Heparin	Sigma-Aldrich
L-glutamine (100x)	Gibco, Thermo Fisher Scientific
Lipofectamine 2000	Invitrogen, Thermo Fisher Scientific
Lipofectamine RNAiMAX	Invitrogen, Thermo Fisher Scientific
Luciferase Assay System	Promega
Matrigel Matrix Basement Membrane Matrix	Corning
MgCl ₂	Applied Biosystems, Thermo Fisher Scientific
Minimum Essential Medium Eagle (MEME)	Sigma-Aldrich
MuLV (Moloney Murine Leukemia Virus) Reverse Transcriptase (200U/μL)	Applied Biosystems, Thermo Fisher Scientific
Non-Essential Amino Acids (NEAA) (100x)	Gibco, Thermo Fisher Scientific
NP40 Cell Extraction Buffer	Invitrogen, Thermo Fisher Scientific
NuPAGE 4-12% Bis-Tris Nupage gel	Invitrogen, Thermo Fisher Scientific
NuPAGE 4x loading dye buffer (for SDS PAGE)	Invitrogen, Thermo Fisher Scientific
OptiMEM+GlutaMAX	Gibco, Thermo Fisher Scientific
Penicillin/Streptomycin (P/S) (10000U/mL) (100x)	Gibco, Thermo Fisher Scientific
Phenylmethanesulfonyl Fluoride	Sigma-Aldrich
Phosphate-Buffered Saline (PBS)	Gibco, Thermo Fisher Scientific
Pierce Protein assay BCA kit	Thermo Fisher Scientific
Platinum qPCR SuperMix-UDG with ROX	Invitrogen, Thermo Fisher Scientific
Polyvinylidene Difluoride (PVDF) Membranes	Millipore
ProLong® Gold antifade mountant	Thermo Fisher Scientific

Propidium Iodide (PI)	Sigma-Aldrich
Protease Inhibitor cocktail (100x)	Sigma-Aldrich
Qiagen RNeasy mini kit	Qiagen
QIASHredder	Qiagen
Quant-iT PicoGreen dsDNA Assay Kit	Invitrogen, Thermo Fisher Scientific
Random Hexamer Primers	Applied Biosystems, Thermo Fisher Scientific
RNase Inhibitor	Applied Biosystems, Thermo Fisher Scientific
RNase/DNase-free distilled water	Gibco, Thermo Fisher Scientific
RPMI1640+GlutaMAX	Gibco, Thermo Fisher Scientific
SensiFAST Probe Hi-ROX one-step kit	BIOLINE
Sodium Pyruvate (100x)	Gibco, Thermo Fisher Scientific
β -Mercaptoethanol	Sigma-Aldrich

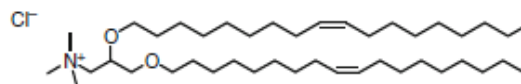
2.1.3. Lipids

Name		Supplier
DOPE	1,2-dioleoyl-sn-glycero-3-phosphoethanolamine	Avanti Polar Lipids
DOPG	1,2-dioleoyl-sn-glycero-3-phospho-(1'-rac-glycerol)	Avanti Polar Lipids
DOTMA	1,2-di-O-octadecenyl-3-trimethylammonium propane	Avanti Polar Lipids
DOPE-PEG2000	1,2-dioleoyl-sn-glycero-3-phosphoethanolamine-N-[methoxy(polyethylene glycol)-2000]	Avanti Polar Lipids
DPPE-PEG2000	1,2-dipalmitoyl-sn-glycero-3-phosphoethanolamine - N-[methoxy(polyethylene glycol)-2000]	Avanti Polar Lipids

2.1.3.1. Structure of lipid

DOTMA (C18)

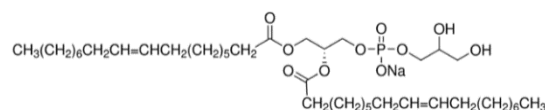
1,2-Di-((Z)-octadec-9-enyloxy)-N,N,N-trimethylammonium propane chloride



Cationic (Hart 2010)

DOPG

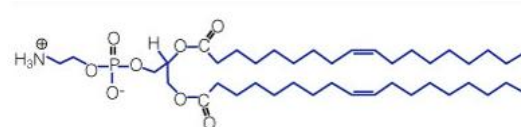
1,2-Dioleoyl-*sn*-glycero-3-phospho-*rac*-(1-glycerol) sodium salt



Anionic (Sigma-Aldrich homepage)

DOPE

1,2-Dioleoyl-*sn*-glycero-3-phosphoethanolamine



Neutral (Promega homepage)

2.1.3.2. Composition of Lipid nanoparticle

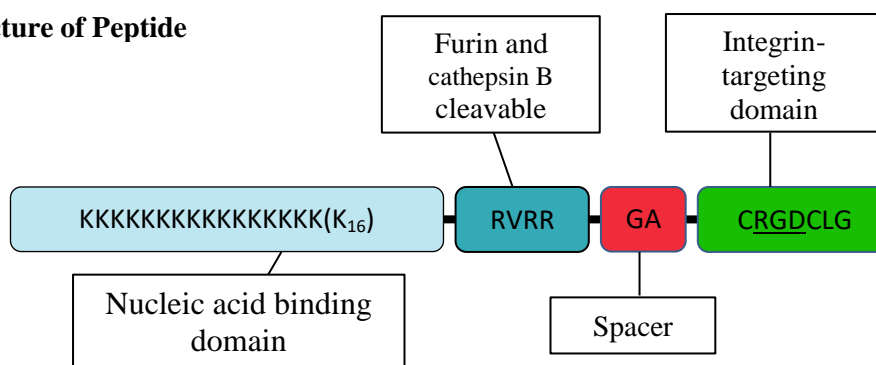
LIPOSOME NAME	Lipid1	Lipid 2	Lipid 3	Polarity
DOTMA:DOPE(DD)	DOTMA (50.0%)	DOPE(50.0%)	-	Cationic
GK25	DOPG (47.5%)	DOPE (47.5%)	DOPE-PEG2000 (5%)	Anionic
AT1	DOTMA (49.5%)	DOPE (49.5%)	DPPE-PEG2000 (1%)	Cationic
AT3	DOPG (49.5%)	DOPE (49.5%)	DPPE-PEG2000 (1%)	Anionic

2.1.4. Peptides

Name	Composition	Supplier
ME27	K ₁₆ RVRRGACRGDCLG	China Peptides Co.

ME72	K ₁₆ RVRRGA <u>CR</u> GECLG	China Peptides Co.
K ₁₆	KKKKKKKKKKKKKKKKKK(K ₁₆)	China Peptides Co.

2.1.4.2. Structure of Peptide



2.1.5. siRNAs

Name	Sequence	Supplier
siMYCN3	Sense 5'-CAGCAGUUGC UAAAGAAAAUU-3' Antisense 5'-UUUUCUUUAGCAACUGCUGUU-3'	Dharmacon, GE Healthcare
siNCYM*	Sense 5'-UGGCAAUUGC UUGUCAU UAAAAUU-3' Antisense 5'-UUUAAUGACAAGCAAUUGCCAUU-3'	Dharmacon, GE Healthcare
Silencer GAPDH	Sense: 5'-GGUCAUCCAUGACAACUUUTT-3' Antisense 5'-AAAAAGUUGUCAUGGAUGACC-3'	Invitrogen, Thermo Fisher Scientific
Silencer Firefly Luciferase (GL2+GL3)	Proprietary sequence	Invitrogen, Thermo Fisher Scientific
siMYCN	Sense 5'-CGGAGAUGCUGCUUGAGAA-3', Antisense 5'-UUCUCAAGCAGCAUCUCCG-3',	Dharmacon, GE Healthcare
siMYCN2	Sense 5'-CGGAGUUGGUAAAGAAUGA-3' Antisense 5'-UCAUUCUUUACCAACUCCG-3'	Dharmacon, GE Healthcare
siNeg (non-targeting pool)	Proprietary sequence Catalogue # D-001810-10-50 ON-TARGET plus	Dharmacon, GE Healthcare
Dy677 control siRNA	Proprietary sequence	Dharmacon, GE Healthcare
FAM-labelled control siRNA	Proprietary sequence	Invitrogen, Thermo Fisher Scientific

*siNCYM was designed on the basis of the anti-NCYM shRNA in Suenaga et al. (2014)

siMYCN and siNCYM were custom siRNAs of ON-TARGET plus (Dharmacon, GE Helthcare)

2.1.6. Taqman Assays (FAM-labelled probes) (Applied Biosystems, Thermo Fisher Scientific)

Name	Catalogue #
Human ACTB	Hs01060665_g1
Human MYCN	Hs00232074_m1
Human MDM2	Hs01066930_m1
Human GAPDH	Hs02758991_g1
Human MYCNOS (NCYM)	Hs01032821_m1
Human TP53	Hs01034249_m1
Human NTRK1	Hs01021011_m1
Mouse ACTB	Mm02619580_g1
Mouse GAPDH	Mm99999915_g1

2.1.7. Primary antibodies for immunoblotting

Name	Supplier	Catalogue #	Dilution
Anti-MYCN B8.4.B	Santa Cruz	sc-53993	1:1000 or 1:10000*
β -Actin (AC-74)	Sigma-Aldrich	A2228-100 μ L	1:10000
Pan Trk (B-3)	Santa Cruz	sc-7268	1:2000*-5000*
Pan Trk (C-15) (Discontinued)	Santa Cruz	sc-139	1:1000

For secondary antibody, Horseradish peroxidase-conjugated (HRP-conjugated) secondary antibody (Dako, Agilent Technologies) (1:10000) was used. * shows the dilution for membranes transferred using Bio-Rad transfer system.

2.1.8. Complete culture media

Cell lines	Composition
Kelly, SK-N-BE(2)	RPMI1640+GlutaMAX, 10% FBS, 25 mM HEPES, 100 U/mL P/S (optional)
LAN5, SK-N-SH	MEM, 10% FBS, 2mM L-Glutamine, 100 U/mL P/S (optional)
Neuro-2A	DMEM+GlutaMAX, 10% FBS, 1 mM Sodium Pyruvate, NEAA, 100 U/mL P/S (optional)

2.1.9. Recipes

Name	Composition
TE buffer	10 mM Tris-HCl pH8, 1mM EDTA
TBST	50 mM Tris-HCl pH 7.5, 150 mM NaCl, 0.2% Tween-20
Phosphate-citrate buffer (washing buffer of fixed cells)	0.2 M Na ₂ HPO ₄ :0.1 M Citric acid pH 7.8=192:8
PI solution	50 µg/ml Propidium iodide in PBS
Stripping buffer	0.2 M NaOH in water

2.2. Methods

2.2.1. Cell culture

Human MYCN-amplified NB cell lines: Kelly, LAN-5, SK-N-BE(2), non MYCN-amplified cell line SK-N-SH, and murine neuroblastoma cell line Neuro-2A were used in this study. Kelly and SK-N-BE(2) were cultured in RPMI1640+GlutaMAX with 10% FBS, 25 mM HEPES buffer and 100 U/mL P/S. LAN-5 and SK-N-SH cells were cultured in MEM with 10% FBS, 2mM L-glutamine and 100 U/mL P/S. Neuro-2A was in DMEM+GlutaMAX supplemented with 10% FBS, 100 U/mL P/S, 1mM sodium pyruvate and NEAA. Recipes of all media used are shown in Section 2.1.8. Media in flasks were changed every 2-3 days.

Cells were passaged when they were 70-80% confluent. Cells were washed with PBS once, and 0.05% trypsin-EDTA was added. Cells were incubated in an incubator at 37 °C in 5% CO₂ for 5 minutes. After cells were detached, trypsin was neutralised by adding complete media. Cells were centrifuged at 1200 rpm for 5 minutes and one tenth of cells were transferred into a new flask with complete media. All cells were incubated in a mycoplasma free incubator at 37 °C in 5% CO₂.

2.2.2. Receptor targeting nanocomplexes (RTNs)

RTN formulations consisted of lipids, peptide and siRNA/pDNA at various ratios depending on the type of liposome employed as shown in Table 2.2.1. The ratios have been previously optimised for anionic formulations as described in Tagalakis et al. (2011) and for anionic formulations in Tagalakis et al. (2014) while the manuscript describing optimisation of the mixing ratio of the double layered nanocomplex, LPRL3, is in preparation. We used lipids/peptide/DNA or siRNA (LPD or LPR) and double layered RTNs, cationic lipid/peptide/ siRNA (or DNA) covered with anionic lipid (LPR(or D)L). The LPR formulation is binding siRNA with the peptide and enveloped within the bilayer liposome.

On the other hand, the LPRL3 formulation is DD/ME27/siRNA (cationic RTN) covered with anionic lipid AT3. The ratios of cationic and anionic liposomes used in this study (shown in

Table. 2.2.1. Weight ratio of each RTN

Name	Ratio (weight)
DD/P/siRNA or DNA	1:4:1
AT1/P/siRNA or DNA	1:4:1
GK25/ME27, ME72 or Y/siRNA or DNA	19:2.7:1
GK25/K16/siRNA or DNA	19:3:1
AT3/ME27, ME72 or Y/siRNA or DNA	20:2.7:1
AT3/K16/siRNA or DNA	20:3:1
LPRL3(DD/ME27/siRNA/AT3)	0.75:3:1:19

Section 2.1.3.2), were investigated in order to optimise RTN transfection efficiency. DD is cationic non-PEGylated liposome. AT1 are cationic PEGylated liposomes, while GK25 and AT3 are PEGylated anionic liposomes. Four peptides were screened, and ME27 was chosen as the optimal peptide for transfections for neuroblastoma cells (data not shown). The cationic peptide ME27 targets integrin receptors while ME72 and K16 were used as negative control peptides (non-targeting). 250 ng pDNA packaged within RTNs in 200 μ L OptiMEM was added to cells per well in 96 well plates. 75 or 100 nM siRNA were added onto the cells per well. siRNA transfections were normally performed in 12 well plates or 24 well plates and the final volumes were 1000 μ L and 500 μ L, respectively.

OptiMEM is widely used for siRNA transfections (Zhao et al. 2008) and the use of OptiMEM is recommended by the company protocol of RNAiMAX. We used OptiMEM in all preparations of transfections because cationic, non-PEGylated RTNs aggregate in serum-containing media (Grosse et al. 2010), while cells can survive in OptiMEM.

To prepare cationic RTNs, liposome, peptide and nucleic acid were mixed (total 200 μ L), and were incubated for 30 minutes at RT. For anionic RTNs, peptide and nucleic acid were mixed first and were incubated for 15 minutes. Anionic liposome was then added into the mixture and they were incubated for 30 minutes at RT. For LPR(D)L3, DD, peptide and nucleic acid were mixed and incubated for 30 minutes at RT. AT3 was then mixed with them and they were incubated for 20 minutes at RT. All RTNs were prepared in 200 μ L OptiMEM and were diluted with OptiMEM to appropriate volume after incubation.

Tagalakis et al. (2014) showed that the order of mixing liposome, peptide and siRNA affects the percentage of siRNA packaging in anionic RTNs. Mixing in the order PRL (peptide and siRNA are mixed first, and then liposome is added) achieved better packaging than LRP (liposome and siRNA are mixed, and then peptide is added). Therefore, all the anionic formulations were made with the PRL method of mixing.

2.2.3. Luciferase plasmid DNA transfection

Luciferase pDNA (Grosse et al. 2010) transfections were performed as described in Tagalakis et al. (2011). Cells were seeded at 2.5×10^4 cells for human NB cell lines or at 2.0×10^4 cells for Neuro-2A cells per well in 96 well plates in complete media without P/S, and were incubated overnight in an incubator at 37 °C in 5% CO₂. The confluency reached 60-70% the next day. The weight ratio of each formulation is shown in Table 2.2.1 while all RTNs were prepared in OptiMEM with 250 ng Luciferase pDNA (pCI-Luc, GL2+GL3) mixed with lipids and peptide added to cells per well in 96-well plates. DNA transfections were performed in 5 or 6 repeats per condition.

For example, for 6 wells of DNA transfection using a cationic formulation in 96 well plates, 250x8 ng liposome, 1000x8 ng peptide and 250x8 ng pDNA were prepared in 60 µL, 80 µL and 60 µL OptiMEM respectively. They were mixed in 15 mL tube and were incubated for 30 minutes. Then 1400 µL OptiMEM were added in the RTN and 200 µL of the RTN was aliquoted into 6 wells.

After the formation of RTNs, they were diluted with OptiMEM in order to aliquot 200 µL per well in 96 well plates. As a positive control, 250 ng pDNA were mixed with 1µL Lipofectamine 2000 (L2K) in OptiMEM (4:1=L2K:DNA weight ratio). After more than 10 minutes incubation, each formulation was topped up to 200 µL with OptiMEM. All nanocomplexes were centrifuged at 1500 rpm for 5 minutes immediately after they added onto cells. The centrifuge step increases transfection efficiency as described in Grosse et al. (2010) and cellular uptake efficiencies of RTNs with or without centrifuge is described in section 4.4.7. in Chapter 4. After 4 or 24 hour incubation in the cell culture incubator, cells were centrifuged at 1500 rpm and for 5 minutes, and then, OptiMEM was replaced with complete culture media. The cells were incubated for 24 hours after transfection in an incubator at 37 °C in 5% CO₂, and were harvested to assess transfection efficiency.

2.2.4. siRNA transfection

siRNA transfections were prepared as described in Tagalakis et al. in (2011) and Tagalakis et al (2014). Cells were seeded at 5×10^4 cells for human NB cell lines or at 3.0×10^4 cells for Neuro-2A cells per well in 24 well plates in complete media without P/S. For 12 well plates, cells were seeded at 1.6×10^5 cells for human NB cell lines or at 1.0×10^5 cells for Neuro-2A cells per well. Cells were incubated overnight in an incubator at 37 °C in 5% CO₂. The confluency reached 30-50% the next day. 75 or 100 nM siRNA was mixed with lipids and peptide in 500µL OptiMEM per well for a 24 well plate or 1000 µL for a 12 well plate. siRNA transfections were performed in duplicate

We used the commercially available lipid-based reagent Lipofectamine RNAiMAX, according to the supplier's instruction. RNAiMAX was mixed with 10 µM siRNA at a 1:1 volume ratio. RNAiMAX and siRNA were mixed in OptiMEM and incubated for more than 10 minutes and were added to cells in complete culture media at 10 nM.

RNAiMAX was also used in order to confirm MYCN siRNA silencing ability in Chapter 3, and the final concentration of the siRNA was 5, 10, 20 and 50 nM. RNAiMAX was mixed with the same volume of 10 µM siRNA. For example, 10 µL of 10 µM siRNA was mixed with 10 µL RNAiMAX. As soon as nanocomplexes were added onto cells, they were centrifuged at 1500 rpm for 5 minutes and were incubated for 4 hours in an incubator at 37 °C in 5% CO₂. RTNs in OptiMEM were replaced with complete media at 4 or 24 hours after centrifuge at 1500 rpm for 5 minutes. The cells were incubated for 48 hours and were harvested for subsequent analysis.

2.2.5. Biophysical characterisation of RTNs

Size and charge (zeta potential) of liposomes and nanocomplexes were measured by Zetasizer nano ZS (Malvern). The Zetasizer measures size using dynamic light scattering,

which measures the diffusion of nanoparticles under the Brownian motion. The software converts the data of the diffusion to the size and the size distribution using the Stokes-Einstein equation (Zetasizer nano series user manual 2009). Charge was measured by Laser Doppler micro-electrophoresis. The device applies electric field to the solution of nanoparticles, and they move with a velocity related to their zeta potential. The velocity is measured by light scattering. The measurement required minimum 1-2 μg DNA/RNA per sample. All the size and zeta potential were measured three times at RT.

All nanocomplexes were prepared in water (RNase and DNase free) at RT because it was shown by previous study that cationic non-PEGylated RTNs were aggregated in PBS (Grosse et al. 2010). RTNs were prepared in small volume of water (less than 50 μL) and were topped up to 900-950 μL with water just before the size and zeta potential were measured. The diluted RTNs were transferred into a cuvette for measurement. Biophysical characterisation of RTNs in trehalose is described in section 2.2.22.

2.2.6. Total RNA extraction

Total RNA was extracted using RNeasy mini kit. A silica-based membrane of the column in this kit can selectively bind RNA suspended in a guanidine thiocyanate containing high-salt buffer (RLT buffer) mixed with ethanol after cells were lysed in the buffer (Tan & Yiap 2009; Chirgwin et al. 1979). After the membrane was washed to remove the salt in the membrane, RNA was eluted with RNase-free water.

Total RNA was extracted according to the supplier's instruction (Qiagen). RLT buffer was freshly supplemented with β -mercaptoethanol (100:1 volume ratio= RLT buffer: β -mercaptoethanol) before used. 350 μL RLT buffer per well in 24 well plates were used. Cell lysates were passed through the QIASHredder column (optional step for *in vitro*) before addition to the RNeasey mini kit column. 70% Ethanol was added into cell lysates at 1:1

volume ratio. After the cell lysate had passed through the column, the membrane was washed with 700 μL RW1 wash buffer, and was centrifuged at 13000 rpm for 1 minute. Then they were washed with 500 μL RPE wash buffer, and were centrifuged at 13000 rpm for 1 minute. Washing with RPE buffer was repeated. To dry the membrane, the spin column was centrifuged at 13000 rpm for 1 minute. 30 μL RNase-free water was dropped directly on the membrane in the column, and it was centrifuged at 13000 rpm for 1 minute to elute total RNA. The concentration of RNA was quantified by measuring OD_{260} with the NP1000 software of Nanodrop. Samples with 260/280: 1.9-2.1 were regarded as having sufficient quality RNA.

2.2.7. Quantitative real-time PCR (qRT-PCR)

qRT-PCR was performed as previously described in Bustin & Nolan (2004) .

Two-step qRT-PCR: For complementary DNA (cDNA) synthesis, 0.1-1 μg total RNA was mixed with 0.8 μL 2 mM dNTPs and 1 μL 50 μM Random Hexamers, and the total volume of each sample was prepared to 12 μL . It was incubated at 70 $^{\circ}\text{C}$ for 10 minutes, and chilled to 4 $^{\circ}\text{C}$. Then it was mixed with 2 μL 10xPCR buffer, 4 μL 25 mM MgCl_2 , 1 μL MuLV reverse transcriptase (200 U/ μL) and 1 μL RNase inhibitor (20 U/ μL). The sample was incubated at 42 $^{\circ}\text{C}$ for 90 minutes, at 80 $^{\circ}\text{C}$ for 5 minutes and cooled at 4 $^{\circ}\text{C}$. qRT-PCR was performed with 1 μL MYCN TaqMan assay (primer/probe mix) or GAPDH assay in 10 μL 2x Platinum qPCR superMix-UDG with ROX. The sample was topped up to 20 μL with water. The cDNA was diluted 1 in 5 with water. MYCN mRNA expression level (or GAPDH mRNA expression level) was normalised using the housekeeping gene ActB. The qRT-PCR conditions were as follows: 50 $^{\circ}\text{C}$ heating for 2 minutes and then at 95 $^{\circ}\text{C}$ for 10 minutes for activation, followed by 40 repeats of the PCR cycle: 95 $^{\circ}\text{C}$ for 15 seconds and 60 $^{\circ}\text{C}$ for 1 minute in the ABI prism or Bio-Rad 96 CFX .

One-step qRT-PCR: 10-50 ng total RNA were mixed with 1 μ L TaqMan assay, 10 μ L 2x qPCR master mix, 0.2 μ L reverse transcriptase and 0.4 μ L RNase Inhibitor (all from the SensiFAST Probe Hi-ROX one-step kit). The qRT-PCR reactions were preheated at 45 °C for 20 minutes and then at 96 °C for 2 minutes, followed by 40 cycles of 95 °C for 10 seconds and at 60 °C for 30 seconds. The cycles were performed in the Bio-Rad 96 CFX. Ct values were obtained on ABI 7000 software or Bio-Rad CFX manager, respectively. The silencing efficiency was calculated using Microsoft Excel using the Delta-Delta Ct analysis.

2.2.8. Statistical Analysis

The error bars are expressed as the mean \pm standard deviation and results were analysed using a two-tailed, unpaired Student t-test unless mentioned otherwise (in those cases one-way ANOVA was performed). Probability values $p < 0.05$ were indicated as *, $p < 0.01$ were indicated as ** and $p < 0.001$ were indicated as ***.

2.2.9. Sub G1 Assay

Sub G1 assay using PI staining was used as described in Riccardi & Nicoletti (2006). Sub G1 assay Cells were seeded at 1.6×10^5 cells per well in the wells of a 12 well plate, and were incubated overnight. The cells were transfected and the transfection media was changed to complete culture media 4 hours after transfection as normal. After 48 hour incubation, media were collected into FACS tubes, and cells were harvested from plates using 0.05% trypsin-EDTA. Cells were neutralised with PBS, and they were transferred to the same FACS tube where the media were collected. They were centrifuged at 1500 rpm for 5 minutes at RT. Supernatant were discarded by decantation. Cell pellets were vortexed and 500 μ L 70% Ethanol were added drop-wise into the tubes. Cells were incubated on ice for 30 minutes, and were centrifuged at 3000 rpm for 5 minutes at RT. 70% ethanol was removed and the pellets were reduced to smaller cell clusters. 1 mL Phosphate-citrate buffer was added, and

cells were centrifuged at 3000 rpm for 5 minutes at RT. The supernatant was removed, and 50 μ L RNase solution and 250 μ L PI solution were added into the cells and the cells were incubated for 15 minutes. Percentages of PI negative cells were measured using a flow cytometer (CyAn or Calibur). The data were analysed using the Flow Jo VX32 software (FlowJo, LCC).

2.2.10. Measurement of neurite length and cell area

The quantification of neurite outgrowth was carried out as described in Clark et al. (2013). SK-N-BE(2) cells were seeded at 5×10^4 cells per well in 12 well plates, and were incubated at 37 °C in 5% CO₂ in an incubator. Anti-MYCN siRNA was transfected with Lipofectamine RNAiMAX at 50, 20, 10 and 5 nM final concentration in a total volume of 1000 μ L complete media. The cells were observed for 6 days. The media was changed to fresh complete media at day 4. Cell images were taken under bright field using a microscope Olympus IX70 with a Canon DS126191 camera attached at day 2 and day 6. 5 images were chosen randomly from each condition.

The data were analysed using software Fiji ImageJ. For measurement of neurite length, extended neurites were defined as longer than the cell itself. Neurites were traced using Straight>Freehand Line function and the lengths were measured in pixels. A macro was created to run interpolate (Edit>Selection>Interpolate), interval=10, smooth in order to smooth and accurate the freehand line. The macro was run every time when a freehand line was drawn. Cell area was measured using the polygon selections function.

2.2.11. Proliferation assay (CCK-8 assay)

This experiment was performed as described in Ishiyama et al. (1997). CCK-8 assay reagent is highly water-soluble tetrazolium salt: WST-8 [2-(2-methoxy-4-nitrophenyl)-3-(4-nitrophenyl)-5-(2,4-disulfophenyl)-2H-tetrazolium, monosodium salt]. A water-soluble

formazan dye (orange) is produced upon reduction in the presence of an electron mediator from WST-8 (colourless). The reduction is occurred when NAD^+ change to NADH, which are coenzymes found in living cells (Blacker et al. 2014), by dehydrogenases in cells. The number of living cells is indicated by the amount of the formazan dye generated by dehydrogenases in cells.

Cells were seeded in a 96 well plate at 6×10^3 in 200 μL complete media per well and incubated overnight. 10 μM siRNA were mixed with the same volume of RNAiMAX, and incubated for 10 minutes. They were prepared at 20 μL and at 20, 10 or 5 nM final concentration, and added into the well. Transfected cells were incubated in an incubator under 5% CO_2 at 37 $^\circ\text{C}$. 10 μL CCKt-8 reagent were added into each well ($n=3$), and incubated for 3.5 hours. The intensity at 450 nm was measured using the FLUOstar Optima plate reader.

2.2.12. Cell Viability assay

The CellTiter 96® AQueous One Solution Reagent is a tetrazolium compound [3-(4,5-dimethylthiazol-2-yl)-5-(3-carboxymethoxyphenyl)-2-(4-sulfophenyl)-2H-tetrazolium, inner salt; MTS(a)] and an electron coupling reagent (phenazine ethosulfate; PES). PES is stably combined with MTS. The MTS tetrazolium compound (Owen's reagent) is reduced by cells into a coloured formazan product. It is likely that this conversion is carried out by NADPH or NADH produced by dehydrogenase enzymes in metabolically active cells (Berridge & Tan 1993). The number of living cells is determined by the amount of the formazan dye generated by dehydrogenases in cells.

Cells were seeded at 1.5×10^4 cells per well in 96 well plates, and were incubated in an incubator under 5% CO_2 at 37 $^\circ\text{C}$ overnight. Cells were transfected with siMYCN and siNeg in replications of six. 4 hours after transfection, complete culture media was added following

the removal of transfection media. 24 hour after transfection, media were changed, and MTS reagent (CellTiter 96 Aqueous One Solution Cell Proliferation Assay) was added into each well as described in Nabatiyan & Krude (2004). Cells were incubated for 2 hours at 37 °C. The absorbance at 492 nm was measured using the FLUOstar Optima plate reader.

2.2.13. Immunoblotting

Approximately 10 µg total proteins was separated by sodium dodecyl sulfate polyacrylamide gel electrophoresis (SDS-PAGE) as described in Towbin et al. (1979) and Bunette (1981). Cells were harvested at 48 hours after transfections. Cells were washed with cold PBS twice, and were re-suspended with cold NP40 Cell Extraction Buffer supplemented with 1 mM Phenylmethanesulfonyl fluoride and 1x Protease Inhibitor cocktail. The cells were vortexed every 10 minutes and were incubated on ice for 30 minutes. The mixture was centrifuged at 13000 rpm for 15 minutes at 4 °C and the supernatant was transferred into new tubes. The concentration of protein lysates were quantified using the BCA kit. Up to 10 µg of total proteins was mixed with 4x loading dye buffer supplemented with 10x DDT. The sample was boiled at 100 °C for 5 minutes. The sample was then electrophoresed on 4-12% Bis-Tris Nupage gel in MOPS buffer at 150 V for 1 hour. The protein bands on the gel were transferred to PVDF membranes at 30 V for 1 hour. Alternatively, the transfer was conducted in Bio-Rad transfer tank at 100 V for 1-1.5 hours. PVDF membranes were blocked with 5% or 10% dried milk in TBST for 1 hour. They were then probed and incubated with anti-MYCN antibody overnight. For anti-β-Actin antibody, the incubation time was 1 hour. The concentration of each antibody used in this study is described in Section 2.1.7. They were gently shaken and washed three times with TBST, each wash for 10 minutes. Then, the membranes were incubated in the secondary antibody diluted with TBST or 10% dried milk buffer. They were washed three times with TBST again, and the protein bands were detected using the ECL chemiluminescence-based detection kit (Bio

Rad), and the bands were visualised in the UVChemi chemiluminescence detection apparatus.

2.2.14. Stripping immunoblotting membranes

Probed PVDF (immunoblotting) membranes were striped before they were probed with other primary antibodies. Immunoblotting membranes were washed with distilled H₂O gently on a shaker for 10 minutes twice. The membranes were incubated in pre-warmed 0.2 M NaOH at 37°C for 20 minutes. Membranes in 0.2 M NaOH were gently stirred on a shaker for 10 minutes. Then membranes were then stirred in TBST buffer for 10 minutes. Membranes were blocked in 5 or 10% dried milk-TBST blocking buffer for 1 hour, and were probed with a primary antibody overnight as described in 2.2.15.

2.2.15. Mass Spectrometry analysis for quantitative protein profiling

The assay was performed by personnel in the UCL Great Ormond Street Institute of Child Health proteomic laboratory. Cells transfected with siMYCN, siNCYM, siNeg and untransfected were freeze-dried, digested with trypsin and cleaned with a C18 column. Total amount of Peptides were quantified and then the samples were diluted to 100 ng/μL. 1 μL of sample was injected into a mass spectrometry instrument, and therefore, approximately 100 ng of the digested peptides were analysed. For quantification, Yeast enolase peptides were used.

2.2.16. Cellular Uptake assay

Cells were seeded at 5×10^4 cells per well in a 24 well plate, and incubated overnight. Fluorescence (AlexaFluor 555) labelled negative control siRNA, BlockIt was mixed with cationic liposome and peptide at a weight ratio of 1:4:1= lipids:peptide:siRNA or a volume ratio of 1:1 = RNAiMAX: 10 nM BlockIt as described in Tagalakis et al. in (2017) and Liu

et al. (2014). Nanocomplexes were incubated for 30 minutes at RT, and then added onto cells without complete media for RTNs or in complete media for RNAiMAX. The cells were then centrifuged at 1500 rpm for 5 minutes if it was necessary. For RTNs, the final concentration was 100 nM. 4 hour after the transfection, nanocomplexes were removed and complete media was replaced if required. The cells were incubated in an incubator at 37 °C in 5% CO₂. When the percentage of cellular uptake was measured, the cells were washed with PBS once and 100 µL of 0.05% trypsin-EDTA were added. They were incubated for 5 minutes in an incubator at 37 °C in 5% CO₂, and then they were neutralised with 400 µL complete culture media. The cells were transferred into FACS tubes. Alexa Fluor 555 positive population was measured through FL2 in FACS Calibur. Ten thousand cells were counted in each sample. The data were analysed using FlowJoVX32.

2.2.17. Heparin Dissociation assay (siRNA release assay)

0.2 µg siRNA was mixed with 1.33 µL PicoGreen (Thermo Fisher Scientific) (150 ng:1 µL ratio) in TE buffer (10 mM Tris-HCl pH 8, 1 mM EDTA) in 100 µL per well, and were incubated in the dark for 10 minutes at RT as described in Tagalakis et al. (2011). The PicoGreen-labelled siRNA was then mixed with 0.2 µg lipids and 0.4 µg peptide in TE buffer in 100 µL in a clear 96 well plate. The nanocomplexes were incubated in the dark for 30 minutes at RT. Several conditions of heparin were prepared. 100 µL Heparin in TE buffer was added in 100 µL nanocomplexes at 0.01, 0.025, 0.05, 0.075, 0.1, 0.15, 0.2, 0.25, 0.5, 0.75, 1, 2, 5 10 U/mL final concentrations and then 100 µL of TE buffer were added in each well. They were incubated in the dark for 30 minutes at RT. Then the fluorescence intensity (Excitation: 492nm, Emission 520) was measured using the FLUOstar Optima plate reader. As a negative control, 1.33µL PicoGreen was mixed with 98.66 µL TE buffer in the dark for 10 minutes at RT. It was then mixed with 100 µL TE buffer, and was incubated for 30 minutes in dark at RT. Then, 100 µL TE buffer were added, and incubated

for 30 minutes in the dark at RT. As a positive control, 0.2 µg siRNA was mixed with 1.33 µL PicoGreen, and was topped up to 100µL with TE buffer, and was incubated in the dark for 10 minutes at RT. It was incubated with 100 µL of TE buffer in the dark for 30 minutes at RT. Then, 100 µL TE buffer were added, and it was incubated for 30 minutes in the dark for 30 minutes. The fluorescence intensity was measured as above.

2.2.18. Luciferase assay

Luciferase activity was measured as described in Tagalakis et al. (2011) and de Wet et al. (1987). Cells were washed with PBS twice, and were lysed with 1x Reporter Lysis Buffer (Promega). Cells were incubate at 4 °C for 20 minutes, and then, at -80°C for 40 minutes. After cell lysates were thawed at RT, they were transferred into white 96 well plates and 50 µL Luciferase substrate was added into each well. The luminescence was measured to assess luciferase activity in transfected cells in a FLUOstar OPTIMA plate reader. The data were normalised by the protein concentration of each sample, which was measured by a Bradford protein assay, and Relative Luminescence Units per mg of protein were calculated.

2.2.19. Bradford protein assay

Protein quantification assay was performed after luciferase assay using Bradford protein assay reagent as described in Bradford (1976). 20 µL of sample (lysate + luciferase substrate) were mixed with 180 µL of 1x Bradford protein assay reagent in each well of a clear 96 well plate, and incubated at least for 5 minutes at RT. The absorbance at 595 nm was measured by the FLUOstar OPTIMA plate reader. Then total protein concentration per well was calculated using a protein curve obtained from several known concentrations of bovine serum albumin (BSA).

2.2.20. Storage of RTN in trehalose

Trehalose was prepared as 50% solution (w/v %) in water. RTNs were prepared in each tube at 0.02 µg/µL, and were suspended in 5, 8, 10 or 20% trehalose solutions. RTNs were stored at 4°C immediately. For the freezing condition, RTNs were frozen immediately in 100% ethanol with dry ice. When RTNs become solid, they were left on dry ice. They were soon transferred and kept in a freezer at -80°C for more than one hour. The RTNs were then moved at 4°C, and were stored there until they were used for transfection or biophysical characterisation.

For biophysical characterisation, 100 µL RTNs were used for measurement of the size and charge using the Zetasizer (Malvern). 100 µL RTN was mixed with 800 µL water and was transferred to a cuvette, and therefore, 2 µg of DNA or siRNA were used for the measurement. The size and zeta potential were measured three times.

For transfections, RTNs were diluted with OptiMEM to the appropriate concentration, and were added onto cells. Cells were centrifuged at 1500 rpm for 5 minutes and were incubated in an incubator at 37 °C in 5% CO₂. 4 hour after transfections, OptiMEM was replaced with complete media. Cells were harvested at 24 hours for luciferase pDNA transfection or at 48 hours for siRNA transfection analyses.

2.2.21. Xenografts in mice as a neuroblastoma *in vivo* model

Cultured cells were trypsinised (0.05% trypsin-EDTA), and were incubated in an incubator for 5 minutes. Cells were re-suspended in media without FBS and supplements to inactivate trypsin, and were centrifuged at 1200 rpm for 5 minutes. After the supernatant was removed, cells were re-suspended in media without FBS and supplements and centrifuged again. Cells (Kelly or SK-N-BE(2)) were re-suspended in small volume of media as above, and were

passed through a 40 µm cell strainer. The cell number was then counted, and the cells were prepared at 3×10^6 cells in 100 µL per mouse as previously described in Tagalakis et al. (2017). 100 µL matrigel kept on wet ice were mixed with the cells with tips that were kept at 4 °C overnight. Tips should be cold because matrigel can be liquid at 4 °C. Cells were kept on ice till the instillation. 3×10^6 cells in 200 µL were then injected subcutaneously into female NOD-SCID gamma (NSG) mice, 6 to 8 week old (Charles River, Margate, UK). The tumour size was checked over the skin every two days. Treatment was performed when the tumour size reached at approximately 5x6 mm.

2.2.22. RTN transfection *in vivo*

Neuroblastoma mouse model was prepared (3 mice per condition) as described in 2.2.23. RTNs were prepared as described in Section 2.2.2. 25 µg siRNA packaged within RTNs were prepared in 100 µL containing 5% dextrose per mouse as described in Tagalakis et al. (2017). RTNs were injected into the mice intravenously. After 48 hours, NB tumours were extracted and frozen till the appropriate assay. The tumour was thawed in the RTL buffer and homogenised using the bead mill homogeniser Precellys 24. Then, total RNA was extracted as usual (Section 2.2.6).

2.2.23. Biodistribution of RTN

Neuroblastoma mouse model was prepared as described in 2.2.23. 0.5 mg/kg siRNA-Dy677 packaged with AT1 and ME27 were intravenously injected into NSG mice developing a tumour (Kelly) (n=3 per each condition) as described in Tagalakis et al. (2017). 4 hours after injection, tumours and organs (kidneys, spleen, heart, liver, and lung) were taken from the mice and imaged using an IVIS Lumina Series III imaging system. The images were processed using the Living Image software (PerkinElnmer).

2.2.24. Tumour uptake image in histology

Neuroblastoma mouse model was prepared as described in 2.2.23 (n=6 for the siRNA treated condition, n=4 for untransfected control). The fluorescence (FAM) signal was investigated in cryo sections of tumours isolated from control untreated mice and from mice following tail-vein injections of nanocomplexes with FAM-labelled siRNA/AT1/ME27 as described in Tagalakis et al. (2017). The tumours were removed 24 hours after the injection. Tissue sections were rinsed in PBS briefly to remove any media components, and fixed in pre-cooled (at -20 °C) acetone for 10 to 15 minutes. Tissue sections were rinsed in PBS three times, 5 minutes each and then, stained with DAPI for 15 minutes at RT in dark. Then tissue sections were washed in PBS (three changes, 5 minutes each). Sections were mounted using ProLong Gold antifade mountant. Micrographs were taken using Leica upright fluorescence.

2.2.25. Caspase -3/7 assay

As described in Tateishi et al. (2016), caspase-3 and -7 activities were measured using the Caspase-Glo® 3/7 Assay. A luminogenic caspase-3/7 substrate interacts with caspase-3/7. When the substrate is added into caspase-3/7, the substrate is cleaved and then luminescent signal is released. In addition, the reagent also lyses cells. The luminescence signal increases according to the amount of caspase present.

Cells were seeded in 96 well plates at 1.8×10^4 cells per well and were incubated over night in a TC incubator. The cells were transfected with siMYCN and siNeg using RNAiMAX (1:1 volume ratio) in 200 μ L complete culture media at 10 nM or 50 nM final concentration. After 48-hour incubation, 100 μ L media was removed from each well and 100 μ L of the Caspase-Glo® 3/7 Assay reagent was added. After 1 hour incubation at RT, the luciferase activity was measured using the FLUOstar Optima plate reader. Protein was also quantified using Bradford protein assay reagent (see details in Section 2.2.19).

CHAPTER 3

Results

MYCN silencing and the downstream effects

induced by RNAi targeting MYCN

3. MYCN silencing and the downstream effects induced by RNAi targeting MYCN

3.1. Introduction

Aggressive neuroblastoma is highly associated with MYCN amplification and it accounts for approximately 15% all the neuroblastoma incidents (Gustafson & Weiss 2010). MYCN is a transcription factor which belongs to the Myc family and regulates many genes controlling essential cellular activities including proliferation, cell cycle, differentiation and apoptosis during development. MYCN upregulates p53, and suppresses TrkA, which has an important role in differentiation of sympathetic neurons in normal cells during development (Dixon & McKinnon 1994). It has been regarded that overexpressed MYCN induces proliferation and cell cycle and suppresses differentiation and apoptosis in MYCN amplified NB, which promotes tumorigenesis of NB (Westermarck et al. 2011). Hence MYCN is a promising target for gene therapy in NB with MYCN application.

p53 mutations are relatively rare, although multiple sessions of chemotherapy may induce p53 mutations in NB tumours (Tweddle et al. 2001). NB cells with p53 mutations are often resistant to anti-cancer drugs, especially those involving the p53 pathway (Huang & Weiss 2013). Patients with MYCN-amplified NB are treated with high dose chemotherapy and during treatment for residual disease they receive 13-*cis*-retinoic acid. However 13-*cis*-retinoic acid has little or no benefit for these particular patients and recently the residual disease therapy has included anti-GD2 antibody-related therapies, combined with the cytokines granulocyte macrophage colony stimulating factor and IL2. This has improved the survival rate for 2 years by 20%, although the prognosis of MYCN-amplified NB remains very poor (Barone et al. 2013; Pleossl et al. 2016). In addition, NB patients can develop resistance toward RA (Clark et al. 2013). Therefore, new therapies are required for NB with MYCN amplification.

We hypothesised that MYCN expression levels in MYCN-amplified NB cells could be silenced by RNAi and that MYCN reduction would induce differentiation and apoptosis, even in MYCN-amplified NB cells with p53 mutations and drug resistance. In addition, genes targeted by MYCN should be up- or down-regulated by MYCN reduction as a downstream effect. We chose TP53, MDM2 upregulated by MYCN, and NTRK1 downregulated by MYCN, as markers of the downstream effects. Furthermore, NTRK1/TrkA is a marker of neuronal differentiation that is negatively regulated by MYCN, and therefore, it was also expected that MYCN silencing might trigger differentiation of NB cells and morphological changes. Differentiated NB cells become more like terminally differentiated neurons that eventually senesce and die. Hence, differentiation by RNAi-mediated MYCN silencing suppresses the NB growth rate.

3.2. Aims

In this chapter, we aim:

1. To silence MYCN using RNAi (siRNA) and investigate silencing efficiency at mRNA and protein levels
2. To observe up/downregulation of TP53, MDM2 and NTRK1 at mRNA and protein levels as downstream effects of MYCN silencing
3. To observe differentiation (morphological changes) and apoptosis induced by siRNA-mediated MYCN silencing
4. To investigate the growth rate of NB cell line after siMYCN transfection of NB cells

3.3. Results

3.3.1. MYCN and NCYM expression differences among neuroblastoma cell lines at mRNA and protein levels

We first observed the expression level differences in MYCN mRNA, MYCN protein and NCYM RNA among several NB cell lines to understand their expression characteristics (Fig. 3.3.1). qRT-PCR and immunoblotting were performed. All values were normalised to those of SK-N-SH, and therefore SK-N-SH expression is set as 1. SK-N-BE(2) cells expressed 2000-fold more MYCN mRNA than SK-N-SH (non-MYCN amplified) cells, whereas Kelly and LAN-5 cells MYCN mRNA levels when compared to SK-N-SH cells were 1612-fold and 510-fold higher, respectively (Fig. 3.3.1.a).

Then, the MYCN protein level was compared among several NB cell lines (Fig. 3.3.1.b). According to the supplier of the anti-MYCN antibody the expected MYCN size was 67 kDa, however, protein bands consistently appeared around 55 kDa (between 51 and 64 kDa). The 55 kDa bands were clear and the intensities agreed with MYCN-amplification or non MYCN-amplification in each cell line. Hence, we concluded the bands at approximately 55 kDa were the MYCN protein bands. SHEP and SK-N-AS are MYCN non-amplified NB cell lines, and SHEP-21N and SKNAS-NmycER, which are conditionally-expressing amplified MYCN protein, were used as positive controls. SHEP-21N contains a MYCN expression cassette that can be switched off by tetracycline exposure. The MYCN protein expression level in SHEP-21N was the same as that in LAN-5 and both were 6-fold higher than that in SK-N-SH with a single copy of the *MYCN* gene. SKNAS-NmycER expresses the MYCN-Estrogen receptor fusion protein, and the fusion protein is activated by the estrogen analogue 4-hydroxytomoxifen (4-OHT) (Koppen et al 2007). Because it is a fusion protein of an estrogen receptor and MYCN, the bands of SKNAS-NmycER 4-OHT +/- were slightly larger (approximately 60 kDa) than those of the other cell lines (approximately 55 kDa), and

the SKNAS-NmycER 4-OHT +/- were not significantly different from each other (7.7 and 7.8, respectively).

The MYCN protein expression level (Fig. 3.3.1.b) in MYCN-amplified cell lines, Kelly, LAN-5 and SK-N-BE(2), was significantly higher than that in non MYCN-amplified SK-N-SH cells by 4-fold, 6-fold and 20-fold, respectively. Interestingly, the MYCN protein expression level in LAN-5 was 1.3 times higher than Kelly cells while the MYCN mRNA expression level was 3 times higher in Kelly than in LAN-5. bEnd3, a murine endothelial cell line, was used as a negative control for MYCN protein expression, and the value relative to SK-N-SH was 0.3. The data of MYCN expression at mRNA and protein levels suggests that the amount of MYCN mRNA does not always closely correlate with the amount of MYCN protein relative to SK-N-SH cells.

We also investigated the NCYM RNA expression level in SK-N-BE(2), Kelly, LAN-5 and SK-N-SH (Fig. 3.3.1.c). NCYM was not expressed as much as MYCN. Although the MYCN mRNA level in Kelly cells was lower than that in SK-N-BE(2), the NCYM RNA expression level in Kelly was slightly higher than that in SK-N-BE(2). The expression level in LAN-5 was 5 times lower than that in Kelly.

This result suggests that the amount of NCYM RNA expression may not have a very linear correlation with MYCN mRNA expression while it is likely that MYCN mRNA and NCYM RNA are co-overexpressed in MYCN-amplified NB cells.

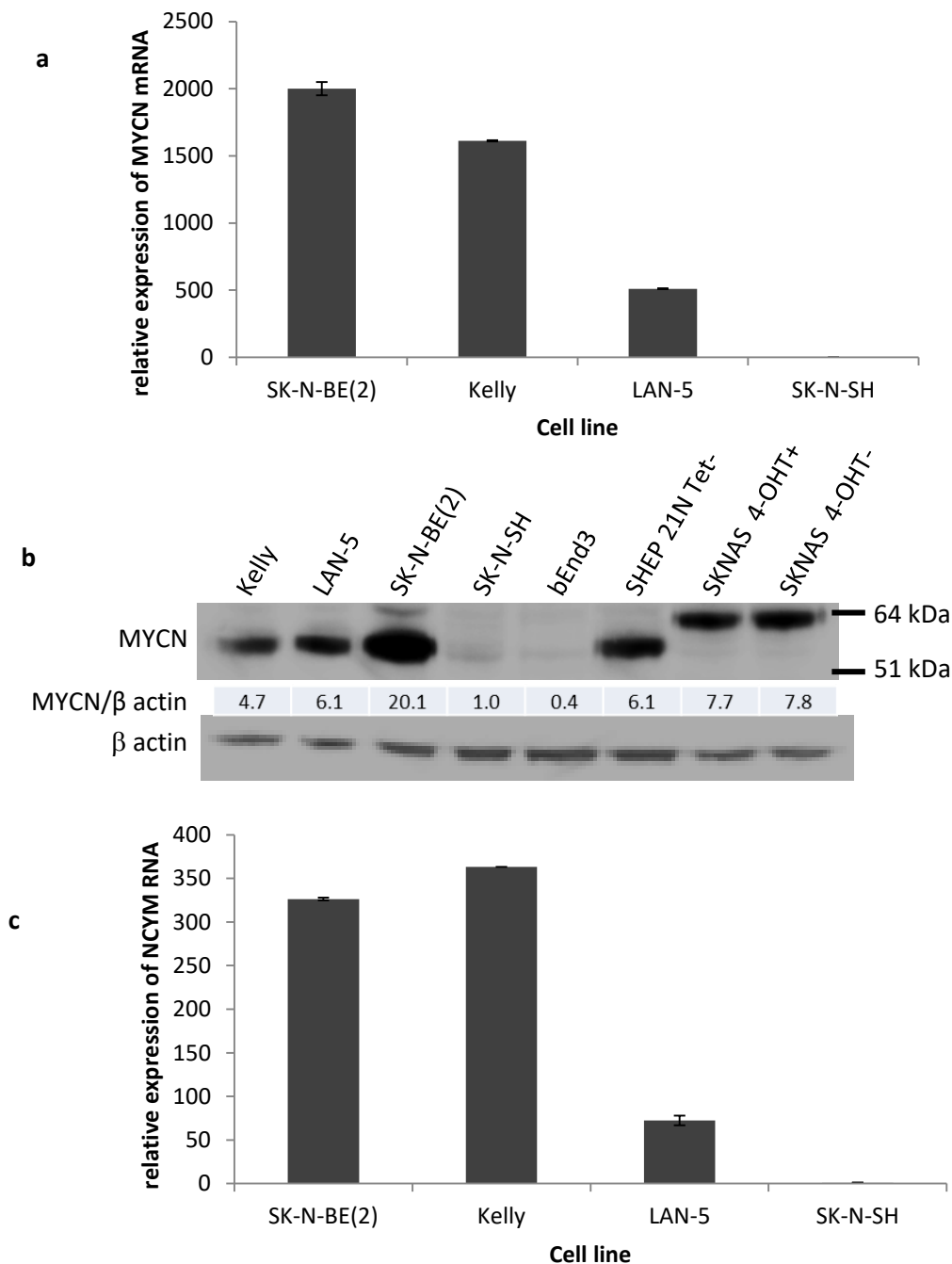


Fig 3.3.1. Differences in MYCN and NCYM expression levels among cell lines. All values were normalised to that of SK-N-SH. i.e. SK-N-SH=1. a) Relative expression level of MYCN mRNA quantified by qRT-PCR. The expression levels in MYCN amplified cell lines were approximately 500-2000-fold higher than those in SK-N-SH. (n=2) b) Immunoblotting analysis of MYCN protein expression level in NB cell lines. The expression levels were quantified using ImageJ according to the intensity. The MYCN protein expression levels in MYCN amplified NB cells were approximately 4-fold to 20-fold greater than that of SK-N-SH. c) Relative expression level of NCYM RNA quantified by qRT-PCR. NCYM is co-amplified with MYCN mRNA in MYCN amplified NB cells while the expression levels of the two are not linearly correlated to each other. (n=2) In all the graphs each column represents the mean± SD.

3.3.2. Transfection efficiency in a NB cell line by Lipofectamine RNAiMAX

Although transfection efficiency does not always represent gene silencing efficiency, it indicates how many cells can take in siRNA and how much siRNA can get into individual cells. To observe the transfection efficiency of Lipofectamine RNAiMAX (RNAiMAX, Thermo Fisher Scientific) and the correlation between transfection and silencing efficiencies, cellular uptake of fluorescence (AlexaFluor 555) labelled negative control siRNA was performed at 50, 20, 10 and 5 nM final concentration at 4, 24 and 48 hour time points in SK-N-BE(2) cells (Fig. 3.3.2.a). 50 and 20 nM siRNA/RNAiMAX achieved the maximum percentage of positive cells at the 4 hour time point with 95.7% and 96.7% uptake respectively, while the percentage at 10 nM and 5 nM showed slightly lower maximum percentages of labelled cells (both at 88.6%).

On the other hand, the mean fluorescence intensity (MFI) of cells treated with 50 nM showed the highest MFI levels between all different concentrations at the 4 hour (529) and 24 hour time points (333), but kept decreasing between 4 and 48 hour time points (Fig. 3.3.2.b). 20 nM was the second highest at 4 and 24 hour time points, and then, was the strongest at 48 hours. MFI at 10 and 5 nM increased between 4 and 24 hour time points, although they decreased between 24 and 48 hour time points. This result suggests that 20 nM siRNA may be the optimal concentration for maximum silencing efficiency at 48 hour time point.

When samples are a cell line, they generally can be sorted to two populations by the size in flow cytometry: the smaller is dust or dead cells and the larger is live cells in a cell line. Therefore, the percentages of the two populations can be regarded as indication of the cell viability. The live cells were selected to analyse the transfection efficiency and MFI in this study (Fig. 3.3.2.c). We noticed the changes in the percentage of the live cells during 48

hours at the 4 different concentrations of siRNA. The percentage at 50 nM at 4 hours (67.1%) was quite low, compared with those of the other conditions. At the 48 hour time point, 50 nM siRNA reduced the live cells to 55.6% and 20 nM to 69.3%, while 10 and 5 nM maintained survival at the same level as untransfected cells.

The data suggest 50 nM was cytotoxic and the MFI was dropped off because the cells were dead. On the other hand, 20 nM achieves higher cellular uptake efficiency during the 48 hours although it was more toxic compared with 10nM and 5 nM. 10 nM and 5 nM siRNA can survive transfection for 48 hours without any difference to untransfected cells. Therefore, we concluded that silencing efficiency at 10 nM can be regarded as a silencing efficiency without cytotoxicity, and 10 nM siRNA is used as a positive control in transfections using RTNs.

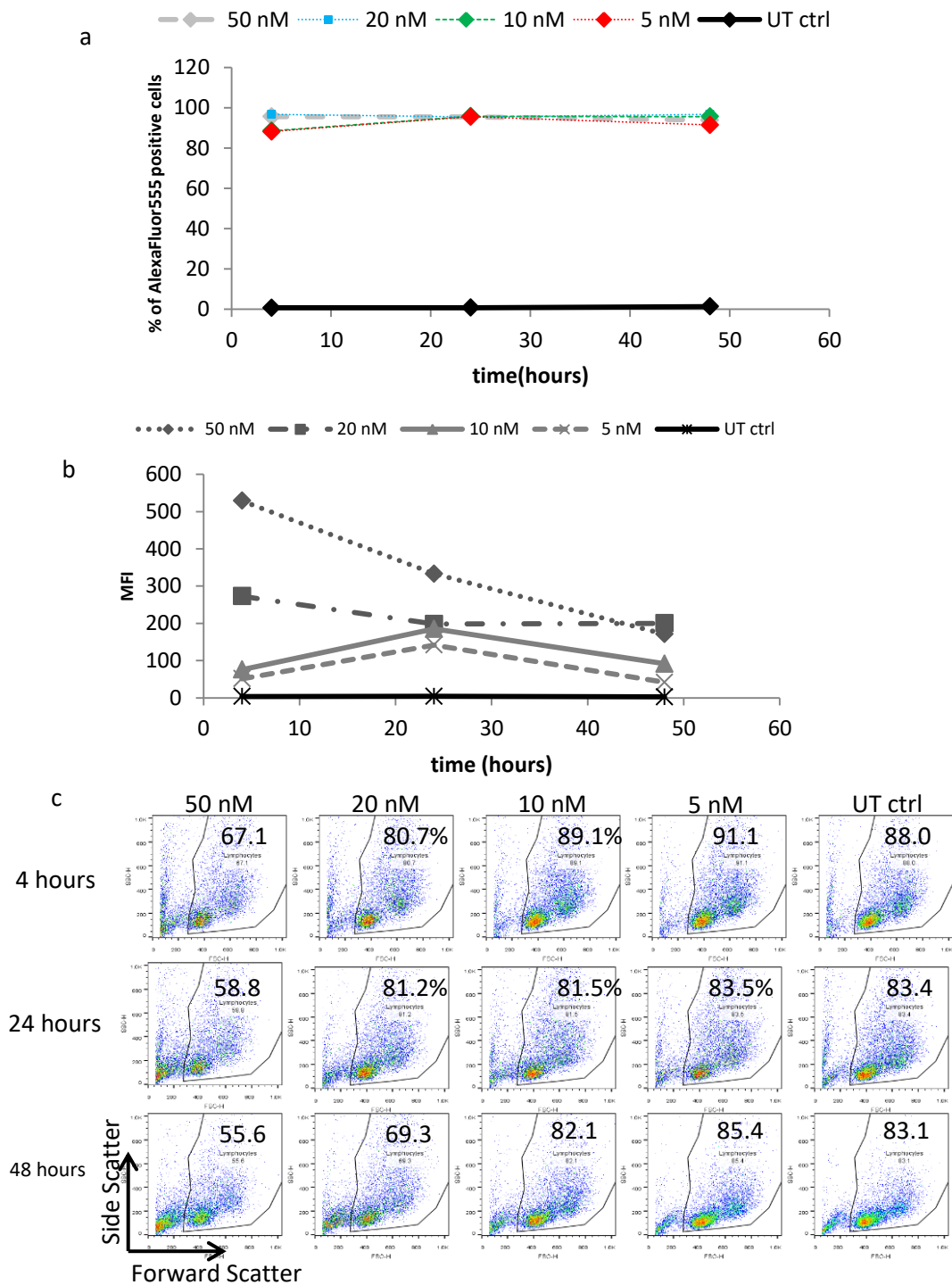


Fig.3.3.2. Cellular uptake of SK-N-BE(2) cells The percentage of AlexaFluor 555-siRNA positive cells treated with 50, 20, 10, and 5 nM siRNA were observed using flow cytometry at 4, 24 and 48 hour time points. **a)** All concentrations of siRNA achieved uptakes of over 95% at 24 hours. **b)** MFI changes during the 48 hours. **c)** Percentage changes of live cells at the 4 different concentrations during 48 hours. The cells were distributed on the plot according to the size and the gated population shown is the live cells. The left panel in each graph shows dead cells and dust. (n=1)

3.3.3. Comparison of MYCN silencing efficiency of 3 different siMYCNs

Three candidate siRNAs targeting 3 different regions (Fig. 3.3.3.a) on *MYCN* gene, were compared to investigate *MYCN* gene silencing efficiency and select the best one for the remaining experiments. 10 nM of each siMYCN was used to transfect Kelly cells using RNAiMAX, and the cells were harvested at 48 hours (n=6) (Fig. 3.3.3.b). As a result, siMYCN 3 achieved the highest silencing efficiency at 55%, followed by siMYCN 2. The siMYCN 2 silenced *MYCN* mRNA at similar levels to siMYCN 3 in one experiment while it did not reduce *MYCN* mRNA levels at all in another experiment. siMYCN 1 did not reduce *MYCN* mRNA in any experiment.

Therefore, we concluded that siMYCN 3 was the most efficient and was used in all subsequent experiments.

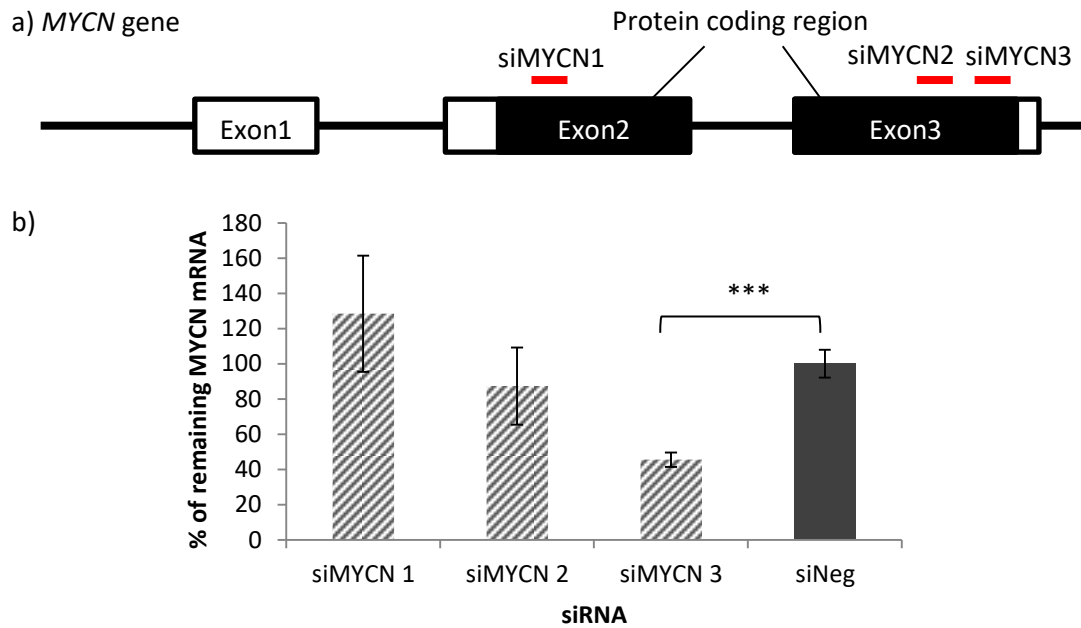


Fig. 3.3.3. Comparison of MYCN silencing efficiency of 3 different siMYCNs in Kelly cells a) the map of *MYCN* gene and the targeted regions by the 3 different siMYCNs b) Three candidate of anti-MYCN siRNAs were transfected at 10 nM into Kelly cells, and MYCN mRNAs were quantified using qRT-PCR 48 hours after the transfection (n=6). 3 achieved the best MYCN silencing at 54.5%. In all the graphs each column represents the mean ± SD. ***p<0.001

3.3.4. MYCN silencing at mRNA level by siMYCN in NB cell lines

To observe MYCN silencing efficiency by siMYCN in NB cell lines, siRNA transfection using RNAiMAX (1:1 volume ratio) was performed in 4 different NB cell lines: SK-N-BE(2), Kelly, LAN-5 and SK-N-SH. Silencing efficiency was assessed at the 48 hours later using qRT-PCR (Fig.3.3.4.).

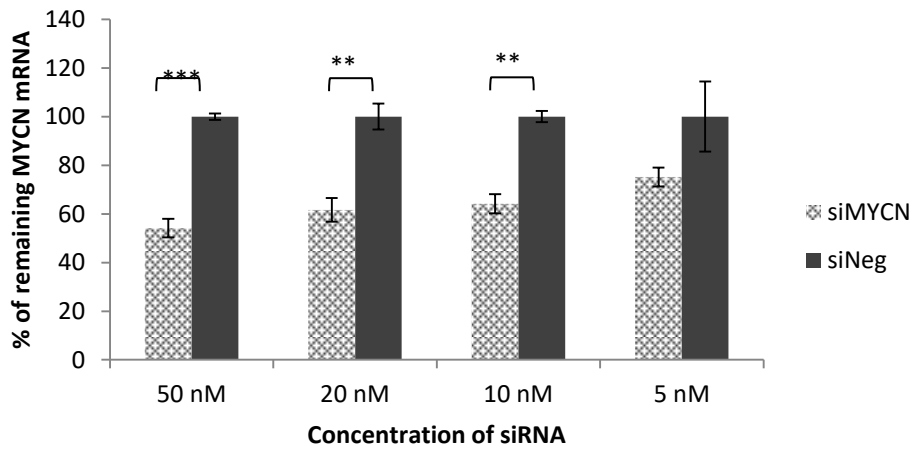
MYCN silencing efficiency by siMYCN at mRNA level achieved 24.8-45.9% in SK-N-BE(2), depending on the dose. 50 nM siMYCN achieved the highest silencing efficiency among the 4 different concentrations, followed by 20 nM siMYCN. The differences between siMYCN and siNeg in 50 nM, 20 nM and 10 nM were statistically different ($p=0.00061$, 0.0098 and 0.002 , respectively) while those for the 5 nM dose were not significantly different ($p=0.22$).

In Kelly cells, the silencing was 36.2%-51.2%, with 20 nM siMYCN achieving the highest knockdown. Overall, MYCN silencing efficiency in Kelly cells was slightly higher than that in SK-N-BE(2) cells by approximately 8% and the difference in the values among the 4 different concentrations of siMYCN was smaller than that in SK-N-BE(2) cells. At 50 nM, 20 nM and 5 nM, the differences between siMYCN and siNeg were significantly different ($p=0.0000016$, 0.00014 and 0.009 , respectively) while those for 10 nM were not ($p=0.09$). In LAN-5, significant silencing of MYCN mRNA was not seen at any concentration. The highest silencing in the cell line was 12.5% at 20 nM siMYCN, although the difference between siMYCN and siNeg at 20 nM was not statistically different ($p=0.058$). The other concentrations of siMYCN were not significantly different from the same concentration of siNeg ($p=0.71$ at 50 nM, $p=0.14$ for 10 nM and $p=0.13$ for 5 nM).

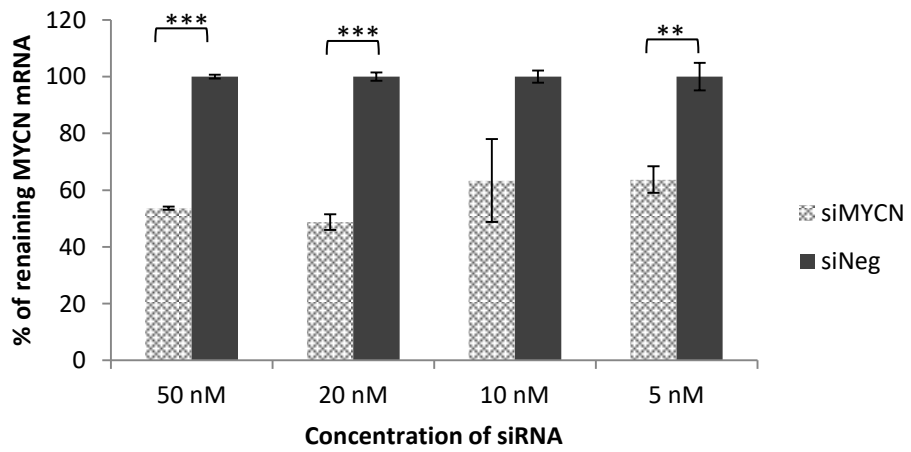
In SK-N-SH cells, 50 nM, 20 nM and 10 nM doses of siMYCN achieved similar silencing efficiency at 54.8-58.6% and the efficiency slightly decreased to 47.1% at 5 nM. The p value of each condition was 0.00041, 0.0018, 0.000069 and 0.075 respectively.

This result suggests siMYCN never achieved 100% knockdown even in the SK-N-SH NB cell line which has a single copy of MYCN. In addition, LAN-5 might be the most difficult cells to be transfected.

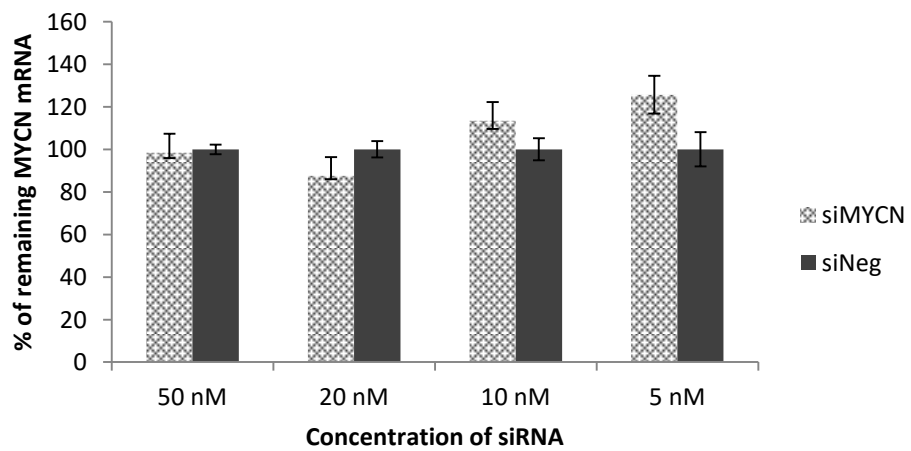
SK-N-BE(2)



Kelly



LAN-5



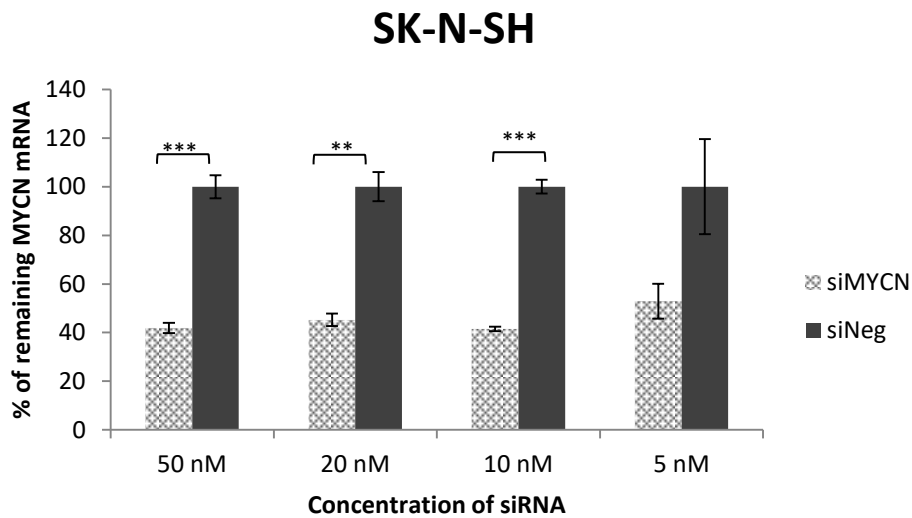


Fig. 3.3.4. Remaining MYCN mRNA in NB cell lines 48 hours after siMYCN transfection quantified using qRT-PCR SK-N-BE(2), Kelly, LAN-5 and SK-N-SH were transfected with siMYCN and siNeg using RNAiMAX (1:1 volume ratio) and were incubated for 48 hours. The MYCN mRNA expression level was quantified using qRT-PCR. The values were normalised by the value of siNeg at each concentration. siMYCN silenced MYCN up to 45.9% in SK-N-BE(2), 51.2% in Kelly, 12.5 in LAN-5 and 67.5% in SK-N-SH. All the concentrations of siMYCN significantly reduced MYCN mRNA in the three cell lines except LAN-5. (n=3) In all the graphs each column represents the mean± SD.
 *p<0.05, **p<0.01, ***p<0.001

3.3.5. TP53, MDM3 and NTRK1 mRNA up/downregulated by MYCN silencing

MYCN is proposed to regulate many downstream genes including TP53 and MDM3, which are essential for cellular activities as a transcription factor. However, it is likely that overexpressed MYCN induces proliferation and cell cycle while it suppresses apoptosis and differentiation. To determine downstream effects of MYCN silencing by RNAi, we chose 3 genes to analyse for protein expression: TP53 (Chen et al. 2010) and MDM2 (Slack et al. 2005) were previously reported to be direct transcriptional targets of MYCN, and NTRK1 expressing TrkA a neuronal differentiation marker. After siMYCN was transfected into SK-N-BE(2), Kelly and LAN-5 cells, mRNA of TP53, MDM2 and NTRK1 was quantified by qRT-PCR (Fig. 3.3.5., 3.3.6., 3.3.7.).

In SK-N-BE(2), the trend of siMYCN-mediated downregulation of TP53 and MDM2 was similar although there was no clear dose dependent response (Fig. 3.3.5.a,b). siMYCN mediated MYCN reduction downregulated TP53 by 1.2-33.0% and MDM2 by 2.2-30.0%. NTRK1 was notably upregulated by siMYCN, and the expression level was 2-3-fold higher than that of siNeg treatment (Fig. 3.3.5.c). In Kelly cells, TP53 and MDM3 mRNA expressions were upregulated following siMYCN silencing at 50 nM, 20 nM and 10 nM, except those in 5 nM (Fig. 3.3.6.a,b). The relative mRNA expression level of TP53 was increased by 10.0-32.7% and of MDM2 by 4.2-30.0% while 5 nM siMYCN downregulated TP53 and MDM2 mRNAs by 22.2-23.4%. Interestingly, NTRK1 was upregulated by all the 4 different concentrations of siMYCN, and the expression level was 1.3-4.4-fold higher than those in siNeg (Fig. 3.3.6.c). In LAN-5, no clear trend and no significant up/downregulation were seen. siMYCN achieved 4.1-12.8% silencing of TP53 and 0-11.3% of MDM2, although 10nM upregulated TP53 by 7.8% (Fig.3.3.7.a,b). In addition, NTRK1 was upregulated by siMYCN by 4.0-31.1% (Fig. 3.3.7.c).

The data suggest downstream effects caused by siMYCN may not always be the same in different cell lines because TP53 and MDM2 were downregulated in SK-N-BE(2) and they were upregulated in Kelly, but they were not significant. On the other hand, NTRK1 was remarkably upregulated by siMYCN mediated MYCN reduction in both SK-N-BE(2) and Kelly. Furthermore, the downstream effect might be affected by the MYCN silencing efficiency because the efficiency in LAN-5 was smaller as well as the change in TP53, MDM2 and NTRK1.

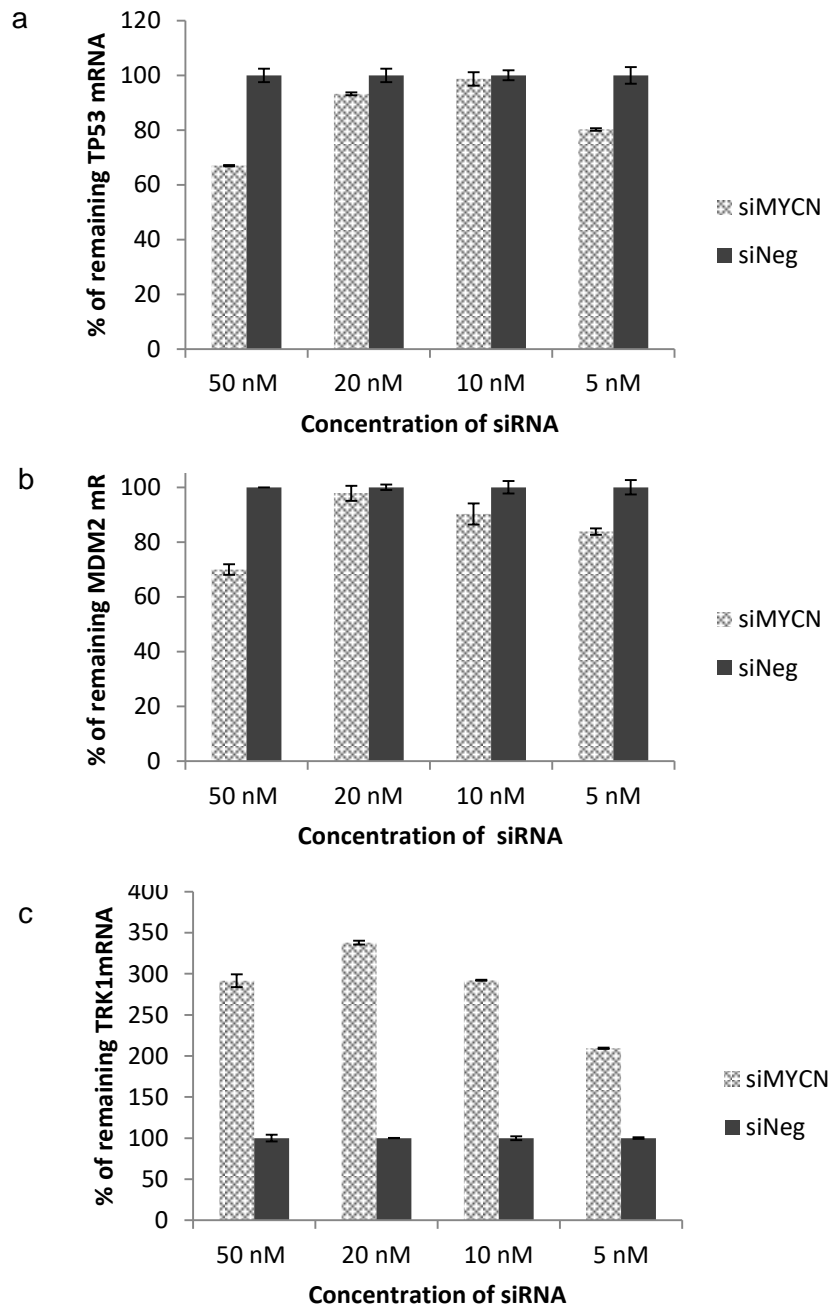


Fig. 3.3.5. TP53, MDM2 and NTRK1 mRNA up/downregulation by siMYCN mediated MYCN reduction in SK-N-BE(2) cells After the transfection, mRNA of a)TP53, b)MDM2 and c)NTRK1 was quantified by qRT-PCR. TP53 and MDM2 were downregulated moderately while NTRK1 was significantly upregulated 2-3-fold compared to cells treated with siNeg. (n=3) In all the graphs each column represents the mean \pm SD.

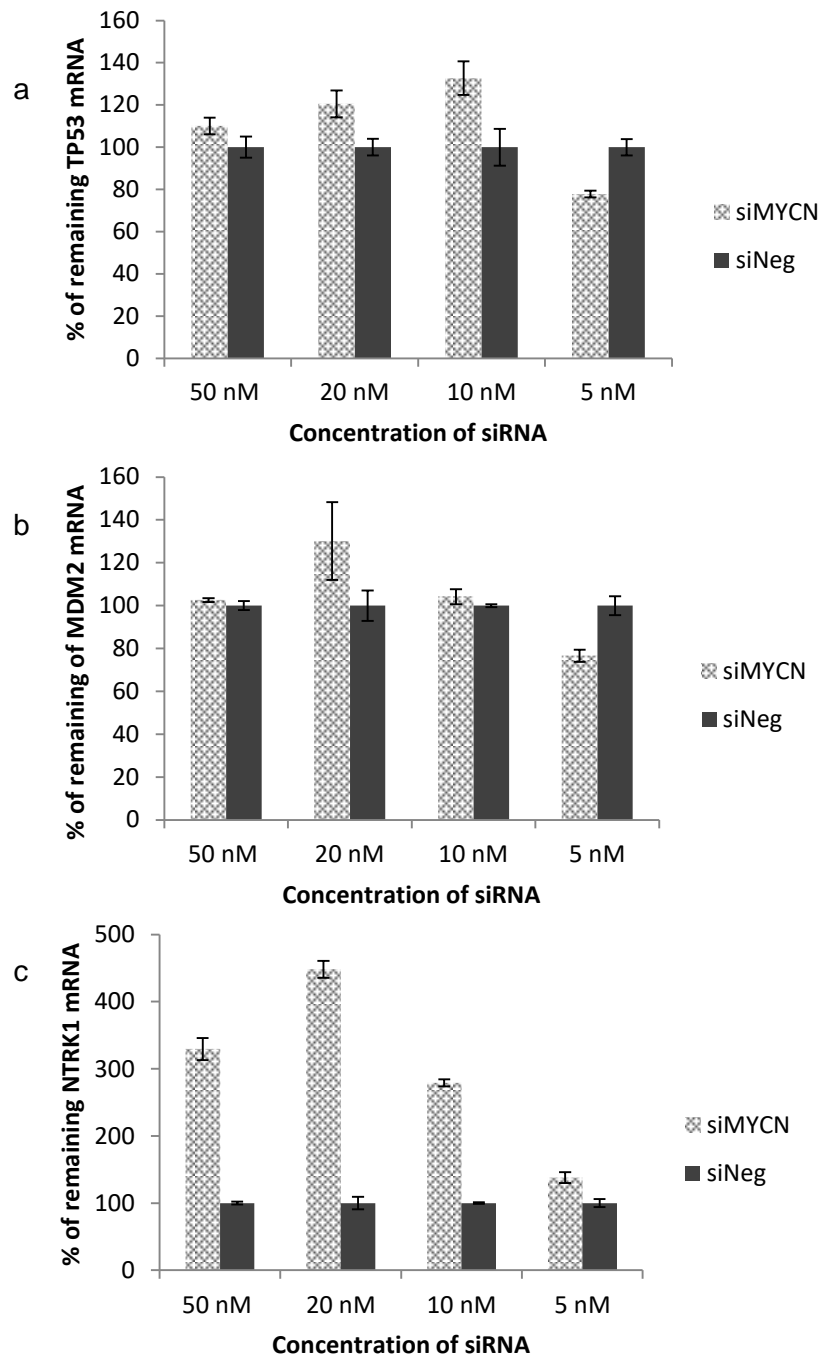


Fig. 3.3.6. TP53, MDM2 and NTRK1 mRNA up/downregulation by siMYCN mediated MYCN reduction in Kelly cells. After the transfection, mRNA of **a)**TP53, **b)**MDM2 and **c)**NTRK1 was quantified by qRT-PCR. TP53 and MDM2 were slightly upregulated except that at 5 nM siMYCN, while NTRK1 was remarkably upregulated. They had 1.3-4.4 times greater mRNA levels compared to cells treated with siNeg. (n=3) In all the graphs each column represents the mean \pm SD.

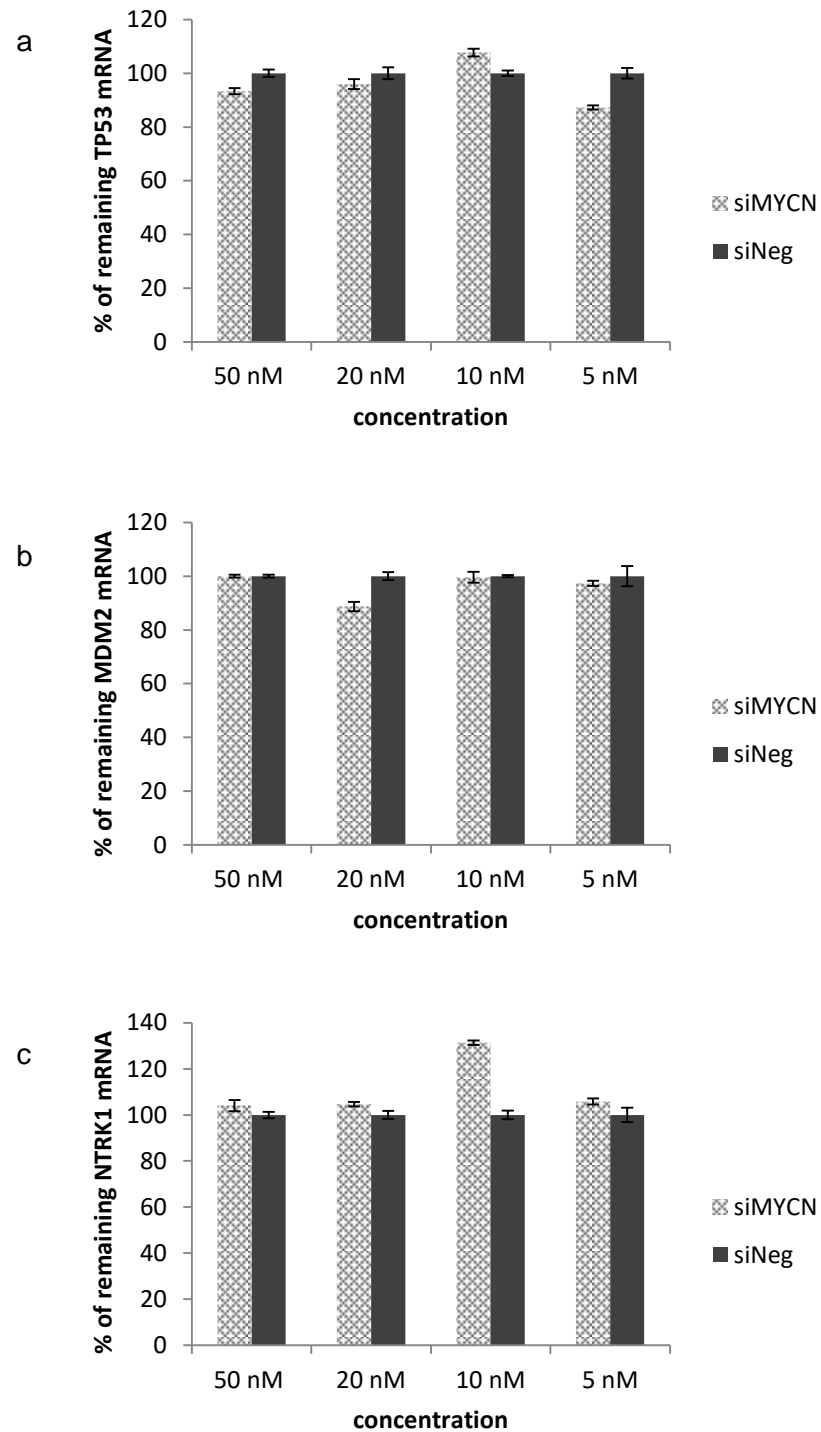


Fig. 3.3.7. TP53, MDM2 and NTRK1 mRNA up/downregulation by siMYCN mediated MYCN reduction in LAN-5 cells After the transfection, mRNA of a)TP53, b)MDM2 and c)NTRK1 was quantified by qRT-PCR. It did not seem that there is up/downregulation by siMYCN transfection as well as siMYCN could not achieve significant MYCN knockdown. (n=3) In all the graphs each column represents the mean \pm SD.

3.3.6. MYCN silencing and Trk upregulation at protein level

We then investigated whether siMYCN mediated MYCN silencing, which reduced mRNA levels, also reduced MYCN protein production assessed by Western blot analysis. SK-N-BE(2) and Kelly cells were transfected with siMYCN or siNeg at 50 nM, 20 nM, 10 nM and 5 nM final concentrations using RNAiMAX (1:1 volume ratio), and were harvested at 72 hour after transfection. The samples were probed with anti-MYCN antibody, a neuronal differentiation marker anti-pan Trk antibody and anti-beta actin as a house keeping gene (Fig. 3.3.8.a, b). The intensity of all bands of MYCN, Trk and beta actin was measured using Image J, and the intensity of MYCN and Trk was normalised to the β actin. Then the values were normalised to the untransfected negative control in order to calculate relative expression levels (untransfected negative control = 1). The relative expression level of each protein is shown under the respective band.

siMYCN reduced MYCN protein level by approximately 70-95% in SK-N-BE(2) and 35-84% in Kelly. There was only a modest decrease in MYCN in SK-N-BE(2) cells with siNeg and a consistent increase in Kelly cells. Furthermore, siMYCN-mediated MYCN silencing upregulated pan Trk expression level by 1.8-2.4-fold in SK-N-BE(2) and 3.3-6.7-fold in Kelly, compared with the respective untransfected cells. siNeg also increased/decreased Trk protein expression level, and it seems to be experimental variation. In addition, in SK-N-BE(2), 10 nM siMYCN silenced approximately 2-fold more the MYCN compared to 5 μ M RA.

These results of SK-N-BE(2) and Kelly transfected with siMYCN suggest that the amount of the MYCN protein reduction and pan Trk upregulation are negatively correlated. In addition, siMYCN may achieve higher percentage of MYCN knockdown than 5 μ M RA in SK-N-BE(2) cells.

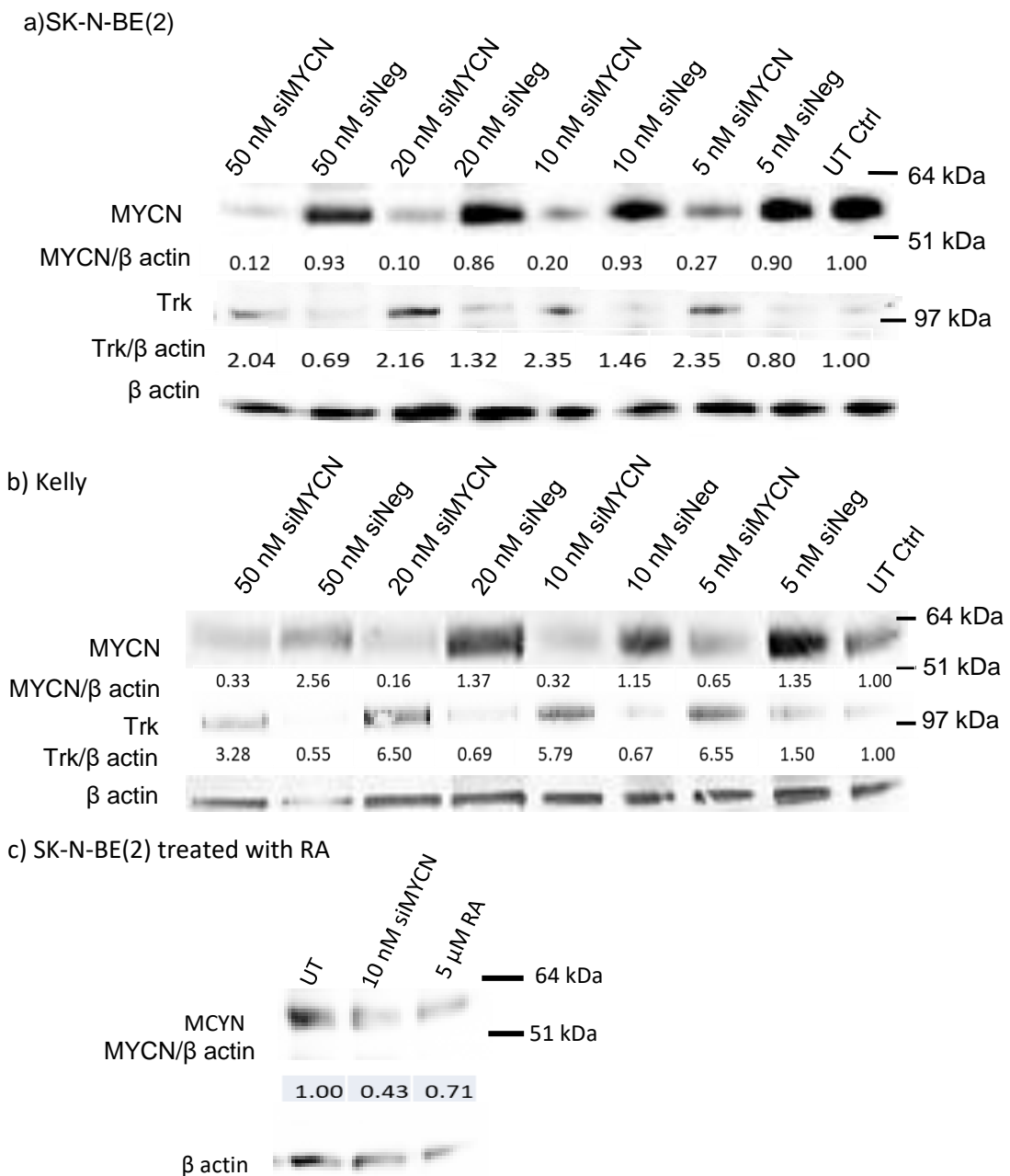


Fig. 3.3.8. Immunoblotting of MYCN and Trk following siMYCN transfections The number under the band is the relative expression level calculated from the intensity of the band. a) SK-N-BE(2) and b) Kelly were transfected with siMYCN/siNeg for 3 days, and the samples were probed with anti-MYCN antibody and anti-Pan-Trk antibody. MYCN bands appeared between 64 and 51 kDa and pan Trk bands above 97 kDa. The bands were quantified and normalised to untransfected negative control. siMYCN induced MYCN reduction and Trk upregulation. c) Comparison of the effects on MYCN expression of treatment with 10nM siMYCN and 5μM RA in SK-N-BE(2) cells. 10 nM siMYCN silenced approximately 2-foldmore the MYCN protein than RA.

3.3.7. Differentiation in SK-N-BE(2) by siMYCN

Overexpression of MYCN has been regarded to suppress differentiation and apoptosis of neuroblastoma cells. This is particularly evident in MYCN-amplified NB cells and is one of the tumourigenic mechanisms in NB. In addition, some NB cells such as SK-N-BE(2) cells have non-functional p53 and they have resistance towards not only against drugs that depend on the p53 pathway (Tweddle et al. 2001) but also on radiotherapy (Gudgov & Komarova, 2003).

We hypothesised that siMYCN can reduce MYCN expression and induce differentiation in neuroblastoma cells with non-functional p53. We then investigated the ability of siMYCN to induce differentiation in SK-N-BE(2), which can be a model of MYCN-amplified NB cells with p53-dependent chemotherapy and radiotherapy resistance, and to change the cells morphologically by quantifying neurite length and the number of neurites.

SK-N-BE(2) cells were transfected with siMYCN or siNeg at 50 nM, 20 nM, 10 nM or 5 nM using RNAiMAX (1:1 volume ratio), and were incubated for 6 days (Fig. 3.3.9). The transfection media was changed to complete media at day 3. siMYCN treatment induced notable neurite elongation and morphological differentiation; extended neurites connected with each other. In addition, the morphology of cells after siMYCN transfection became raised and with a smaller rounder shape, indicative of differentiated cells. Although some neurite extension was also seen in cells treated with siNeg, they were not as long and numerous as those transfected with siMYCN. To quantify neurites, the total neurite length value per image were normalised by the total cell area as it was too difficult to distinguish and count single cells of SK-N-BE(2) as they tend to grow in clumps. The total number of neurites was calculated from the number of neurites that were longer than cells. The experiment was performed twice and 5 images were taken from each experiment.

The neurite extensions appeared from day 2 after transfection, the length induced by siMYCN was around 0.015-0.025 $\mu\text{m}/\mu\text{m}^2$ cell area (Fig. 3.3.10.a). It was significantly longer than the extension by siNeg in all the concentrations. The length of neurites transfected with 20 nM, 10 nM and 5 nM siMYCN at day 6 was longer than that at day 2 by around 0.03 $\mu\text{m}/\mu\text{m}^2$ cell area. However, the neurite length induced by 50 nM siMYCN had variation, and therefore, it was not significantly different from the one of 50 nM siNeg at day 6. The neurite length induced by 5 nM, 10 nM and 20 nM siMYCN at day 6 was significantly different from that by siNeg at each concentration ($p=0.000085$, 0.0000067 and 0.0000074 respectively) while the length was almost the same among the three different concentrations of siMYCN (0.033 - 0.035 $\mu\text{m}/\mu\text{m}^2$ cell area) (Fig. 3.3.10.a).

The number of the extended neurites were counted as a quantifiable marker of differentiation in SK-N-BE(2) cells after siMYCN transfection. The number of the neurites was notably different from cells treated with siNeg at all concentrations at day 2 and day 6. The number was not different between day 2 and day 6 (Fig. 3.3.10.b).

These results suggest that siMYCN can dramatically induce differentiation in NB cells, and it is likely that the efficiency to induce neurite elongation was not significantly different among the 4 different concentrations of siMYCN.

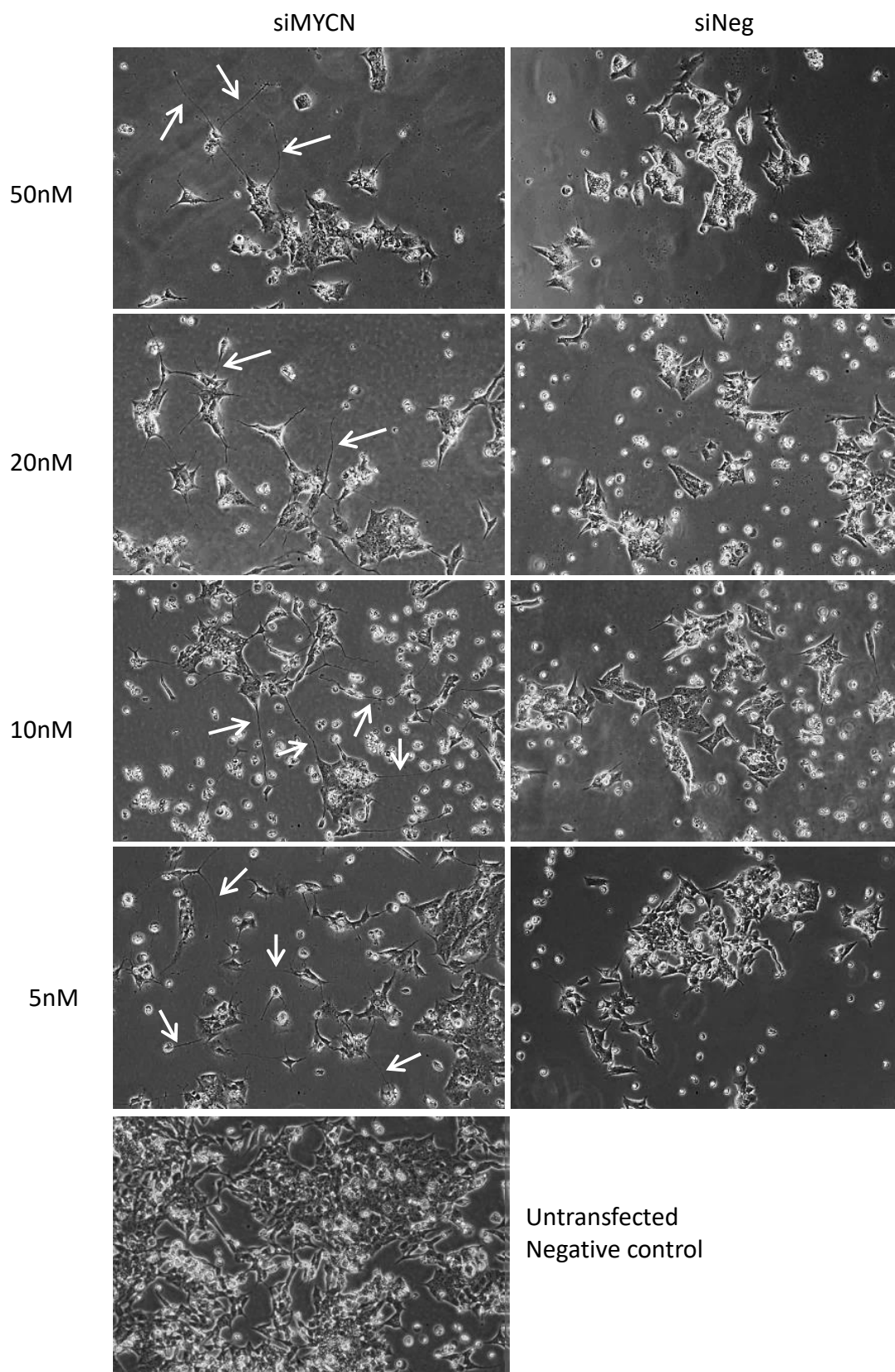
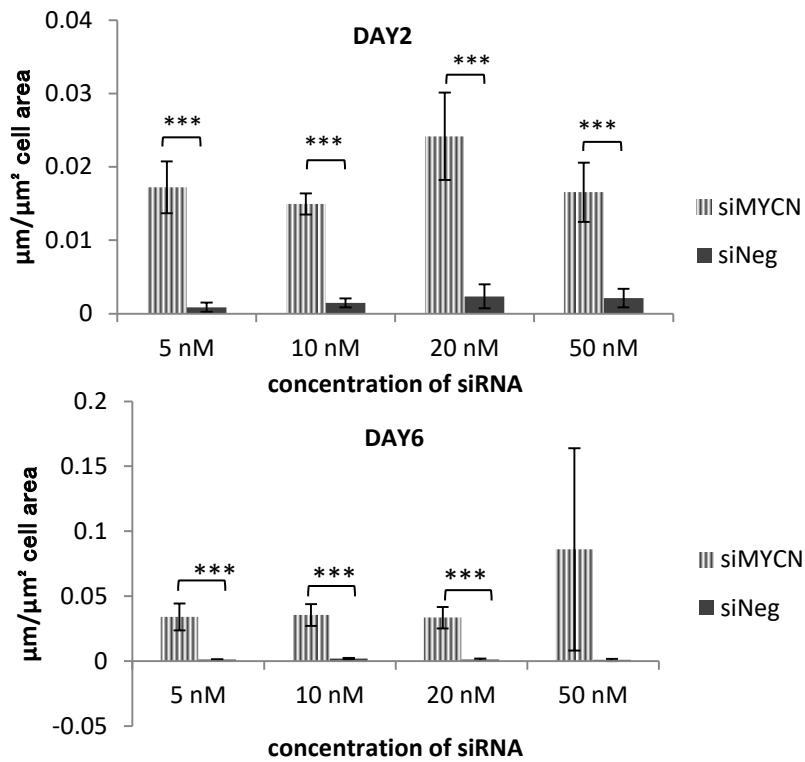


Fig. 3.3.9. Cell morphology changes after siMYCN transfection SK-N-BE(2) cells transfected with siMYCN/siNeg and incubated for 6 days. The morphology was changed by transfection relative to controls with the formation of elongated neurites (arrows) and the presence of rounder and smaller cell bodies.

a) The neurite length per cell



b) The number of the neurites per cell

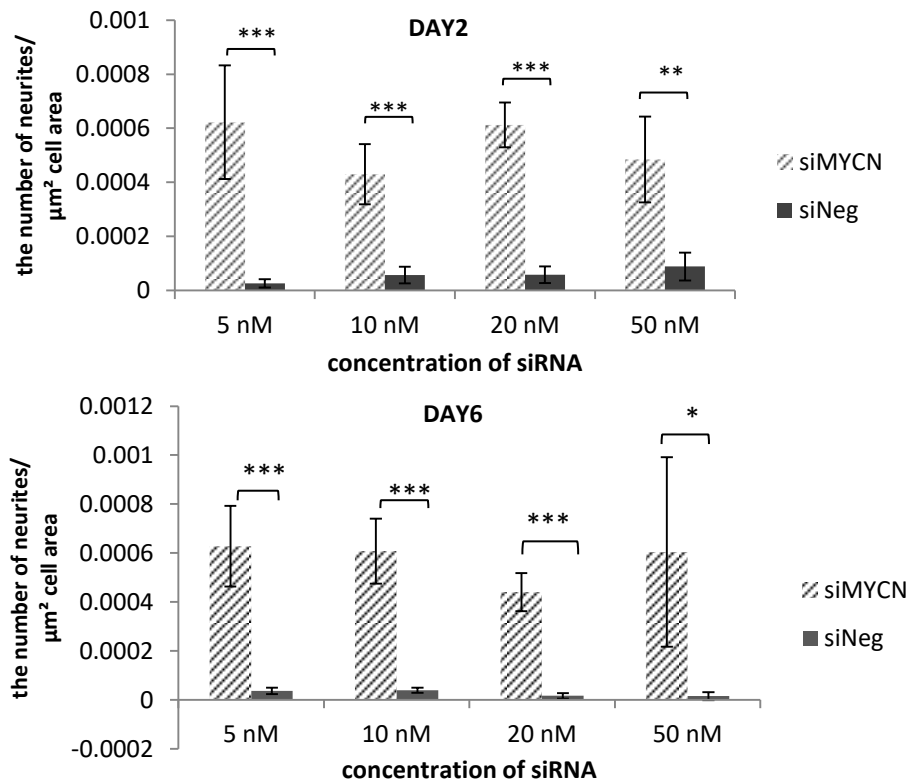


Fig. 3.3.10. Quantification of neurites after siMYCN transfection of SK-N-BE(2) cells: Fig. 3.3.9. siMYCN significantly induced differentiation in SK-N-BE(2) ($n=10$), and there were significant differences in a) the neurite length and b) the number of the neurites between siMYCN and siNeg. The neurite length in day 6 was longer than that in day 2 while the number of the neurites were almost the same during the 4 days. In all the graphs each column represents the mean \pm SD. * $p < 0.05$, ** $p < 0.01$, *** $p < 0.001$

3.3.8. The sensitivity of NB cell lines toward retinoic acid

RA is one of the commonly used drugs in chemotherapy for NB. To observe the sensitivity of the 4 different cell lines: SK-N-BE(2), Kelly, LAN-5 and SK-N-SH towards RA, the cells were treated with 5 and 10 μ M RA for 48 hours (Fig. 3.3.11.). As many papers have reported previously (Clark et al. 2013; Joshi et al. 2007; Akkuratov et al. 2015), SK-N-SH and LAN-5 cells responded toward RA treatment, by morphological changes as well as induction of neurite elongation. In SK-N-SH cell cultures, there are two types of cells, neuronal-type and Schwann-type, and the morphology of the Schwann-type cells were clearly flatter after the RA treatment. The extended neurites formed networks and connected cells. In LAN-5, the extended neurites also formed the networks among the cells although morphological differences in the cells were not seen. On the other hand, SK-N-BE(2) and Kelly did not change significantly with regard to their morphology, and neurite networks were not induced although a few neurite elongations were seen. This result suggests that Kelly and SK-N-BE(2) are likely to have resistance towards RA, and therefore, RA cannot be expected to display efficacy toward certain types of NBs such as Kelly and SK-N-BE(2).

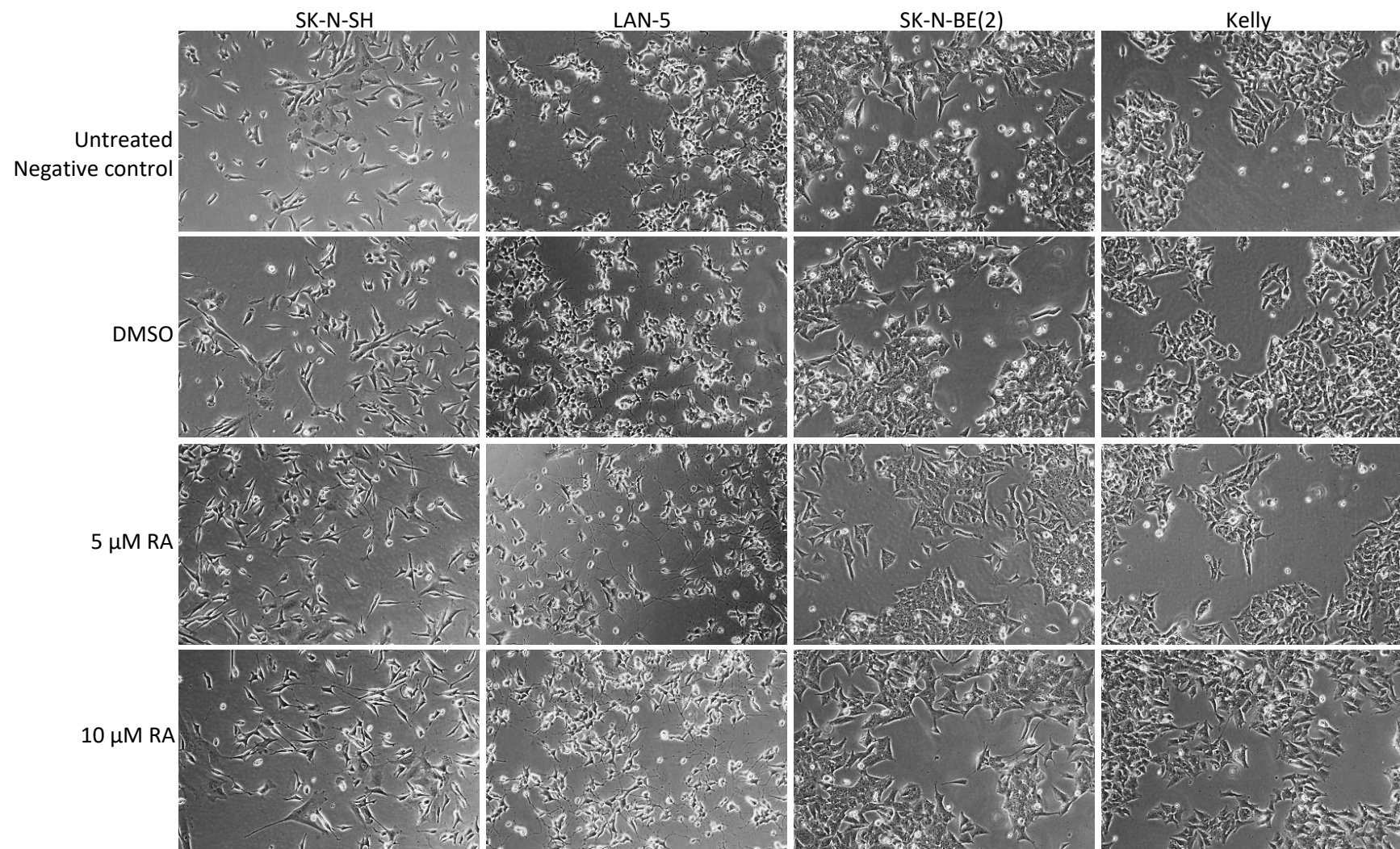


Fig. 3.3.11. Difference in response towards Retinoic Acid among NB cell lines SK-N-SH, LAN-5, SK-N-BE(2) and Kelly cells were treated with 5 or 10 μ M RA for 48 hours. RA induced the neurite elongations in SK-N-SH and LAN-5, while SK-N-BE(2) and Kelly did not respond significantly in the morphology.

3.3.9. Apoptosis induced by MYCN silencing

As mentioned above, it is hypothesised that overexpression of MYCN suppresses differentiation and apoptosis and induces cell proliferation and cell cycle in MYCN-amplified NB cells, which is one of the tumourigenic mechanisms. It was also reported that reduction of MYCN induces apoptosis in MYCN-amplified NB cells (Kang et al. 2006). To investigate the ability of siMYCN to trigger apoptosis in MYCN amplified NB cells, the sub G1 assay using Propidium Iodide (PI) staining and Caspase-3/7 assay were performed. SK-N-BE(2) and Kelly cells were treated with siMYCN and siNeg, and the cells were assessed at 72 hours after the transfection. The sub G1 population consists of apoptotic and necrotic dead cells. However, it is likely that the population in cells transfected with siNeg is only necrotic dead cells. Hence, the percentage difference between samples transfected with siMYCN and siNeg indicates the approximate percentage of apoptotic dead cells.

In SK-N-BE(2), apoptosis was induced by siMYCN with a dose dependent manner while the percentages of G1 populations are varying among different experiments and therefore, the error bars were high (Fig. 3.3.12.a). 50 nM siMYCN treated cells achieved approximately 15% apoptotic dead cells which was the highest percentage of apoptotic dead cells in the 4 different concentrations. The population of apoptotic cells at 20 nM siMYCN was 12%, at 10 nM was 10% and at 5 nM was 2%. None of the cell populations transfected with siMYCN was statistically different from those of both siNeg at the same concentration and untransfected negative control.

In Kelly, siMYCN induced apoptosis in the cell line with a dose independent manner whilst the error bars were high at 20 nM, 10 nM and 5 nM, and therefore, they are not statistically different between siMYCN and siNeg, and among these 3 concentrations of siMYCN (Fig. 3.3.12.b). On the other hand, 50 nM siMYCN achieved 9.0% higher apoptosis, compared

with 50 nM siNeg. The 50 nM siMYCN-treated cells showed statistical significant differences when compared to 50 nM siNeg-treated cells and UT ctrl cells ($p= 0.018$ and 0.0019 , respectively).

In addition, Caspase-3/7 assay was performed in SK-N-BE(2) and Kelly transfected with 50 nM or 10 nM of siMYCN or siNeg using RNAiMAX (Fig.3.3.12.c,d). The cells were incubated for 48 hours after t transfections, and luciferase assay was performed to measure caspase-3/7 activity (see details in Section 2.2.25.). As a result, there were no significant differences between siMYCN and siNeg, and siMYCN and UT ctrl at any concentration in SK-N-BE(2) and at 50 nM in Kelly. In Kelly, there was a significant difference between 10 nM siMYCN and UT control ($p=0.0071$) but there was also a significant difference between 10 nM siNeg and UT control ($n=0.00016$). Therefore, it is not likely that the difference between 10 nM siMYCN and UT control in Kelly shows apoptosis induced by siMYCN.

This results suggests that siMYCN may not be able to induce apoptosis in SK-N-BE(2) cells. Kelly cells with a dose of 50 nM or potentially higher needed to obtain significant differences, according to the PI staining data, but Caspase-3/7 assay did not show siMYCN-induced apoptosis at any concentration in either SK-N-BE(2) or Kelly cells.

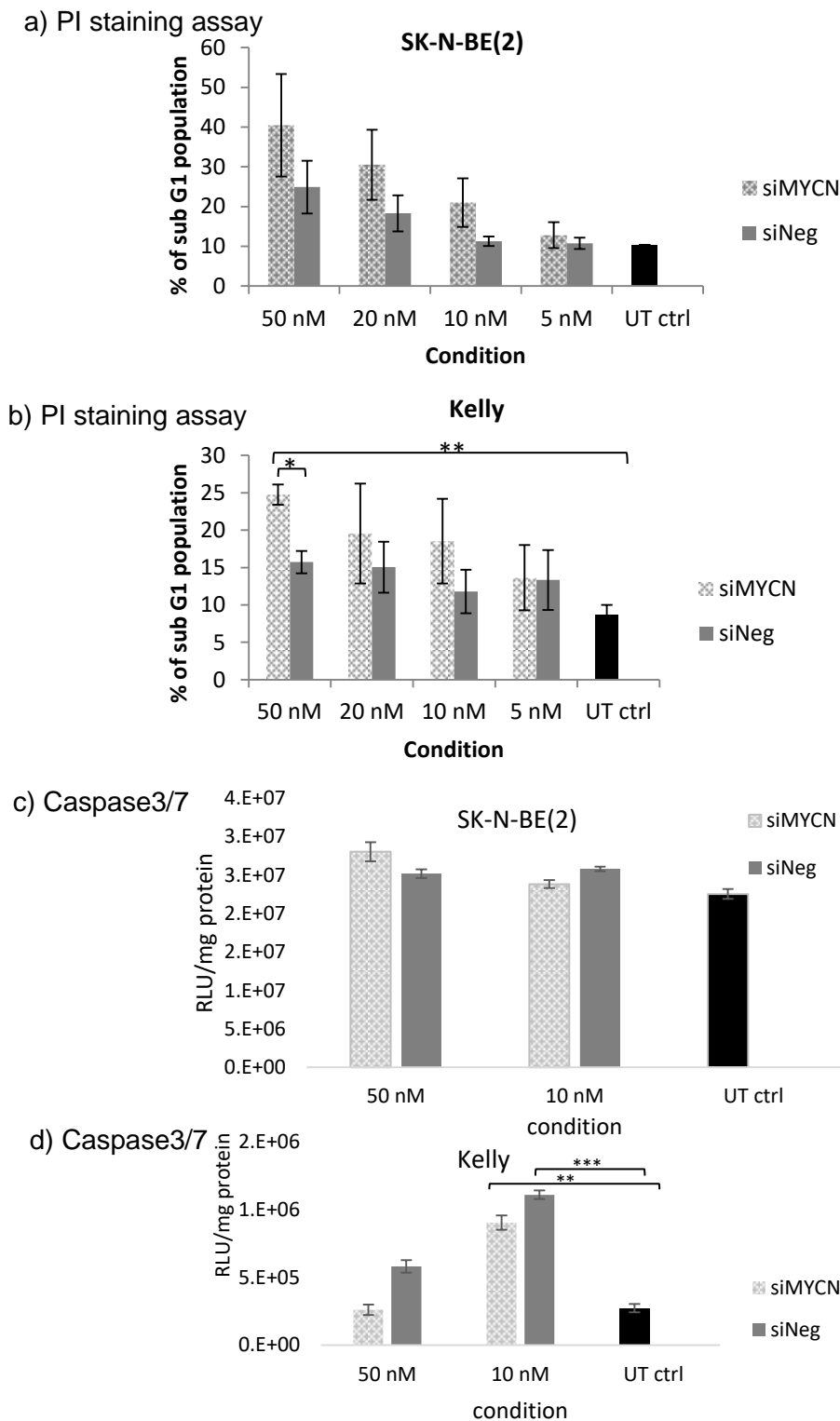


Fig. 3.3.12. Sub G1 assay using PI staining and Caspase 3/7 assay. Percentage of Sub G1 population was observed using PI staining by flow cytometry. **a)** SK-N-BE(2) and **b)** Kelly cells were treated with siMYCN or siNeg, and were harvested 72 hours later. Both siMYCN and siNeg increased the sub G1 population with a dose dependent manner while it showed clear difference between siMYCN and siNeg in some comparisons in Kelly cells. Caspase3/7 assay was performed using **c)** SK-N-BE(2) and **d)** Kelly. There were not significant differences among siMYCN, siNeg and UT ctrl. In all the graphs each column represents the mean \pm SD. * $p < 0.05$, ** $p < 0.01$, *** $p < 0.001$

3.3.10. MYCN and NCYM gene silencing by siNCYM and NCYM RNA silencing by siMYCN

Suenaga et al. (2014) reported that NCYM RNA is co-amplified with MYCN in MYCN amplified NB cells, and the two genes enhance the expression levels of each other. Furthermore, Suenaga et al (2014) pointed out that NCYM RNA was reduced as much as MYCN mRNA by shMYCN in a human neuroblastoma cell line CHP134. Their data suggested that a putative E-box is located just 2 base pairs upstream of the transcript start site of the NCYM gene and MYCN activates NCYM transcription, and therefore, shMYCN can indirectly silence NCYM RNA (Suenaga et al. 2014).

We investigated the silencing efficiency of NCYM by siMYCN in SK-N-BE(2) and Kelly cells and found that siMYCN at 20 nM, 10 nM and 5 nM silenced NCYM RNA in both cell lines but not when 50 nM were used. The silencing efficiencies of NCYM achieved were 4.6-15.4% in SK-N-BE(2) and 7.2-38.8% in Kelly cells (Fig. 3.3.13.a, b).

To investigate the ability of siNCYM to silence NCYM RNA, and MYCN mRNA and to upregulate NTRK1, SK-N-BE(2) cells were transfected with 50 nM, 20 nM, 10 nM and 5nM siNCYM and siMYCN using RNAiMAX (1:1 volume ratio), and were incubated for 48 hours. siNCYM decreased NCYM RNA dramatically and achieved 79-92% silencing (n=4) (Fig. 3.3.14.a). The efficiency was significantly different between siNCYM and siNeg treated cells at all concentrations ($p < 0.0001$). On the other hand, MYCN silencing by siNCYM was lower; with 20 nM and 5 nM siNCYM achieving 5-8% knock down of MYCN mRNA while 50 nM and 10 nM did not show any reduction. Only the 20 nM siNCYM silencing of MYCN was statistically different from 20 nM siNeg ($p=0.0263$) (Fig. 3.3.14.b). Interestingly 5 nM siNCYM with 5 nM siMYCN silenced MYCN mRNA as much as 10 nM

siMYCN, which was approximately 80% knockdown and 4-fold higher than that of 10 nM siNCYM (Fig.3.3.14.c).

siNCYM did not significantly upregulate NTRK1 (Fig. 3.3.15.a) (n=2). MYCN silencing by siNCYM or siMYCN and siNCYM at the protein level was investigated by immunoblotting (n=2). siNCYM at 50 nM, 20 nM, 10 nM and 5 nM siNCYM with 5 nM siMYCN reduced MYCN protein level and, normalised to the value of siNeg, silencing efficiency was 18% for 50 nM siNCYM, 3% for 20 nM, 20% for 10 nM and 90% for 5 nM siNCYM with 5 nM siMYCN. While the values of siNCYM and siNeg in each concentration were not statistically significant, the trend was clear; siNCYM decreased MYCN protein. However, siNCYM at 50 nM, 20 nM and 10 nM did not upregulate pan Trk. 5 nM siNCYM seemed to upregulate Trk while it did not reduce MYCN protein. Therefore, the upregulation by 5 nM seems to be a experimental error. On the other hand, 5 nM siNCYM with 5 nM siMYCN upregulated pan Trk 1.7 times compared to untransfected negative control cells, which was higher than that achieved by 10 nM siMYCN (Fig. 3.3.15.b).

These results suggest that siNCYM significantly reduced NCYM RNA and it downregulated the MYCN protein level. In addition, it is likely that siMYCN has the ability to silence NCYM RNA in SK-N-BE(2). However, it does not appear to silence MYCN mRNA as much as siMYCN does, which agrees with the data which Suenaga et al. (2014) reported.

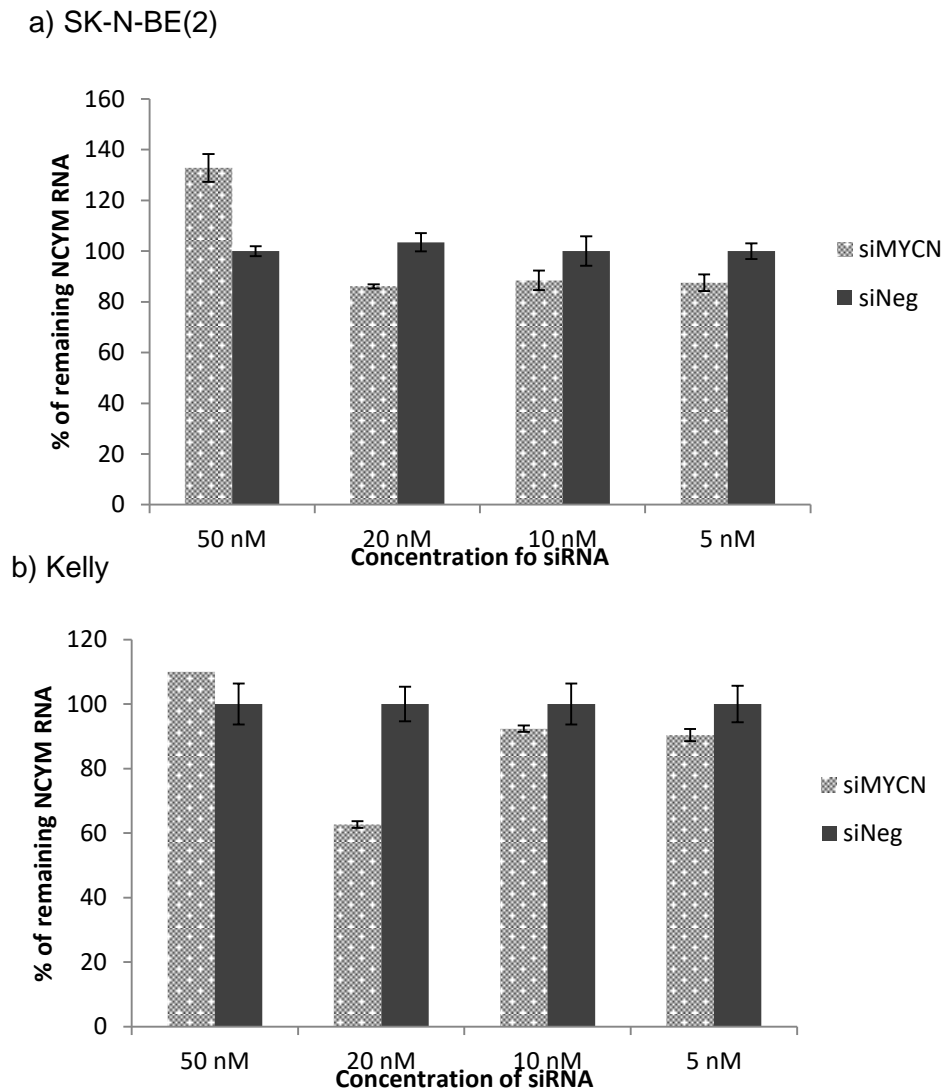


Fig. 3.3.13. NCYM RNA expression levels in SK-N-BE(2) and Kelly treated with siMYCN. siMYCN silenced 12.5-14% NCYM RNA in a) SK-N-BE(2) and 7.4-37.4% in b) Kelly at 5,10 and 20 nM. 50 nM siMYCN did not decrease NCYM RNA. (n=2) In all the graphs each column represents the mean \pm SD.

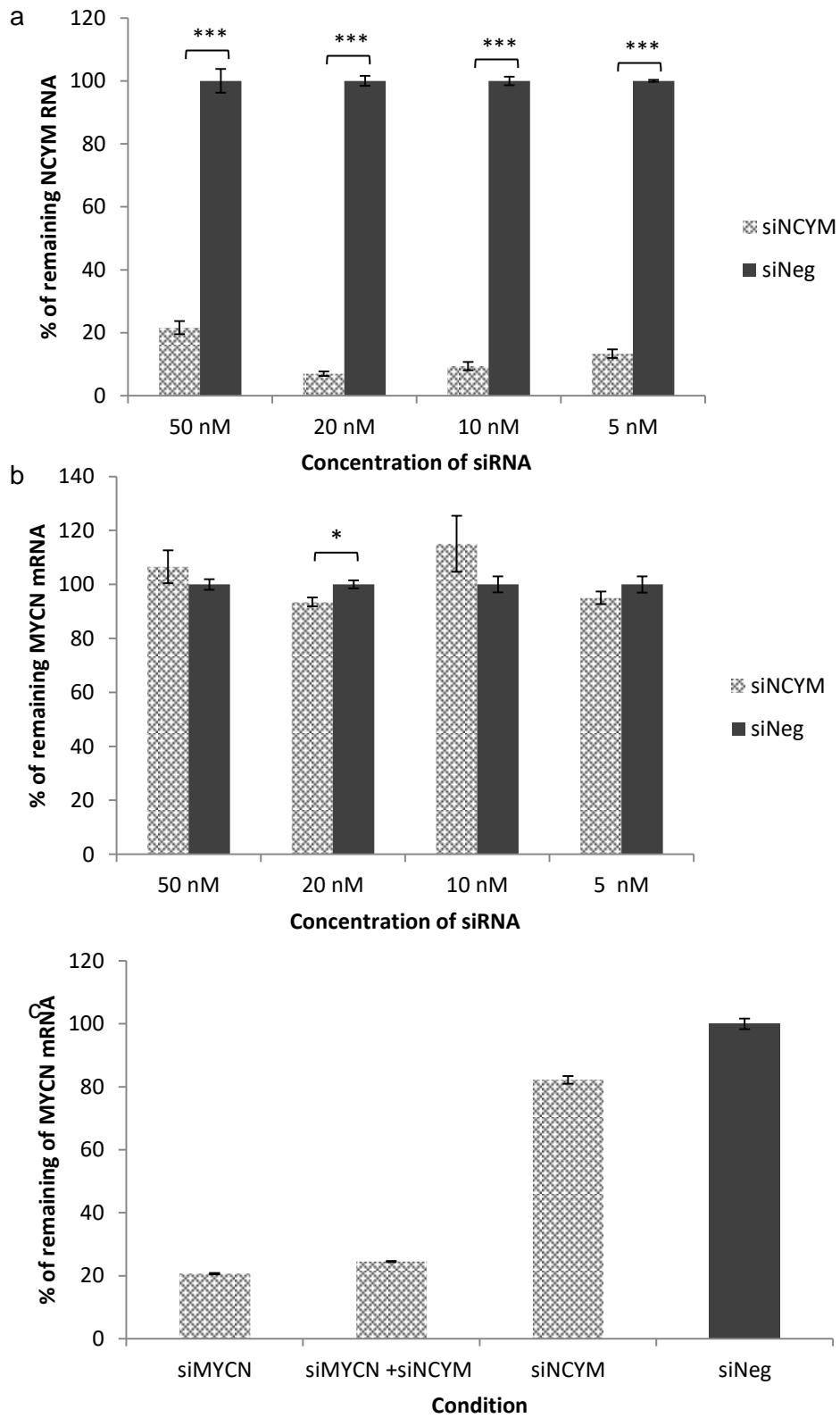


Fig. 3.3.14. NCYM/MYCN silencing by siNCYM (anti-NCYM siRNA) in SK-N-BE(2) cells. a) siNCYM achieved 78.4-93.0% NCYM RNA silencing (n=4) although b) it silenced up to 10% MYCN mRNA at 20 and 5nM. (n=4) c) MYCN silencing by 10 nM siMYCN, 5 nM siMYCN+ 5 nM siNCYM and 10 nM siNCYM (n=2) In all the graphs each column represents the mean± SD. *p<0.05, ***p<0.001

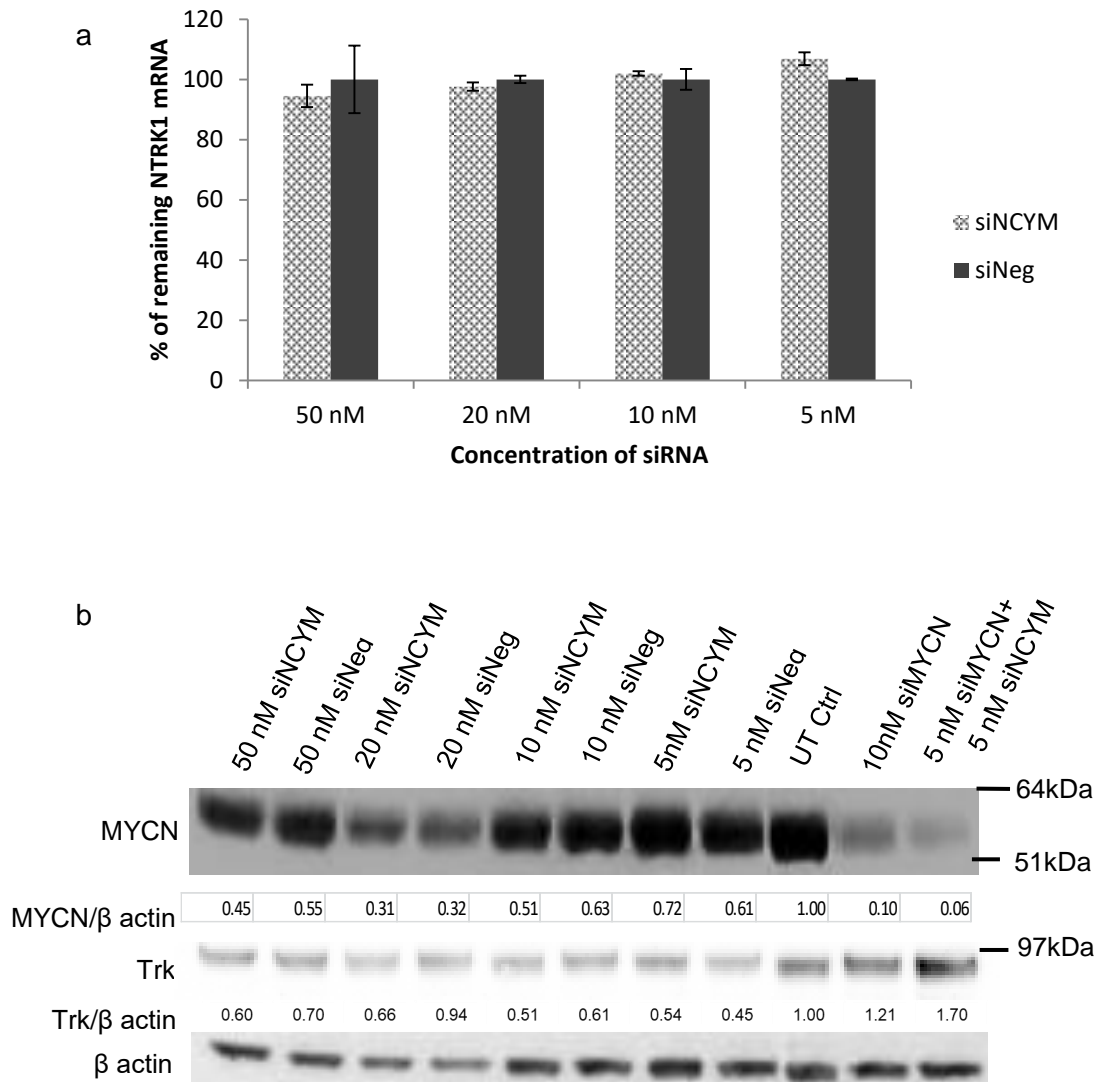


Fig. 3.3.15. NTRK1 mRNA expression and MYCN /pan Trk protein expression levels in SK-N-BE(2) treated with siNCYM The number under the band is the relative protein expression level calculated from the intensity of the band. a) NTRK1 mRNA expression levels in SK-N-BE(2) treated with siNCYM/siNeg for 48 hours as quantified by qRT-PCR. It is likely that siNCYM does not affect the mRNA expression. (n=2) b) MYCN and pan Trk expression at protein level 72 hours after siNCYM transfection. MYCN were slightly reduced while it seems that siNCYM downregulated pan Trk protein level at all the concentrations. This experiment was performed two times. In all the graphs each column represents the mean \pm SD.

3.3.11. Differentiation in SK-N-BE(2) by siNCYM

siNCYM reduced MYCN mRNA and MYCN protein expressions while the efficiency is not as high as siMYCN. We hypothesised, therefore, that siNCYM might induce differentiation in SK-N-BE(2) cells. These cells were transfected with 50 nM, 20 nM, 10 nM and 5nM siNCYM using RNAiMAX (1:1 volume ratio), then incubated for 6 days. At day 3, the transfection media was changed to complete media. As a result, siNCYM induced neurite elongation in the cell lines. However, the morphology of the neurites was not the same as in siMYCN transfected cells. Neurites induced by siNCYM were straighter and thicker and shorter than the ones by siMYCN (Fig. 3.3.9). When NB cell lines are exposed to stress such as cytotoxic reagents, some of them extend the neurites and the morphology is straight and thick as well as the shape of the cells become slightly rounder. The morphology induced by siNCYM was slightly similar to the ones induced by stress. On the other hand, the morphology of the transfected cells do become raised, smaller and rounder in shape, indicating differentiation. The neurite length in the cells transfected with siNCYM was significantly longer than those transfected with siNeg at all concentration tested at both days 2 and 6 (Fig. 3.3.17.a). However, the length difference between day 2 and day 6 were approximately 0.001-0.003 $\mu\text{m}/\mu\text{m}^2$ cell area and the length became longer between day 2 and day 6 in cells transfected with 50 nM, 20 nM and 5 nM siNCYM. However, the ones transfected with 10 nM siNCYM became shorter from day 2 to day 6. In addition, the concentration differences of siNCYM did not make differences in the neurite length.

The number of the neurites per cell area at day 2 and day 6 was also quantified. While there was a significant difference between the one treated with siNCYM and siNeg at all the concentrations, the number was the almost the same at 20 and 50 nM between day 2 and day 6. The number of neurites at day 6 was slightly more than at day 2 by 0.00007 at 5 nM and 0.00004 at 10 nM.

Overall, it is likely that siNCYM can induce modest differentiation in SK-N-BE(2) although morphological differences are not as significant as those obtained by siMYCN. However, the differences between siNCYM and siNeg were statistically different at all the 4 different concentrations.

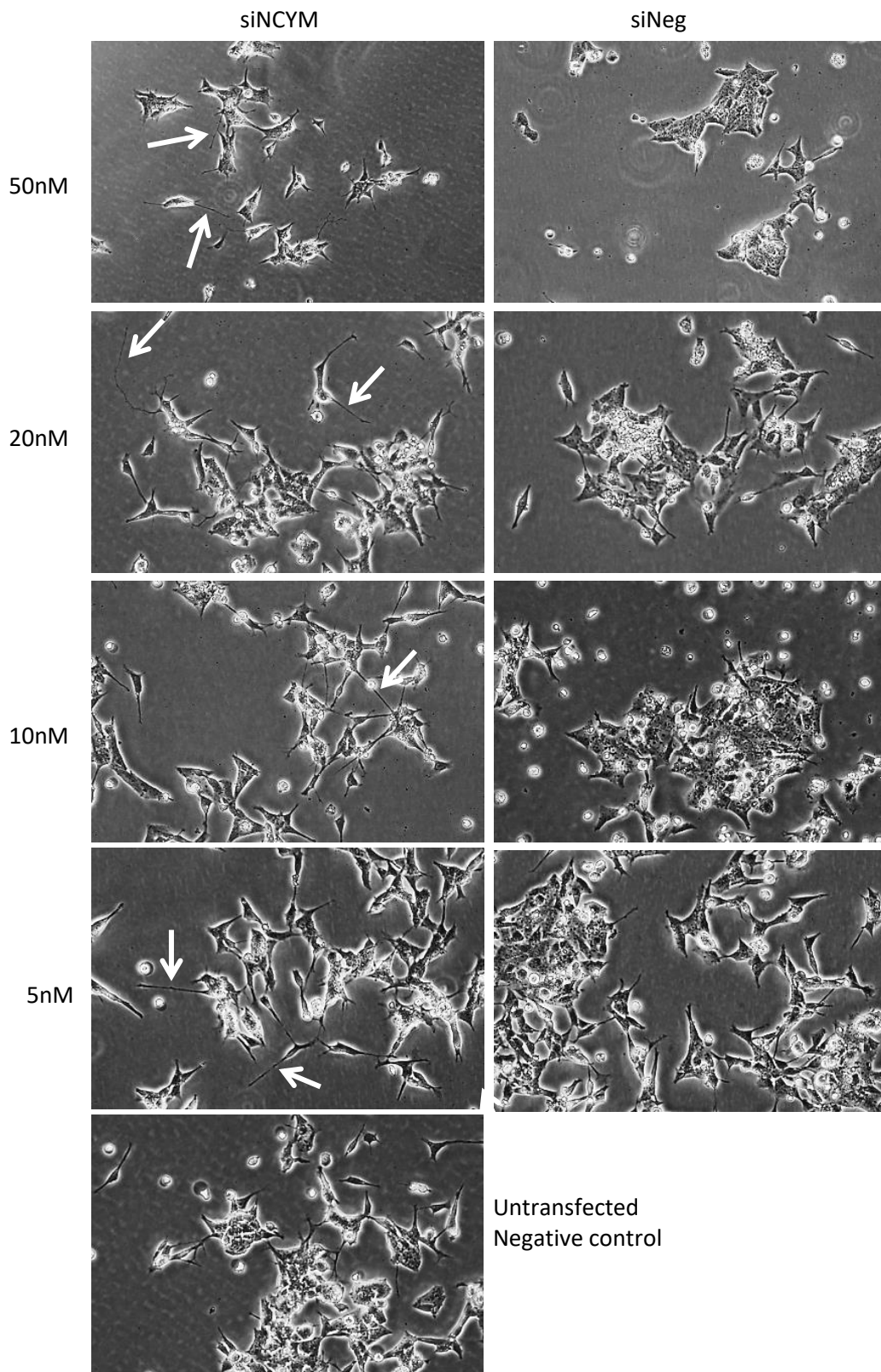
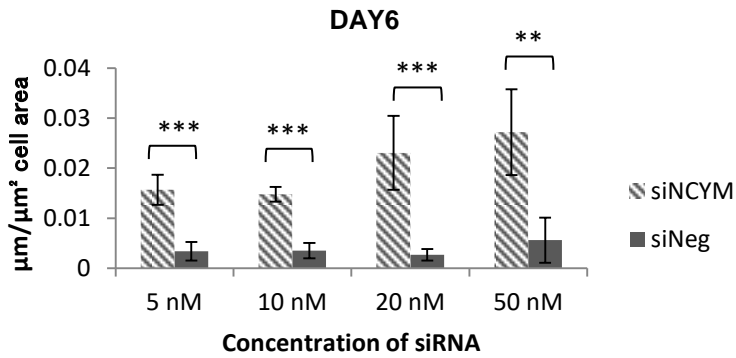
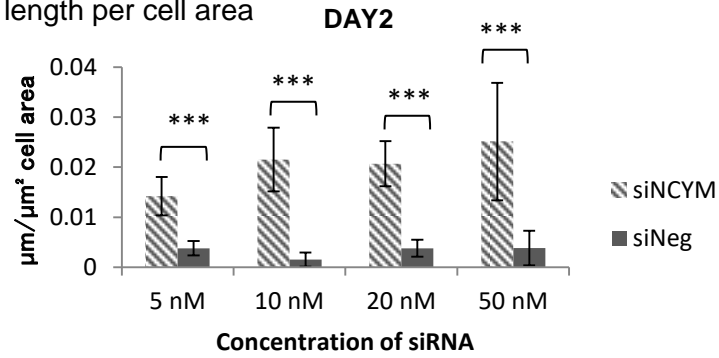


Fig. 3.3.16. Morphology changes of SK-N-BE(2) cells transfected with siNCYM
 siNCYM induced differentiation in SK-N-BE(2). The morphology of the neurites was different from the ones differentiated by siMYCN (white arrows). The number of the extended neurites was clearly different from the ones treated with siNeg. Therefore, it was concluded that siNCYM induced differentiation. The images of the morphology change induced by siMYCN are Fig. 3.3.9.

a) The neurite length per cell area



b) The number of the neurites per cell area

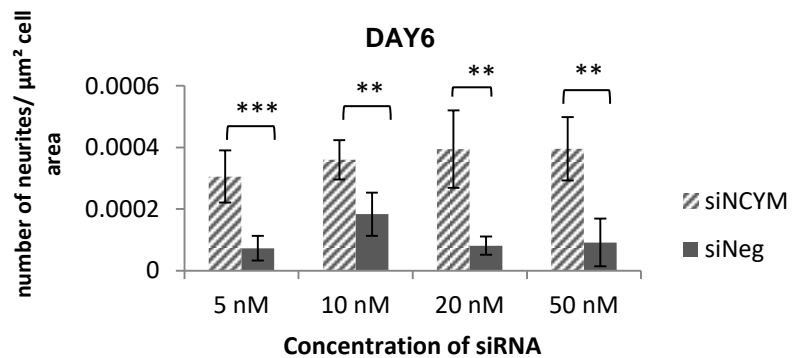
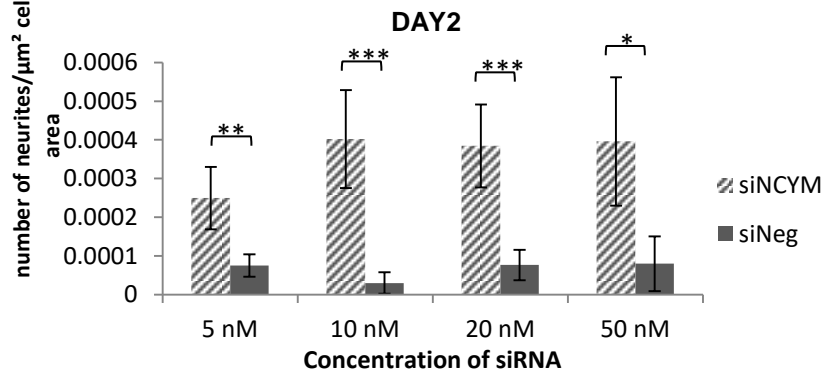


Fig. 3.3.17. The neurite length and the number of the neurites per cell area induced by siNCYM at day 2 and day 6 Quantified data of Fig. 3.3.16. **a)** The total neurite length were normalised by the total of the cell area per image. **b)** the total number of the neurites normalised by total cell area. (n=10) In all the graphs each column represents the mean \pm SD. *p<0.05, **p<0.001, ***p<0.0001

3.3.12. Cell viability (cytotoxicity) assay

To investigate the toxicity of siMYCN and siNeg transfections, we then, performed cell viability assays in siMYCN and siNeg transfections using RNAiMAX at 50 and 10 nM in SK-N-BE(2) cells (Fig. 3.3.19). As a result, 50 nM siMYCN and siNeg were significantly toxic, and the intensities were 0.36 and 0.42, respectively and the value of 50 nM siMYCN was significantly different from the ones of 10 nM siMYCN and untransfected control cells, and the p values were 0.00181 between 50 nM siMYCN and 10 nM siMYCN, and 0.000442 between 50 nM siMYCN and untransfected control cells. In addition, the values between 50 nM siNeg and untransfected control cells were also statistically different with $p=0.00154$. On the other hand, there were no significant differences between 10 nM siMYCN and untransfected control cells, and 10 nM siNeg and untransfected control cells. These results suggest that cells treated with 50 nM siMYCN with RNAiMAX decrease the viability due to the toxicity of the transfection, rather than MYCN reduction, while cells treated with 10 nM siMYCN were as viable as untransfected control cells.

These results suggest that siRNA transfections at 50 nM using RNAiMAX were significantly cytotoxic and decreased cell viability, while siRNA transfections at 10 nM did not affect or slightly affected cell viability. There was no significant difference between 10 nM siRNA treated and untransfected cells.

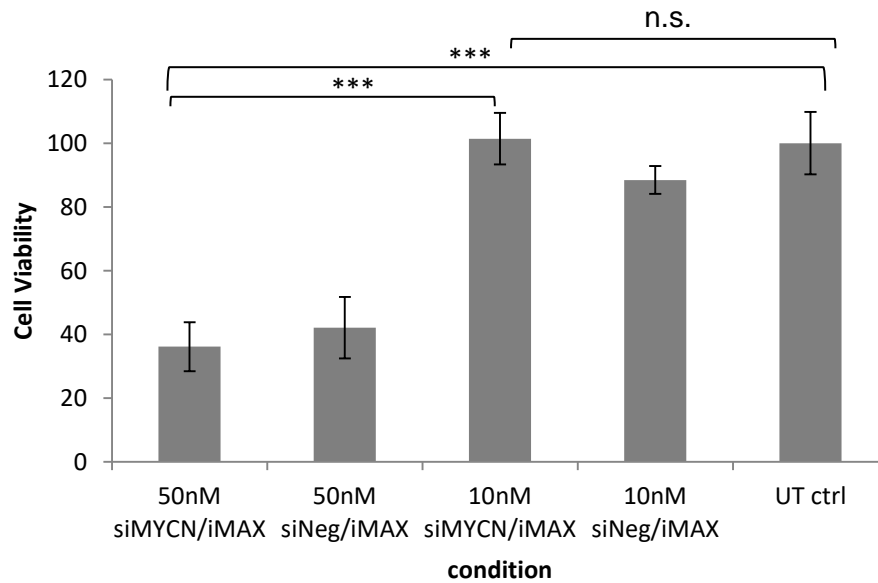


Fig. 3.3.18. Cell viability (toxicity) assay Cell viability of SK-N-BE(2) cells treated with 50 nM or 10 nM siMYCN/siNeg were assessed using MTS assay reagent. SiRNA transfection at 50 nM using RNAiMAX was notably toxic while the cell viability of the cells treated with 10 nM was almost the same or slightly lower (statistically non-significant) to the one of untransfected negative control cells. The intensity was normalised to untransfected negative control cells. (n=5) In all the graphs each column represents the mean± SD. ***p<0.001

3.3.13. Suppression of cell proliferation by siMYCN and siNCYM

In MYCN amplified NB cells, overexpressed MYCN induces proliferation and cell growth. To use siMYCN for therapeutics, the ability to suppress proliferation is critical. We performed proliferation assays using a cell counting assay kit -8 (CCK-8) after siMYCN and siNCYM were transfected into SK-N-BE(2) cells. Firstly, the ability of 20 nM siMYCN/siNeg, 5 nM siMYCN/siNeg and untransfected controls were compared at 3 time points after transfection: at 24 h, 48 h and 72 h (n=3) (Fig.3.3.20.a). SiRNA transfection slowed down the growth rate of the treated cells and 20 nM siMYCN particularly suppressed proliferation. At 24 hours, there was no significant difference between the different concentrations of MYCN siRNA and untransfected controls. At 48 hours, there was a difference between 20 nM siMYCN and untransfected control cells. Although 20 nM siMYCN suppressed the cell growth more than that treated with 20 nM siNeg, it did not reach statistical significance. At 72 hours, the number of the cells treated with siMYCN was lower than any other condition. 20 nM siNeg slowed down the cell growth at almost the same level to the one by 5 nM siMYCN/siNeg. The difference between 20 nM siMYCN and siNeg, and 20 nM siMYCN and untransfected control cells were statistically significant ($p=0.049$ and 0.0062 , respectively).

Secondly, we compared cell growth after transfections with 10 nM siMYCN, siNCYM, 5nM MYCN + 5 nM NCYM, 10 nM siNeg and untransfected control cells (n=3) (Fig. 3.3.20.b). The growth rate of each condition was measured at days 0, 1, 2 and 3. The values of each condition at different time points were normalised by the value of the same condition at day 0 and therefore, all values at day 0 were set as 1. SiRNA transfections slowed down the growth rate in this experiment again. 10 nM siMYCN suppressed the proliferation during the 3 days, and the cell growth rate was remarkably different, compared with siNeg at day 1 ($p=0.00084$), day 2 ($p=0.000011$) as well as untransfected control cells at day 1 ($p=0.00021$),

day 2 ($p=0.0044$) and day 3 ($p=0.037$). 5 nM siMYCN+5 nM NCYM slowed down the growth rate at day 1, compared with 10 nM siNCYM, siNeg ($p=0.0060$) and untransfected control ($p=0.000069$), and the rate, however, became faster after day 2 and it was almost the same level as that in siNCYM and siNeg. On the other hand, the growth rate in 10 nM siNCYM were almost the same as that in siNeg during the 3 days although it was statistically different from siNeg only at day 1 ($p=0.0025$).

These results show that 10 nM or higher concentrations of siMYCN are likely to suppress proliferation in SK-N-BE(2), while siNeg also can suppress it. However, there is a clear difference of growth rate between siMYCN and siNeg, and therefore, we concluded siMYCN could be used to decrease cell growth rate. In addition, it seems that siNYCM cannot decrease the cell growth rate.

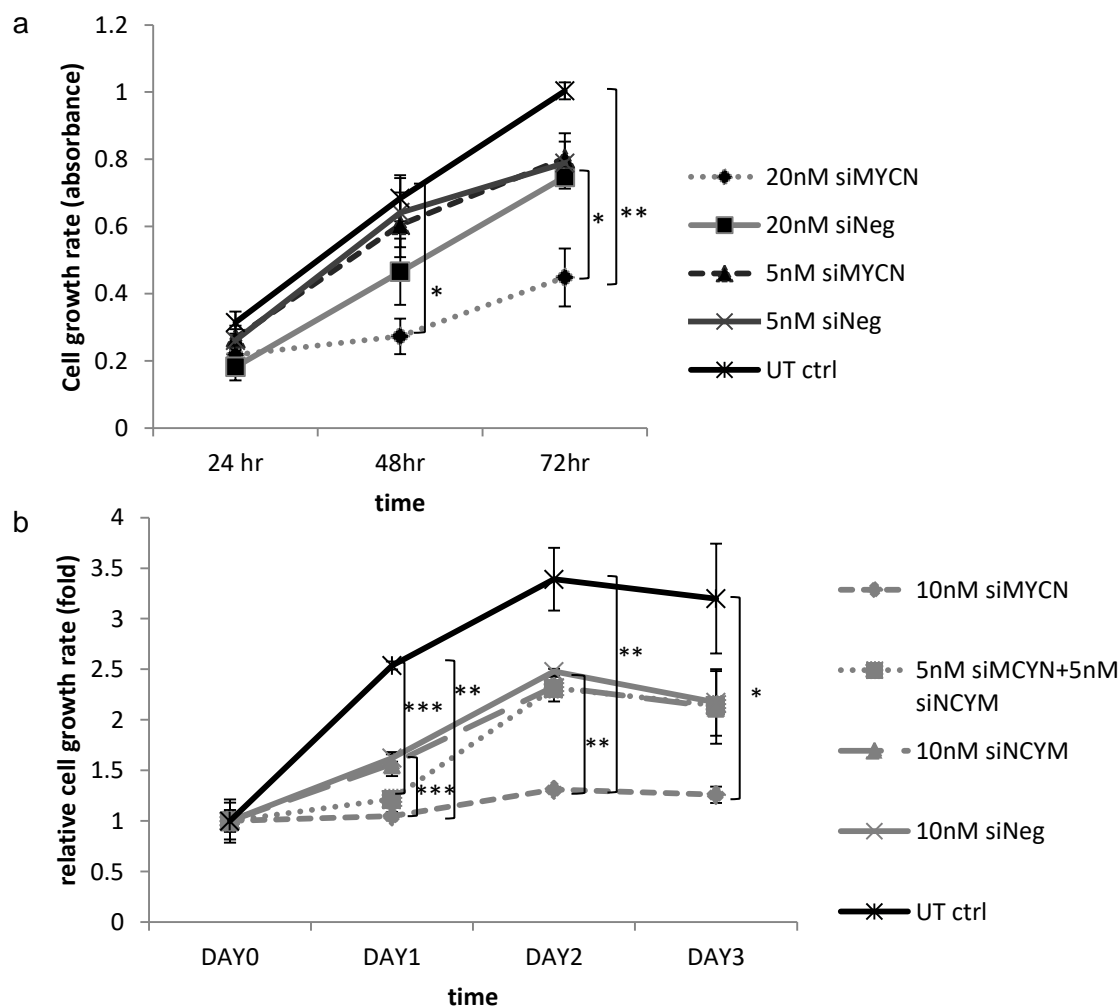


Fig. 3.3.19. Suppression of proliferation by siMYCN and siNCYM in SK-N-BE(2) cells SK-N-BE(2) cells were treated with siMYCN/siNCYM, and the cell growth rates were measured using the CCK-8 assay reagent at 3 or 4 time points. a) The cells were seeded at 1.5×10^4 cells per well, and treated with 20 nM or 5 nM siMYCN/siNeg. 20 nM siMYCN significantly suppressed the cell growth from 48 hours. b) The cells were seeded at 1.0×10^4 per well, and were treated with 10 nM siMYCN, siNCYM or siNeg or 5 nM siMYCN+5 nM siNCYM. 10nM siMYCN remarkably reduced the growth rate during the 3 days. (n=3) * $p < 0.05$, ** $p < 0.01$, *** $p < 0.001$

3.4. Discussion

The aims in this chapter were to investigate the ability of siRNA targeting MYCN and NCYM to silence MYCN, and whether the MYCN knockdown induces downstream effects such as up/downregulation of genes targeted by MYCN and differentiation of the NB cells.

Nara et al. (2007) previously showed that MYCN silencing induces apoptosis and differentiation including neurite extension, as well as NTRK1 and NTRK3 (TrkC) mRNA upregulation in MYCN-amplified NB cell line NB-1. Similarly, Kang et al. (2006) also reported that MYCN silencing by siMYCN, induces apoptosis in MYCN-amplified NB cell lines (LAN-1 and IMR-32) and differentiation in BE(2)-C, LAN-1 and IMR-32 cells as well as upregulation at protein level of a neuronal differentiation marker, neuron specific enolase (NSE) . However, the two studies have not quantified the neurite length and the number of the neurites induced by siMYCN. Furthermore, these studies have not been shown Trk upregulation at protein level and down/upregulation of genes targeted by MYCN. Here, we performed experiments to address these shortfalls in NB, MYCN-silenced cells.

We firstly characterised four different NB cell lines: SK-N-BE(2), Kelly, LAN-5 and SK-N-SH at mRNA and protein levels in terms of MYCN. Among the 4 cell lines, the MYCN expression levels of both mRNA and protein in SK-N-BE(2) were the highest. Interestingly, the MYCN protein expression level in Kelly cells was lower than that in LAN5 while the mRNA level in Kelly was higher than that in LAN5. The data agree with those in Durbas et al. (2016), which showed that MYCN mRNA expression level in Kelly is approximately 2 times higher than that in LAN-5 while the MYCN protein levels in the two cells lines were the same. These results suggest that the MYCN mRNA/protein metabolism in Kelly may be different from that in the other cells. For example, MYCN protein in Kelly cells may be degraded faster than in SK-N-BE(2) and LAN5 and the proteins that are associated with

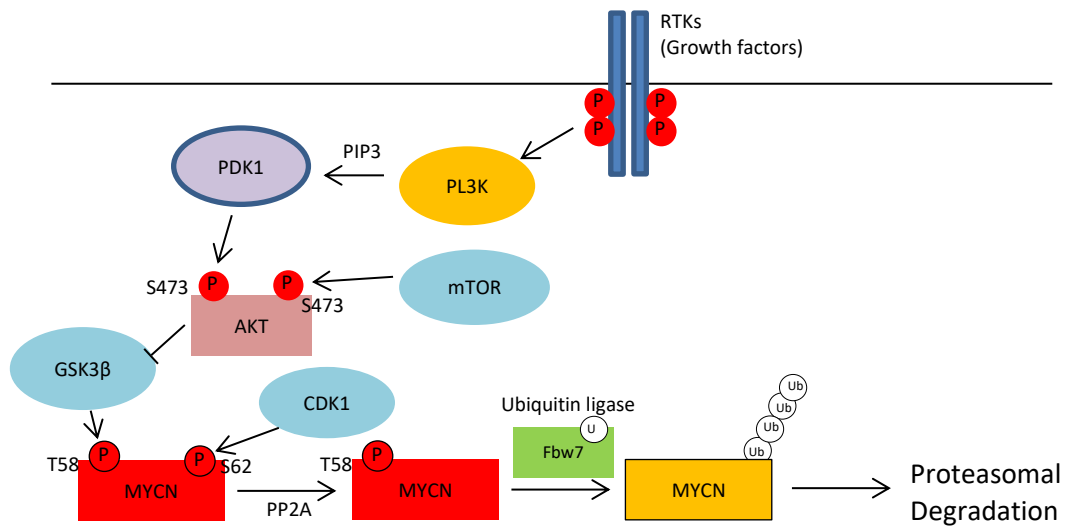


Fig. 3.4.1. MYCN protein stability and proteasomal degradation PL3K/AKT pathway promotes stability of MYCN protein via GSK3β inactivation. GSK3β and Fbw7 are associated with MYCN proteasomal degradation. Fbw7 is an ubiquitin ligase which drives ubiquitination. (modified from Barone et al 2013)

the degradation of MYCN protein such as GSK3β and Fbw7 are more active, or the ones stabilising MYCN protein such as the PL3K/AKT pathway are less active in Kelly than the other NB cells (Fig. 3.4.2)

RNAiMAX is a widely-used, commercially-available, liposome-based transfection reagent. The transfection efficiency is consistently high although it is toxic at higher concentrations (Fig.3.3.2). The percentages of the dead cells and live cells in each concentration of siRNA, which are shown in Fig.3.3.2.c, agreed with those seen under a microscope when cell morphology and confluency were checked before harvesting the cells 48 hours after transfection. Hence, the cellular uptake efficiency measured using flow cytometry is likely to be reliable. Furthermore, the MFI changed during the 48 hour incubation. A possible reason is cytotoxicity of higher concentration of siRNA. It can be considered that the cells took more siRNA and the intensity was the highest at increasing concentrations, compared with

those at lower concentrations. However, too much uptake was toxic for the cells and many cells were dying during the 48 hour time period. On the other hand, cells taking up less siRNA survived better at the 48 hour time point. Therefore, the cells at 10 nM and 5 nM were probably growing and the fluorescent intensity was diluted.

RA is well-known as a differentiating agent, and it is used for high-risk neuroblastoma for controlling minimal residue after high-dose chemotherapy (Hämmerle et al. 2013; American Cancer Society website). We treated the 4 NB cell lines SK-N-SH, LAN-5, SK-N-BE(2) and Kelly with RA to compare the ability of RA and siMYCN to induce differentiation in the cell lines. The 4 NB cell lines reacted differently towards RA treatment: SK-N-SH and LAN-5 showed morphological characteristics of differentiation by RA while SK-N-BE(2) and Kelly did not show a clear response and significant morphology changes were not seen in either of these cell lines. SK-N-BE(2) did not appear to respond towards RA. However, a sub-clone cell line of SK-N-BE(2) named SK-N-BE(2)-C (Memorial Sloan Kettering Cancer Center), and another reported by Andres et al. (2013), BE(2)-M17, are differentiated in morphology by RA. These data may suggest that SK-N-BE(2) cells consist of mixed populations and there are cells responding towards RA.

Westmarke et al. (2011) mentioned that RA targets the retinoic acid receptor/retinoic X receptor (RAR/RXR) in normal neuronal cells and that RA induces differentiation in both MYCN amplified and non-MYCN amplified tumour cells. In addition, MYCN downregulation was seen before RA-mediated differentiation. They pointed out that these results suggested that RA may directly regulate MYCN expression at transcription level (Westmarke et al. 2011). Furthermore, Haskell et al. (1987) reported that RA induced morphological differentiation and increased TrkA expression in LAN-1 cells. Iraci et al. (2011) found that MYCN downregulates TrkA expression by forming a repression complex

with transcription factors SP-1 and MIZ-1 at the core promoters of TrkA, and the complex recruits the histone deacetylase HDAC1 to suppress the transcription.

In SK-N-BE(2), as it was mentioned above, probably only a small percentage of the cells can respond towards RA treatment, which agrees with the data in Joshi et al. (2007), which is why we found that RA achieved approximately 10% MYCN silencing only. On the other hand, we successfully demonstrated that siMYCN was able to drastically induce morphological differentiation in SK-N-BE(2), which has resistance towards RA and anti-cancer drugs depending on the p53 pathway. Our data showed that siMYCN silenced MYCN and upregulated Trk at mRNA and protein levels. Furthermore, the morphology changes in the neurites and the cells are another strong evidence which shows the SK-N-BE(2) cells were indeed differentiated.

RA is a powerful chemotherapeutic drug to differentiate NB cells without RA resistance. However, the response of NB cells towards RA treatment is not homogeneous as NB is a heterogeneous disease. Our data suggest that siMYCN might be promising for a therapy in cases of NB with resistance towards RA and drugs relying on the p53 pathway, as observed with SK-N-BE(2) cells.

In addition, SK-N-BE(2) cells treated with siNCYM also showed evidence of differentiation although the morphology of the neurites was different from that of cells transfected with siMYCN, while NTRK1 and Trk were not upregulated by siNCYM. We concluded that the cells were differentiated because the total length per cell area induced by siNCYM was significantly longer than that by siNeg (Section 3.3.11). There is another pathway to induce differentiation, the estrogen receptor alpha (ER α) pathway, which is upregulated by MYCN reduction. If this pathway was upregulated by siNCYM, it could be a reason why neurite elongation was induced by siNCYM transduction in SK-N-BE(2) without Trk upregulation.

However, the correlation between siNCYM treatment and the pathway is unknown. Therefore, it is necessary to investigate the mechanism of the differentiation pathways and the morphological differentiation.

Interestingly, Kelly cells did not show any significant morphological changes after either RA or siMYCN treatments even though NTRK1 and pan Trk were significantly upregulated by siMYCN (not assessed though in Kelly cells treated with RA). Henriksen et al. (2011) showed that Kelly cells differentiated after retrovirally transduction with MYCN shRNA at the 3 day time point and the silencing efficiency was approximately 45%, which is similar to our efficiency. Therefore, Kelly has the ability to differentiate and change morphologically by siMYCN treatment as well as possibly RA treatment, however, it was not observed in our experiments. It is not known whether it is due to the shorter incubation duration after siMYCN transfection in our experiments or it is due to other differences in experimental conditions or cells, including the passage number. To observe the correlation among MYCN downregulation and Trk upregulation by RA or siMYCN and Trk upregulation and morphological modifications, further experiments may be required.

We performed qRT-PCR and immunoblotting to assess TP53 and MDM2 expression levels at the mRNA and protein levels, respectively. We expected that p53 would be upregulated when amplified MYCN was silenced by siMYCN because p53 is suppressed by MDM2, which is upregulated by MYCN (Huang & Weiss 2015). qRT-PCR successfully showed that TP53 was upregulated by siMYCN-mediated MYCN silencing in Kelly, although it was downregulated in SK-N-BE(2). In LAN-5, there were no significant differences in the amount of TP53 and MDM2 among the cells treated with the 4 different siMYCN concentrations, because the amount of MYCN silencing by siMYCN probably did not reach the level which can cause downstream effects. Unfortunately, neither TP53 nor MDM2

could be assessed by immunoblotting due to the quality of the antibodies but this should be done in the future.

It was reported that Kelly cells are mutated for TP53 (Gogolin et al. 2013) while other researchers claim that it is wild type for TP53 (Afanasyeva et al. 2011, Shahbazi et al. 2014). According to van Maerken et al. (2011), TP53 in Kelly cells has a point mutation in codon 177, which converts proline to threonine. Our qRT-PCR showed TP53 was upregulated by siMYCN, while MDM2 was not significantly downregulated. This result may imply that the MDM2-p53 pathway is functional.

SK-N-BE(2) has non-functional p53 (Keshelava et al. 2001) due to a point mutation at codon 135 on p53 with the consequence that a cysteine is converted to phenylalanine (Goldschneider et al. 2006). Interestingly, the qRT-PCR data showed that MDM2 and p53 were downregulated by siMYCN, while p53 was supposed to be upregulated by MYCN and MDM2 reduction in normal cells. One possible explanation of this result is that siMYCN-mediated MYCN silencing decreased MDM2 as MYCN upregulates MDM2, however, the pathway to upregulate p53 by MDM2 silencing may not have worked because of the DNA damage in SK-N-BE(2) by radiotherapy and chemotherapy. Tweddle et al. (2001) also reported that p53 and MDM2 in SK-N-BE(2) did not react toward irradiation treatment while wild type p53 increased after DNA damage and MDM2 increased at 4 hours after the treatment in SK-N-BE(1), another NB cell line sampled from the same patient before chemotherapy sessions. Our data and the results in Tweddle et al. (2001) suggest that SK-N-BE(2) may not apoptose via the p53-dependent pathway even though it is treated with siMYCN.

Then, we carried out a PI staining assay to assess the ability of siMYCN to induce apoptotic death in the NB cell lines. Overall, the results of the PI staining assay did not always agree

with the percentage of dead cells seen under a microscope before the cells were harvested. That is because it is difficult to collect and not to lose the small fragments of apoptotic cells through the procedure of the staining. Especially the data of the subG1 population/PI staining in SK-N-BE(2) were underestimated and with high variability leading to large error bars. However, more than 50% of the cells treated with 50 nM siMYCN that were checked under a microscope and the percentages of dead and live cells counted were similar to the percentages in the data measured by flow cytometry in Fig.3.3.3.c. In addition, the supernatant was discarded in the data of Fig.3.3.3.c, and therefore, it is likely that the percentages in the data are also underestimated.

Even though the data of PI staining/sub G1 assay may not be accurate, there were consistent differences in the percentages between siMYCN and siNeg treated cells in both SK-N-BE(2) and Kelly cells and the difference may be regarded as apoptotic dead cells. In SK-N-BE(2), they were induced by a p53-independent pathway. However, the pathway to trigger apoptosis after siMYCN mediated MYCN reduction is unknown, and further studies are required to reveal this pathway. In addition, it may be useful to find another target for apoptosis induction via p53-independent for anticancer therapy.

We conducted siNCYM transfections to assess the ability of the siRNA to reduce MYCN at mRNA and protein levels and to upregulate Trk and induce morphological differentiation. While Armstrong and Krystal (1992) firstly described NCYM mRNA, it has been unclear whether it codes for a functional protein. Suenaga et al. (2014) firstly reported that mRNA of NCYM indeed codes for a functional protein and proposed that the protein stabilises MYCN protein via inhibition of GSK3 β , a kinase promoting MYCN degradation. Therefore, the shRNA-mediated silencing of NCYM downregulated MYCN protein although MYCN mRNA was not reduced. In addition, MYCN overexpression enhances NCYM promoter activity and so siMYCN decrease NCYM mRNA (Suenaga et al. 2014).

Our data partially agreed with their data in that siMYCN reduced NCYM mRNA in both SK-N-BE(2) and Kelly cells and siNCYM at 50 nM, 20 nM and 10 nM decreased MYCN protein although the silencing level was lower than that in Suenaga et al. (2014). One possible reason for the disagreement in the silencing level is the use of different cell lines, as mentioned in the Results (Section 3.3.10). The Suenaga research group used CHP134 cells and Durbas et al. (2006) showed that the cell line expresses about 60% of MYCN mRNA and 1.1 times less MYCN protein than Kelly cells and therefore, it might be easier to silence the MYCN mRNA and protein in CHP134 compared to Kelly cells.

On the other hand, Liu et al. (2016) recently reported that their NCYM siRNA (purchased from Qiagen) silenced MYCN by approximately 50% in SK-N-BE(2)-C. In addition, another research group showed MYCN mRNA and protein knockdown by NCYM shRNA in SK-N-BE(2)-C (Zhao et al. 2016). Importantly, one of the NCYM shRNAs in Zhao et al. (2016) is targeting the same region on NCYM mRNA as the one targeted by anti-NCYM shRNA in Suenaga et al. (2014) as well as our siNCYM, and therefore, the silencing efficiency of the shRNA targeting NCYM in the two groups should be the same. However, MYCN mRNA was silenced by the NCYM shRNA in Lui et al. (2016) although it was not in Suenaga et al. (2014). There is not publication in which compared SK-N-BE(2) and SK-N-BE(2)-C regarding MYCN mRNA expression level, while Huang et al. (2011) reported that the MYCN mRNA expression level in SK-N-BE(2)-C was lower than those in the other sub-clones of SK-N-BE(2), BE(2)-S and BE(2)-N. It may be possible that the differences in the response towards NCYM siRNA/shRNA resulted from the differences in the MYCN expression level between SK-N-BE(2) and the sub-cloned cell line BE(2)-C.

Furthermore, the relationship between MYCN and NCYM is still not clear. Zhao et al. (2016) mentioned that they were not able to detect the protein of NCYM even though they tried two antibodies. We also tried to detect the protein using a commercially available

antibody but it did not work and their recommended positive control cell line was a human liver cancer cell line Hep G2, which overexpresses c-Myc, rather than MYCN. NCYM co-expresses with MYCN, and therefore, we concluded the anti-NCYM antibody would not work. It is necessary to confirm whether the RNA of NCYM is coding a protein and how it stabilises MYCN protein in a further study. Zhao et al. (2016) claimed that CCCTC-binding factor (CTCF) binds with NCYM non-coding RNA and the two promote MYCN expression. On the other hand, Liu et al. (2016) reported that lncUSMycN, a novel long non-coding RNA upstream of MYCN, upregulates NCYM RNA expression and NCYM RNA post-transcriptionally upregulates MYCN by binding to the RNA binding protein NonO. The complex of NonO and NCYM RNA allows MYCN mRNA to translate and increase MYCN protein compared, with the mRNA in the normal translation. In addition, the mechanisms such as the main promoter of MYCN expression in NB cells are unknown (Zhao et al. 2016), even though MYCN is well-recognised as a good target in the therapy. There are still many studies required for understanding MYCN and the knowledge will help make gene therapy targeting MYCN more efficient and applicable to heterogeneous MYCN amplified NB cells.

In conclusion, we have successfully demonstrated that siMYCN can silence MYCN at mRNA and protein levels and that MYCN silencing induces NTRK1/Trk upregulation in SK-N-BE(2) and Kelly cells. Importantly, siMYCN and siNCYM significantly trigger morphological differentiation in SK-N-BE(2), a NB cell line that has a p53 mutation and has resistance towards RA and drug depending p53-pathway. Therefore, MYCN silencing by siRNA may provide a novel therapy for NB with drug resistance.

CHAPTER 4

Results

MYCN silencing by siRNA delivered using RTNs

4. MYCN silencing by siRNA delivered using RTNs

4.1. Introduction

RNAi induced by siRNA has been studied in various diseases *in vitro* for many purposes including developing gene therapy and investigation of the function of target genes. siRNA delivery requires the development of efficient vectors. Lipid nanoparticles have been used widely for siRNA delivery owing to their abilities to protect nucleic acids from extra- and intracellular enzymatic degradation and deliver siRNA to tissues *in vivo* (Elsabahy, Nazarali & Foldvan 2011). In addition, lipid based vehicles in cancer therapy are required to promote: 1) longer circulation times in blood without interaction with blood proteins, 2) accumulation and penetration within the tumour 3) internalisation to cells within the targeted tissues and 4) siRNA release to the cytoplasm (Xu et al. 2016).

We have developed receptor-targeting nanocomplexes (RTNs) consisting of liposome, receptor-targeting peptide and nucleic acids to deliver the RTNs to target tissues specifically. We are developing cationic, non-PEGylated RTNs *in vitro* for *in vivo* use, as cationic non-PEGylated RTNs interact with serum proteins in blood and are sensed by immune cells (Judge & MacLachlan 2008). Polyethylene glycol (PEG) is now commonly used for lipid based nanoparticle to solve these problems, PEG generates a protective hydrophilic layer on cationic liposome surface, and it changes the surface properties, decrease opsonisation by blood protein. PEG also reduces phagocytosis, called steric stabilisation effects (Allan et al. 2002; Huang et al. 2008). Those properties allow PEGylated RTNs can increase circulation time in blood, and increase opportunity that PEGylated RTNs reach target tissues (Hart 2010). On the other hand, PEGylation can prevent RTNs cellular uptake (Huang et al. 2010; Mishra et al. 2004) and siRNA endosomal escape (Oliveira et al. 2015). PEG also might not sufficiently protect siRNA against enzymatic degradation (*ibid*).

In our group, for the endosomal escape of siRNA, there is a cleavable linker in integrin receptor targeting peptide ME27 in our RTNs. The cleavable linker is degraded by the endosomal proteinases furin and cathepsin B, and it allows siRNA release to the cytoplasm. In addition, the integrin- targeting motif in peptide ME27 enables targeted delivery to specific cells.

We have also developed anionic RTNs consisting anionic liposomes, cationic peptide and nucleic acids. Anionic liposomes cannot get into cells because of the repulsion to the plasma membrane of the target cells, and only the receptor-target peptide on anionic RTNs can bind the targeted receptor. Then the RTNs are internalised via endocytosis. The internalisation of anionic RTNs is induced only when the receptor catches the receptor-targeting peptide. Therefore, anionic RTNs can specifically deliver siRNA into the target tissues while cationic RTNs can bind to unspecific cells and be internalised.

We hypothesised that the transfection/silencing efficiency (internalisation) of cationic non-PEGylated RTNs would be predicted to be higher than PEGylated RTNs. On the other hand, anionic RTNs would be delivered more specifically, compared with cationic RTNs.

4.2. Aims

We aim:

1. To screen optimal RTNs and to optimise transfection conditions in NB cells *in vitro*
2. To investigate MYCN silencing efficiency of RTNs *in vitro* and *in vivo*
3. To observe specific delivery by ME27 into NB cells *in vitro* and *in vivo*

4.3. Results

4.3.1. Differences in pDNA transfection efficiency among RTNs

We first performed DNA transfection of RTNs consisting of liposome, peptide ME27 and Luciferase pDNA in Kelly to compare the differences in transfection efficiencies of 4 different liposomes: DD (cationic, non-PEGylation), AT1 (cationic, 1% PEGylation), AT3 (anionic, 1% PEGylation) and GK25 (anionic, 5% PEGylation) (the details of the components in each liposome, see 2.1.3.2 in Material and Methods chapter). 4 hours after the transfections, the transfection media was replaced with complete media. The transfected cells were incubated for 24 hours and the lysates were extracted in order to measure the luciferase activity.

The RTN consisting of non-PEGylated DD achieved the highest RLU/mg protein in the four RTNs and it was approximately 14-times larger than that of AT1, 1% PEGylated cationic (Fig. 4.3.1.a). The efficiencies of the two anionic RTNs were 1/1000 of DD. However, the efficiency differences between cationic and anionic RTNs were not consistent in different cell lines and experiments (Fig. 4.3.1.b). The transfection efficiency of DD was approximately 10-times higher in Neuro-2A and 40-times in Kelly than those of AT3. The efficiency of another anionic RTN LPDL3, which consists of DD, ME27 and Luc pDNA covered with an outer layer of AT3 liposome was dramatically increased to levels similar to those of DD-containing RTNs in both Neuro-2A and Kelly cell lines, while the efficiency of AT3-containing RTNs was much lower than that of DD.

The data may suggest that the cationic RTNs achieve higher transfection efficiencies, compared with anionic RTNs, and PEGylation decreases the efficiency even in cationic RTNs. The double layered formulation improved the efficiency of anionic RTNs, compared with anionic single layered RTNs.

We hypothesised that anionic RTNs can specifically bind to the targeting receptors on cells because anionic RTNs are negatively charged and cannot bind to negatively charged plasma membrane on cells due to the repulsion. Only the receptor-targeting peptide in anionic RTNs can bind to the targeted receptor on cells, and the binding to cells is specific while their efficiencies are lower than those of cationic. Then we performed an experiment where three different peptides: integrin receptor targeting ME27, negative control peptides ME72 and K16 (for the details, see 2.1.4. in Materials and Methods chapter), to observe the specificity of the three peptides in cationic and anionic RTNs, DD and GK25 (anionic, 5% PEGylation) (Fig. 4.3.1.c). As a result, the efficiencies of the cationic RTNs containing DD were not significantly different among the three different peptides although they were all approximately 4-times higher than that of anionic RTNs. On the other hand, the efficiency of the anionic RTNs containing the integrin targeting peptide ME27 was significantly higher than those of RTNs with ME72 and K16 in anionic formulations.

These results may imply that the specificity of the transfections by cationic RTNs is low and they bind cells non-specifically, and therefore, their efficiencies look high. On the other hand, anionic RTNs bind targeted cells specifically while the efficiencies are lower because they can bind cells only via the interaction of the receptor-targeting peptide and the targeted receptor. However, the anionic double layered RTN LPDL3 showed higher transfection efficiency than the single layered anionic RTNs.

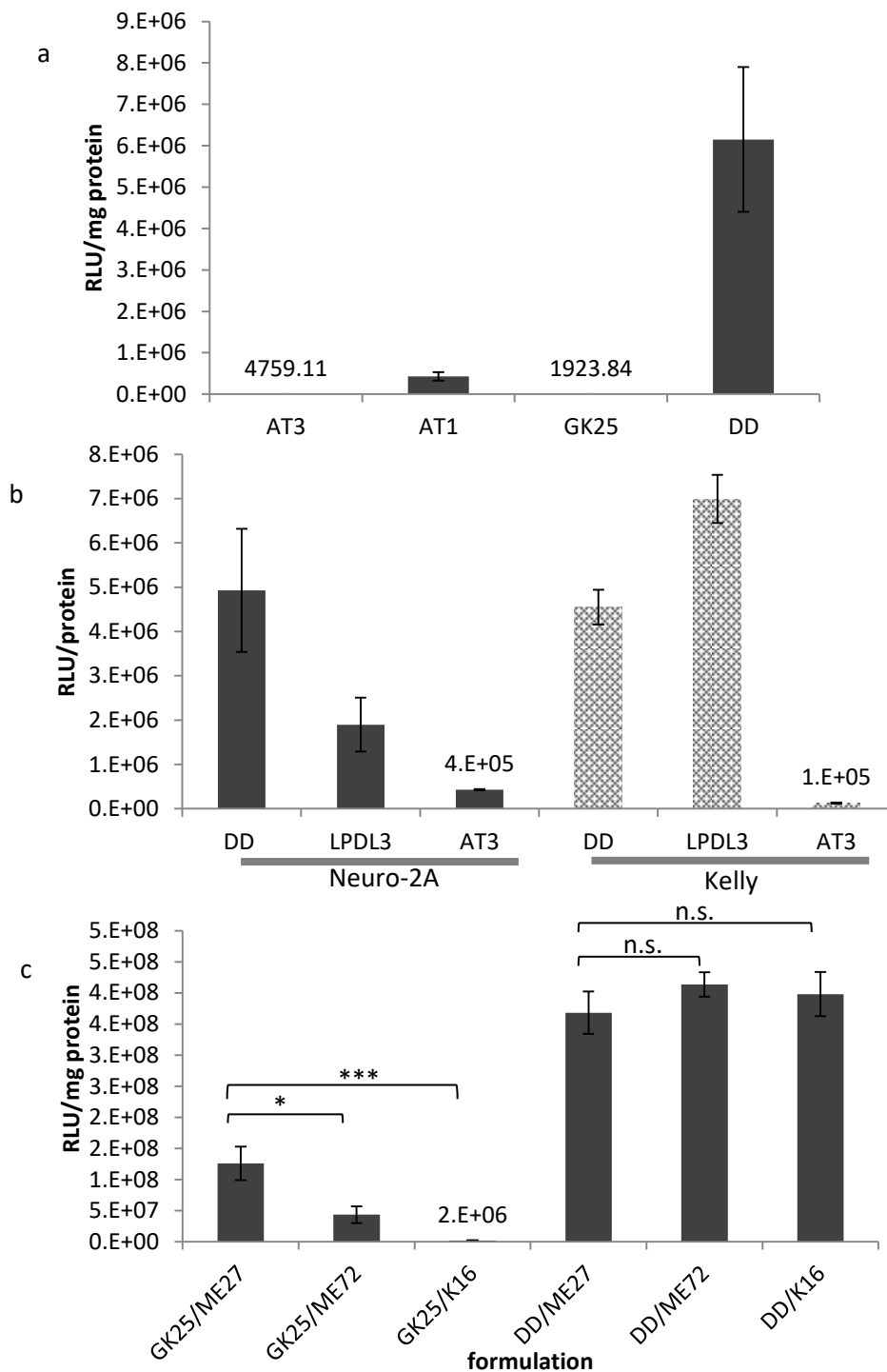


Fig. 4.3.1. Luciferase pDNA transfection using RTNs a) Differences in transfection efficiencies among RTNs containing AT3 (anionic 1% PEG), AT1 (cationic 1% PEG), GK25 (anionic 5% PEG), DD (cationic non-PEG) in Kelly. (n=6) b) Differences in transfection efficiencies among three different RTNs in Neuro-2A and Kelly. LPDL3 is a double layered formulation consisting of DD/ME27/DNA covered with AT3. (n=6) c) Differences in specificity between a cationic and an anionic RTNs. ME72 and K16 are negative control peptides. (n=6) In all the graphs each column represents the mean \pm SD. * $p < 0.05$, *** $p < 0.001$

4.3.2. MYCN silencing efficiency of siMYCN delivered by RTNs *in vitro*

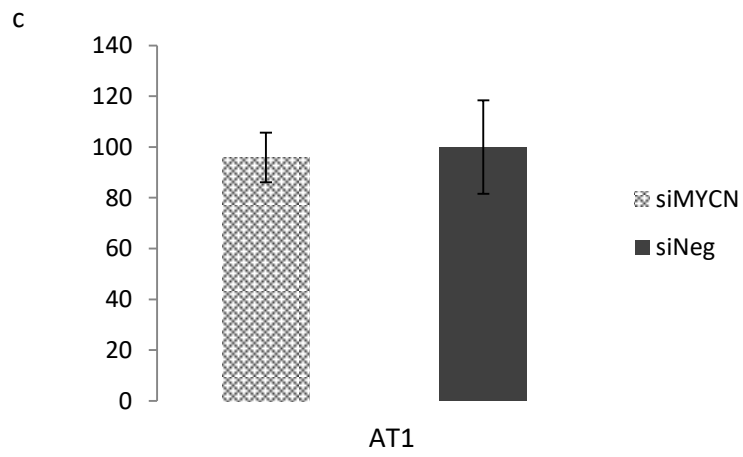
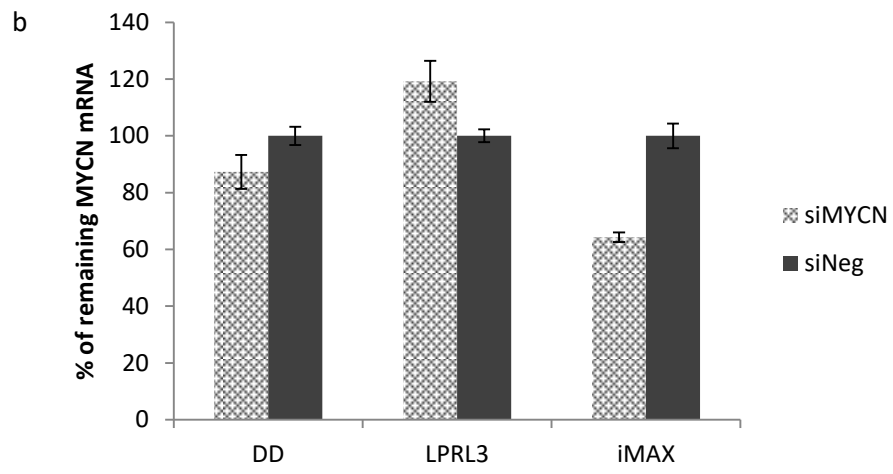
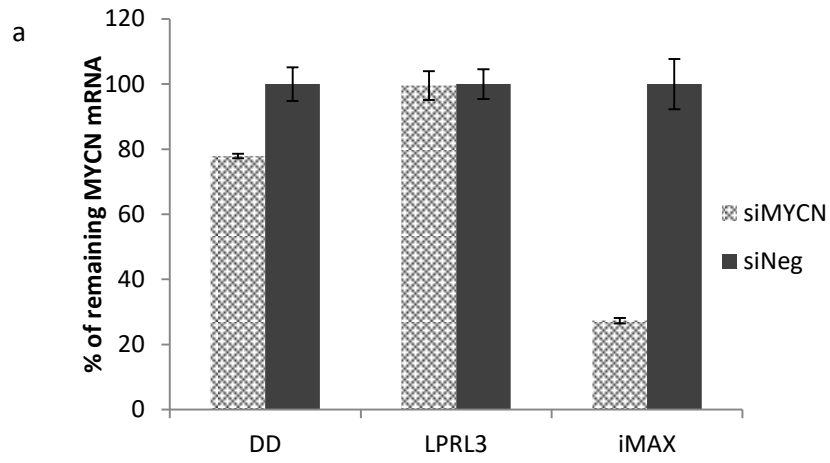
To observe MYCN silencing efficiency using RTNs *in vitro*, we performed experiments where siMYCN were transfected into Kelly and SK-N-BE(2) using DD/ME27 and LPRL3: DD/ME27/siRNA/AT3 formulations. The transfected cells were incubated for 48 hours and the RNA was extracted. The remaining MYCN mRNA was measured by qRT-PCR.

As a result, DD achieved 22.1% MYCN silencing in Kelly and 12.7% in SK-N-BE(2) (Fig.4.3.2.a,b). The efficiency of siMYCN seemed to be different from that in siNeg in only Kelly. On the other hand, LPRL3 did not silence MYCN in either Kelly or SK-N-BE(2).

We also tested the cationic RTN containing AT1/ME27 to compare the MYCN silencing efficiencies of cationic non-PEGylated and PEGylated RTNs in SK-N-BE(2) (Fig.4.3.2.c). The RTN achieved only approximately 5% MYCN silencing and it was not statistically different from the value of the siNeg.

These results suggest that non-PEGylated, cationic RTNs can silence MYCN mRNA, although, PEGylated cationic and anionic RTNs did not significantly reduce the mRNA.

The MTS assay was performed in transfections of cationic RTNs containing DD in SK-N-BE(2) to observe the toxicity of RTN transfections in a NB cell line (Fig. 4.3.2.d). The transfection media was changed to complete media 4 hours after the transfection and the cells were incubated for 24 hours (n=5). The viability of the cells transfected with RTN was not significantly different from that of untransfected negative control (p=0.73 for siMYCN and 0.23 for siNeg). It seems that transfections of RTNs containing DD are not cytotoxic.



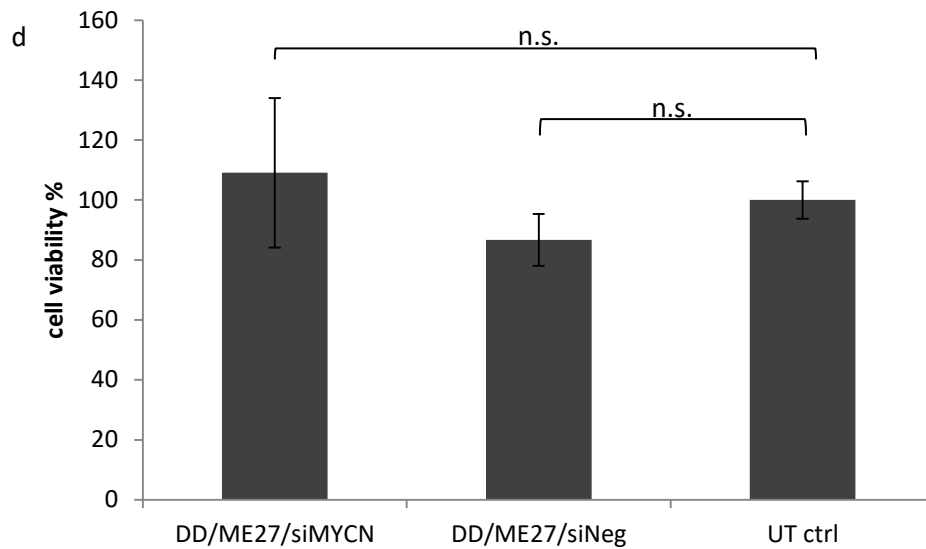


Fig. 4.3.2. siMYCN transfections using RTNs and the cell viability iMAX was used at 10 nM as a positive control. a) MYCN silencing efficiencies by cationic DD and anionic LPRL3 RTNs in Kelly. (n=2) b) MYCN silencing by cationic and anionic RTNs in SK-N-BE(2). (n=2) c) MYCN silencing by RTN containing cationic AT1 in SK-N-BE(2). (n=2) d) Cell viability (MTS) assay in SK-N-BE(2) cells transfected with DD /ME27/siMYCN or siNeg at 24 hour time point (n=5). In all the graphs each column represents the mean \pm SD. *p<0.05

4.3.3. MYCN silencing *in vivo*

We investigated the MYCN silencing efficiency of siMYCN packaged with cationic 1% PEGylated liposome AT1 (composition shown in 2.1.3.2. in the Material and Methods chapter) and peptide ME27 in a NB animal model of NOD SCID Gamma (NSG) mice xenografted with Kelly and SK-N-BE(2) cell lines. When the size of the tumour was approximately 5x6 mm (it took about two weeks after the xenograft), the RTNs were injected into the lateral tail vein. After 48 hour incubation, the tumours were taken and total RNA were extracted. The qRT-PCR data were normalised to untransfected negative control. The experiment was performed in collaboration with a colleague from our group (Dr A Tagalakis).

In Kelly cell xenografts, administered to mice by intravenous, tail vein injection, the relative amounts of remaining MYCN mRNA after siMYCN treatment (n=6) was 0.70 and siNeg (n=5) was 0.86, normalised to untransfected negative control (n=3). The relative expression of siMYCN normalised to siNeg was 0.73 (Fig. 4.3.3.a). Hence, siMYCN achieved 29.3% silencing to untransfected negative control and 26.5% to siNeg. In addition, the values of siMYCN were significantly different from both untransfected negative control and siNeg (p=0.0007 and 0.0005, respectively) while siNeg and untransfected control were not different from statistics (p=0.83).

In SK-N-BE(2) tumours, the relative expression of samples transfected with siMYCN was approximately 0.40, siNeg was 0.66 (all n=3). In addition, the relative expression of siMYCN was approximately 0.61 normalised to siNeg (Fig. 4.3.3.b). Therefore, siMYCN achieved 60.0% silencing to untransfected control and 39.1% to siNeg. The values of siMYCN were significantly different from those of untransfected control (p=0.02) although it was not statistically different from those of siNeg due to the high error bar of siNeg

($p=0.83$) because this was a pilot study using SK-N-BE(2) and the sample number was minimum ($n=3$).

These results suggest that the MYCN silencing efficiency *in vitro* may not agree with that *in vivo* and MYCN silencing efficiency *in vivo* is higher and that *in vitro* even in the same RTNs.

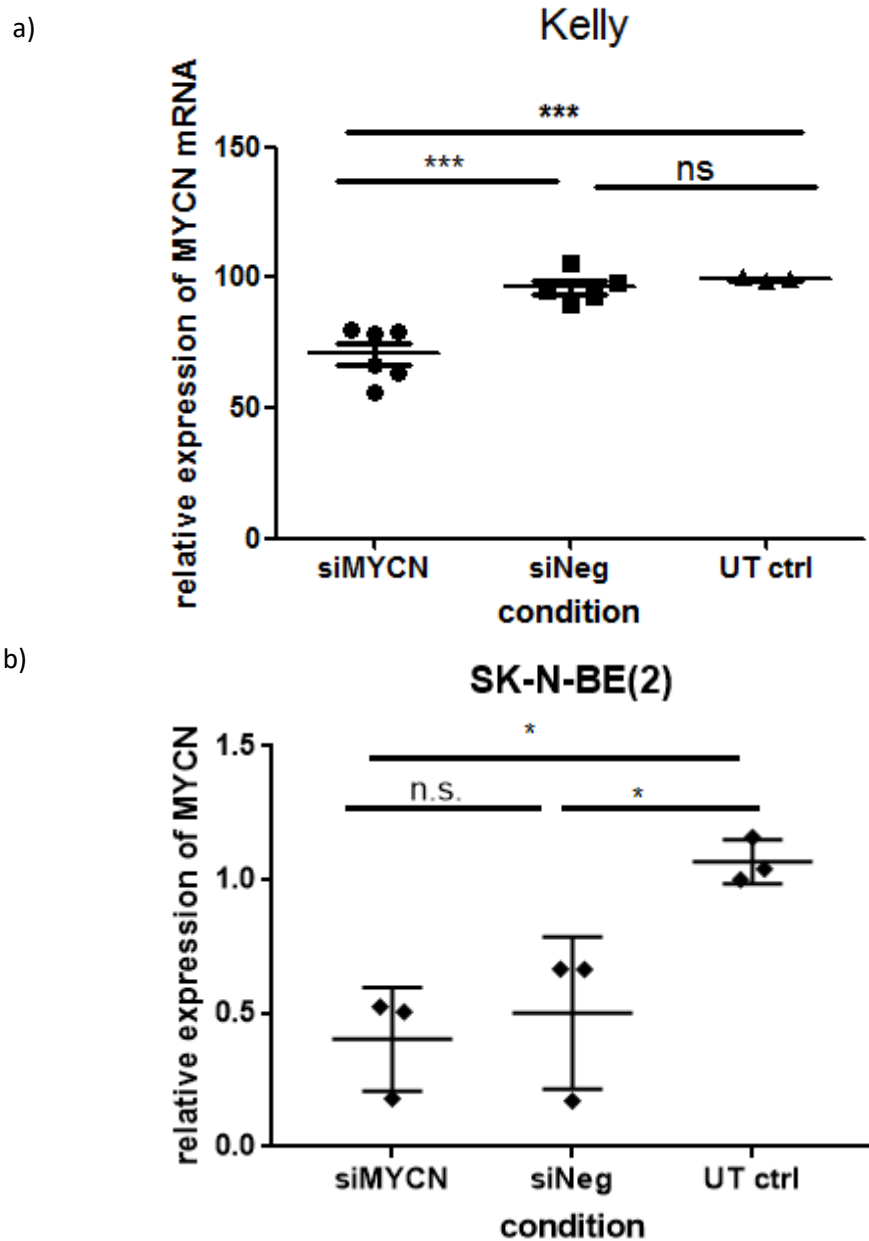


Fig. 4.4.3. MYCN silencing using AT1/ME27/siMYCN *in vivo* siMYCN was transfected in NB animal model which is NOD SCID mice xenografted a) with Kelly (n=6 for siMYCN, n=5 siNeg, n=3 UT ctrl) and b) with SK-N-BE(2) (n=3 each). 25µg siMYCN or siNeg/mouse was injected. After 48 hours, the tumour was taken, and the MYCN mRNA in each sample was quantified by qRT-PCR. The qRT-PCR was run in duplicate two times. One-way ANOVA with Bonferonni post-test used to assess significance. The bar represents mean ±SD. n.s.≥0.05, *p<0.05, ***p<0.001

4.3.4. Tumour uptake of a cationic PEGylated RTN and the biodistribution *in vivo*

Then we observed how much cationic PEGylated RTN was taken in tumours and where the RTN was delivered in organs in mice. NOD SCID Gamma (NSG) mice were xenografted with Kelly cells and when the size of the tumour was approximately 5x6 mm (it took about two weeks after the xenograft), the RTN formulation containing fluorescence-labelled siRNA was injected intravenously by tail vein. The tumours were removed 24 hours after intravenous administration for analysis of tumour uptake of the nanoparticles. The biodistribution of the RTN was observed 4 hours after the intravenous administration. This experiment was performed with assistance from a colleague, Dr A Tagalakis.

Fluorescence labelled siRNA was observed in most of the cells in the tumour while the untransfected tumours were completely negative for fluorescence (negative control) (Fig. 4.3.4.a). In terms of the specificity of siRNA delivery by the RTN, only tumours received the RTN while other organs including lung, liver and spleen showed no uptake of the RTNs (Fig. 4.3.4.a).

These may imply the RTN delivered siRNA to target tumour specifically and most of the RTN accumulated in the tumours with 4 hours.

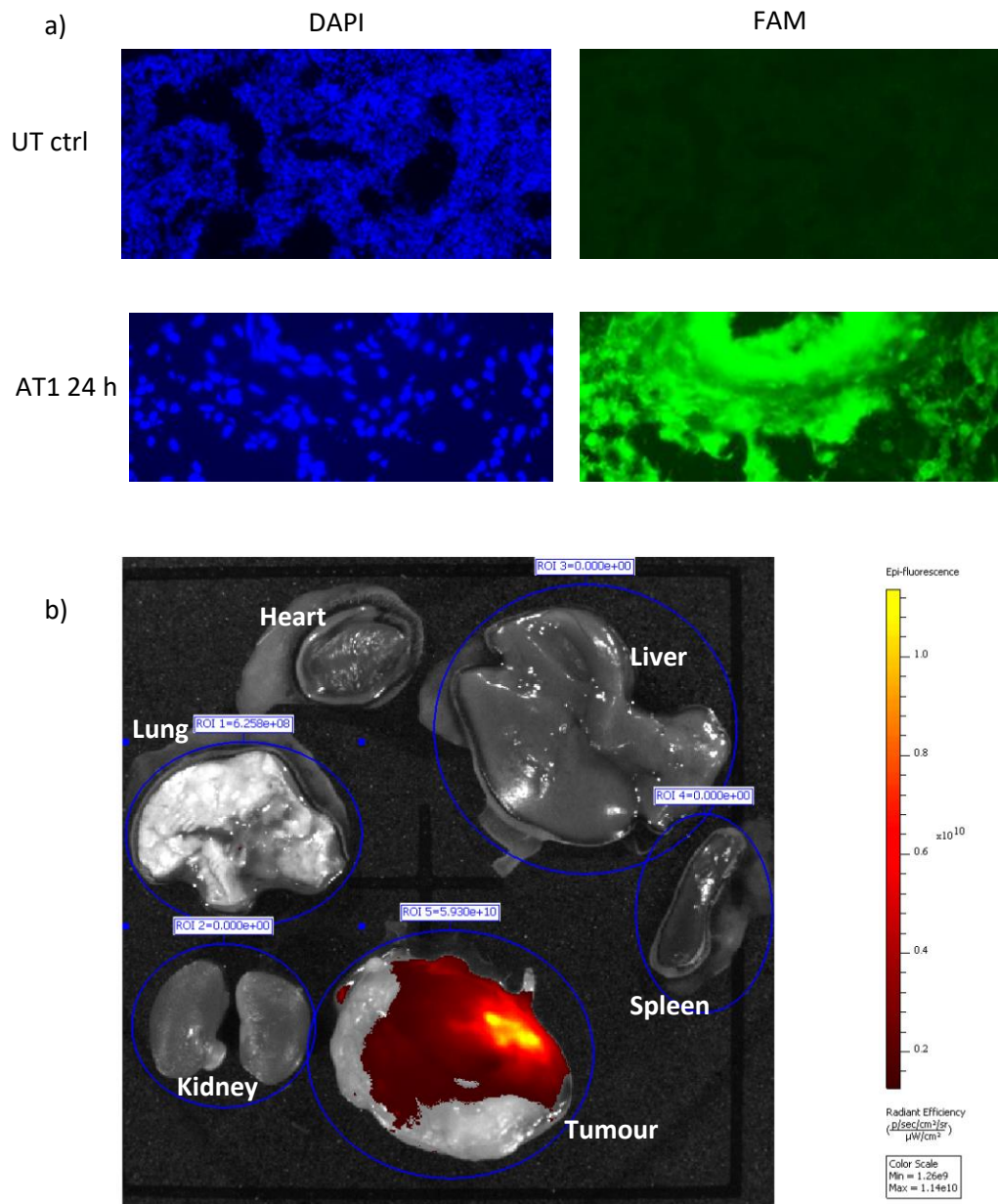


Fig. 4.3.4. Tumour uptake and the biodistribution of the RTN (AT1/ME27/FAM labelled siRNA) a) Histological images of tumours from mice which received the cationic RTN or did not injected (negative control). The tumours were taken 24 hours after the administration. b) Image of organs (tumour, spleen, liver, heart, lung and kidney) in mice which was intravenously injected with the cationic RTN (0.5 mg/kg, 16 $\mu\text{g}/\text{mouse}$). The image was taken 4 hour after the administration.

4.3.5. Cellular uptake of DD with cholesterol *in vitro*

We then aimed to investigate whether higher cellular uptake and transfection efficiencies might be obtained using DD stabilised with cholesterol. We performed Alexa 555-labelled negative control siRNA transfection in SK-N-BE(2) and measured the percentage of fluorescent cells using flow cytometry at three different time points: 4, 24 and 48 hours after the transfections to observe differences in cellular uptake among DD, DD with 10% and 20% cholesterol. The percentage of the fluorescence positive cells transfected by DD without cholesterol was the highest in the three different RTNs, which was 67.2% at 4-hour time point (Fig. 4.3.5.a). DD with 20% cholesterol was the second highest and was 59.2%. DD with 10% cholesterol was 52.6%. At the 24-hour time point, DD with 20% cholesterol achieved the highest cellular uptake, which was 80.7%. DD became the second highest and was 76.5%. At the 48-hour time point, all formulations showed reduced percentages of fluorescent cells by approximately 1/3 while that of DD with 20% cholesterol was still the largest of the three. DD was 43.5% and DD with 10% cholesterol was 42.8%.

In addition, the MFI of DD with 20% cholesterol was the highest at the three time points while that of DD was the second largest (Fig. 4.3.5.b). The MFI of DD with 10% cholesterol was as low as that of untransfected control at the 48-hour time point.

We also observed the ability of DD with 30% cholesterol at the 24-hour time point and compared it with DD with 20% cholesterol (Fig. 4.3.6.). As a result, DD with 30% cholesterol achieved higher cellular uptake, at 89.6%, while DD with 20% cholesterol was 84.9%.

These results may imply that 20% and 30% cholesterol in DD improve the cellular uptake in SK-N-BE(2) while 10% cholesterol did not.

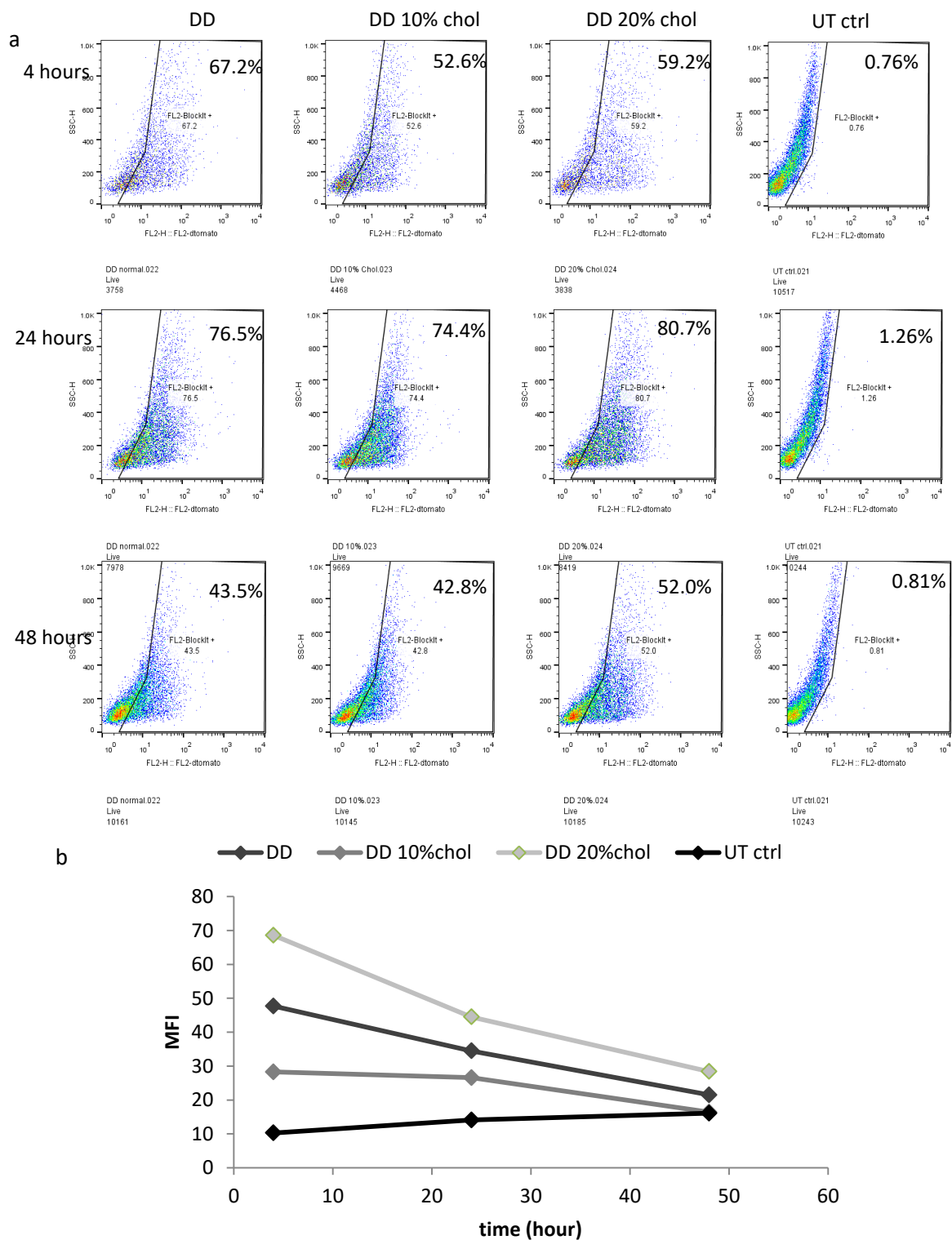


Fig. 4.3.5. Differences in cellular uptake and MFI among DD, DD with 10% and 20% cholesterol a) Cellular uptake of RTNs containing DD, DD with 10% cholesterol and DD with 20% cholesterol at 4 hour, 24 hour and 48 hour time points. (n=1) b) Changes in the MFIs of the RTNs containing DD, DD with 10% cholesterol and DD with 20% cholesterol during 48 hours. The values were quantified from a) the cellular uptake experiment. (n=1)

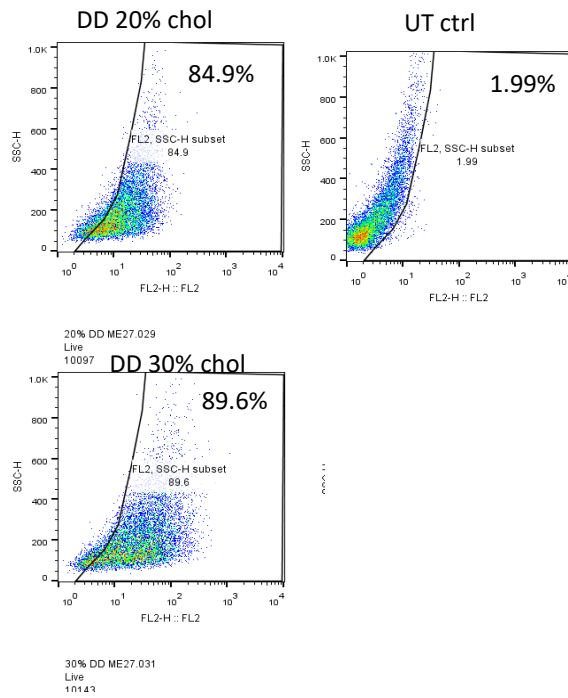


Fig. 4.3.6. Difference in cellular uptake of RTNs containing DD with 20% and 30% cholesterol at 24 hour time point (n=1) The cellular uptake of the RTN containing DD with 30% cholesterol was higher than that of DD with 20% cholesterol.

4.3.6. MYCN silencing efficiency of DD with cholesterol

To investigate MYCN silencing efficiency of DD with cholesterol, we transfected siMYCN packaged with ME27 and DD, DD with 10% or 20% cholesterol in SK-N-BE(2) *in vitro*, and incubated the cells for 48 hours. As a result, siMYCN delivered with DD with 10 and 20% did not silence MYCN while DD silenced mRNA levels by 15.2% (Fig. 4.3.7.a). The positive control siMYCN transfected with RNAiMAX at 10 nM achieved 40% MYCN silencing, and therefore, it seems that the cells and siRNA worked properly.

Similarly, the silencing efficiency of DD with 30% cholesterol was observed (Fig. 4.3.7.b). Surprisingly, siMYCN transfected with DD with 30% cholesterol also did not silence MYCN mRNA while fluorescently-labelled siRNA delivered by DD with 30% cholesterol achieved 89.6% cellular uptake.

The data suggest that cholesterol in DD decreased MYCN silencing efficiency in SK-N-BE(2) although it seems to help the transfection efficiency.

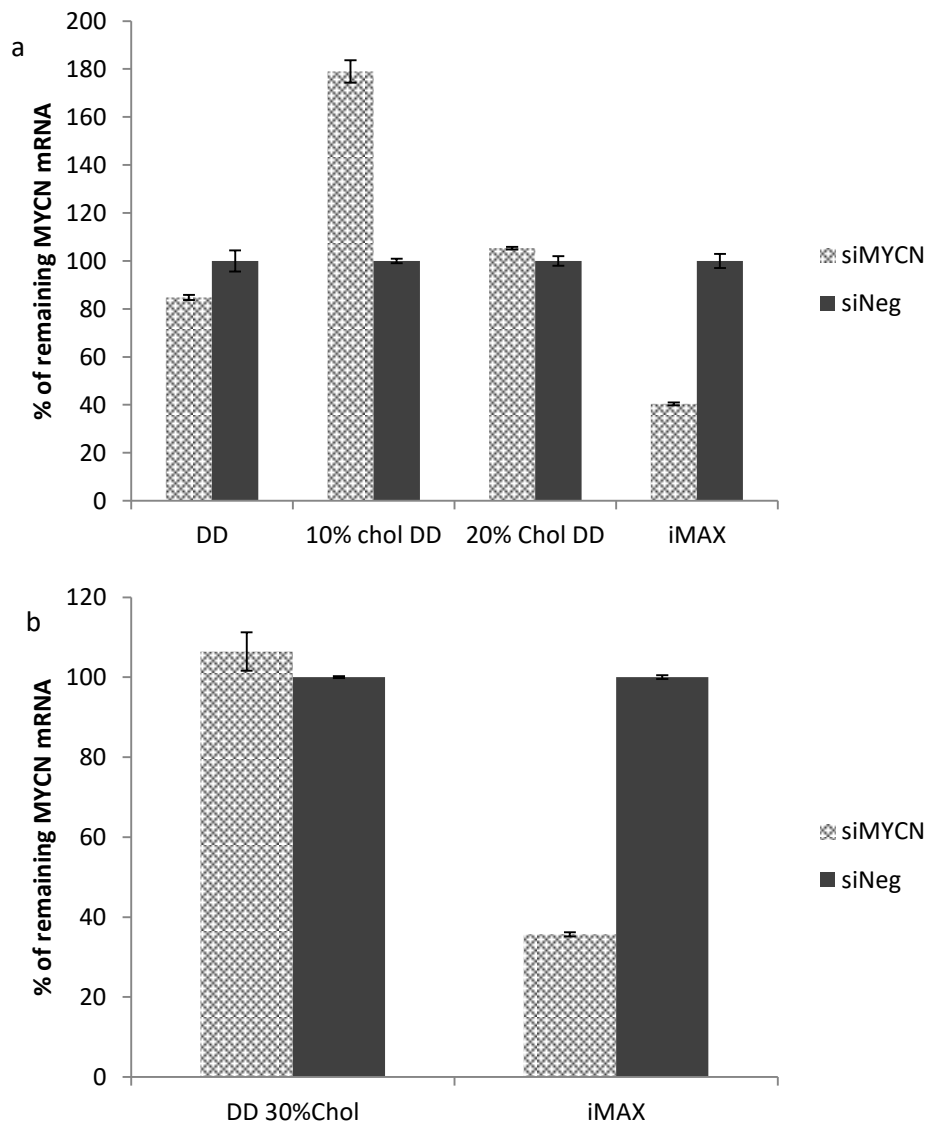


Fig. 4.3.7. siMYCN transfections using RTNs containing DD, DD with 10, 20 and 30% cholesterol. a) The MYCN silencing efficiencies of RTNs containing DD, DD with 10% cholesterol and DD with 20% cholesterol. (n=2) b) The RTN containing DD with 30% cholesterol did not silence MYCN. (n=2). In all the graphs each column represents the mean \pm SD.

4.3.7. siRNA release assay (heparin dissociation assay)

We then investigated the stability and dissociation properties of RTNs containing DD, DD with 20% and 30% cholesterol in heparin because there was disagreement between the cellular uptake and the MYCN silencing efficiency. Heparin is a highly negatively-charged molecule and is widely used to assess the stability of cationic nanocomplexes. The stability indicates how easily the nanocomplexes release siRNA in cells because high concentration of polyanion such as protein, mRNA and nucleic acids may dissociate cationic nanocomplexes in the biological environment. Hence, heparin solution is a model of the environment in a cell (Tagalakis et al. 2013). The siRNA was fluorescence-labelled with PicoGreen and the RTNs were exposed to different concentrations of heparin (0-10.0 U/mL). The packaging efficiency shows the extent of siRNA protection. A percentage of siRNA release was calculated using the value of free siRNA and the heparin concentration of 50% siRNA release was compared among the three RTNs.

At 0 U/mL heparin, the RTN containing DD packaged 98.8%, DD with 20% cholesterol was 96.0% and DD with 30% cholesterol was 96.7%. The heparin concentration of 50% siRNA release (50% dissociation heparin concentration U/mL) in DD with 30% cholesterol was lowest, which was 0.374 U/mL, and DD with 20% cholesterol followed it with 0.385 U/mL (Fig. 4.3.8.). The RTNs containing DD was more stable than those of DD with 20 and 30% cholesterol and the 50% heparin dissociation concentration was 0.417 U/mL. In addition, DD with 20 and 30% cholesterol achieved 100% siRNA release while DD was 94% maximum (Fig. 4.3.8. black arrow).

The data may suggest that DD with 20 and 30% cholesterol are less stable to the packaging of siRNA compared with DD while the packaging efficiency at 0 U/mL heparin was not

different among DD, DD with 20% and 30% heparin. In addition, it seems that RTNs containing DD does not release all siRNA.

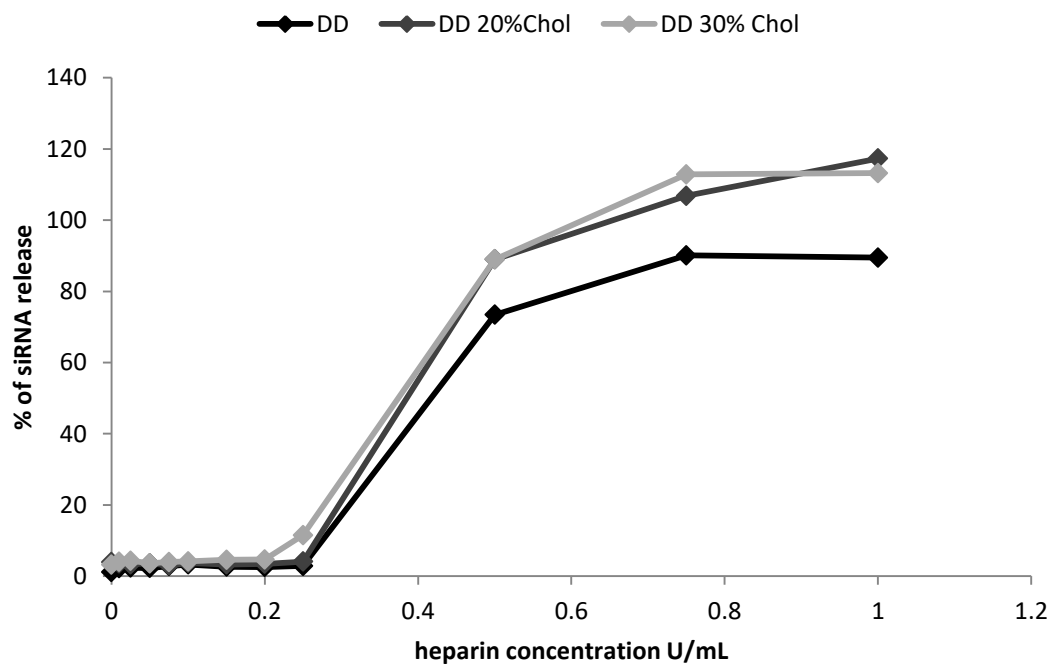


Fig. 4.3.8. The stability and dissociation property of RTNs containing DD, DD with 20 and 30% cholesterol. Heparin dissociation assay (0.01-10 U/mL) was performed to investigate the stability of the RTNs (n=3). The range of 0.01-1 U/mL was shown on the figure.

4.3.8. Differences in cellular uptake efficiency among different conditions of media change and centrifuge

We then observed the differences in cellular uptake efficiencies when cells were transfected with different conditions of media. There was disagreement between the cellular uptake and the MYCN silencing efficiencies of DD with 20 and 30% cholesterol. One possible reason was the difference in the condition of media change. In the cellular uptake assay of Fig. 4.3.5. and Fig. 4.3.6., the transfection media (RTNs in OptiMEM) was not changed for 48 hours while the transfection media was changed to complete media 4 hours after transfection in our standard protocol as well as in the MYCN silencing in Fig.4.3.7. Then we hypothesised that the disagreement may be due to the change of the transfection media with RTNs to normal culture media and that cellular uptake of RTNs may increase if the transfected cells are centrifuged before media change.

We transfected fluorescently-labelled negative control siRNA (BlockIt) packaged with DD with 20% cholesterol and ME27 in SK-N-BE(2) and incubated with different conditions in media and centrifuge (Fig. 4.3.9.a). The cellular uptake was measured at 4 and 24 hour time points.

At the 4 hour time point, there was no significant difference in the percentage of the fluorescent cells in the samples with and without centrifugation just after the transfection (Fig. 4.3.9.b). The MFIs of the two samples were also the same (Fig. 4.3.9.c). At 24 hours, the cellular uptake efficiencies in No3 and No4, which were kept in OptiMEM (transfection media), were similar to each other at 84.9% and 85.5% respectively, and they were higher than those of No4 and No6 with media change (Fig. 4.3.9.b). No4 with media without centrifuge achieved only 38.8%, which was less than half of those of No3 and No5, while No6 with centrifuge and media change achieved 68.1%. Interestingly, the MFI of No6 was

as high as those of No3 and No5 while the cellular uptake efficiency in No6 was approximately 20% lower than those of No3 and No5. The MFI of No4 was lower than the others (Fig. 4.3.9.c).

These results suggest that the step of changing transfection media with complete culture media generally reduced the cellular uptake efficiency of the RTNs. Especially, transfections with changing media without centrifugation such as No4 significantly decreased the cellular uptake efficiency and the MFI, compared with the ones with centrifugation and changing media.

4.3.9. MYCN silencing difference with different conditions of media

To investigate MYCN silencing efficiency among different conditions in media as well as two different time points, we carried out siMYCN transfections with 4 different conditions (Fig. 4.3.10.a). The cells were harvested at 24 and 48 hour time points to compare the silencing efficiency at different time points because the cellular uptake assay (Fig. 4.3.5.a) showed the percentage of the fluorescence positive cells at the 24-hour time point was higher than that at the 48-hour time point. As a result, all of the RTNs did not silence MYCN mRNA while siMYCN with RNAiMAX reduced it 50-68% (Fig. 4.3.10.b).

This result implies that the lower silencing efficiency of the RTN containing DD with 20% cholesterol resulted from the liposome rather than the transfection conditions.

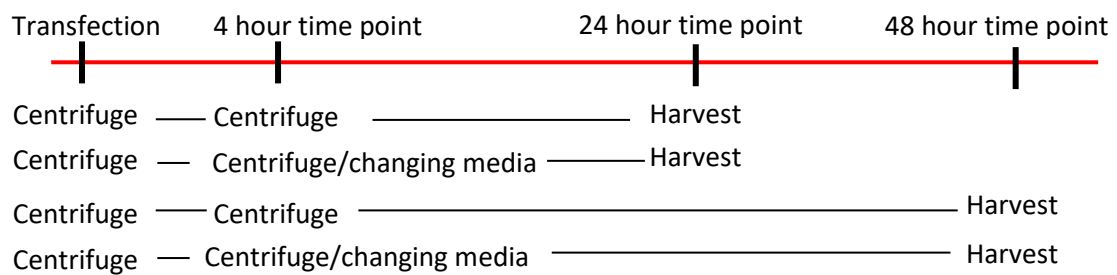
Then we performed siMYCN transfection using a RTN containing DD without cholesterol to investigate if MYCN silencing efficiency was changed when the media was not replaced at the 4 hour time point (Fig. 4.3.11.a). The transfection media was changed at 24 hours after the transfection because changing media at 4 hours after transfection reduce the cellular uptake efficiency (Fig. 4.3.9.b). The transfection cells were harvested at 24 and 48 hour time points to compare the silencing efficiency at two different time points as described above.

As a result, the MYCN silencing efficiency of the cells kept in transfection media for 24 hours (Fig. 4.3.11.b) was slightly higher (22.4% and at 24 hour time point and 23.5% at 48 hour time point) than that with changing media at 4 hour after transfection (Fig.4.3.2.b, 4.3.6.a) by approximately 7-10%.

The data suggest that DD without cholesterol silence MYCN mRNA and the efficiency was higher than that with 20% cholesterol while the transfection efficiency of DD in flow cytometry was lower than that with 20% cholesterol. In addition, the MYCN silencing

efficacy by RTNs containing DD was slightly improved by the method that involved incubation in the transfection media for 24 hours, although, it was not as high as that by RNAiMAX at 10nM.

a



b

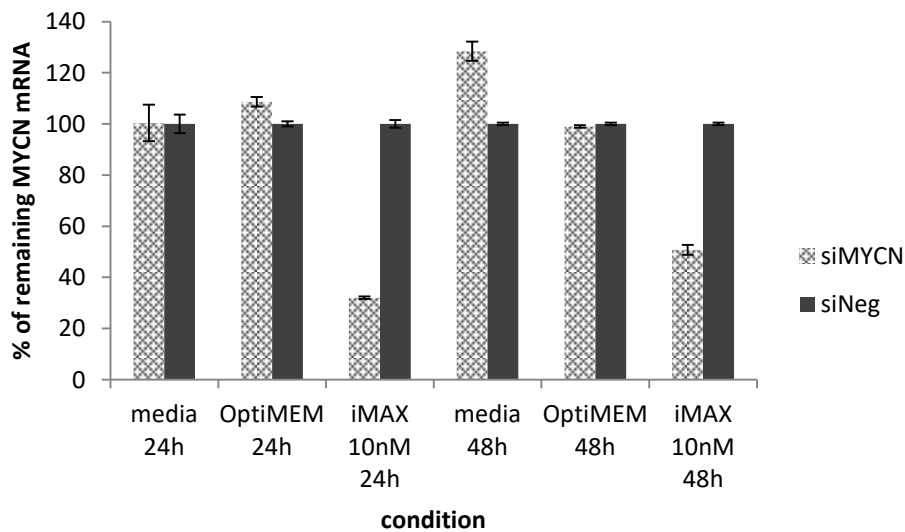


Fig. 4.3.10. siMYCN transfections using RTN containing DD with 20% cholesterol in SK-N-BE(2) a) Conditions used in this experiment. b) siMYCN delivered by the RTN containing DD with 20% cholesterol did not silence MYCN in any condition. (n=2) In all the graphs each column represents the mean± SD.

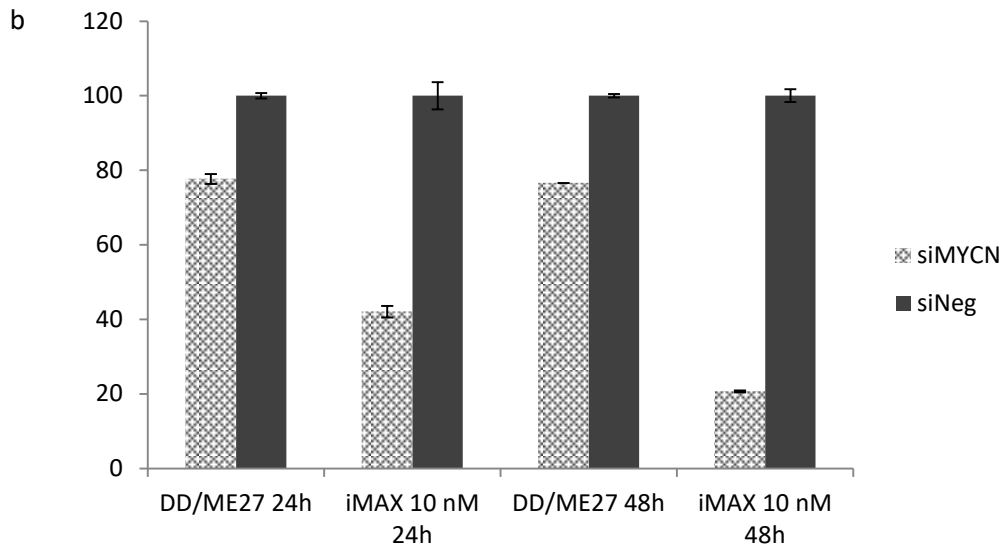
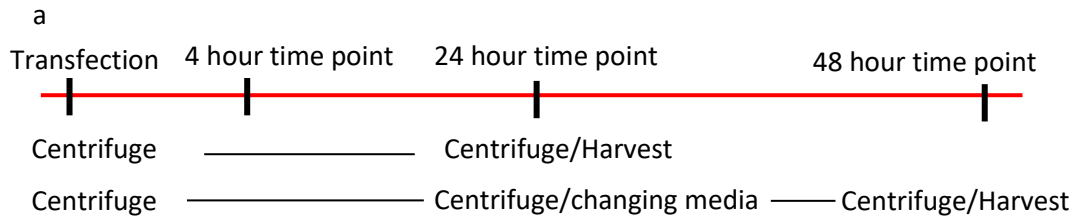


Fig. 4.3.11. MYCN silencing by RTN containing DD/ME27/siMYCN a) time table and procedure of each condition. b) MYCN silencing efficiency of the RTN at two different time point. (n=2) In all the graphs each column represents the mean± SD. **p<0.01, ***p<0.001

4.3. Discussion

We observed the transfection efficiency and silencing efficiency of RTNs in NB cells because commercially available lipid-based reagents such as Lipofectamine RNAiMAX cannot be used *in vivo*. For gene delivery of therapeutics in clinical use, it is necessary to optimise RTNs.

Feng et al. (2010) and Zhu et al. (2013) group reported that anti-MYCN siRNA delivered by liposomes targeting folate receptor was transfected in LAN-5 *in vitro* and *in vivo*. The liposomes are containing cholesterol and are PEGylated. Their formulation achieved 79.2% knockdown at mRNA level and 71.3% at protein level *in vitro* as well as 53.1% at mRNA level and about 60% at protein level *in vivo* (Feng et al. 2010, Zhu et al. 2013). Interestingly, their anti-MYCN siRNA is targeting the same site as that siMYCN1 in chapter 3 (Fig. 3.3.3.a) in our study is. This may imply that the most efficient site for MYCN knockdown is different among NB cells.

Our RTNs for NB cells normally contain peptide ME27, which target the integrin $\alpha_5\beta_1$, $\alpha_v\beta_3$ and $\alpha_v\beta_5$ receptors expressed on cancer cells and are binding to fibronectin and vitronectin of extracellular matrix, and the expression of the receptors in Kelly and SK-N-BE(2) has been confirmed in the previous study by colleges in our group (data not shown). RTNs containing DD normally achieves higher transfection and silencing efficiency compared with RTNs with PEGylated liposomes *in vitro*. A possible reason why LPDL3 achieved higher transfection efficiency compared with single layered anionic RTNs is that DNA was enveloped with non-PEGylated DD, rather than directly packaged by anionic PEGylated liposomes, and the structure made DNA released easier from PEG motif.

On the other hand, non-PEGylated cationic RTNs cannot be used *in vivo* because negatively charged serum in blood shields the cationic RTNs and LPRL3 did not achieve MYCN

knockdown. Therefore, AT1 (1% PEGylation, cationic) was chosen for *in vivo* work in this study. RTN consisting of AT1 achieved 26.5% and 29% MYCN silencing to siNeg in Kelly and SK-N-BE(2) respectively, and 29.3% and 60% to untransfected negative control respectively *in vivo* although it silenced only 4.2% to siNeg in SK-N-BE(2) *in vitro*. The *in vivo* study using Kelly successfully showed that MYCN silencing by siMYCN, which was significantly different from siNeg and untransfected negative control while there was not different between siNeg and untransfected control. On the other hand, the study using SK-N-BE(2) *in vivo* was a pilot experiment that 3 samples were prepared per condition. There was not a significant difference between siMYCN and siNeg due to the high error bar of siNeg. For further study, it will be necessary to increase the sample size in SK-N-BE(2) *in vivo* study and investigate MYCN silencing at the protein level in order to confirm the data at mRNA level as well as the downstream effects of MYCN silencing, such as NTRK1/TrkA upregulation. In addition, it may be useful for therapy to carry out multiple doses of siMYCN and investigate the silencing efficiency and the tumour growth rate *in vivo*.

On the other hand, there was a disagreement in the silencing efficiency of AT1 between *in vitro* and *in vivo*. One possible reason may be that the uptake efficiency of RTNs. The experiment of cellular uptake of a RTN (DD with 20% cholesterol/ME27/siRNA) using flow cytometry (Fig. 4.3.9.b) revealed that the transfection efficiency in the cells in complete media changed 4 hours after the transfection without centrifugation, our standard protocol, was only 38.8%, which was almost half of that in the cells in the transfection media for 24 hours. It may imply that there are RTNs not binding to the cells at the 4 hour time point, and they are washed away by changing to fresh complete media because the cellular uptake efficacy of the cells in changed media without centrifuge was the same as that of the transfected cells at the 4 hour time point. In addition, most of the fluorescence positive cells at 4 hour time point were just binding the fluorescent RTN while the ones at 24 hour time

point internalised the RTN. For further study, it will be useful to distinguish the two kinds of the fluorescent cells by quenching cells just binding fluorescent RTNs using trypan blue.

On the other hand, the data of the tumour uptake and the biodistribution of the RTN (Fig. 4.3.4.a,b) may show that the RTN was specifically delivered to the tumours within 4 hours and the cells of the tissues took the RTN probably due to the circulation of blood and the EPR effect. The EPR effect is a phenomenon that nanoparticles and liposomes are easily accumulated in cells in tumours because the vessel veins around tumours are inflammatory and there are gaps between the endothelial cells of vessel vein and it allows more than 500 nm nanoparticles to pass the wall and accumulate in tumours (Li & Szoka 2007). In addition, RTNs *in vivo* are circulating in the bloodstream while the one not taken by cells are eventually captured by the liver (Samuelsson et al. 2017). PEGylated liposomes are less captured by the liver or the spleen compared with non-PEGylated liposomes, and approximately 15% of intravenously injected PEGylated liposome were detected in the liver after 24 hours while more than 80% were remaining in plasma in mice (ibid). In addition, Xu et al, (2016) reported that the terminal elimination half-life of their nanocomplexes consisting of siRNA and liposome with PEGylation and cholesterol was approximately 15 hours in blood. These data suggest that injected RTNs are stably exposed to NB cells via the bloodstream and the dose is not dramatically reduced by capture by the liver or by degradation *in vivo*. Therefore, the transfection efficiency *in vivo* is higher than that *in vitro* in the same RTNs, which may have made the disagreement in the silencing efficiency between *in vitro* and *in vivo*.

We also aimed to improve silencing efficiency by RTNs and used liposomes with cholesterol because one possible reason of lower silencing efficiency is instability of liposomes. Many researchers have been investigating liposomes with cholesterol and it was reported that adding cholesterol at more than 25mol% stabilises liposomes and improves cellular uptake

and (Schroeder et al. 2009). DD with 20% and 30% cholesterol improved the transfection efficiency in SK-N-BE(2) compared with DD without cholesterol while DD with 10% reduced the transfection efficiency. However, the MYCN silencing efficiency of the RTN with 20 and 30% cholesterol was lower than that without cholesterol.

Then we hypothesised from these results from the two experiments that 20 and 30% cholesterol in DD may have stabilised RTNs and it may have made siRNA release difficult and performed the heparin dissociation assay to compare the stability of the three liposomes. As a result, DD was the most stable and can hold siRNA compared with DD with 20 and 30% cholesterol and the data did not support our hypothesis.

A possible reason for the disagreement among the three experiments is that the data in the heparin dissociation assay is just a model and shows the physical ability to hold siRNA of liposomes and did not show the actual stability and the ability to release siRNA the liposomes in NB cells. In addition, the transfection and MYCN silencing efficiency of RTNs with 20% cholesterol were reproducible in our study (Fig. 4.3.5. a., Fig. 4.3.6. and Fig. 4.3.9.b. for the cellular uptake efficiency, Fig. 4.3.7. and Fig.4.3.10. for the silencing efficiency). However, there is no publication clearly mentioning the accuracy of the heparin dissociation assay compared with the actual ability to hold/release siRNA in cells. Therefore, the reason of the disagreement is not clear.

In addition, higher percentage such as 40-50% of cholesterol might improve silencing efficiency *in vivo*. Lin et al. (2014) reviewed that several research groups have delivered siRNA by liposomes with 48% cholesterol *in vivo*. It is necessary for further study in which the correlation between silencing efficiency and cholesterol concentration is investigated as well as the efficiency of liposomes with higher cholesterol.

RTNs consisting of DD achieved approximately 22.1% MYCN silencing in Kelly and 12-17% in SK-N-BE(2) *in vitro* with the method in which the transfection media (OptiMEM and the RTN) was changed to complete media 4 hours after the transfections (No4 in Fig. 4.3.9.b). After the cellular uptake experiments revealed the lower transfection efficiency in our standard protocol (No4), we performed transfection by changing media at 24 hours after transfection (No3). It seemed to improve the MYCN silencing efficiency in SK-N-BE(2) by the RTN consisting of DD, which achieved 23.5% silencing. The silencing efficiency *in vitro* was not significantly different from that of AT1 *in vivo*. In addition, it was similar to that of 5 nM siMYCN with RNAiMAX, which was approximately 25% silencing (Fig. 3.3.4), while the cellular uptake of siRNA by DD (Fig. 4.3.5.) and the MFI was lower those of 5 nM RNAiMAX (Fig. 3.3.2.a,b). These results may imply that the efficiency of siRNA release by DD is higher than that by RNAiMAX and it is possible that siMYCN delivered by DD induced differentiation and NTRK1/TrkA upregulation in SK-N-BE(2). On the other hand, the cell viability of several cell lines decreases in OptiMEM when the transfection media are not changed 4 hours after transfections. That is why we replace transfection media with fresh complete culture media 4 hours after transfection in our standard protocol and the viability of cells transfected with both siMYCN and siNeg in the standard protocol were not significantly different from that of untransfected cells (Fig. 4.3.2.d). Therefore, it is necessary to conduct optimisation of the methods and investigation of downstream effects of MYCN reduction induced by RTNs for further study.

Conclusion

We performed transfections with RTNs containing siMYCN for MYCN silencing *in vitro* and *in vivo*. As a result, a RTN consisting AT1, ME27 and siMYCN successfully silenced approximately 30% MYCN mRNA normalised to siNeg in Kelly xenografted to mice while the MYCN silencing efficiency by the same RTN was approximately 5% in SK-N-BE(2) *in*

vitro. In addition, a RTN containing DD achieved about 23.5% MYCN silencing in SK-N-BE(2) after the optimisation of the protocol (n=2), which is a similar efficiency to that by 5 nM RNAiMAX. Therefore, differentiation and NTRK1/TrkA upregulation might be induced by RTNs and it is necessary to observe them for further study. It is also necessary to increase the number of replications in the experiments of siMYCN transfections using DD.

CHAPTER 5

Results

Long term storage of RTNs in trehalose

5. Long term storage of RTNs in trehalose

5.1. Introduction

Lipid nanoparticles can load a wide range of reagents from small molecule drugs to biologicals including nucleic acids such as siRNA and mRNA (Hart 2010). Furthermore, gene/drug delivery by lipid or polymer-based nanoparticles that target cells is promising and will be a novel therapy in the future for cancers and other diseases. Receptor –Targeted Nanocomplexes (RTN) are described in this thesis for neuroblastoma therapy but a therapeutic product will be required to remain stable for storage and transportation, and that maintain their biophysical characteristics and transfection properties.

Trehalose is a non-reducing disaccharide that has been used as a cryoprotectant in the food, cosmetic and pharmaceutical industries. Anchrdoquy, Carpenter & Kroll, (1997) demonstrated that trehalose maintained the transfection efficiency and biophysical characteristics of freeze-dried lipid/DNA nanocomplexes after re-suspension in water. In addition, it was reported that trehalose enhanced DNA transfection efficiency and transgene expression levels by stabilising the liposomes (Tseng et al. 2007). Furthermore, Ball et al. (2017) showed that siRNA packaged by liposomes in 20% trehalose achieved higher silencing compared with those in water or 5% trehalose.

To assess the ability of trehalose to maintain the biophysical characters and the functions of RTNs, we performed DNA and siRNA transfections suspended in several concentrations of trehalose and stored at 4 °C or -80 °C overnight or for longer periods, and compared with RTNs stored in the same conditions in water. In this study, we carried out the experiment only at -80 °C without lyophilisation.

We hypothesised that trehalose should enable RTNs to retain their biophysical and functional properties after storage at -80 °C while the RTNs stored at -80 °C in water should be disrupted by ice crystals.

5.2. Aims

In this chapter, we aim:

1. To confirm the ability of trehalose to maintain the biophysical characters and transduction/silencing efficiency of RTNs suspended in different concentrations of trehalose at 4 °C or -80 °C
2. To investigate the better time to thaw RTNs when they are transfected: one kept at -80 °C just before transfections or one thawed and kept at 4 °C
3. To observe the ability of trehalose to enhance transfection/silencing efficiency in NB cell line
4. To investigate if the ability of trehalose can be applied to both cationic and anionic RTNs

5.3. Results

5.3.1. Biophysical character and function of the RTNs consisting of DD, ME27 and Luciferase plasmid DNA stored at 4 °C or -80 °C in trehalose

We first observed the ability of trehalose to maintain the biophysical characteristics and the functionality of RTNs containing pDNA. RTNs were prepared in 5%, 8%, 10% and 15% trehalose stored at 4 °C or -80 °C. The size and the zeta potential of the RTNs were measured before storing at 4 °C or -80 °C, and they are called as ‘the original’ in this study. The RTNs stored at -80 °C were first snap-frozen in an ethanol bath with dried ice floating before placing into storage at -80 °C, and then stored at -80 °C overnight or more. The RTNs were transferred at 4 °C till transfection or measurement of the sizes and the zeta potentials. RTNs to be stored under each condition were prepared once a week for 4 weeks, and at day 29, those RTNs were removed then transfected into Neuro-2A to compare the function of the RTNs stored under different conditions with freshly made RTNs as well as their sizes and the zeta potentials (Fig. 5.3.1.a).

The sizes of the 4 original RTNs were between 142.30 nm and 201.63 nm and Batch w4 was the biggest (Fig. 5.3.1.b). The polydispersity index (PDI) was almost the same among week 1, 2 and 3 while after 4 weeks storage the PDI was 0.41, which means it was slightly more heterogenous (Fig. 5.3.1.c). In the RTNs stored at 4 °C, the size in water was 130 nm - 140 nm and so slightly smaller than those of the RTNs in trehalose. In the trehalose solutions, the sizes were 150 nm -200 nm and not significantly different among the different concentrations (Fig. 5.3.1.d, Fig. 5.3.2.a). In -80 °C, the size of RTNs in water of Batch w1 and w2 were about 10 times bigger than those of RTNs in trehalose and approximately 2-fold greater than those in water at Batch w3 and w4. In addition, the population was more homogenous after the storage, except the RTN in 15% trehalose at Batch w1 where the PDI

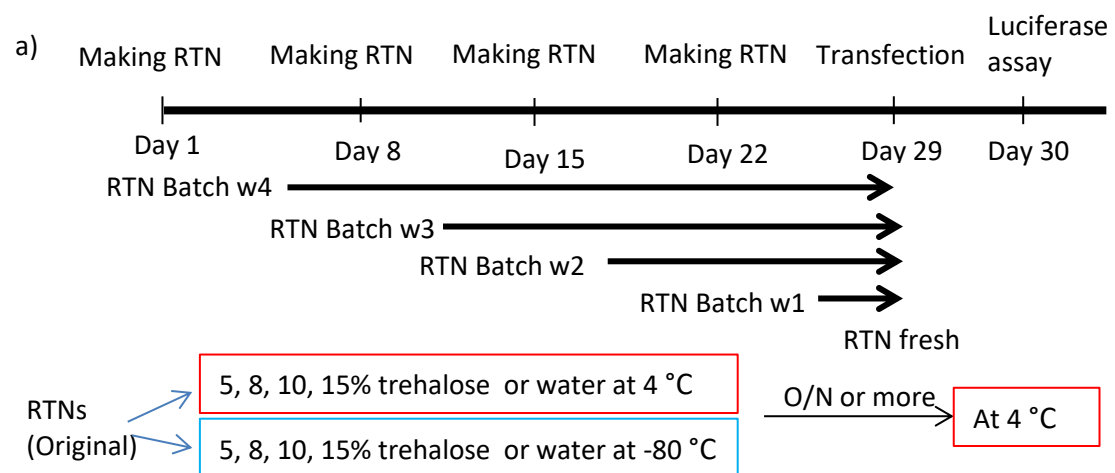
was approximately 0.20-0.35. The PDI of Batch w3 and w4 storing in water at -80 °C was about 0.75 and was higher than RTNs stored under any other conditions (Fig. 5.3.1.c, Fig. 5.3.2.a,b). The sizes and PDIs of the RTNs stored at 4 °C or -80 °C were similar to those of freshly prepared RTNs, except for the RTN in water, stored frozen at -80 °C. On the other hand, the zeta potentials of the 4 original RTNs (Fig. 5.3.1.b) were 23.5 mV - 39.6 mV which is lower than the ones stored at both 4 °C and -80 °C (Fig. 5.3.2.b). Those of the RTNs stored at both 4 °C and -80 °C did not change among the different conditions including water at -80 °C although it tended to be slightly higher when the size was bigger. They were around 40-60 mV (Fig. 5.3.2.b). These values were slightly higher than those of the freshly prepared RTNs, which were about 41-44 mV.

These results imply that trehalose protects RTNs stored at -80 °C from ice crystal and maintains the biophysical properties. In addition, the storage at 4 °C for more than 1 week seems to improve the PDI of the RTNs stored at -80 °C. In addition, it is likely that 5% or 10% of trehalose achieves better transfection efficiency.

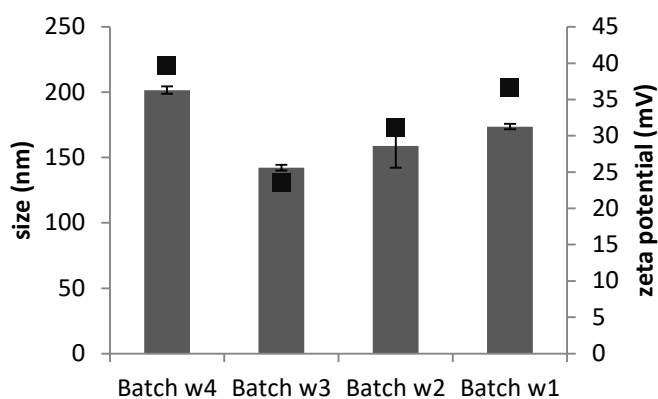
We then transfected Luciferase pDNA enveloped with DD and ME27 into the murine neuroblastoma cell line, Neuro-2A, and compared them with those of the freshly made RTNs (Fig. 5.3.2.d). Lipofectamine 2000 (L2K) was used as a positive control at 2:1 weight ratio (=L2K: DNA). Freshly made RTNs achieved approximately 5×10^8 RLU/mg protein, which was 83% of the efficiency of the L2K. In RTNs in trehalose stored for 1 week (Batch w1), all the RTNs in trehalose at 4 and -80 °C except 10% at 4 °C achieved higher than 5×10^8 RLU/mg protein of the freshly made RTNs and the positive control. In the RTNs stored for 2 weeks (Batch w2), the efficiencies of the ones in stored at 4 °C and in 5% at -80 °C were greater than that of the positive control, although those of 8, 10, 15 % and water were lower than that of positive control. The RTNs stored for 3 and 4 weeks (Batch w3 and w4) did not achieve higher efficiency than that of the positive control. RTNs in 5% stored at 4 or -80 °C

and in water maintained similar transfection efficiency to those of the freshly made RTNs while the others dropped down the values of RLU/mg protein, which is lower than half of the value in Batch w4 each condition.

The data suggest that the transfection efficiency can be improved by up to 2 week storage at 4 °C and 1 week at -80 °C. However, more than 3 week storage at 4 °C and more than 2 weeks in -80 °C seems to reduce the transfection efficiency while there are no differences in the biophysical properties associated with the duration of storage. It is likely that even the size and zeta potential do not change by long term storage at 4 degrees, the junctions may have changed. The junction between peptide and DNA or siRNA might have been tighter, which induce less DNA/siRNA release.



b) Before storage ■ size ■ zeta potential



c)

	size	PDI
Batch w4	201.63	0.41
Batch w3	142.30	0.36
Batch w2	159.00	0.35
Batch w1	173.67	0.36

d) After storage

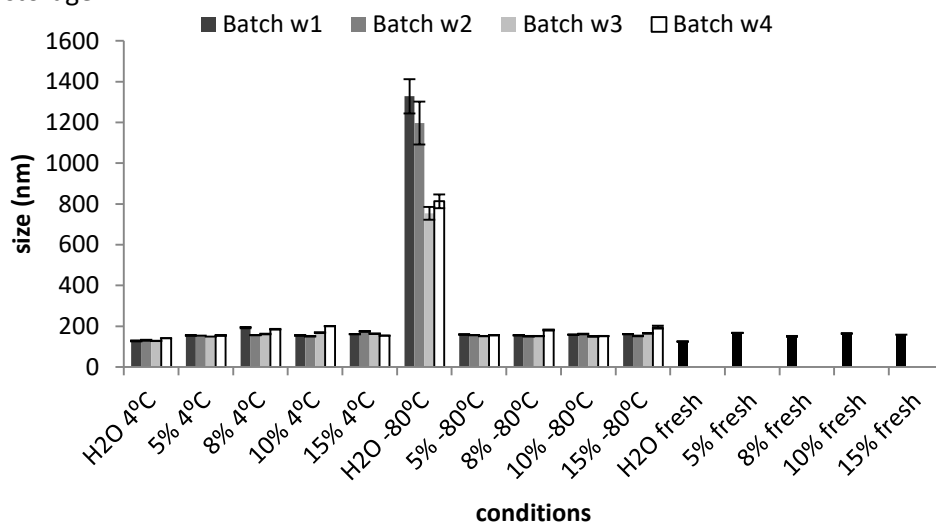


Fig. 5.3.1. Biophysical data of RTNs consisting of DD/ME27/Luc DNA in trehalose or water stored at 4 or -80 °C a) Work flow of this experiment. RTNs were prepared each week during 4 weeks and stored at 4 °C or -80 °C in trehalose or water. (n=3) b) the sizes and zeta potentials of each nanocomplex before storage (called 'original'). (n=3) c) the size and PDI of the original RTNs. The same data of b). d) the sizes of the RTNs stored at 4 °C or -80 °C in trehalose or water compared with the freshly prepared RTNs. (n=3) In all the graphs each column represents the mean ± SD.

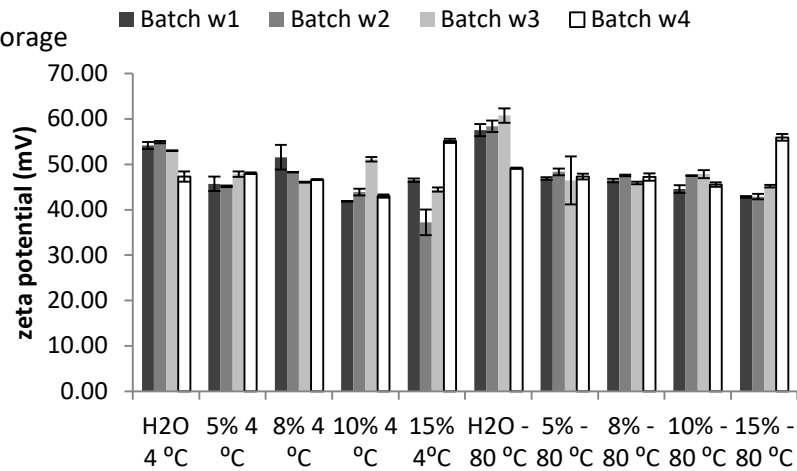
a) After storage

	Batch w1		Batch w2		Batch w3		Batch w4	
	size	PDI	size	PDI	size	PDI	size	PDI
H2O 4 °C	128.17	0.23	131.13	0.26	127.80	0.25	141.37	0.21
5% 4 °C	154.97	0.23	154.27	0.24	148.77	0.25	155.07	0.32
8% 4 °C	193.97	0.34	156.37	0.25	161.70	0.27	185.27	0.32
10% 4 °C	154.93	0.24	150.60	0.23	169.40	0.34	200.90	0.21
15% 4 °C	161.57	0.26	174.47	0.35	163.53	0.32	154.00	0.26
H2O -80 °C	1328.00	0.70	1197.00	0.76	753.47	0.59	813.10	0.22
5% -80 °C	159.77	0.24	156.43	0.26	151.83	0.25	156.03	0.30
8% -80 °C	156.10	0.23	150.67	0.24	151.33	0.25	181.10	0.21
10% -80 °C	158.93	0.24	162.07	0.30	150.63	0.26	151.93	0.29
15% -80 °C	161.13	0.26	151.87	0.25	165.37	0.34	195.10	0.54

b)

	size	PDI	zeta potential
H2O fresh	125.87	0.21	44
5% fresh	166.53	0.29	41.60
8% fresh	151.93	0.22	41.67
10% fresh	162.60	0.29	42.23
15% fresh	158.23	0.25	41.07

c) After storage



d)

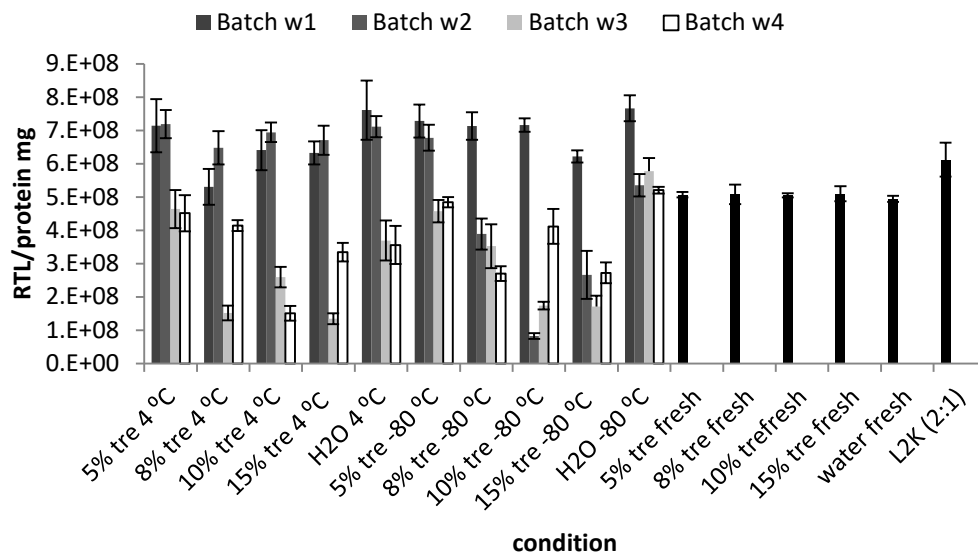


Fig. 5.3.2. Biophysical data and the function of data of RTNs consisting of DD/ME27/Luc DNA in trehalose or water stored at 4 or -80°C a) the sizes and the PDI of RTNs stored at 4 or -80°C in trehalose or water. (n=3) The same data of Fig. 5.3.1.d. b) the sizes, PDI and the zeta potential of the freshly made RTNs in d). (n=3) c) the zeta potential of RTNs stored at 4 or -80°C in trehalose or water. (n=3) d) the transfection efficiency of RTNs stored at 4 or -80°C in trehalose or water compared with the freshly prepared RTNs. (n=6). In all the graphs each column represents the mean± SD.

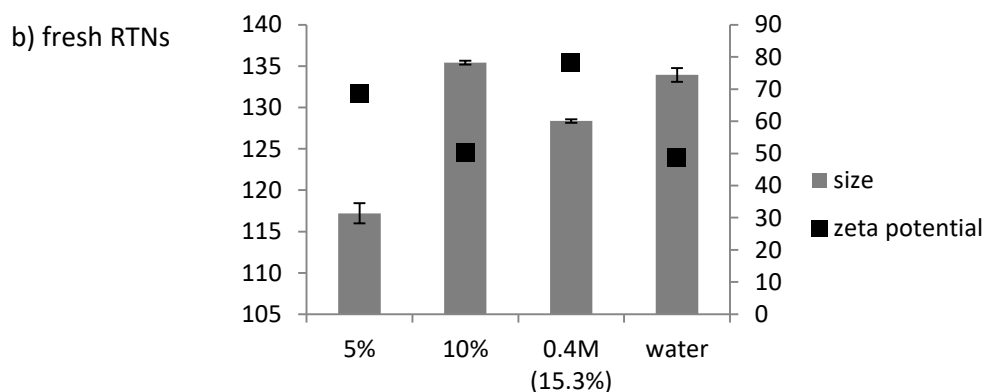
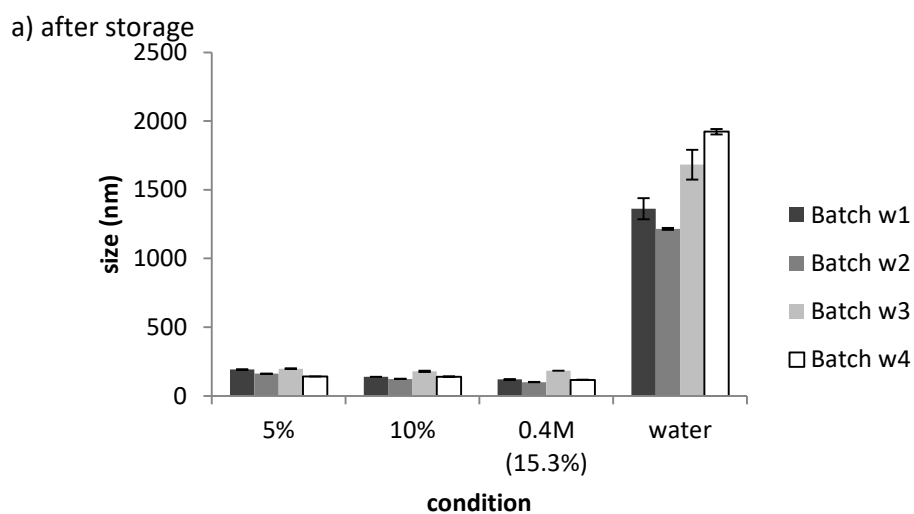
5.3.2. RTNs in trehalose kept at -80 °C

The results of 5.3.1. showed that RTNs stored at 4 °C for 3 weeks or more dropped the transfection efficiency. We hypothesised that storage at -80 °C can keep the function of RTNs compared with 4 °C, and investigated the biophysical character and the function of RTNs kept at -80 °C for 1-4 weeks. We prepared RTNs in 5%, 10% and 0.4 M (approximately 15.3%) trehalose kept at -80 °C once each week for 4 weeks and thawed them just before transfection into Nuero-2A. The sizes, PDIs, zeta potentials were measured, and the Luciferase expression was assessed as the transfection efficiency.

The sizes and PDIs of the RTNs kept at -80 °C were similar to those of the RTNs frozen at -80 °C and stored at 4 °C (Fig. 5.3.3.a,b,c) while the zeta potentials were higher. The sizes were between 100-200 nm in the RTNs in trehalose while RTNs in water became significantly larger, which is approximately 1200-1900 nm. Overall, they were not significantly different from those of the freshly prepared RTNs, except the RTNs in water. The zeta potentials of RTNs in 5% and 10% trehalose and water were around 45-65 mV while those of 0.4 M trehalose were about 90-99mV. Except for the RTNs in 0.4 M trehalose, the zeta potentials were similar to those of the freshly prepared RTNs.

The transfection efficiency was compared with that of freshly made RTNs. The transfection efficiencies of RTNs in 5% and 10% trehalose stored for 1, 2 and 3 weeks were almost the same and were higher than those of the freshly prepared RTNs. RTNs in 15% trehalose did not achieve the same levels of transfection efficiency as those in 5% and 10% stored for 1, 2 and 3 weeks while that in 10% stored for 4 weeks dropped down. RTNs in water did not show any trend, and they were inconsistent (Fig. 5.3.3.d).

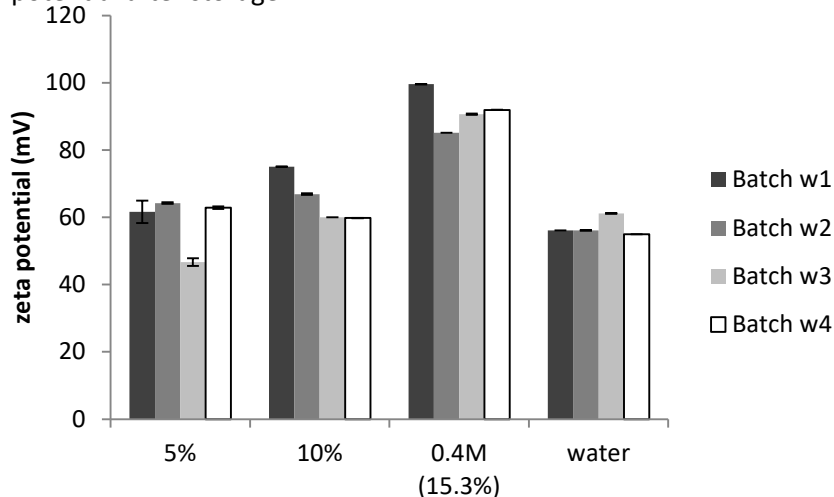
These results suggest that storage at -80 °C until transfection kept more stably of the function compared with stored at 4 °C.



c) size and PDI of fresh RTNs and stored RTNs

	Fresh		Batch w1		Batch w2		Batch w3		Batch w4	
	size	PDI	size	PDI	size	PDI	size	PDI	size	PDI
5%	117.20	0.24	191.57	0.38	161.40	0.32	198.00	0.35	140.87	0.29
10%	135.40	0.22	138.23	0.32	122.80	0.22	178.63	0.38	139.73	0.39
0.4M (15.3%)	128.37	0.39	119.00	0.44	99.57	0.39	183.40	0.33	116.33	0.35
water	133.93	0.33	1361.00	0.68	1214.33	0.61	1682.67	0.72	1922.33	0.96

d) zeta potential after storage



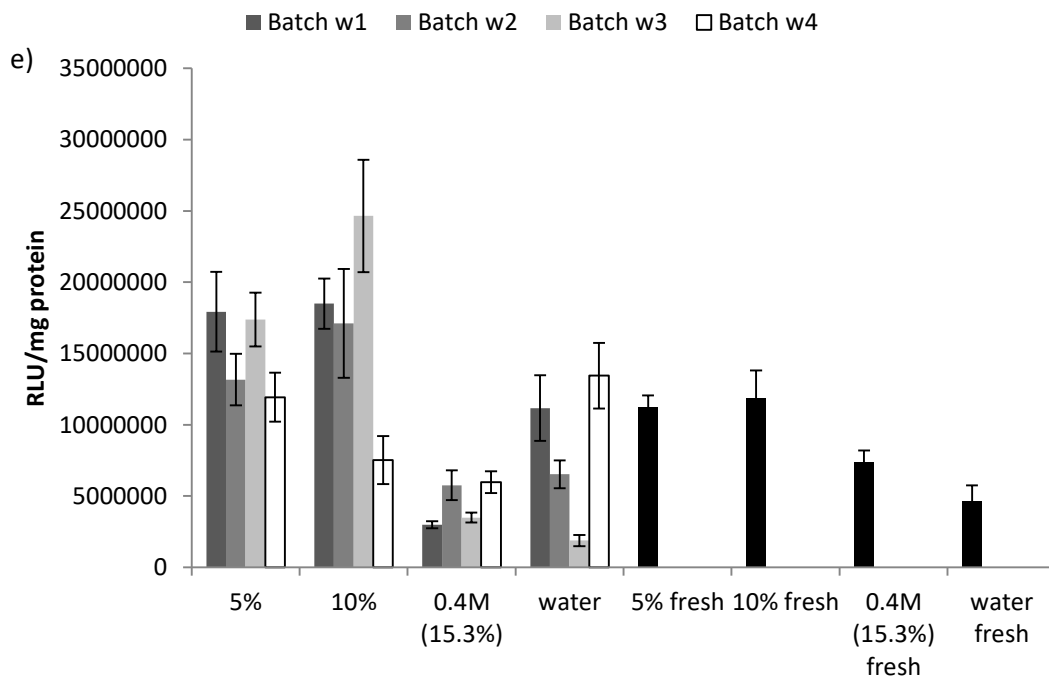


Fig. 5.3.3. the biophysical characters and the function of RTNs kept at -80 °C a) the size of RTNs kept at -80 °C in trehalose or water. b) the size and zeta potentials of the freshly prepared RTNs. (n=3) c) the sizes and PDIs of RTNs kept at -80 °C and freshly prepared when they were transfected. (n=3) d) zeta potentials of the RTNs kept at -80 °C. (n=3) e) the transfection efficiency of the RTNs kept at -80 °C and freshly prepared. (n=6). In all the graphs each column represents the mean± SD.

5.3.3. Luciferase silencing by siRNA delivered by RTNs in trehalose stored at 4 °C or -80 °C

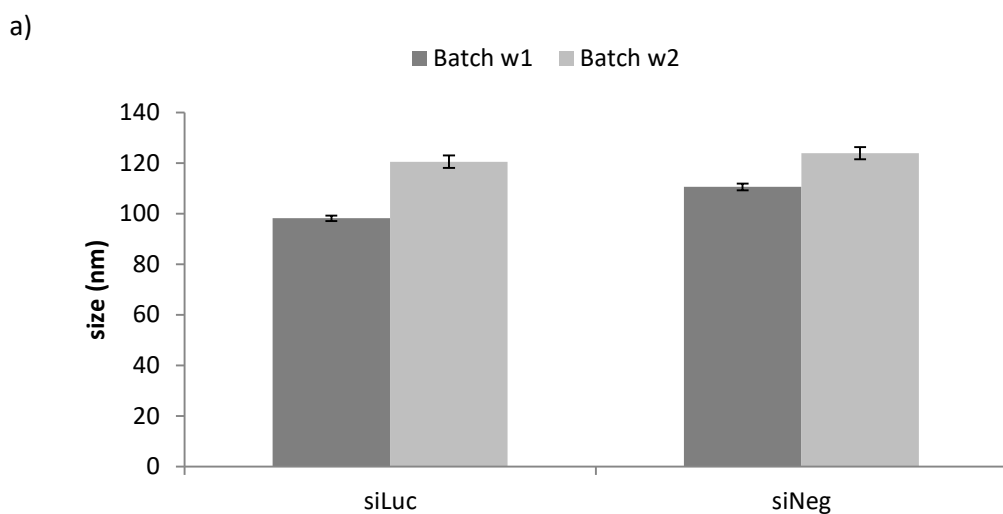
We then performed Luciferase siRNA transfection into Neuro-2A transduced and expressing Luciferase to observe the ability of trehalose to retain the biophysical character and the function of RTNs containing siRNA. RTNs consisting of DD, ME27 and anti-Luciferase siRNA (siLuc)/Negative control siRNA (siNeg) were made and prepared in 5, 10 and 20% trehalose. The RTNs were prepared once each week for 2 weeks and were stored at 4 °C or -80 °C. RTNs stored at -80 °C were transferred to 4 °C until the transfection after stored at -80 °C overnight, rather than kept at -80 °C until transfection. The biophysical character of the RTNs was observed, and the silencing efficiency was measured by luciferase expression level. They were compared with those of freshly prepared RTNs.

The size of the original RTNs in Batch w2 was slightly smaller than that of Batch w1 in both siLuc and siNeg, and the PDI was 0.28-0.37 (Fig. 5.3.4.a,b). The zeta potential of RTNs containing siLuc was approximately 44 mV, which is higher than that of siNeg by 10 mV (Fig. 5.3.4.b). Although the freshly made RTN of siLuc in water was slightly bigger than the original RTNs in Batch w1, w2 and the other freshly made RTNs of siLuc and siNeg, they were all approximately 100-150 nm and the zeta potential was about 30-50 mV (Fig. 5.3.4.c). In the RTNs stored at 4 °C or -80 °C in trehalose, overall they were approximately 100-150 nm and are similar to those of the freshly prepared RTNs. On the other hand, the RTNs in water stored at -80 °C were more than 500 nm. The PDIs of the RTNs in trehalose at 4 °C or -80 °C and water at 4 °C did also not significantly change while the PDIs of the RTN in water at -80 °C was almost twice that of the others (Fig. 5.3.4.d).

The zeta potentials of the RTNs in trehalose at 4 °C or -80 °C and water at 4 °C were similar, and those were around 30-50 mV. On the other hand, the zeta potentials of the RTNs in water stored at -80 °C were bigger and were about 60-70 mV (data not shown).

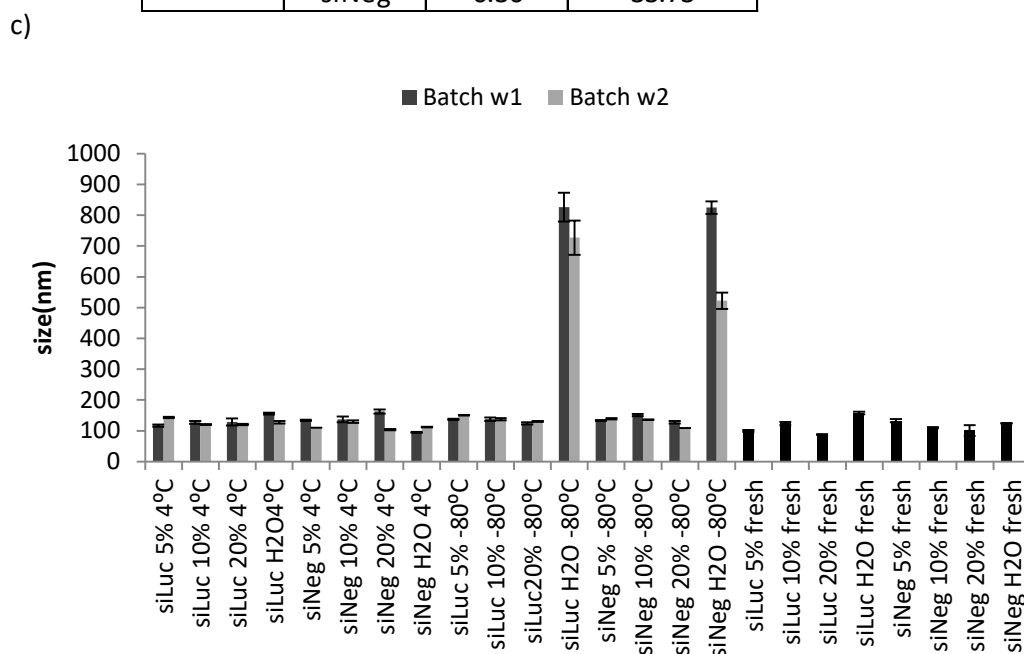
In the silencing efficiency, the RTNs Batch w1 except water at -80 °C achieved approximately 5% - 10% silencing while those in water at -80 °C did not show knockdown (Fig. 5.3.4.e). On the other hand, the silencing efficiencies of RTNs Batch w1 were various among the conditions. The RTN in 10% trehalose stored at 4 °C achieved the highest silencing at 25.6% following by 20% at -80 °C, which achieved 19.6% silencing. The other RTNs Batch w2 except 20% 4 °C and 10% at -80 °C achieved similar knockdown efficiency to those of the ones Batch w1, which was approximately 10% knockdown. In the freshly prepared RTNs, 5% and 10% achieved about 9.0% and 1.8% silencing respectively, and the others did not. 5% trehalose achieved slightly better silencing efficiency in the freshly prepared RTNs.

The data may imply that trehalose can maintain the biophysical character of RTNs containing siRNA and the storage at both 4 °C and -80 °C seems to improve the function slightly. In addition, storage at both 4 °C and -80 °C for 1 week gives better silencing efficiency than that for 2 weeks. It is likely that storage in around 10% trehalose at 4 °C for a week achieves the highest efficiency.



b)

		PDI	zeta potential
Batch w1	siLuc	0.28	46.00
	siNeg	0.37	34.40
Batch w2	siLuc	0.33	42.53
	siNeg	0.36	33.73



d)

PDI		siLuc 5%	siLuc 10%	siLuc 20%	siLuc H2O	siNeg 5%	siNeg 10%	siNeg 20%	siNeg H2O
Batch w1	4°C	0.34	0.39	0.56	0.35	0.41	0.38	0.55	0.28
	-80°C	0.36	0.34	0.39	0.54	0.33	0.36	0.45	0.62
Batch w2	4°C	0.36	0.30	0.48	0.37	0.32	0.38	0.45	0.33
	-80°C	0.34	0.37	0.38	0.53	0.34	0.34	0.37	0.50
fresh		0.29	0.39	0.49	0.39	0.40	0.45	0.44	0.39

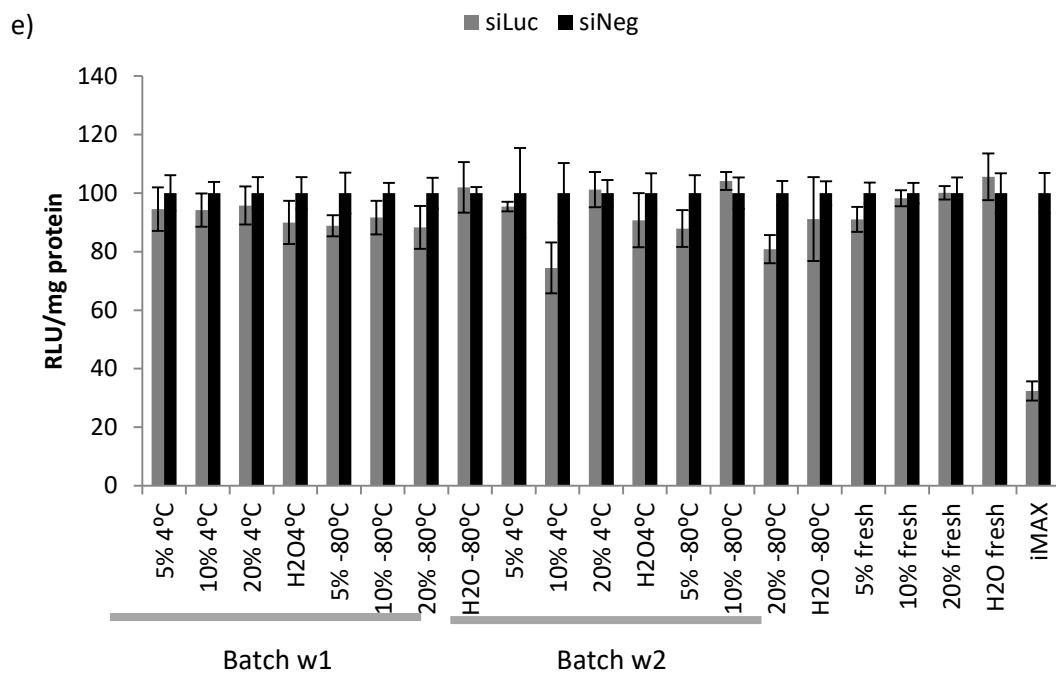


Fig. 5.3.4. the sizes and zeta potentials of RTNs containing siLuc and the silencing efficiency a) the size of the original RTNs containing DD, ME27 and siLuc/siNeg. (n=3,technical replicates) b) the PDIs and zeta potentials of the original RTNs. (n=3,technical replicates) c) the sizes of the RTNs stored at 4 °C or -80 °C and the freshly prepared RTNs. (n=3,technical replicates) d) the PDIs of the RTNs stored at 4 °C or -80 °C and the freshly prepared RTNs. e) Luciferase silencing efficiency of the RTNs. (n=6, biological replicates) In all the graphs each column represents the mean± SD.

5.3.4. GAPDH silencing by siRNA delivered by RTNs in trehalose stored at 4 °C or -80 °C

We then performed GAPDH silencing by anti-GAPDH siRNA (siGAPDH) packaged with DD and ME27 in Neuro-2A to investigate the ability of trehalose to retain the biophysical character and the function of RTNs containing another siRNA, anti-GAPDH siRNA. The RTNs were prepared in 8 or 10% trehalose and were stored at 4 °C overnight, or were frozen at -80 °C for 3 hours and then transferred to 4 °C and stored overnight. The size and zeta potential of these RTNs were measured as well as their transfection efficiencies, and compared with freshly prepared RTNs. The biophysical properties of the RTNs just after the storage at -80 °C for 3 hours before transfer to 4 °C were also measured this time.

The sizes of the original RTNs of siGAPDH and siNeg (: the RTNs before the storage) (Fig. 5.3.5.a) were slightly larger than those in the siLuc RTNs experiment above (Fig. 5.3.4.b). They were approximately 143.0 nm -194.5 nm. The PDIs were more than 0.44, and the highest was 0.77 in siNeg in water, which means they were heterogeneous. The zeta potentials of the original ones were about 61.2-81.0 mV, which is 1.5-2 times higher than those of the siLuc RTNs experiment.

The sizes of the RTNs containing siGAPDH stored at 4 °C or -80 °C was also overall slightly bigger than those of the RTNs containing siLuc experiment above (Fig. 5.3.4.c) at 150 nm -230 nm: the smallest one of siNeg in 10% trehalose stored at -80 °C was 138.76 nm and the largest one of siGAPDH stored at 4 °C in water was 231.53 nm (Fig. 5.3.5.a,b). In addition, the size of RTNs stored at -80 °C became slightly smaller after the storage at 4 °C overnight in all the conditions. The PDIs were also higher than those of the RTNs in the siLuc experiment above, and were approximately 0.40 to 0.87 (Fig. 5.3.5.b). The sizes of the freshly prepared RTNs were similar to those of the original RTNs (Fig. 5.3.5.a,d). The PDIs

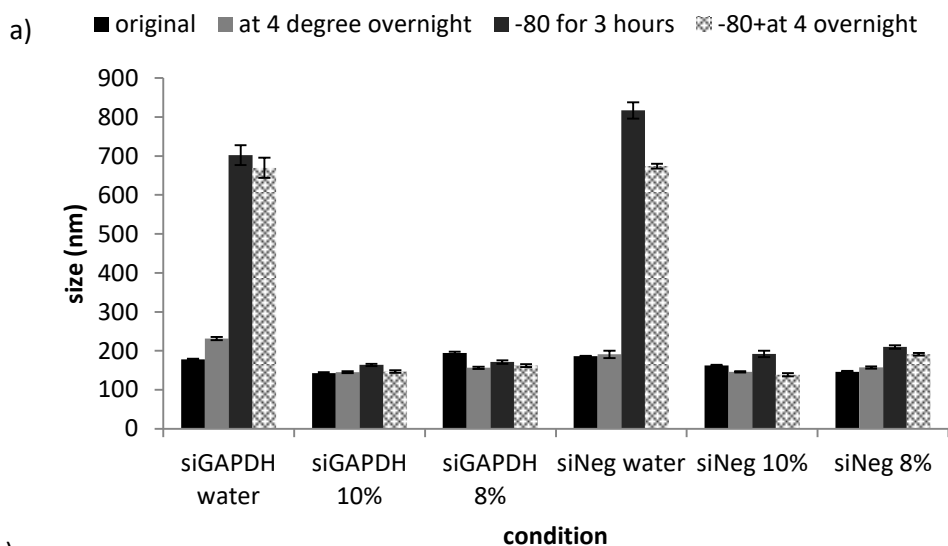
were 0.40-0.62 in both the stored and the fresh RTNs, which suggest there are multiple populations in the RTNs (Fig. 5.3.5.b, d).

The zeta potentials of the RTNs containing siGAPDH and siNeg in this experiment were 59.4 mV - 87.3 mV, which is almost twice higher than those of the siLuc RTNs experiment (Fig. 5.3.5.c). The zeta potentials of the RTNs in water were relatively stable among the different storage conditions while the size in water at -80 °C was dramatically changed. On the other hand, RTNs in trehalose tended to be more positively charged and to be changed among the different storage conditions. Overall, the zeta potentials of the RTNs stored at 4 °C or -80 °C were similar to those of the freshly prepared RTNs (Fig. 5.3.5.c,d).

In terms of transfection efficiency, overnight storage at 4 °C in 10% trehalose and at -80 °C in water and 8% trehalose improved the silencing efficiency (Fig. 5.3.5.e). The RTN in 10% at 4 °C achieved 71.1% and the one in 8% at -80 °C did 54.7%, which is higher than 53.0% of the positive control RNAiMAX. Interestingly, the large RTN in water at -80 °C also achieved 71.1%, which is the same silencing efficiency as that of in 10% at 4 °C. In addition, the overnight storage at 4 °C in water improved the efficiency at approximately 34.7% while the fresh one in water did 11.8%. However, the silencing efficiencies of the RTNs in trehalose except 10% at 4 °C and 8% at -80 °C were similar among the different storage conditions, which were 42.3-27.2%. There were no significant differences between siGAPDH and siNeg of the fresh RTN in water and of the RTN in 10% trehalose stored at -80 °C while there were significant differences between siGAPDH and siNeg of the other conditions.

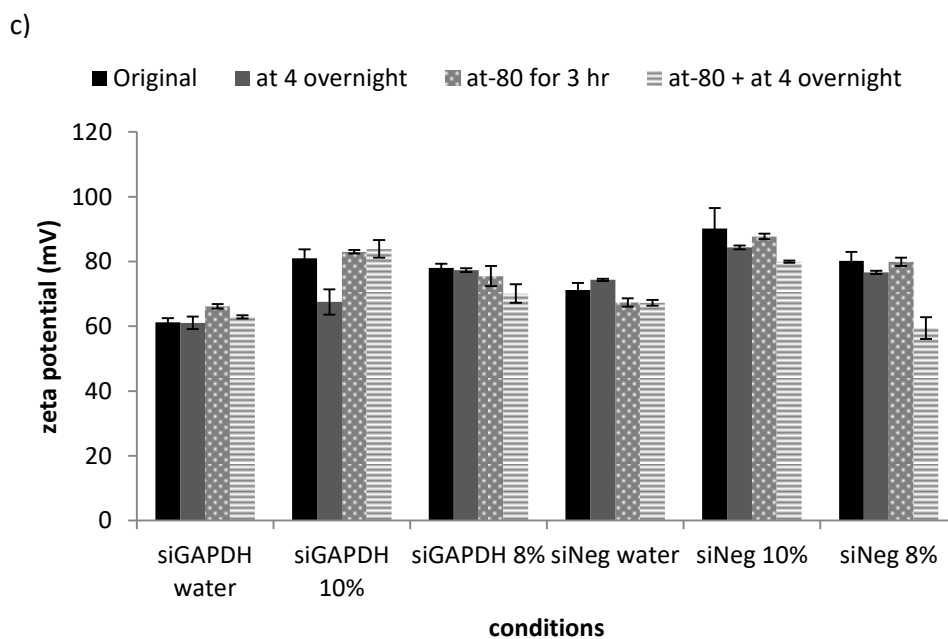
The data may imply that trehalose and longer incubation could improve the function and the 8% trehalose at 4 °C seemed to give the best result. The conditions of adding trehalose did not show affection to the sizes and PDI, and however, the RTNs in trehalose tended to have

higher zeta potentials. That might suggest that higher zeta potential can give better silencing efficiency rather than smaller size and PDI *in vitro*.



b)

PDI	condition			
	original	4°C	-80°C for 3 hours	-80°C + 4°C
siGAPDH H2O	0.48	0.54	0.52	0.40
siGAPDH 10%	0.44	0.46	0.58	0.42
siGAPDH 8%	0.64	0.49	0.45	0.43
siNeg H2O	0.77	0.53	0.54	0.52
siNeg 10%	0.55	0.65	0.81	0.76
siNeg 8%	0.56	0.74	0.87	0.79



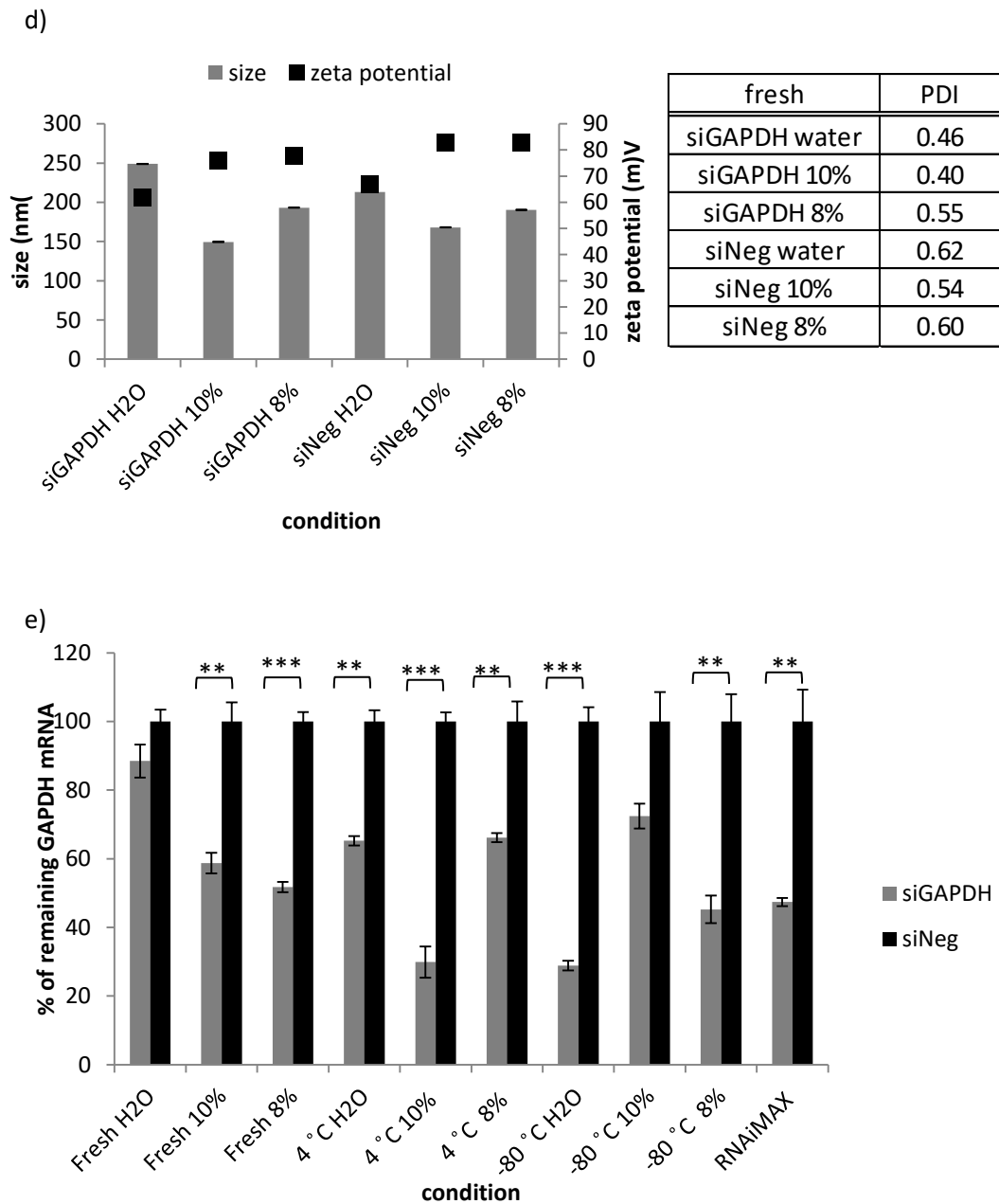


Fig. 5.3.5. The biophysical character and the function of RTNs consisting of siGAPDH/siNeg, DD and ME27 a) the sizes of the original and the stored RTNs. RTNs stored at $-80\text{ }^{\circ}\text{C}$ were measured twice: just after thawing the RTNs and after transferred and stored at $4\text{ }^{\circ}\text{C}$. (n=3) b) the PDI of the original and the stored RTNs. c) the zeta potentials of the original and the stored RTNs. (n=3) d) the sizes, PDI and the zeta potentials of the fresh RTNs. (n=3) e) GAPDH silencing efficiency by the stored and the freshly prepared RTNs. (n=3) In all the graphs each column represents the mean \pm SD. **p<0.01, ***p<0.0001

5.3.5. MYCN silencing by siMYCN delivered with RTNs stored at 4 °C or -80 °C in trehalose or water

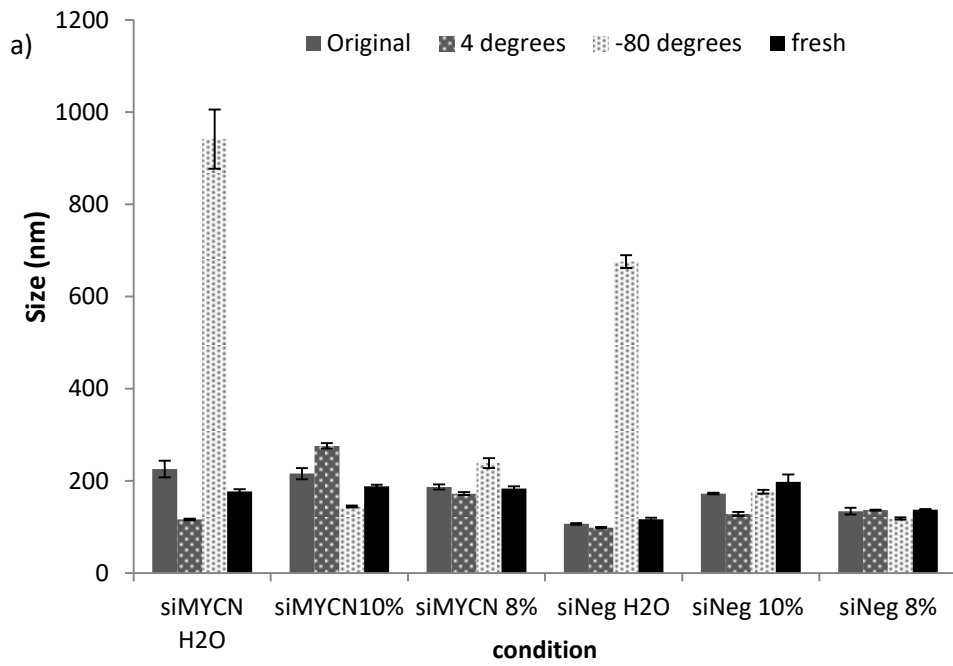
To observe the effect of trehalose in MYCN silencing by siRNA, we performed MYCN silencing by siMYCN in the MYCN-amplified NB cell line, Kelly. RTNs consisted of DD, ME27 and siMYCN or siNeg and were prepared in 8% or 10% trehalose, or water and stored at 4 °C or -80 °C.

The sizes of the original RTNs containing siMYCN (the ones not stored at 4 °C or -80 °C yet) were overall slightly larger than those of siNeg (Fig. 5.3.6.a). After storage, the RTNs in water at -80 °C became dramatically larger than the others while there were no clear trends in the size of the other conditions. The PDIs were similar among the RTNs of siMYCN and siNeg as well as among the original, the stored and the fresh RTNs (Fig. 5.3.6.b). The average zeta potentials of each condition showed the similar trend between siMYCN and siNeg; the RTNs in water and 8% trehalose were approximately 50 mV while the ones in 10% trehalose were around 65 mV (Fig. 5.3.6.c). There were no significant effects of storage on zeta potential, and the error bars of the average zeta potentials were small in all the conditions.

In terms of silencing function, the results of qRT-PCR analysis of MYCN silencing showed different trends from those of siGAPDH (Fig. 5.3.6.d). Especially, the freshly prepared RTNs showed completely different trends. The freshly RTN in water achieved better silencing ($p=0.0016$) compared with the RTNs in trehalose and that of RNAiMAX which silenced only 17.2% MYCN mRNA ($p=0.12$). The second best was the RTN in 8% trehalose at 4°C and achieved 38.2% silencing (0.00047). Similarly, the RTN in 10% trehalose at 4°C silenced 25.7% and it was significantly different from the siNeg in the same condition ($p=0.00047$). The RTNs in 10% trehalose at -80°C achieved 37.5%, and however, it was not

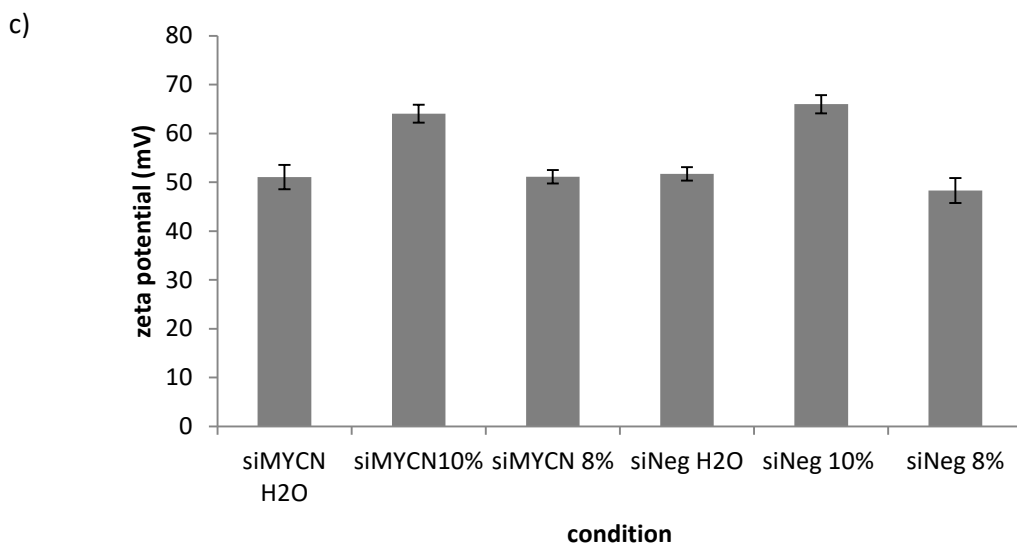
statistically significant ($p=0.099$) because it had a larger error bar. Surprisingly, the RTNs in water stored at $-80\text{ }^{\circ}\text{C}$ achieved 21.1% ($p=0.00091$), which is higher than those of water at $4\text{ }^{\circ}\text{C}$, 8% at $-80\text{ }^{\circ}\text{C}$ and fresh 10% and 8%.

These results suggest that trehalose can enhance the silencing efficiency in RTNs stored at $4\text{ }^{\circ}\text{C}$ compared with, and can protect the biophysical characters of RTNs containing siMYCN even though they are thawed after freezing at $-80\text{ }^{\circ}\text{C}$.



b)

PDI	Original	4 degrees	-80 degrees	fresh
siMYCN H2O	0.58	0.56	0.55	0.63
siMYCN10%	0.74	0.57	0.46	0.57
siMYCN 8%	0.68	0.47	0.66	0.47
siNeg H2O	0.51	0.43	0.40	0.49
siNeg 10%	0.79	0.55	0.78	0.61
siNeg 8%	0.44	0.45	0.48	0.44



d)

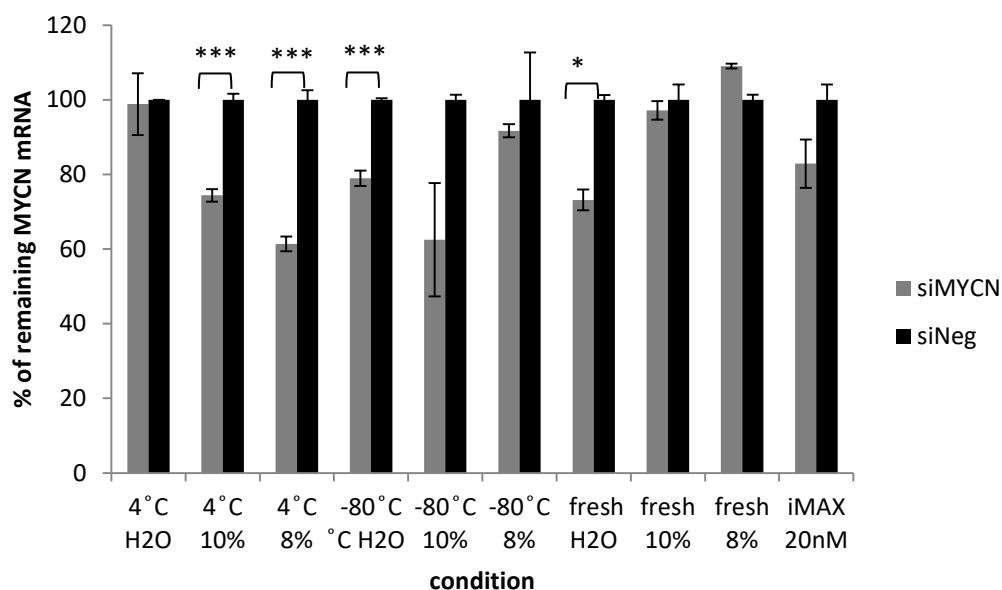


Fig. 5.3.6. The biophysical character and the function of RTNs consisting of siMYCN/siNeg, DD and ME27 a) the sizes of the original and the stored RTNs. b) the PDI of the original and the stored RTNs. c) the average of the zeta potentials of the original and the stored RTNs. d) MYCN silencing efficiency by the stored and the freshly prepared RTNs in human NB cell line Kelly. In all the graphs each column represents the mean \pm SD. * $p < 0.05$, *** $p < 0.0001$

5.3.6. Anionic RTNs in 8% trehalose stored at 4 °C overnight

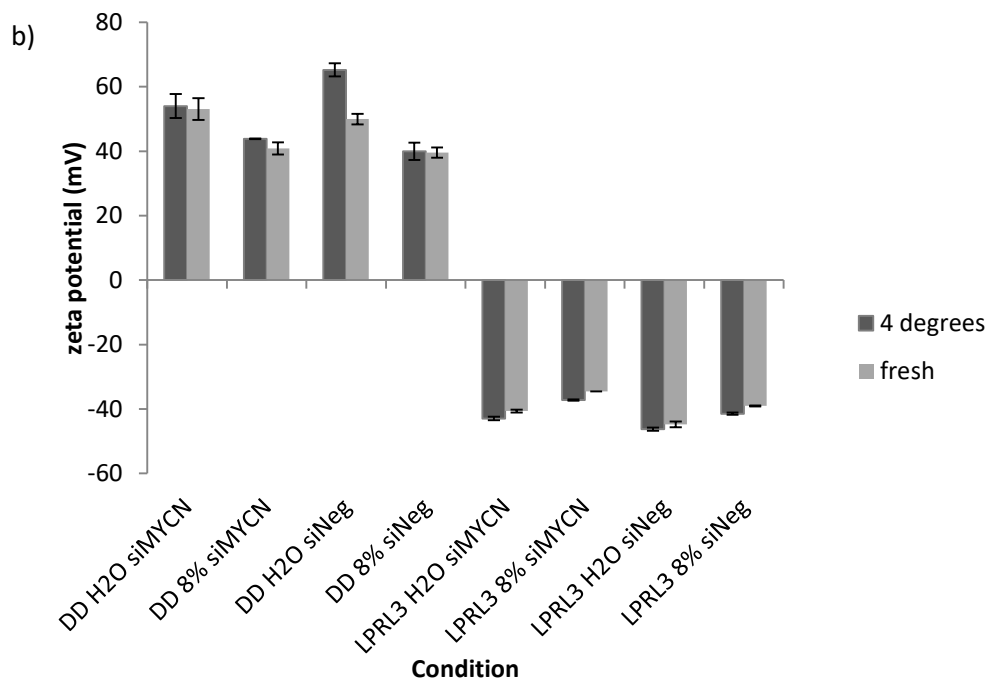
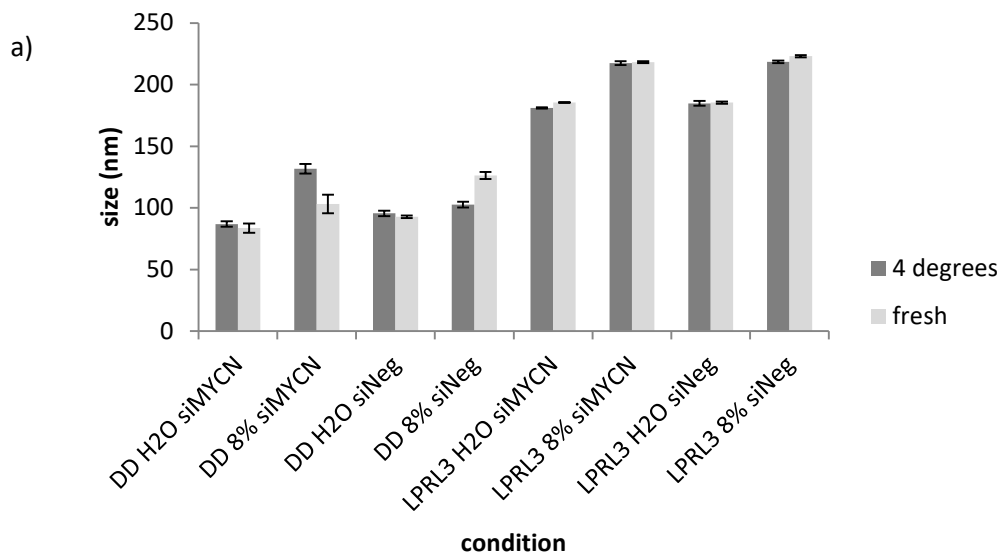
Finally, we observed the ability of trehalose in anionic formulations. We carried out an experiment where anionic RTNs consisting of DD (cationic liposome), AT3 (anionic liposome), ME27 and siMYCN/siNeg. To prepare the anionic RTNs, DD, ME27 and siRNA were mixed and cationic RTNs were formed first. Then anionic liposome was mixed with the cationic RTNs and the anionic liposome covers the cationic RTNs. The RTNs were stored at 4 °C overnight to investigate the efficiency of trehalose under the condition. In this time, the RTNs were not stored at -80 °C because the biophysical character and the function of the RTNs in trehalose stored at -80 °C were not significantly different from those of the RTNs stored at 4 °C in the experiments above.

In general, cationic formulations were almost half the size of the anionic, double-layered formulations (Fig. 5.3.7.a). There were no differences between the sizes of the RTNs stored at 4 °C and those prepared freshly, before the transfection, while the RTNs in 8% trehalose were slightly larger than those in water. The cationic RTNs were smaller than the cationic RTNs containing siLuc or siGAPDH in the experiments above (Fig. 5.3.6.a). The zeta potentials of the cationic RTNs were similar to those of the cationic RTNs above (Fig. 5.3.6.c, Fig. 5.3.7.b) while the cationic RTNs in water had higher zeta potentials than those in 8% trehalose. The anionic RTNs in water were more negatively charged than RTNs in 8% trehalose. In terms of RTN heterogeneity, the cationic formulations had much higher PDIs while the anionic ones were very low at approximately 0.18-0.23 (Fig. 5.3.7.c). However, the PDIs of the cationic RTNs were similar to those of the cationic RTNs containing siLuc and siGAPDH above (Fig. 5.3.6.b).

In terms of silencing function, the cationic RTNs in water at 4°C and the fresh cationic and anionic RTN in water were able to achieve higher silencing, of 59.9%, 61.4% and 66.4%

respectively, than 58.0% of RNAiMAX (Fig. 5.3.7.d). In addition, they were all significantly different from that of siNeg in each condition ($p=0.013$, 0.00062 and 0.00031 , respectively). The other formulations also successfully silenced MYCN, at 36.5% - 46.5% knockdown. The RTNs in the same solution at 4 °C and the freshly prepared showed similar silencing efficiency except LPRL3 in water. In addition, there were not significant differences between siMYCN and siNeg in the cationic RTN in 8% trehalose at 4 °C, the anionic RTN in water at 4 °C and freshly prepared anionic RTN in 8% trehalose. On the other hand, the LPRL3 in 8% trehalose at 4 °C, the freshly prepared in 8% trehalose were significant ($p=0.016$ and 0.00036 , respectively).

The data imply that trehalose also maintains the biophysical character and function of anionic RTNs on freezing at -80 °C and thawing to 4 °C.



c) PDI

	4 degrees	fresh
DD H2O siMYCN	0.44	0.34
DD 8% siMYCN	0.51	0.47
DD H2O siNeg	0.32	0.31
DD 8% siNeg	0.42	0.45
LPRL3 H2O siMYCN	0.19	0.20
LPRL3 8% siMYCN	0.18	0.19
LPRL3 H2O siNeg	0.23	0.21
LPRL3 8% siNeg	0.23	0.19

d)

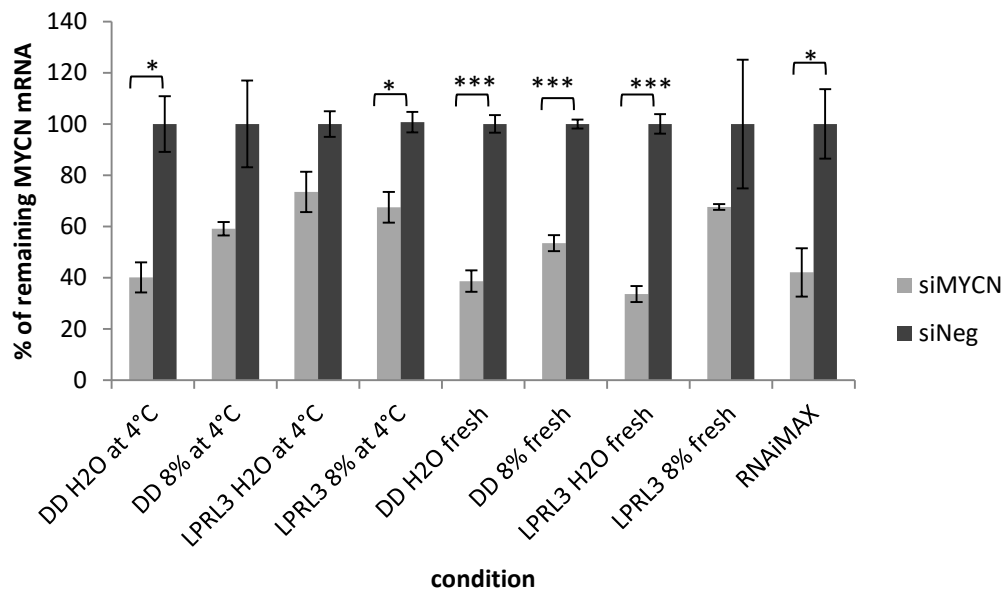


Fig. 5.3.7. The biophysical character and the function of RTNs consisting of siMYCN/siNeg, DD and ME27 a) the sizes of the RTNs stored at 4 °C and the fresh RTNs. (n=3) b) the PDI of the RTNs stored at 4 °C and the fresh RTNs. (n=3) c) the average of the zeta potentials of the RTNs stored at 4 °C and the fresh RTNs. (n=3) d) MYCN silencing efficiency by the stored and the freshly prepared RTNs in human NB cell line Kelly. (n=3) In all the graphs each column represents the mean± SD. *p<0.05, ***p<0.0001

5.4. Discussion

We conducted experiments in which RTNs in trehalose were stored at 4 °C or -80 °C. The biophysical characteristics and transfection/silencing efficiency were measured in order to observe the ability of trehalose to protect the RTNs from destruction by inhibiting formation of ice-crystals.

Trehalose is a non-reducing sugar and disaccharide, consisting of two α -glucose molecules bound by an α,α -1,1-glucoside bond (Fig. 5.4.1). Trehalose has high resistance to acid hydrolysis, and can exist in a closed-ring form because of the bonding (trehalose: CID 7427, PubChem). Because there are no internal hydrogen bonds, trehalose can easily form hydrogen bonds with the head groups of lipids. This maintains the space between the head groups, and keeps the membrane in the fluid phase (Peraira et al. 2004). Therefore, water is replaced by the trehalose molecule, and is located close to the lipid polar head groups (water-replacement hypothesis) (Jain & Roy, 2008).

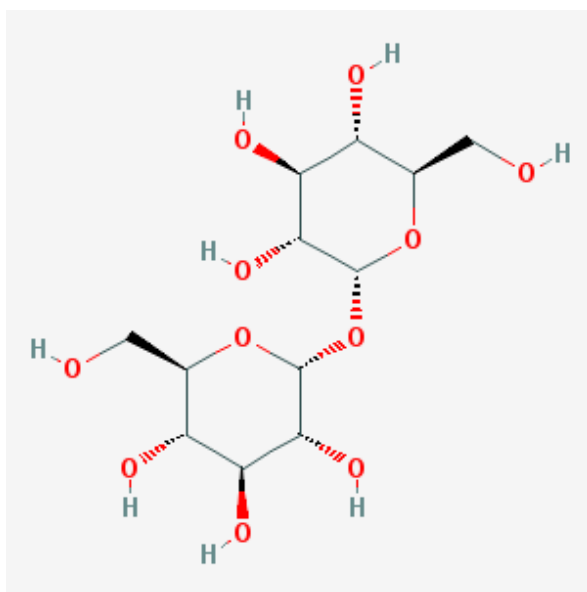


Fig. 5.4.1. Structure of trehalose Taken from (PubChem website)

In addition, trehalose inhibits the growth of ice-crystals in space between lipids. The melting point of a solution containing trehalose is lower than that expected from depression of the molecular freezing point because trehalose promotes a disruptive effect on the tetrahedral hydrogen-bond network of pure water (Uchida et al. 2012), resulting in smaller ice-crystals even after freezing of the trehalose solution (TREHA, Hayashibara website). Furthermore, the viscosity of trehalose increases with decreasing temperature, also affecting the growth process of ice- crystals (Uchida et al. 2012).

In our study, trehalose successfully maintained the biophysical properties of the RTNs containing DNA or siRNA at -80 °C, at all concentrations. In addition, incubation at 4 °C overnight or more tends to improve the PDI. Even the PDI of RTNs containing DNA stored at -80 °C in water became smaller when they were incubated at 4 °C for three weeks or more (Fig. 5.3.2.a), while the ones kept at -80 °C in water, and thawed just before transfection, showed higher PDIs. In general, smaller RTNs showed higher charges in cationic formulations.

In our study, the RTNs were prepared at 0.02 mg/mL at a range of trehalose concentrations from 5-20%. We observed that even at the lowest concentration of 5% trehalose, RTNs were able to maintain their biophysical characteristics. Date et al. (2010) reported that 20% trehalose was able to retain the sizes of nanoparticles packaging antibiotics up to 32 mg/mL at -40 °C and -70 °C, and that there was significant increase in size above that concentration. Similarly, Ball et al. (2017) pointed out that there was no significant difference in the size of lipid nanoparticles containing siLuc, prepared at 0.125 mg/mL in 20% trehalose at -80 °C, while the size and PDI became larger in nanoparticles in 1, 5 and 10% trehalose. These results suggest that our formulations were diluted, compared to the concentrations in the other studies, and that lower concentrations of trehalose were able to maintain the size of the RTNs. However, RTNs at concentrations higher than 32 mg/mL might require more than

20% trehalose solution to preserve their biophysical character, according to Date et al. (2010).

In terms of function, the RTNs for all trehalose concentrations (one or two weeks storage at 4 °C) achieved higher transfection efficiencies with Luciferase pDNA than those stored at 4 °C in either water or trehalose for three or four weeks. In addition, the RTNs stored at -80 °C for one week (frozen at -80 °C and then stored at 4°C till needed) or just kept at -80 °C also achieved high transfection efficiency. Tseng et al. (2007a,b) reported that trehalose at an optimal concentration can enhance transfection efficiency of GFP pDNA/polyethylenimine (PEI) complexes in vitro, and GFP pDNA/lipid complexes in vivo, although it should be noted that the lipids used in this study differ from the ones used in our own work, and trehalose was added in transfection media instead of to the RTN suspension. We tested the transfection methods in Tseng et al. (2007b) in which the trehalose was added in complete media before transfection and the concentration of the trehalose was kept in the transfection media too. However, transfection efficiency was not improved compared with the RTNs that were prepared in trehalose solution, and were transfected without additional trehalose. Therefore, trehalose was not added to transfection media in our experiments.

Tseng et al. (2007a) explained that a possible reason why trehalose might enhance transfection efficiency is that the disaccharide might increase the cellular entry of nucleic acid by stabilising the lipid-based liposome. Furthermore, Ball et al. (2017) reported that siRNA in liposomes in 20% trehalose achieved higher silencing efficiency, compared with those in 1%, 5% and 10% trehalose, which is not in line with our findings where 5-10% trehalose showed higher transfection/silencing efficiencies. Tseng et al (2007a) noted that the most effective concentration of trehalose is different among cell lines. This is a potential explanation for this disagreement between optimal trehalose concentrations.

On the other hand, there were no significant differences in efficiency among different conditions in the siLuc transfection. The siLuc transfections showed overall lower silencing efficiency, compared with the other silencing experiments. A possible reason for this is that the Neuro-2A cells used, stably express luciferase by transduction. This may lead them to express very high levels of luciferase as they possibly contain many copies of the transduced Luciferase gene. However, with RNAiMAX approximately 55% silencing was achieved. Hence, the silencing efficiency of the RTNs was not high. The reason for this low silencing efficiency is not clear.

Another possible reason the efficiency may have been affected is the batch of DD used, or the RTNs in the experiment had a lower positive charge than the ones in the experiments of siGAPDH and siMYCN transfections, which achieved good transfection/silencing efficiencies. RTNs with a higher positive charge are more easily attracted to a negatively-charged cell membrane. The zeta potentials of the RTNs in the siLuc transfections were approximately 33 to 46 mV, while those of the RTNs containing siGAPDH were >60 mV, achieving higher than 30% silencing overall. The fresh anionic RTNs containing siMYCN, however, achieved approximately 65% MYCN silencing, and the same formulations containing siMYCN in water stored at 4 °C with similar zeta potentials showed different silencing efficiency (Fig. 5.3.7.b and d). Therefore, this is difficult to explain the lower efficiency using only zeta potentials.

Interestingly, RTNs stored at -80 °C in water showed better transfection/silencing efficiencies, compared with the other conditions in the Luciferase pDNA and siGAPDH transfections. Probably, this is because larger RTNs can sediment faster than the others, and thus they stay on the bottom of the plate and can bind cells faster. In addition, Tseng et al. (2007a) argued that liposomes larger than 500 nm might enter cells via micropinocytosis. However, it would be difficult to deliver large RTNs, such as those >500 nm, to NB tumour

cells via the blood stream in vivo because of the blood-brain barrier. Therefore, this is only relevant to in vitro transfections.

Trehalose can maintain the biophysical characteristics of RTNs containing DNA/siRNA, and the function of RTNs in trehalose stored at 4 °C or -80 °C for up to two weeks, is not significantly different from that of the freshly prepared RTNs in DNA transfection. It may be necessary to perform experiments to investigate the function and biophysical characteristics of RTNs containing siRNA in trehalose for a longer time because we have not observed the function and biophysical character of RTNs stored for longer than 2 weeks. Lyophilisation of RTNs has the potential for further study. Although lyophilisation is more expensive than deep freezing, it is easier to transport anywhere in the world. In addition, trehalose is an ideal cryoprotectant because its glass transition temperature is one of the highest in sugars we commonly use, including sucrose, and the moisture absorbency of materials containing trehalose become lower through vitrification.

In conclusion, trehalose is very effective as a cryoprotectant when RTNs are stored at -80 °C. The biophysical characteristics of RTNs at 0.02 mg/mL is successfully retained in 5-20% trehalose at -80 °C, and it is likely that around 5-10% is the optimal concentration for the transfection/silencing efficiencies in the murine NB cell line, Neuro-2A, and a human NB cell line, Kelly. Function was maintained when the RTNs were stored at 4 °C for up to 2 weeks, or were kept at -80 °C and thawed just before transfection, or were thawed and stored at 4 °C for a week. This knowledge would be useful to keep RTNs long-term during transportation, although it will be necessary to perform further studies.

CHAPTER 6

General discussion and conclusion

6. General discussion and conclusion

In this study, we aimed to silence MYCN using siRNA and to induce differentiation and apoptosis for a novel therapy for NB. We first performed MYCN silencing by siMYCN using RNAiMAX (Thermo Fisher Scientific), a commercial lipid-based reagent to investigate MYCN silencing efficiency at mRNA and protein levels as well as downstream effects of MYCN reduction, described in Chapter 3. Then, we investigated MYCN silencing efficiency of siMYCN delivered by RTNs, described in Chapter 4. Finally, we assessed the potential for storage of RTNs at -80 °C using trehalose cryoprotectant and the ability to maintain the biophysical characters and the function of the RTNs, described in Chapter 5.

We successfully demonstrated MYCN silencing by siMYCN, NTRK1/TrkA upregulation as a downstream effect of MYCN reduction and slower growth rate of SK-N-BE(2) transfected with siMYCN *in vitro*. In addition, the morphological changes of SK-N-BE(2) transfected with siMYCN confirmed the differentiation in the cells. These results suggest that siMYCN silences MYCN at the mRNA and protein levels. In addition, siMYCN can induce differentiation in NB cells, such as SK-N-BE(2), with non-functional p53 and developing resistance toward RA (Joshi et al. 2007) and drugs dependent on p53 pathway after multiple sessions of chemotherapy and radiotherapy (Tweddle et al. 2001; Huang & Weiss 2013). siMYCN could be a novel therapy for relapsed NB after the standard therapy.

siMYCN delivered by cationic PEGylated RTN also successfully silenced MYCN mRNA *in vivo*, although it did not achieve sufficient knockdown *in vitro*. The achieved level of silencing may be induced by MYCN reduction at the protein level and Trk upregulation, according to the results in Chapter 3. In addition, the experiments of tumour uptake and biodistribution of the RTNs revealed that RTNs *in vivo* are specifically delivered to NB tumours and are internalised by the tumour. For further study, it will be necessary to

investigate the downstream effects, including TrkA upregulation triggered by siMYCN delivered by RTNs *in vitro* and *in vivo*. In addition, it is necessary to observe tumour mass changes after multiple doses of RTNs as an assessment of the therapeutic potential and inflammation in the tissues that might be induced by the injections by histology.

In addition, increasing the silencing efficiency is essential. Multiple injections of siMYCN may achieve higher knockdown because higher doses of RTNs can accumulate in the NB tissue. It may be possible to optimise RTNs for better internalisation into NB cells, for instance, using more than one peptide to target multiple receptors such as folate and glucose receptors. Silencing another mRNA or non-coding RNA such as NCYM, which are associated with MYCN transcription and/or MYCN stabilisation, also might achieve higher MYCN silencing.

Although MYCN has been widely studied, the transcription mechanisms have not been fully revealed (Zhao et al. 2016). Lui et al. (2016) reported that MYCN mRNA transcription may be unregulated by NCYM RNA binding with NonO, but the effects of NCYM on MYCN expression are still poorly understood, and it remains controversial as to whether the transcript of NCYM encodes a protein. When the relationships among NCYM, MYCN and lncUSMycN are fully revealed, there are potentials that the pathway can be a target to silence MYCN and that may enhance the MYCN silencing efficacy.

Another possible therapeutic approach may be Clustered Regularly Interspaced Short Palindromic Repeats (CRISPR) and the CRISPR-associated protein 9 (Cas9) (CRISPR/Cas9). Recently, a CRISPR/Cas9 system has been rapidly spread in gene therapy (Zhang et al. 2017), and we also used the system to non-MYCN amplified NB cell line SK-N-SH and amplified cell line SK-N-BE(2) (the experiments were conducted by a previous master's degree student in our group. The data are not shown). As a result, mRNA of CRISPR/Cas9

with gRNA was able to cut the target area on MYCN on SK-N-SH, which was confirmed by T7 endonuclease assay, and the MYCN protein was reduced by three rounds of transfections, while it was not seen in SK-N-BE(2) in either T7 endonuclease assay or immunoblotting. A possible reason for this result is SK-N-BE(2) have more than 100 copies of MYCN (Harenza et al. 2017). It may be difficult to induce indels using CRISPR/Cas9 as much as the indels can be seen in T7 endonuclease assay or MYCN protein reduction can be detected in immunoblotting.

On the other hand, Aguirre et al. (2016) showed that the DNA breaks were induced when genes of high copy number were targeted by CRISPR/Cas9, leading to reduction of proliferation via G2 cell cycle arrest. Therefore, targeting MYCN by CRISPR/Cas9 in MYCN amplified NB cells may eventually induce cell cycle arrest, which could be another strategy for therapy in NB.

Another promising approach might be CRISPR interference (CRISPRi). In this strategy, targeted genes are silenced via methylation by dCas9-KRAB (Krüppel-associated box) (Gilbert et al. 2014). sgRNA guides dCas9-KRAB to the target region of a gene, and dCas9 forms a complex with the target region on DNA and the gRNA (Thakore et al. 2015). Then, KRAB employs a heterochromatin-forming complex that triggers histone methylation and deacetylation, and the transcription of the gene is repressed (ibid.). The effective target regions are promoter regions, 5' untranslated regions and proximal enhancer elements (ibid.). The advantages of the strategy are reversible knockdown (Boettcher & McManus 2015) and no DNA breaks (Gilbert et al. 2014).

We also successfully showed that trehalose maintained the biophysical characters and function of RTNs at -80 °C. The data suggest that it is possible to prepare large amounts of RTNs, store the aliquots in trehalose at -80 °C and use them in different experiments, which

allows consistency in the conditions among experiments as well as transporting them for long distance. However, it is still necessary to investigate the maximum concentrations of RTNs towards trehalose and the effect in anionic double layered RTNs containing MYCN siRNA as well as the effects in RTNs in lyophilisation.

Transportation and stable storage at -80 °C are not always available, and they are more expensive than those at room temperature. On the other hand, freeze-dried reagents have longer shelf life and it is easier to transport them everywhere in the world. This method can be applied for RTNs consisting of not only siRNA but also drugs nucleus acids including pDNA or mRNA of CRISPR/Cas9. It may help to transport gene therapy reagents using lipid-based nanoparticles in clinical application in the future.

In conclusion, siMYCN silenced MYCN at mRNA and protein levels and that induced significant differentiation as well as morphological change showing differentiation in the transfected NB cell line with MYCN amplified developing drug resistance. These results may imply that therapy using siMYCN is promising even for relapse NB with drug resistance. siNCYM also silenced differentiation in SK-N-BE(2), although the MYCN silencing efficiency at mRNA and protein levels was not as significant as that of siMYCN. On the other hand, NCYM may play a crucial role in the mechanisms of MYCN transcription. Hence, further investigation of the mechanisms is required for enhancement of MYCN silencing.

In addition, siMYCN delivered by a cationic PEGylated RTN also achieved MYCN silencing in NB tumour developed in SCID mice injected with human NB cell lines Kelly and SK-N-BE(2). The siMYCN delivered using the RTNs successfully silenced MYCN mRNA in both Kelly and SK-N-BE(2) *in vivo*. The results suggest that it may be the efficacy of systemic injection of siMYCN packaged with RTNs for therapy in NB. At the same time,

it is necessary to investigate the therapeutic efficacy of siMYCN for longer periods and the downstream effects of MYCN reduction that was observed in vitro. In addition, it is essential to observe immune responses after the injection and the specificity of the location where the RTNs are delivered.

Trehalose can maintain the biophysical characteristics and function of RTNs at -80 °C. In addition, transfection/silencing efficiency was more stably preserved when RTNs were kept at -80 °C. It is necessary to observe function of RTNs in trehalose stored at -80 °C for longer time such as 6 months and the ability of trehalose to preserve RTNs at higher concentration.

7. References

- Aagaard, L & Rossi, JJ 2007, '*RNAi therapeutics: principles, prospects and challenges*', *Adv Drug Deliv Rev.*, vol. 59, no. 2-3, pp. 75-86.
- Afanasyeva, EA, Mestdagh, P, Kumps, C, Vandesompele, J, Ehemann, V, Theissen, J, Fischer, M, Zapatka, M, Brors, B, Savelyeva, L, Sagulenko, V, Speleman, F, Schwab, M & Westermann, F 2011, '*MicroRNA miR-885-5p targets CDK2 and MCM5, activates p53 and inhibits proliferation and survival*', *Cell Death Differ.*, vol. 18, no. 6, pp. 974-84.
- Aguirre, AJ, Meyers, RM, Weir, BA, Vazquez, F, Zhang, CZ, Ben-David, U, Cook, A, Ha, G, Harrington, WF, Doshi, MB, Kost-Alimova, M, Gill, S, Xu, H, Ali, LD, Jiang, G, Pantel, S, Lee, Y, Goodale, A, Cherniack, AD, Oh, C, Kryukov, G, Cowley, GS, Garraway, LA, Stegmaier, K, Roberts, CW, Golub, TR, Meyerson, M, Root, DE, Tsherniak, A & Hahn WC 2016, '*Genomic Copy Number Dictates a Gene-Independent Cell Response to CRISPR/Cas9 Targeting*', *Cancer Discov.*, vol. 6, no. 8, pp. 914-29
- Akkuratov, EE, Wu, J, Sowa, D, Shah, ZA & Liu, L 2015, '*Ouabain-Induced Signaling and Cell Survival in SK-N-SH Neuroblastoma Cells Differentiated by Retinoic Acid*', *NS Neurol Disord Drug Targets.*, vol. 14, no. 10, pp. 1343–1349.
- Allen, C, Dos Santos, N, Gallagher, R, Chiu, GN, Shu, Y, Li, WM, Johnstone, SA, Janoff, AS, Mayer, LD, Webb, MS & Bally, MB 2002, '*Controlling the physical behavior and biological performance of liposome formulations through use of surface grafted poly(ethylene glycol)*', *Biosci Rep.*, vol. 22, no. 2, pp. 225-50.
- Almeida, R & Allshire, RC 2005, '*RNA silencing and genome regulation*', *Trends Cell Biol.*, vol. 15, no. 5, pp. 251-8.
- American Cancer Society 'Retinoid Therapy for Neuroblastoma': <https://www.cancer.org/cancer/neuroblastoma/treating/retinoid-therapy.html> Retrieved on 30.10.2017.
- Anchordoquy, TJ, Carpenter, JF & Kroll, DJ 1997, '*Maintenance of transfection rates and physical characterization of lipid/DNA complexes after freeze-drying and rehydration*', *Arch Biochem Biophys.*, vol. 348, no. 1, pp. 199-206.
- Andres, D, Keyser, BM, Petrali, J, Benton, B, Hubbard, KS, McNutt, PM & Ray R 2013, '*Morphological and functional differentiation in BE(2)-M17 human neuroblastoma cells by treatment with Trans-retinoic acid*', *BMC Neurosci.*, vol. 18, no. 14, p49
- Armstrong, BC & Krystal, GW 1992, '*Isolation and characterization of complementary DNA for N-cym, a gene encoded by the DNA strand opposite to N-myc*', *Cell Growth Differ.*, vol. 3, no. 6, pp. 385-90.
- Bachetti, T, Di Paolo, D, Di Lascio, S, Mirisola, V, Brignole, C, Bellotti, M, Caffa, I, Ferraris, C, Fiore, M, Fornasari, D, Chiarle, R, Borghini, S, Pfeffer, U, Ponzoni, M,² Ceccherini, I, & Perri, P 2010, '*PHOX2B-Mediated Regulation of ALK Expression: In Vitro Identification of a Functional Relationship between Two Genes Involved in Neuroblastoma*', *PLoS One.*, vol. 5, no. 10.

- Bader, AG, Brown, D & Winkler, M 2010, '*The promise of microRNA replacement therapy*', *Cancer Res.*, vol. 70, no. 18, pp. 7027-30.
- Balazs, DA & Godbey, W 2011, '*Liposomes for use in gene delivery*', *J Drug Deliv.*, vol. 2011, p. 326497.
- Ball, RL, Bajaj, P & Whitehead, KA 2016, '*Achieving long-term stability of lipid nanoparticles: examining the effect of pH, temperature, and lyophilization*', *Int J Nanomedicine.*, vol. 30, no. 12, pp. 305-315.
- Banelli, B, Gelvi, I, Di Vinci, A, Scaruffi, P, Casciano, I, Allemanni, G, Bonassi, S, Tonini, GP & Romani, M 2005, '*Distinct CpG methylation profiles characterize different clinical groups of neuroblastic tumors*', *Oncogene.*, vol. 24, no. 36, pp. 5619-28.
- Barone, G, Anderson, J, Pearson, AD, Petrie, K & Chesler, L 2013, '*New strategies in neuroblastoma: Therapeutic targeting of MYCN and ALK*', *Clin Cancer Res.*, vol. 19, no. 21, pp. 5814-21.
- Bartlett, DW & Davis, ME 2006, '*Insights into the kinetics of siRNA-mediated gene silencing from live-cell and live-animal bioluminescent imaging*', *Nucleic Acids Res.*, vol. 34, no. 1, pp. 322-33.
- Bell, E, Chen, L, Liu, T, Marshall, GM, Lunec, J & Tweddle, DA 2010, '*MYCN oncoprotein targets and their therapeutic potential*', *Cancer Lett.*, vol. 293, no. 2, pp. 144-57.
- Beltran, H 2014, '*The N-myc Oncogene: Maximizing its Targets, Regulation, and Therapeutic Potential*', *Mol Cancer Res.*, vol. 12, no. 6, pp. 815-22.
- Berridge, MV & Tan, AS 1993, '*Characterization of the cellular reduction of 3-(4,5-dimethylthiazol-2-yl)-2,5-diphenyltetrazolium bromide (MTT): subcellular localization, substrate dependence, and involvement of mitochondrial electron transport in MTT reduction*', *Arch Biochem Biophys.*, vol. 303, no. 2, pp. 474-82.
- Birmingham, A, Anderson, EM, Reynolds, A, Ilsley-Tyree, D, Leake, D, Fedorov, Y, Baskerville, S, Maksimova, E, Robinson, K, Karpilow, J, Marshall, WS & Khvorova, A 2006, '*3' UTR seed matches, but not overall identity, are associated with RNAi off-targets*', *Nat Methods.*, vol. 3, no. 3, pp. 199-204.
- Blacker, TS, Mann, ZF, Gale, JE, Ziegler, M, Bain, AJ, Szabadkai, G & Duchon, MR 2014, '*Separating NADH and NADPH fluorescence in live cells and tissues using FLIM*', *Nat Commun.*, vol. 5, p. 3936
- Boettcher, M & McManus, MT 2015, '*Choosing the Right Tool for the Job: RNAi, TALEN, or CRISPR*', *Mol Cell.*, vol. 58, no. 4, pp. 575-85.
- Bonvini, P, Nguyen, P, Trepel, J & Neckers, LM 1998, '*In vivo degradation of N-myc in neuroblastoma cells is mediated by the 26S proteasome*', *Oncogene.*, vol. 16, no. 9, pp. 1131-9.

- Briuglia, ML, Rotella, C, McFarlane, A & Lamprou, DA 2015, 'Influence of cholesterol on liposome stability and on in vitro drug release', *Drug Deliv Transl Res.*, vol. 5, no. 3, pp. 231-42.
- Brockmann, M, Poon, E, Berry, T, Carstensen, A, Deubzer, HE, Rycak, L, Jamin, Y, Thway, K, Robinson, SP, Roels, F, Witt, O, Fischer, M, Chesler, L & Eilers, M 2013, 'Small molecule inhibitors of aurora-a induce proteasomal degradation of N-myc in childhood neuroblastoma', *Cancer Cell.*, vol. 24, no. 1, pp. 75-89.
- Brodeur, GM 2003, 'Neuroblastoma: biological insights into a clinical enigma', *Nat Rev Cancer.*, vol. 3, no. 3, pp. 203-16.
- Brodeur, GM & Bagatell, R 2014, 'Mechanisms of neuroblastoma regression', *Nat Rev Clin Oncol.*, vol. 11, no. 12, pp. 704-13.
- Brodeur, GM, Pritchard, J, Berthold, F, Carlsen, NL, Castel, V, Castelberry, RP, De Bernardi, B, Evans, AE, Favrot, M & Hedborg F 1993, 'Revisions of the international criteria for neuroblastoma diagnosis, staging, and response to treatment', *J Clin Oncol.*, vol. 11, no. 8, pp. 1466-77.
- Broering, R, Real, CI, John, MJ, Jahn-Hofmann, K, Ickenstein, LM, Kleinehr, K, Paul, A, Gibbert, K, Dittmer, U, Gerken, G & Schlaak, JF 2014, 'Chemical modifications on siRNAs avoid Toll-like-receptor-mediated activation of the hepatic immune system in vivo and in vitro', *Int Immunol.*, vol. 26, no. 1, pp. 35-46
- Buechner, J & Einvik, C 2012, 'N-myc and noncoding RNAs in neuroblastoma', *Mol Cancer Res.*, vol. 10, no. 10, pp. 1243-53.
- Burnette, WN 1981, 'Western blotting": electrophoretic transfer of proteins from sodium dodecyl sulfate--polyacrylamide gels to unmodified nitrocellulose and radiographic detection with antibody and radioiodinated protein A', *Anal Biochem.*, vol. 112, no. 2, pp. 195-203.
- Bustin S. ed 2004, 'A-Z of Quantitative PCR (IUL Biotechnology Series)', International University Line, La Jolla, California
- Calvaresi, EC & Hergenrother, PL 2013, 'Glucose conjugation for the specific targeting and treatment of cancer', *Chem Sci.*, vol. 4, no. 6, pp. 2319-2333.
- Cancer research uk n. d. *Neuroblastoma*. Retrieved February 13, 2018, from https://www.childrenwithcancer.org.uk/childhood-cancer-info/cancer-types/neuroblastoma/?__ja=tsid:90000%7ccid:1044373102%7cagid:49320487617%7ctid:kwd-354093838721%7ccrid:246886640762%7cnw:g%7crnd:3952980537010990436%7cdvc:c%7cadp:1t2%7cmt:b%7cloc:9046033&gclid=EA1aIQobChMIjPzG7cSj2QIVirztCh1E3wlDEAAYAiAAEgJqN_D_BwE
- Casciano, I, Banelli, B, Croce, M, De Ambrosis, A, di Vinci, A, Gelvi, I, Pagnan, G, Brignole, C, Allemanni, G, Ferrini, S, Ponzoni, M & Romani, M 2004, 'Caspase-8 gene expression in neuroblastoma', *Ann N Y Acad Sci.*, vol. 1028, pp. 157-67.

- Chen L, Iraci, N, Gherardi, S, Gamble, LD, Wood, KM, Perini, G, Lunec, J & Tweddle, DA 2010, '*p53 is a direct transcriptional target of MYCN in neuroblastoma*', *Cancer Res.*, Vol. 70, no. 4, pp. 1377-88.
- Chesler, L, Goldenberg, DD, Collins, R, Grimmer, M, Kim, GE, Tihan, T, Nguyen, K, Yakovenko, S, Matthay, KK & Weiss, WA 2008, '*Chemotherapy-induced apoptosis in a transgenic model of neuroblastoma proceeds through p53 induction*', *Neoplasia.*, vol. 10, no. 11, pp. 1268-74.
- Chesler, L, Schlieve, C, Goldenberg, DD, Kenney, A, Kim, G, McMillan, A, Matthay, KK, Rowitch, D & Weiss WA 2006, '*Inhibition of phosphatidylinositol 3-kinase destabilizes Mycn protein and blocks malignant progression in neuroblastoma*', *Cancer Res.*, vol. 66, no. 16, pp. 8139-46.
- Cheung, NK & Dyer, MA 2013, '*Neuroblastoma: developmental biology, cancer genomics and immunotherapy*', *Nat Rev Cancer.*, vol. 13, no. 6, pp. 397-411.
- Chipumuro, E, Marco, E, Christensen, CL, Kwiatkowski, N, Zhang, T, Hatheway, CM, Abraham, BJ, Sharma, B, Yeung, C, Altabef, A, Perez-Atayde, A, Wong, KK, Yuan, GC, Gray, NS, Young, RA & George, RE 2014, '*CDK7 inhibition suppresses super-enhancer-linked oncogenic transcription in MYCN-driven cancer*', *Cell.*, vol. 159, no. 5, pp. 1126-1139.
- Chirgwin, JM, Przybyla, AE, MacDonald, RJ & Rutter, WJ 1979, '*Isolation of biologically active ribonucleic acid from sources enriched in ribonuclease*', *Biochemistry.*, vol. 18, no. 24, pp. 5294-9.
- Clark, O, Daga, S, Stoker, AW 2013, '*Tyrosine phosphatase inhibitors combined with retinoic acid can enhance differentiation of neuroblastoma cells and trigger ERK- and AKT-dependent, p53-independent senescence*', *Cancer Lett.*, vol. 328, no. 1, pp. 44-54.
- Cong, L, Ran, FA, Cox, D, Lin, S, Barretto, R, Habib, N, Hsu, PD, Wu, X, Jiang, W, Marraffini, LA & Zhang, F 2013, '*Multiplex genome engineering using CRISPR/Cas systems*', *Science.*, vol. 339, no. 6121, pp. 819-23.
- Corvetta, D, Chayka, O, Gherardi, S, D'Acunto, CW, Cantilena, S, Valli, E, Piotrowska, I, Perini, G & Sala A 2013, '*Physical interaction between MYCN oncogene and polycomb repressive complex 2 (PRC2) in neuroblastoma: functional and therapeutic implications*', *J Biol Chem.*, vol. 288, no. 12, pp. 8332-41.
- Cotterman, R & Knoepfler, PS 2009, '*N-Myc regulates expression of pluripotency genes in neuroblastoma including lif, klf2, klf4, and lin28b*', *PLoS One*, vol. 4, no. 6.
- Cotterman, R, Jin, VX, Krig, SR, Lemen, JM, Wey, A, Farnham, PJ & Knoepfler, PS 2008, '*N-Myc regulates a widespread euchromatic program in the human genome partially independent of its role as a classical transcription factor*', *Cancer Res.*, vol. 68, no. 23, pp. 9654-62.
- Crespi, B & Summers, K 2005, '*Evolutionary biology of cancer*', *Trends Ecol Evol.*, vol. 20, no. 10, pp. 545-52.

- Crowe, JH, Crowe, LM, Carpenter, JF & Wistrom CA 1987, '*Stabilization of dry phospholipid bilayers and proteins by sugars*', *Biochem J.*, vol. 242, no. 1, pp. 1–10.
- Dana, H, Chalbatani, GM, Mahmoodzadeh, H, Karimloo, R, Rezaiean, O, Moradzadeh, A, Mehmandoost, N, Moazzen, F, Mazraeh, A, Marmari, V, Ebrahimi, M, Rashno, MM, Abadi, SJ & Gharagouzlo, E 2017, '*Molecular Mechanisms and Biological Functions of siRNA*', *Int J Biomed Sci.*, vol. 13, no. 2, pp. 48-57.
- Dardenne, E, Beltran, H, Benelli, M, Gayvert, K, Berger, A, Puca, L, Cyrta, J, Sboner, A, Noorzad, Z, MacDonald, T, Cheung, C, Yuen, KS, Gao, D, Chen, Y, Eilers, M, Mosquera, JM, Robinson, BD, Elemento, O, Rubin, MA, Demichelis, F & Rickman, DS 2016, '*N-Myc Induces an EZH2-Mediated Transcriptional Program Driving Neuroendocrine Prostate Cancer*', *Cancer Cell.*, vol. 30, no. 4, pp. 563-577.
- Dash, TK & Konkimalla, VB 2013, '*Nanoformulations for delivery of biomolecules: focus on liposomal variants for siRNA delivery*', *Crit Rev Ther Drug Carrier Syst.*, vol. 30, no. 6, pp. 469-93.
- Date, PV, Samad, A & Devarajan, PV 2010, '*Freeze thaw: a simple approach for prediction of optimal cryoprotectant for freeze drying*', *AAPS PharmSciTech.*, vol. 11, no. 1, pp.304-13.
- de Wet, JR, Wood, KV, DeLuca, M, Helinski, DR & Subramani, S 1987, '*Firefly luciferase gene: structure and expression in mammalian cells*', *Mol Cell Biol.*, vol. 7, no. 2, pp. 725-37.
- Deniz, A, Sade, A, Severcan, F, Keskin, D, Tezcaner, A & Banerjee, S 2010, '*Celecoxib-loaded liposomes: effect of cholesterol on encapsulation and in vitro release characteristics*', *Biosci Rep.*, vol. 30, no. 5, pp. 365-73.
- Desgrosellier, JS & Cheresch, DA 2010, '*Integrins in cancer: biological implications and therapeutic opportunities*', *Nat Rev Cancer.*, vol. 10, no. 1, pp. 9-22.
- Dewitt, J, Ochoa, V, Urschitz, J, Elston, M, Moisyadi, S & Nishi, R 2014, '*Constitutively active TrkB confers an aggressive transformed phenotype to a neural crest-derived cell line*', *Oncogene.*, vol. 33, no. 8, pp. 977-85.
- Dharmacon, '*Off-target Effects: Disturbing the Silence of RNA interference (RNAi)*': <http://dharmacon.gelifesciences.com/uploadedFiles/Resources/off-target-tech-review-technote.pdf> Retrieved on 30.10.2017.
- Dharmacon, '*What are off-target effects and how can these be addressed in an siRNA experiment?*': <http://dharmacon.gelifesciences.com/resources/faqs/what-off-target-effects-how-addressed-sirna-experiment/> Retrieved on 30.10.2017.
- Dixon, JE & McKinnon, D 1994, '*Expression of the trk gene family of neurotrophin receptors in prevertebral sympathetic ganglia*', *Brain Res Dev Brain Res.*, vol. 77, no. 2, pp. 177-82.

- Domingo-Fernandez, R, Watters, K, Piskareva, O, Stallings, RL & Bray, I 2013, '*The role of genetic and epigenetic alterations in neuroblastoma disease pathogenesis*', *Pediatr Surg Int*, no. 29, pp101–119.
- Duffy, DJ, Krstic, A, Schwarzl, T, Higgins, DG & Kolch, W 2013, '*GSK3 inhibitors regulate MYCN mRNA levels and reduce neuroblastoma cell viability through multiple mechanisms, including p53 and Wnt signaling*', *Mol Cancer Ther.*, vol. 13, no. 2, pp. 454-67.
- Durbas, M, Horwacik, I, Boratyn, E & Rokita, H 2016, '*Downregulation of the PHLDA1 gene in IMR-32 neuroblastoma cells increases levels of Aurora A, TRKB and affects proteins involved in apoptosis and autophagy pathways*', *Int J Oncol.*, vol. 49, no. 2, pp. 823-37.
- Eggert, A, Grotzer, MA, Zuzak, TJ, Wiewrodt, BR, Ho, R, Ikegaki, N & Brodeur, GM 2001, '*Resistance to tumor necrosis factor-related apoptosis-inducing ligand (TRAIL)-induced apoptosis in neuroblastoma cells correlates with a loss of caspase-8 expression*', *Cancer Res.*, vol. 61, no. 4, pp. 1314-9.
- Elbashir, SM, Lendeckel, W & Tuschl, T 2001, '*RNA interference is mediated by 21- and 22-nucleotide RNAs*', *Genes Dev.*, vol. 15, no. 2, pp. 188-200.
- Elsabahy, M, Nazarali, A & Foldvari, M 2011, '*Non-viral nucleic acid delivery: key challenges and future directions*', *Curr Drug Deliv.*, vol. 8, no. 3, pp. 235-44.
- Esteller, M 2011, '*Non-coding RNAs in human disease*', *Nat Rev Genet.*, vol. 12, no. 12, pp. 861-74.
- Faye, C, Inforzato, A, Bignon, M, Hartmann, DJ, Muller, L, Ballut, L, Olsen, BR, Day, AJ & Ricard-Blum, S 2010, '*Transglutaminase-2: a new endostatin partner in the extracellular matrix of endothelial cells*', *Biochem J.*, vol. 427, no. 3, pp. 467-75.
- Feng, C, Wang, T, Tang, R, Wang, J, Long, H, Gao, X & Tang, S 2010, '*Silencing of the MYCN gene by siRNA delivered by folate receptor-targeted liposomes in LA-N-5 cells*', *Pediatr Surg Int.*, vol. 26, no. 12, pp.1185-91.
- Feng, C, Wang, T, Tang, R, Wang, J, Long, H, Gao, X & Tang, S 2010, '*Silencing of the MYCN gene by siRNA delivered by folate receptor-targeted liposomes in LA-N-5 cells*', *Pediatr Surg Int.*, vol. 26, no. 12, pp. 1185-9.
- Fire, A, Xu, S, Montgomery, MK, Kostas, SA, Driver, SE & Mello, CC 1998, '*Potent and specific genetic interference by double-stranded RNA in *Caenorhabditis elegans**', *Nature.*, vol. 391, no. 6669, pp. 806-11.
- Fulda, S, Lutz, W, Schwab, M, Debatin, KM 2000, '*MycN sensitizes neuroblastoma cells for drug-triggered apoptosis*', *Med Pediatr Oncol.*, vol. 35, no. 6, pp. 582-4.
- Gherardi, S, Valli, E, Erriquez, D & Perini, G 2013, '*MYCN-mediated transcriptional repression in neuroblastoma: the other side of the coin*', *Front Oncol.*, vol.3, no. 42.

- Gilbert, LA, Horlbeck, MA, Adamson, B, Villalta, JE, Chen, Y, Whitehead, HE, Guimaraes, C, Panning, B, Ploegh, HL, Bassik, MC, Qi, LS, Kampmann, M, & Weissman, JS 2014, '*Genome-Scale CRISPR-Mediated Control of Gene Repression and Activation*', *Cell.*, vol. 159, no. 3, pp. 647–661.
- Gladson, CL, Hancock, S, Arnold, MM, Faye-Petersen, OM, Castleberry RP & Kelly, DR 1996, '*Stage-specific expression of integrin alphaVbeta3 in neuroblastic tumors*', *Am J Pathol.*, vol. 148, no. 5, pp. 423-34.
- Golan, T, Khvalevsky, EZ, Hubert, A, Gabai, RM, Hen, N, Segal, A, Domb, A, Harari, G, David, EB, Raskin, S, Goldes, Y, Goldin, E, Eliakim, R, Lahav, M, Kopleman, Y, Dancour, A, Shemi, A, Galun, E 2015, '*RNAi therapy targeting KRAS in combination with chemotherapy for locally advanced pancreatic cancer patients*', *Oncotarget.*, vol. 6, no. 27, pp. 24560-70.
- Goldschneider, D, Horvilleur, E, Plassa, LF, Guillaud-Bataille, M, Million, K, Wittmer-Dupret, E, Danglot, G, de Thé, H, Bénard, J, May, E & Douc-Rasy S 2006, '*Expression of C-terminal deleted p53 isoforms in neuroblastoma*', *Nucleic Acids Res.*, vol. 34, no. 19, pp. 5603-12.
- Gomes-da-Silva, LC, Fonseca, NA, Moura, V, Pedroso de Lima, MC, Simões, S & Moreira, JN 2012, '*Lipid-based nanoparticles for siRNA delivery in cancer therapy: paradigms and challenges*', *Acc Chem Res.*, vol. 45, no. 7, pp. 1163-71.
- Goswami, S 2013, '*Importance of integrin receptors in the field of pharmaceutical & medical science*', *Scientific Research Advances in Biological Chemistry*, vol. 3, no.2, pp. 224-252
- Grosse, SM, Tagalakis, AD, Mustapa, MF, Elbs, M, Meng, QH, Mohammadi, A, Tabor, AB, Hailes, HC & Hart, SL 2010 '*Tumor-specific gene transfer with receptor-mediated nanocomplexes modified by polyethylene glycol shielding and endosomally cleavable lipid and peptide linkers*', *FASEB J.*, vol. 24, no. 7, pp. 2301-13.
- Gu, L, Zhang, H, He, J, Li, J, Huang, M & Zhou, M 2012, '*MDM2 regulates MYCN mRNA stabilization and translation in human neuroblastoma cells*', *Oncogene.*, vol. 31, no. 11, pp. 1342-53.
- Gudkov, AV & Komarova, EA 2003, '*The role of p53 in determining sensitivity to radiotherapy*', *Nat Rev Cancer.*, vol. 3, no. 2, pp. 117-29.
- Guglielmi, L, Cinnella, C, Nardella, M, Maresca, G, Valentini, A, Mercanti, D, Felsani, A & D'Agnano, I 2014, '*MYCN gene expression is required for the onset of the differentiation programme in neuroblastoma cells*', *Cell Death Dis.*, vol. 5.
- Gustafson, WC & Weiss, WA 2010, '*Myc proteins as therapeutic targets*', *Oncogene.*, vol. 29, no. 9, pp. 1249-59.
- Hamilton, AJ & Baulcombe, DC 1999, '*A species of small antisense RNA in posttranscriptional gene silencing in plants*', *Science.*, vol. 286, no. 5441, pp. 950-2.

- Hämmerle, B, Yañez, Y, Palanca, S, Cañete, A, Burks, DJ, Castel, V & Font de Mora J 2013, 'Targeting neuroblastoma stem cells with retinoic acid and proteasome inhibitor', PLoS One., vol. 8, no. 10.
- Hanahan, D & Weinberg, RA 2011, 'Hallmarks of cancer: the next generation', Cell., vol. 144, no. 5, pp. 646-74.
- Harenza, JL, Diamond, MA, Adams, RN, Song, MM, Davidson, HL, Hart, LS, Dent, MH, Fortina, P, Reynolds, CP & Maris, JM 2017, 'Transcriptomic profiling of 39 commonly-used neuroblastoma cell lines', Sci Data., vol. 28, no. 4, p. 170033.
- Harris, RG, White, E, Phillips, ES, Lillycrop, KA 2002, 'The expression of the developmentally regulated proto-oncogene Pax-3 is modulated by N-Myc', J Biol Chem., vol. 277, no. 38, pp. 34815-25.
- Hart, SL 2010, 'Multifunctional nanocomplexes for gene transfer and gene therapy', Cell Biol Toxicol, vol. 26, no. 1, pp. 69-81.
- Haskell, BE, Stach, RW, Werrbach-Perez, K & Perez-Polo, JR 1987, 'Effect of retinoic acid on nerve growth factor receptors', Cell Tissue Res., vol. 247, no. 1, pp. 67-73.
- He, S, Liu, Z, Oh, DY & Thiele, CJ 2013, 'MYCN and the epigenome', Front Oncol., vol. 3, p.1.
- Henriksen, JR, Haug, BH, Buechner, J, Tømte, E, Løkke, C, Flaegstad, T & Einvik, C 2011, 'Conditional expression of retrovirally delivered anti-MYCN shRNA as an in vitro model system to study neuronal differentiation in MYCN-amplified neuroblastoma', BMC Dev Biol., vol. 11, no. 1.
- Ho, R, Minturn, JE, Simpson, AM, Iyer, R, Light, JE, Evans, AE & Brodeur, GM 2011, 'The effect of P75 on Trk receptors in neuroblastomas', Cancer Lett., vol. 305, no. 1, pp. 76-85.
- Hornung, V, Guenther-Biller, M, Bourquin, C, Ablasser, A, Schlee, M, Uematsu, S, Noronha, A, Manoharan, M, Akira, S, de Fougères, A, Endres, S & Hartmann, G 2005, 'Sequence-specific potent induction of IFN-alpha by short interfering RNA in plasmacytoid dendritic cells through TLR7', Nat Med., vol. 11, no. 3, pp. 263-70.
- Huang, R, Cheung, NK, Vider, J, Cheung, IY, Gerald, WL, Tickoo, SK, Holland, EC & Blasberg, RG 2011, 'MYCN and MYC regulate tumor proliferation and tumorigenesis directly through BMI1 in human neuroblastomas', FASEB J, vol. 25, no. 12, pp. 4138-49.
- Huang, R, Cheung, NK, Vider, J, Cheung, IY, Gerald, WL, Tickoo, SK, Holland, EC & Blasberg, RG 2011, 'MYCN and MYC regulate tumor proliferation and tumorigenesis directly through BMI1 in human neuroblastomas', FASEB J., vol. 25, no. 12, pp. 4138-49.
- Huang, Y, Chen, J, Chen, X, Gao, J & Liang, W 2008, 'PEGylated synthetic surfactant vesicles (Niosomes): novel carriers for oligonucleotides', J Mater Sci Mater Med., vol. 19, no. 2, pp. 607-14.

- Inge, TH, Casson, LK, Priebe, W, Trent, JO, Georgeson, KE, Miller, DM & Bates, PJ 2002, 'Importance of *Sp1* consensus motifs in the *MYCN* promoter', *Surgery.*, vol. 132, no. 2, pp. 232-8.
- Iraci, N, Diolaiti, D, Papa, A, Porro, A, Valli, E, Gherardi, S, Herold, S, Eilers, M, Bernardoni, R, Della Valle G & Perini G 2011, 'A *SP1/MIZ1/MYCN* repression complex recruits *HDAC1* at the *TRKA* and *p75NTR* promoters and effects neuroblastoma malignancy by inhibiting the cell response to NGF', *Cancer Res.*, vol. 71, no. 2, pp. 404-12.
- Ishiyama, M, Miyazono, Y, Sasamoto, K, Ohkura, Y, Ueno, K 1997, 'A highly water-soluble disulfonated tetrazolium salt as a chromogenic indicator for NADH as well as cell viability', *Talanta.*, vol. 44, no. 7, pp. 1299-305.
- Jackson, AL & Linsley, PS 2010, 'Recognizing and avoiding siRNA off-target effects for target identification and therapeutic application', *Nat Rev Drug Discov.*, vol. 9, no. 1, pp. 57-67.
- Jackson, AL, Burchard, J, Schelter, J, Chau, BN, Cleary, M, Lim, L & Linsley, PS 2006, 'Widespread siRNA "off-target" transcript silencing mediated by seed region sequence complementarity', *RNA.*, vol. 12, no. 7, pp. 1179-87.
- Jain, NK & Roy, I 2009, 'Effect of trehalose on protein structure', *Protein Sci.*, vol. 18, no. 1, pp. 24-36.
- Joshi, S, Guleria, RS, Pan, J, Dipette, D & Singh, US 2007, 'Heterogeneity in retinoic acid signaling in neuroblastomas: Role of matrix metalloproteinases in retinoic acid-induced differentiation', *Biochim Biophys Acta.*, vol. 1772, no. 9, pp. 1093-102.
- Judge, A & MacLachlan, I 2008, 'Overcoming the innate immune response to small interfering RNA', *Hum Gene Ther.*, vol. 19, no. 2, pp. 111-24.
- Judge, AD, Sood, V, Shaw, JR, Fang, D, McClintock, K & MacLachlan, I 2005, 'Sequence-dependent stimulation of the mammalian innate immune response by synthetic siRNA', *Nat Biotechnol.*, vol. 23, no. 4, pp. 457-62.
- Jung, S, von Thülen, T, Laukemper, V, Pigisch, S, Hangel, D, Wagner, H, Kaufmann, A & Bauer, S 2015, 'A single naturally occurring 2'-O-methylation converts a TLR7- and TLR8-activating RNA into a TLR8-specific ligand', *PLoS One.*, vol. 10, no. 3
- Kang, J, Rychahou, PG, Ishola, TA, Mourot, JM, Evers, BM & Chung, DH 2008, '*N-myc* is a novel regulator of *PI3K*-mediated *VEGF* expression in neuroblastoma', *Oncogene.*, vol. 27, no. 28, pp. 3999-4007.
- Kang, JH, Rychahou, PG, Ishola, TA, Qiao, J, Evers, BM & Chung, DH 2006, '*MYCN* silencing induces differentiation and apoptosis in human neuroblastoma cells', *Biochem Biophys Res Commun.*, vol. 351, no. 1, pp. 192-7.

- Kapeli, K, Hurlin, PJ 2011, '*Differential regulation of N-Myc and c-Myc synthesis, degradation, and transcriptional activity by the Ras/mitogen-activated protein kinase pathway*', J Biol Chem., vol. 286, no. 44, pp.38498-508.
- Karikó, K, Weissman, D & Welsh, FA 2004, '*Inhibition of toll-like receptor and cytokine signaling--a unifying theme in ischemic tolerance*', J Cereb Blood Flow Metab., vol. 24, no. 11, pp. 1288-304.
- Karki, R, Mariani, M, Andreoli, M, He, S, Scambia, G, Shahabi, S & Ferlini, C 2013, ' *β III-Tubulin: biomarker of taxane resistance or drug target?*', Expert Opin Ther Targets., vol. 17, no. 4, pp. 461-72.
- Kearns, NA, Genga, RM, Enuameh, MS, Garber, M, Wolfe, SA & Maehr, R 2014, '*Cas9 effector-mediated regulation of transcription and differentiation in human pluripotent stem cells*', Development., vol. 141, no. 1, pp.219-23.
- Kedmi, R, Ben-Arie, N & Peer, D 2010, '*The systemic toxicity of positively charged lipid nanoparticles and the role of Toll-like receptor 4 in immune activation*', Biomaterials., vol. 31, no. 26, pp. 6867-75.
- Keshelava, N, Zuo, JJ, Chen, P, Waidyaratne, SN, Luna, MC, Gomer, CJ, Triche, TJ & Reynolds, CP 2001, '*Loss of p53 function confers high-level multidrug resistance in neuroblastoma cell lines*', Cancer Res., vol. 61, no. 16, pp. 6185-93.
- Kim, SS, Shago, M, Kaustov, L, Boutros, PC, Clendening, JW, Sheng, Y, Trentin, GA, Barsyte-Lovejoy, D, Mao, DY, Kay, R, Jurisica, I, Arrowsmith, CH & Penn, LZ 2007, '*CUL7 is a novel antiapoptotic oncogene*', Cancer Res., vol. 67, no. 20, pp. 9616-22.
- Knoepfler, PS, Zhang, XY, Cheng, PF, Gafken, PR, McMahon, SB & Eisenman, RN 2006, '*Myc influences global chromatin structure*', EMBO J., vol. 25, no. 12, pp. 2723-34.
- Koldehoff, M, Steckel, NK, Beelen, DW & Elmaagacli, AH 2007, '*Therapeutic application of small interfering RNA directed against bcr-abl transcripts to a patient with imatinib-resistant chronic myeloid leukaemia*', Clin Exp Med., vol. 7, no. 2, pp. 47-55.
- Koppen, A, Ait-Aissa, R, Hopman, S, Koster, J, Haneveld, F, Versteeg, R & Valentijn LJ 2007, '*Dickkopf-1 is down-regulated by MYCN and inhibits neuroblastoma cell proliferation*', Cancer Lett, vol. 256, no. 2, pp. 218-28.
- Kramps, C, Strieder, V, Sapetschnig, A, Suske, G & Lutz, W 2004, '*E2F and Sp1/Sp3 Synergize but are not sufficient to activate the MYCN gene in neuroblastomas*', J Biol Chem., vol. 279, no. 7, pp. 5110-7.
- Lam, JK, Chow, MY, Zhang, Y & Leung, SW 2015, '*siRNA Versus miRNA as Therapeutics for Gene Silencing*', Mol Ther Nucleic Acids., vol. 4,
- Lanzkowsky, P, Lipton, J & Fish, J 2016, '*Lanzkowsky's Manual of Pediatric Hematology and Oncology: 6th Edition*', Academic Press

- Lázcoz, P, Muñoz, J, Nistal, M, Pestaña, A, Encío, I & Castresana, JS 2006, '*Frequent promoter hypermethylation of RASSF1A and CASP8 in neuroblastoma*', BMC Cancer., vol. 25, no. 6, p. 254.
- Lee, SH, Anekal, P, Lim, CJ, Liu CC & Ginsberg MH 2013, '*Two modes of integrin activation form a binary molecular switch in adhesion maturation*', Mol Biol Cell., vol. 24, no.9, pp. 1354-62.
- Li, J, Ma, FK, Dang, QF, Liang, XG & Chen, XG 2014 '*Glucose-conjugated chitosan nanoparticles for targeted drug delivery and their specific interaction with tumor cells*', Frontiers of Materials Science, vol. 8, no. 4, pp 363–372
- Li, W & Szoka, FC Jr 2007, '*Lipid-based nanoparticles for nucleic acid delivery*', Pharm Res., vol. 24, no, 3, pp. 438-49.
- Lin, CY, Lovén, J, Rahl, PB, Paranal, RM, Burge, CB, Bradner, JE, Lee, TI, Young, RA 2012, '*Transcriptional amplification in tumor cells with elevated c-Myc*', Cell., vol. 151, no. 1, pp. 56-67.
- Lin, Q, Chen, J, Zhang, Z & Zheng, G 2014, '*Lipid-based nanoparticles in the systemic delivery of siRNA*', Nanomedicine (Lond)., vol. 9, no. 1, pp. 105-20.
- Liu, PY, Erriquez, D, Marshall, GM, Tee, AE, Polly, P, Wong, M, Liu, B, Bell, JL, Zhang XD, Milazzo, G, Cheung, BB, Fox, A, Swarbrick, A, Hüttelmaier, S, Kavallaris, M, Perini, G, Mattick, JS, Dinger, ME & Liu, T 2014, '*Effects of a novel long noncoding RNA, lncUSMycN, on N-Myc expression and neuroblastoma progression*', J Natl Cancer Inst., vol. 106, no. 7.
- Liu, T, Tee, AE, Porro, A, Smith, SA, Dwarthe, T, Liu, PY, Iraci, N, Sekyere, E, Haber, M, Norris, MD, Diolaiti, D, Della, Valle G, Perini, G & Marshall, GM 2007, '*Activation of tissue transglutaminase transcription by histone deacetylase inhibition as a therapeutic approach for Myc oncogenesis*', Proc Natl Acad Sci U S A., vol. 104, no. 47, pp. 18682-7.
- Liu, XQ, Sun, CY, Yang, XZ & Wang, J 2013, '*Polymeric-Micelle-Based Nanomedicine for siRNA Delivery*', Particle & Particle Systems Characterization , vol. 30, no. 3, pp. 211–228.
- Liu, Y, Zhu, YH, Mao, CQ, Dou, S, Shen, S, Tan, ZB & Wang J 2014, '*Triple negative breast cancer therapy with CDK1 siRNA delivered by cationic lipid assisted PEG-PLA nanoparticles*', J Control Release., vol. 192, pp. 114-21.
- Liu, PY, Atmadibrata, B, Mondal, S, Tee, AE, Liu, T 2016, '*NCYM is upregulated by lncUSMycN and modulates N-Myc expression*', Int J Oncol., vol. 49, no. 6, pp. 2464-2470.
- Liu, T, Tee, AE, Porro, A, Smith, SA, Dwarthe, T, Liu, PY, Iraci, N, Sekyere, E, Haber, M, Norris, MD, Diolaiti, D, Della, Valle, G, Perini, G, Marshall, GM 2007, '*Activation of tissue transglutaminase transcription by histone deacetylase inhibition as a therapeutic approach for Myc oncogenesis*', Proc Natl Acad Sci U S A., vol. 104, no. 47, pp. 18682-7.
- Lu, X, Pearson, A & Lunec, J 2003, '*The MYCN oncoprotein as a drug development target*', Cancer Lett., vol. 197, no. 1-2, pp. 125-30.

- Macmillan Cancer support website, '*neuroblastoma in children*': https://www.macmillan.org.uk/cancerinformation/cancertypes/childrenscancers/typesofchildrenscancers/neuroblastoma.aspx#DynamicJumpMenuManager_6_Anchor_6 Retrieved on 30.10.2017.
- Maris, JM, Hogarty, MD, Bagatell, R & Cohn SL 2007, '*Neuroblastoma*', *Lancet*, vol. 369, no. 9579, pp. 2106-20.
- Maris, JM 2010, 'Recent advances in neuroblastoma', *N Engl J Med.*, vol. 362, no. 23, pp. 2202-11.
- Maris, JM, Mosse, YP, Bradfield, JP, Hou, C, Monni, S, Scott, RH, Asgharzadeh, S, Attiyeh, EF, Diskin, SJ, Laudenslager, M, Winter, C, Cole, KA, Glessner, JT, Kim, C, Frackelton, EC, Casalunovo, T, Eckert, AW, Capasso, M, Rappaport, EF, McConville, C, London, WB, Seeger, RC, Rahman, N, Devoto, M, Grant, SF, Li, H & Hakonarson, H 2008, '*Chromosome 6p22 locus associated with clinically aggressive neuroblastoma*', *N Engl J Med.*, vol. 358, no. 24, pp. 2585-93.
- Marshall, GM, Carter, DR, Cheung, BB, Liu, T, Mateos, MK, Meyerowitz, JG & Weiss, WA 2014, '*The prenatal origins of cancer*'. *Nat Rev Cancer.*, vol. 14, no. 4, pp. 277-89.
- Martínez-Cerdeño, V, Lemen, JM, Chan, V, Wey, A, Lin, W, Dent, SR & Knoepfler PS 2012, '*N-Myc and GCN5 regulate significantly overlapping transcriptional programs in neural stem cells*', *PLoS One.*, vol. 7, no. 6
- Mattes, MJ 2007, '*Apoptosis assays with lymphoma cell lines: problems and pitfalls*', *Br J Cancer*, vol. 96, no. 6, pp. 928-936.
- McCarroll, JA, Gan, PP, Liu, M & Kavallaris M. 2010, '*betaIII-tubulin is a multifunctional protein involved in drug sensitivity and tumorigenesis in non-small cell lung cancer*', *Cancer Res.*, vol. 70, vol. 12, pp. 4995-5003.
- Memorial Sloan Kettering Cancer Center; <https://www.mskcc.org/research-advantage/support/technology/tangible-material/sk-n-be-2-c-human-neuroblastoma-cell-line> Retrieved on 30.10.2017.
- Meyer, A, van Golen, CM, Kim, B, van Golen, KL & Feldman, EL 2004, '*Integrin expression regulates neuroblastoma attachment and migration*', *Neoplasia.*, vol. 6, no. 4, pp. 332-42.
- Mishra, S, Webster, P & Davis, ME 2004, '*PEGylation significantly affects cellular uptake and intracellular trafficking of non-viral gene delivery particles*', *Eur J Cell Biol*, vol. 83, no. 3, pp. 97-111.
- Monclair, T, Brodeur, GM, Ambros, PF, Brisse, HJ, Cecchetto, G, Holmes, K, Kaneko, M, London, WB, Matthay, KK, Nuchtern, JG, von Schweinitz, D, Simon, T, Cohn SL & Pearson, AD; INRG Task Force. 2009, '*The International Neuroblastoma Risk Group (INRG) staging system: an INRG Task Force report*', *J Clin Oncol.*, vol. 27, no. 2, pp. 298-303.

- Mossé, YP, Laudenslager, M, Longo, L, Cole, KA, Wood, A, Attiyeh, EF, Laquaglia, MJ, Sennett, R, Lynch, JE, Perri, P, Laureys, G, Speleman, F, Kim, C, Hou C, Hakonarson, H, Torkamani, A, Schork, NJ, Brodeur, GM, Tonini, GP, Rappaport, E, Devoto, M & Maris, JM 2008, '*Identification of ALK as a major familial neuroblastoma predisposition gene*', *Nature.*, vol. 455, no. 7215, pp. 930-5.
- Motegi, A, Fujimoto, J, Kotani, M, Sakuraba, H & Yamamoto, T 2004, '*ALK receptor tyrosine kinase promotes cell growth and neurite outgrowth*', *J Cell Sci.*, vol. 117. Pt 15, pp. 3319-29.
- Mueller S, Matthay KK. 2009, '*Neuroblastoma: biology and staging*', *Curr Oncol Rep*, vol. 11, no. 6, pp. 431-8.
- Murphy, JM & La Quaglia, MP 2014 '*Advances in the surgical treatment of neuroblastoma: a review*', *Eur J Pediatr Surg*, vol. 24, no. 6, pp. 450-6.
- Mustapa, MF, Grosse, SM, Kudsiova, L, Elbs, M, Raiber, EA, Wong, JB, Brain, AP, Armer, HE, Warley, A, Keppler, M, Ng, T, Lawrence, MJ, Hart SL, Hailes, HC & Tabor, AB 2009, '*Stabilized integrin-targeting ternary LPD (lipopolyplex) vectors for gene delivery designed to disassemble within the target cell*', *Bioconjug Chem.*, vol. 20, no. 3, pp. 518-32.
- Nabatiyan, A & Krude, T 2004, '*Silencing of chromatin assembly factor I in human cells leads to cell death and loss of chromatin assembly during DNA synthesis*', *Mol Cell Biol.*, vol. 24, no. 7, pp. 2853-62.
- Nakagawa, M, Takizawa, N, Narita, M, Ichisaka, T & Yamanaka, S 2010, '*Promotion of direct reprogramming by transformation-deficient Myc*', *Proc Natl Acad Sci U S A.*, vol. 107, no. 32, pp. 14152-7.
- Nakagawara, A, Arima-Nakagawara, M, Scavarda, NJ, Azar, CG, Cantor, AB & Brodeur, GM 1993, '*Association between high levels of expression of the TRK gene and favorable outcome in human neuroblastoma*', *N Engl J Med.*, vol. 328, no. 12, pp. 847-54.
- Nara, K, Kusafuka, T, Yoneda, A, Oue, T, Sangkhathat, S & Fukuzawa, M 2007, '*Silencing of MYCN by RNA interference induces growth inhibition, apoptotic activity and cell differentiation in a neuroblastoma cell line with MYCN amplification*', *Int J Oncol*, Vol. 30, no. 5, pp. 1189-96.
- Nie, Z, Hu, G, Wei, G, Cui, K, Yamane, A, Resch, W, Wang, R, Green, DR, Tessarollo, L, Casellas, R, Zhao, K & Levens, D 2012, '*c-Myc is a universal amplifier of expressed genes in lymphocytes and embryonic stem cells*', *Cell.* vol. 151, no. 1, pp. 68-79.
- Noland, CL & Doudna, JA 2013, '*Multiple sensors ensure guide strand selection in human RNAi pathways*', *RNA.*, vol. 19, no. 5, pp. 639-48.
- Ochiai, H, Takenobu, H, Nakagawa, A, Yamaguchi, Y, Kimura, M, Ohira, M, Okimoto, Y, Fujimura, Y, Koseki, H, Kohno, Y, Nakagawara, A & Kamijo, T 2010, '*Bmi1 is a MYCN target gene that regulates tumorigenesis through repression of KIF1Bbeta and TSLC1 in neuroblastoma*', *Oncogene.*, vol. 29, no. 18, pp. 2681-90.

- Ohtake, S & Wang, YJ 2011, '*Trehalose: current use and future applications*', J Pharm Sci., vol. 100, no. 6, pp.2020-53.
- Oliveira, AC, Raemdonck, K, Martens, T, Rombouts, K, Simón-Vázquez, R, Botelho, C, Lopes, I, Lúcio, M, González-Fernández, Á, Real Oliveira, ME, Gomes, AC & Braeckmans K 2015, '*Stealth monoolein-based nanocarriers for delivery of siRNA to cancer cells*', Acta Biomater., vol. 25, pp. 216-29.
- Otto, T, Horn, S, Brockmann, M, Eilers, U, Schüttrumpf, L, Popov, N, Kenney, AM, Schulte, JH, Beijersbergen, R, Christiansen, H, Berwanger, B & Eilers, M 2009, '*Stabilization of N-Myc is a critical function of Aurora A in human neuroblastoma*', Cancer Cell., vol. 15, no. 1, pp.67-78.
- Pandey, GK, Mitra, S, Subhash, S¹, Hertwig, F, Kanduri, M, Mishra, K, Fransson, S, Ganeshram, A, Mondal, T, Bandaru, S, Ostensson, M, Akyürek, LM, Abrahamsson, J, Pfeifer, S, Larsson, E, Shi, L, Peng, Z, Fischer, M, Martinsson, T, Hedborg, F, Kogner, P, Kanduri, C 2014, '*The risk-associated long noncoding RNA NBAT-1 controls neuroblastoma progression by regulating cell proliferation and neuronal differentiation*', Cancer Cell., vol. 26, no. 5, pp. 722-37.
- Patist, A & Zoerb, H 2005, '*Preservation mechanisms of trehalose in food and biosystems*', Colloids Surf B Biointerfaces., vol. 40, no. 2, pp. 107-13.
- Payne, SR & Kemp, CJ 2005, '*Tumor suppressor genetics*', Carcinogenesis, vol. 26, no. 12, pp. 2031–2045.
- Pereira, CS, Lins, RD, Chandrasekhar, I, Freitas, LC & Hünenberger, PH 2004, '*Interaction of the disaccharide trehalose with a phospholipid bilayer: a molecular dynamics study*', Biophys J., vol. 86, no. 4, pp. 2273-85.
- Pichler, M & Calin, GA 2014, '*Long noncoding RNA in neuroblastoma: new light on the (old) N-Myc story*', J Natl Cancer Inst., vol. 106, no. 7.
- Ploessl, C, Pan, A, Maples, KT & Lowe, DK 2016, '*Dinutuximab: An Anti-GD2 Monoclonal Antibody for High-Risk Neuroblastoma*', Ann Pharmacother, vol. 50, no. 5, pp. 416-22.
- Promega <https://www.promega.co.uk/resources/product-guides-and-selectors/protocols-and-applications-guide/transfection/> Retrieved on 30.10.2017.
- PubChem, trehalose: CID 7427, <https://pubchem.ncbi.nlm.nih.gov/compound/trehalose> Retrieved on 30.10.2017.
- Reiff, T, Huber, L, Kramer, M, Delattre, O, Janoueix-Lerosey, I & Rohrer, H 2011, '*Midkine and Alk signaling in sympathetic neuron proliferation and neuroblastoma predisposition*', Development., vol. 138, no. 21, pp. 4699-708.
- Riccardi, C & Nicoletti, I 2006, '*Analysis of apoptosis by propidium iodide staining and flow cytometry*', Nat Protoc., vol. 1, no. 3, pp. 1458-61.

- Richards, AB, Krakowka, S, Dexter, LB, Schmid, H, Wolterbeek, AP, Waalkens-Berendsen, DH, Shigoyuki, A & Kurimoto, M. 2002, '*Trehalose: a review of properties, history of use and human tolerance, and results of multiple safety studies*', *Food Chem Toxicol.*, vol. 40, no. 7, pp. 871-98.
- Sait, S & Modak S. 2017, '*Anti-GD2 immunotherapy for neuroblastoma*', *Expert Rev Anticancer Ther.*, vol. 17, no. 10, pp. 889-904.
- Samuelsson, E, Shen, H, Blanco, E, Ferrari, M & Wolfram, J 2017, '*Contribution of Kupffer cells to liposome accumulation in the liver*', *Colloids Surf B Biointerfaces.*, vol. 1, no. 158, pp. 356-362.
- Schaffner, F, Ray, AM & Dontenwill, M 2013, '*Integrin $\alpha 5\beta 1$, the Fibronectin Receptor, as a Pertinent Therapeutic Target in Solid Tumors*', *Cancers (Basel).*, vol. 5, no. 1, pp. 27-47.
- Schlee, M, Hornung, V & Hartmann, G 2006, '*siRNA and isRNA: two edges of one sword*', *Mol Ther.*, vol. 14, no. 4, pp. 463-70..
- Schönherr, C, Yang, HL, Vigny, M, Palmer, RH & Hallberg, B 2010, '*Anaplastic lymphoma kinase activates the small GTPase Rap1 via the Rap1-specific GEF C3G in both neuroblastoma and PC12 cells*', *Oncogene.*, vol. 29, no. 19, pp. 2817-30.
- Schroeder, A, Levins, CG, Cortez, C, Langer, R & Anderson, DG 2010, '*Lipid-based nanotherapeutics for siRNA delivery*', *J Intern Med.*, vol. 267, no. 1, pp. 9-21.
- Schwab, M, Alitalo, K, Klempnauer, KH, Varmus, HE, Bishop, JM, Gilbert, F, Brodeur, G, Goldstein, M & Trent, J 1983, '*Amplified DNA with limited homology to myc cellular oncogene is shared by human neuroblastoma cell lines and a neuroblastoma tumour*', *Nature*, vol. 305, no. 5931, pp. 245-8.
- Seeger, RC, Brodeur, GM, Sather, H, Dalton, A, Siegel, SE, Wong, KY & Hammond, D 1985, '*Association of multiple copies of the N-myc oncogene with rapid progression of neuroblastomas*', *N Engl J Med.*, vol. 313, no. 18, pp. 1111-6.
- Shahbazi, J, Scarlett, CJ, Norris, MD, Liu, B, Haber, M, Tee, AE, Carrier, A, Biankin, AV, London, WB, Marshall, GM, Lock, RB & Liu T 2014, '*Histone deacetylase 2 and N-Myc reduce p53 protein phosphorylation at serine 46 by repressing gene transcription of tumor protein 53-induced nuclear protein 1*', *Oncotarget.*, vol. 5, no. 12, pp. 4257-68.
- Sigma <http://www.sigmaaldrich.com/catalog/product/sigma/74384?lang=en®ion=GB>
Retrieved on 30.10.2017.
- Singh, SK & Hajeri, PB 2009, '*siRNAs: their potential as therapeutic agents--Part II. Methods of delivery*', *Drug Discov Today*, vol. 14, no. 17-18, pp. 859-65.
- Sioud, M 2005, '*Induction of inflammatory cytokines and interferon responses by double-stranded and single-stranded siRNAs is sequence-dependent and requires endosomal localization*', *J Mol Biol.*, vol. 348, no. 5, pp. 1079-90.

- Sjostrom, SK, Finn, G, Hahn, WC, Rowitch, DH & Kenney, AM 2005, '*The Cdk1 complex plays a prime role in regulating N-myc phosphorylation and turnover in neural precursors*', *Dev Cell.*, vol. 9, no. 3, pp. 327-38.
- Slack, A, Chen, Z, Tonelli, R, Pule, M, Hunt, L, Pession, A & Shohet, JM 2005, '*The p53 regulatory gene MDM2 is a direct transcriptional target of MYCN in neuroblastoma*', *Proc Natl Acad Sci U S A.*, vol. 102, no. 3, pp. 731-6.
- Sledz, CA, Holko, M, de Veer, MJ, Silverman, RH & Williams, BR 2003, '*Activation of the interferon system by short-interfering RNAs*', *Nat Cell Biol.*, vol. 5, no. 9, pp. 834-9.
- Soucek, L & Evan, G 2010, '*The ups and downs of Myc biology*', *Curr Opin Genet Dev.*, vol. 20, no. 1, pp. 91-5.
- Spencer, DS, Puranik, AS & Peppas, NA 2015, '*Intelligent Nanoparticles for Advanced Drug Delivery in Cancer Treatment*', *Curr Opin Chem Eng.*, vol. 7, pp. 84-92.
- Strasser, A, Harris, AW, Bath, ML & Cory, S 1990, '*Novel primitive lymphoid tumours induced in transgenic mice by cooperation between myc and bcl-2*', *Nature.*, vol. 348, no. 6299, pp. 331-3.
- Suenaga, Y, Islam, SM, Alagu, J, Kaneko, Y, Kato, M, Tanaka, Y, Kawana, H, Hossain, S, Matsumoto, D, Yamamoto, M, Shoji, W, Itami, M, Shibata, T, Nakamura, Y, Ohira, M, Haraguchi, S & Nakagawara, A 2014, '*NCYM, a Cis-antisense gene of MYCN, encodes a de novo evolved protein that inhibits GSK3 β resulting in the stabilization of MYCN in human neuroblastomas*', *PLoS Genet.*, vol. 10, no. 1.
- Suenaga, Y, Kaneko, Y, Matsumoto, D, Hossain, MS, Ozaki, T & Nakagawara, A 2009, '*Positive auto-regulation of MYCN in human neuroblastoma*', *Biochem Biophys Res Commun.*, vol. 390, no. 1, pp. 21-6.
- Swarbrick, A, Woods, SL, Shaw, A, Balakrishnan, A, Phua, Y, Nguyen, A, Chanthery, Y, Lim, L, Ashton, LJ, Judson, RL, Huskey, N, Belloch, R, Haber, M, Norris, MD, Lengyel, P, Hackett, CS, Preiss, T, Chetcuti, A, Sullivan, CS, Marcusson, EG, Weiss, W, L'Etoile, N & Goga, A 2010, '*miR-380-5p represses p53 to control cellular survival and is associated with poor outcome in MYCN-amplified neuroblastoma*', *Nat Med.*, vol. 16, no. 10, pp. 1134-40.
- Taft, RJ, Pang, KC, Mercer, TR, Dinger, M & Mattick, JS 2010, '*Non-coding RNAs: regulators of disease*', *J Pathol.*, vol. 220, no. 2, pp. 126-39.
- Tagalakis, AD, Lee do, HD, Bienemann, AS, Zhou, H, Munye, MM, Saraiva, L, McCarthy, D, Du, Z, Vink, CA, Maeshima, R, White, EA, Gustafsson, K & Hart, SL 2014, '*Multifunctional, self-assembling anionic peptide-lipid nanocomplexes for targeted siRNA delivery*', *Biomaterials.*, vol. 35, no. 29, pp. 8406-15.
- Tagalakis, AD, Maeshima, R, Yu-Wai-Man, C, Meng, J, Syed, F, Wu, LP, Aldossary, AM, McCarthy, D, Moghimi, SM & Hart, SL 2017, '*Peptide and nucleic acid-directed self-assembly of cationic nanovehicles through giant unilamellar vesicle modification*:

- Targetable nanocomplexes for in vivo nucleic acid delivery*, Acta Biomater., vol. 15, no. 51, pp. 351-362.
- Tagalakis, AD, He, L, Saraiva, L, Gustafsson, KT & Hart, SL 2011 'Receptor-targeted liposome-peptide nanocomplexes for siRNA delivery', Biomaterials., vol. 32, no. 26, pp. 6302-15
- Tagalakis, AD, Saraiva, L, McCarthy, D, Gustafsson, KT & Hart, SL 2013, 'Comparison of nanocomplexes with branched and linear peptides for siRNA delivery', Biomacromolecules., vol. 14, no. 3, pp. 761-70.
- Tan, SC & Yiap, BC 2009, 'DNA, RNA, and protein extraction: the past and the present', J Biomed Biotechnol., vol. 2009, p. 574398
- Tateishi, K, Iafrate, AJ, Ho, Q, Curry, WT, Batchelor, TT, Flaherty, KT, Onozato, ML, Lelic N, Sundaram, S, Cahill, DP, Chi, AS & Wakimoto, H 2016, 'Myc-Driven Glycolysis Is a Therapeutic Target in Glioblastoma', Clin Cancer Res., vol. 22, no. 17, pp. 4452-65
- Thakore, PI, D'Ippolito, AM, Song, L, Safi, A, Shivakumar, NK, Kabadi, AM, Reddy, TE, Crawford, GE & Gersbach CA 2015, 'Highly specific epigenome editing by CRISPR-Cas9 repressors for silencing of distal regulatory elements', Nat Methods., vol. 12, no. 12, pp. 1143-9.
- Towbin, H, Staehelin, T & Gordon, J 1979, 'Electrophoretic transfer of proteins from polyacrylamide gels to nitrocellulose sheets: procedure and some applications', Proc Natl Acad Sci U S A., vol. 76, no. 9, pp. 4350-4.
- TREHA web, Hayashibara <http://treha.jp/knowledge/function/6.php> [in Japanese] Retrieved on 30.10.2017.
- Tseng, WC, Tang, CH, Fang, TY & Su, LY 2007b, 'Trehalose enhances transgene expression mediated by DNA-PEI complexes', Biotechnol Prog., vol. 23, no. 6, pp. 1297-304.
- Tseng, WC, Tang, CH, Fang, TY 2007a & Su LY 2007a, 'Using disaccharides to enhance in vitro and in vivo transgene expression mediated by a lipid-based gene delivery system', J Gene Med., vol. 9, no. 8, pp. 659-67.
- Tweddle, DA, Malcolm, AJ, Bown, N, Pearson, AD & Lunec, J 2001, 'Evidence for the development of p53 mutations after cytotoxic therapy in a neuroblastoma cell line', Cancer Res., vol. 61, no. 1, pp. 8-13.
- Uchida, T, Takeya, S, Nagayama, M & Gohara K 2012, 'Crystallization and Materials Science of Modern Artificial and Natural Crystals, Chapter 9: Freezing Properties of Disaccharide Solutions: Inhibition of Hexagonal Ice Crystal Growth and Formation of Cubic Ice', InTechpp, pp.203-224
- Valentijn, LJ, Koster, J, Haneveld, F, Aissa, RA, van Sluis, P, Broekmans, ME, Molenaar, JJ, van Nes, J & Versteeg, R 2012, 'Functional MYCN signature predicts outcome of

- neuroblastoma irrespective of MYCN amplification*', Proc Natl Acad Sci U S A., vol. 109, no. 47, pp.19190-5.
- Valli, E, Trazzi, S, Fuchs, C, Erriquez, D, Bartesaghi, R, Perini, G & Ciani, E 2012, '*CDKL5, a novel MYCN-repressed gene, blocks cell cycle and promotes differentiation of neuronal cells*', Biochim Biophys Acta., vol. 1819, no. 11-12, pp. 1173-85.
- Valsesia-Wittmann, S, Magdeleine, M, Dupasquier, S, Garin, E, Jallas, AC, Combaret, V, Krause, A, Leissner, P & Puisieux, A 2004, '*Oncogenic cooperation between H-Twist and N-Myc overrides failsafe programs in cancer cells*', Cancer Cell., vol. 6, no. 6, pp. 625-30.
- van den Boorn, JG, Schlee, M, Coch, C, Hartmann, G 2011, '*SiRNA delivery with exosome nanoparticles*', Nat Biotechnol., vol. 29, no. 4, pp. 325-6.
- Van Maerken, T, Rihani, A, Dreidax, D, De Clercq, S, Yigit, N, Marine, JC, Westermann, F, De Paepe, A, Vandesompele, J & Speleman, F 2011, '*Functional analysis of the p53 pathway in neuroblastoma cells using the small-molecule MDM2 antagonist nutlin-3*', Mol Cancer Ther., vol. 10, no. 6, pp. 983-93.
- Varlakhanova, NV, Cotterman, RF, deVries, WN, Morgan, J, Donahue, LR, Murray, S, Knowles, BB & Knoepfler, PS 2010, '*myc maintains embryonic stem cell pluripotency and self-renewal*', Differentiation., vol. 80, no. 1, pp. 9-19.
- Venturelli, L, Nappini, S, Bulfoni, M, Gianfranceschi, G, Dal Zilio, S, Coceano, G, Del Ben, F, Turetta, M, Scoles, G, Vaccari, L, Cesselli, D & Cojoc D 2016, '*Glucose is a key driver for GLUT1-mediated nanoparticles internalization in breast cancer cells*', Sci Rep., vol. 6, p 21629.
- Videira, M, Arranja, A, Rafael, D, Gaspar, R 2014, '*Preclinical development of siRNA therapeutics: towards the match between fundamental science and engineered systems*', Nanomedicine., vol. 10, no. 4, pp. 689-702.
- Waehler, R, Russell, SJ & Curiel, DT 2007, '*Engineering targeted viral vectors for gene therapy*', Nat Rev Genet., vol. 8, no. 8, pp. 573-87.
- Wakamatsu, Y, Watanabe, Y, Nakamura, H, Kondoh, H 1997, '*Regulation of the neural crest cell fate by N-myc: promotion of ventral migration and neuronal differentiation*', Development., vol. 124, no. 10, pp. 1953-62.
- Wang, C, Liu, Z, Woo, CW, Li, Z, Wang, L, Wei, JS, Marquez, VE, Bates, SE, Jin, Q, Khan, J, Ge, K & Thiele, CJ 2012, '*EZH2 Mediates epigenetic silencing of neuroblastoma suppressor genes CASZ1, CLU, RUNX3, and NGFR*', Cancer Res., vol. 72, no. 1, pp. 315-24
- Wang, L, Zhang, X, Jia, LT, Hu, SJ, Zhao, J, Yang, JD, Wen, WH, Wang, Z, Wang, T, Zhao, J, Wang, RA, Meng, YL, Nie, YZ, Dou, KF, Chen, SY, Yao, LB, Fan, DM, Zhang, R & Yang, AG 2014, '*c-Myc-mediated epigenetic silencing of MicroRNA-101 contributes to dysregulation of multiple pathways in hepatocellular carcinoma*', Hepatology., vol. 59, no. 5, pp. 1850-63.

- Westermarck, UK, Wilhelm, M Frenzel, A & Henriksson, MA 2011, '*The MYCN oncogene and differentiation in neuroblastoma*', *Semin Cancer Biol.*, vol. 21, no. 4, pp. 256-66.
- Whitfield, JR & Soucek, L 2012, '*Tumor microenvironment: becoming sick of Myc*', *Cell Mol Life Sci*, vol. 69, no. 6, pp. 931-4.
- Whittle, SB, Smith, V, Doherty, E, Zhao, S, McCarty, S & Zage, PE, 2017, '*Overview and recent advances in the treatment of neuroblastoma*', *Expert Rev Anticancer Ther.*, vol. 17, no. 4, pp. 369-386.
- Winter, E, Dal Pizzol, C, Locatelli, C & Crezkynski-Pasa, TB 2016, '*Development and Evaluation of Lipid Nanoparticles for Drug Delivery: Study of Toxicity In, Vitroand In Vivo*', *J Nanosci Nanotechnol.*, vol. 16. No. 2, pp. 1321-30.
- Xu, CF, Zhang, HB, Sun, CY, Liu, Y, Shen, S, Yang, XZ, Zhu, YH & Wang, J 2016, '*Tumor acidity-sensitive linkage-bridged block copolymer for therapeutic siRNA delivery*'. *Biomaterials.*, vol. 88, pp. 48-59.
- Yadava, P, Gibbs, M, Castro, C & Hughes JA 2008, '*Effect of Lyophilization and Freeze-thawing on the Stability of siRNA-liposome Complexes*', *AAPS PharmSciTech.*, vol. 9, no. 2, pp. 335–341.
- Young, SA, Graf, R & Stupack, DG 2013, '*Neuroblastoma, Chapter 9 neuroblastoma integrins, Neuroblastoma*' InTechOpen, pp.189-216
- Yu, M, Ohira, M, Li, Y, Niizuma, H, Oo, ML, Zhu, Y, Ozaki, T, Isogai, E, Nakamura, Y, Koda, T, Oba, S, Yu, B & Nakagawara, A 2009, '*High expression of ncRAN, a novel non-coding RNA mapped to chromosome 17q25.1, is associated with poor prognosis in neuroblastoma*', *Int J Oncol.*, vol. 34, no. 4, pp. 931-8.
- Zatsepin, TS, Kotelevtsev, YV & Koteliansky, V 2016, '*Lipid nanoparticles for targeted siRNA delivery - going from bench to bedside*', *Int J Nanomedicine.*, vol. 11, pp. 3077-86.
- Zhang, F, Nakanishi, G, Kurebayashi, S, Yoshino, K, Perantoni, A, Kim, YS & Jetten, AM 2002, '*Characterization of Glis2, a novel gene encoding a Gli-related, Krüppel-like transcription factor with transactivation and repressor functions Roles in kidney development and neurogenesis*', *J Biol Chem.*, vol. 277, no. 12, pp. 10139-49.
- Zhang, S, Zhao, B, Jiang, H, Wang, B & Ma, B 2007, '*Cationic lipids and polymers mediated vectors for delivery of siRNA*', *J Control Release.*, vol. 123, no. 1, pp. 1-10.
- Zhang, X, Wang, L, Liu, M & Li, D 2017, '*CRISPR/Cas9 system: a powerful technology for in vivo and ex vivo gene therapy*', *Sci China Life Sci.*, vol. 60, no. 5, pp. 468-475.
- Zhang, H, Kolb, FA, Jaskiewicz, L, Westhof, E, Filipowicz, W 2004, '*Single processing center models for human Dicer and bacterial RNase III*', *Cell.*, vol. 118, no. 1, pp. 57-68.
- Zhao, Y, Alakhova, DY, Kim, JO, Bronich, TK & Kabanov, AV 2013, '*A simple way to enhance Doxil® therapy: drug release from liposomes at*

the tumor site by amphiphilic block copolymer', J Control Release., vol. 168, no. 1, pp. 61-9.

Zhao, X, Li, D, Pu, J, Mei, H, Yang, D, Xiang, X, Qu, H, Huang, K, Zheng, L & Tong, Q 2016, '*CTCF cooperates with noncoding RNA MYCNOS to promote neuroblastoma progression through facilitating MYCN expression*', Oncogene., vol. 35, no. 27, 3pp. 565-76.

Zhu, Q, Feng, C, Liao, W, Zhang Y& Tang, S 2013, '*Target delivery of MYCN siRNA by folate-nanoliposomes delivery system in a metastatic neuroblastoma model*', Cancer Cell Int., vol. 13, no. 65.

Zuckerman, JE & Davis, ME 2015, '*Clinical experiences with systemically administered siRNA-based therapeutics in cancer*', Nat Rev Drug Discov., vol. 14, no. 12, pp. 843-56.

8. Appendices

Mass Spectrometry analysis

Results

MYCN is a transcription factor and is controlling many genes. To observe the wide range of proteins up/downregulated by siMYCN/siNCYM mediated MYCN reduction, we analysed siMYCN, siNCYM or siNeg transfected cells using mass spectrometry. This mass spectrometry analysis was performed by a mass spectrometry group in Great Ormond Street Institute of Child Health, UCL. This was a pilot experiment and only one sample was prepared per condition. The analysis here was performed using lysates extracted from whole cells, although it would require another method to extract nucleic proteins if this was needed. 71 proteins were detected in siMYCN treated samples, 78 in siNCYM and 109 in siNeg, while 116 were detected in the untransfected negative control cells. Then, the weight changes of the detected proteins with more than 95% confidence were calculated, and the data were normalised by each value of siNeg. A heatmap was drawn using the data in R. The values that were much higher than the others were removed from the heatmap to show the small differences on the heatmap. The complete data are in the Appendix section.

Interestingly, 7 Tubulins were detected and the amount of each Tubulin is different among samples transfected with siMYCN, siNCYM, siNeg and untransfected negative control cells in the data which are not normalised (Fig. S1.a, the data in appendix). Tubulin beta chain was dramatically upregulated by both siMYCN and siNCYM, which were 0.35 and 0.26 ng, respectively, although it was detected at very low amounts or was absent in samples treated with siNeg and untransfected negative control. Tubulin beta-2A chain was detected in untransfected negative control cells and siMYCN although it was absent in siNCYM and siNeg. In addition, Tubulin alpha-1A chain in siNeg was particularly high at 0.77 ng while the amount of the protein in siMYCN, siNCYM and untransfected negative control cells was

0.020, 0.0064 and 0.027, respectively. Furthermore, Tubulin beta-3, beta-4 and another isotype of Tubulin beta (gene: TUBB, transcript: TUBB-208, protein ID in UniProt: Q5JP53) were detected in siNeg and untransfected negative control, although they were absent or at much lower levels in siMYCN and siNCYM. Tubulin alpha-1B in siMYCN and untransfected negative control cells was almost at the same level although it was half in siNCYM. In addition, the amount of alpha-1A in siNeg was 1/10 of that in untransfected negative control.

Most of the proteins detected were downregulated by siMYCN and siNCYM in the heatmap (Fig. S1.b). The highest value in the heatmap is represented as red, which is Histone H1.2 at 1.09 in siMYCN and 0.67 in siNCYM, and it suggests that siMYCN did not affect the expression level of Histone H1.2. On the other hand, Tubulin alpha-1B chain was dramatically upregulated by both siMYCN and siNCYM at 8.28 and 5.05, respectively (it is not on the heatmap as the values of Histone H1.2 were higher than those of the other proteins), although the amount of the protein in the cells treated with siMYCN/siNCYM/siNeg were decreased, compared to that in untransfected negative control cells.

Most of the values in siNCYM were lower than siMYCN in this analysis, which is similar to the amount of MYCN downregulation and Trk upregulation by siNCYM were lower than those by siMYCN. However, the values of heat shock 70 kDa protein 1A and nucleophosmin in siNCYM were slightly higher than those in siMYCN by approximately 0.1.

There were proteins detected in the siMYCN treated sample which were undetectable in the siNCYM sample: 14-3-3 protein zeta/delta and glutathione S-transferase P. The two proteins were slightly downregulated by siMYCN by 19.7% and 27.2%, respectively.

These results suggest that many proteins might be up/downregulated by both MYCN mRNA and NCYM RNA as MYCN protein regulates those proteins, and it is likely that it is dependent upon the MYCN expression level. However, it may be possible that there are proteins which are directly affected by NCYM RNA level or that the protein up/downregulation is not linear correlation with MYCN reduction.

Discussion

In the mass spectrometry data, seven types of Tubulin were detected. The amount of each tubulin was different among the 4 conditions and it may account for the morphological differences among the conditions. Tubulin alpha and beta polymerise microtubules, which are the main components of cytoskeleton in neurons. Especially Tubulin beta-3 is well-known as a biomarker of differentiation in neuronal cells and is expressed in neuronal and non-neuronal cells in cancer. In addition, it is an essential regulator of survival pathway (Karki et al. 2013, MacCaroll et al. 2010). It has been pointed out that it seems that overexpressed Tubulin beta-3 is associated with tumour aggressiveness. Furthermore, it is likely that the overexpression is a marker of drug resistance such as with taxan, a microtubule targeting agent and mitotic inhibitor (Karki et al. 2013). In untransfected and siNeg-treated SK-N-BE(2), Tubulin beta 3 was detected while the protein was absent or much lower level in the cells treated with siMYCN and siNCYM. This may imply that siMYCN and siNCYM downregulate the protein and that this in turn may induce cell growth arrest.

Glutathione S-transferase P was slightly downregulated by siMYCN although it was not detected in the cells treated with siNCYM. Glutathione S-transferase P downregulates cyclin-dependent kinase 5 (CDK5) activity, which is involved in neuronal differentiation

(Guglielmi et al. 2014). The decrease of the protein may suggest that differentiation was induced by the transfections.

However, the sample number of this experiment was only one, and therefore, it is necessary to analyse more samples to confirm the data. Furthermore, mass spectrometry analysis of nucleus proteins is also essential for further study because MYCN is a transcription factor. It should reveal a more wide range of downstream effects of MYCN silencing by siMYCN.

We observed a widely range of changes in protein in cytoplasm using mass spectrometry (Appendix Fig.S1.). Firstly, our study is a first attempt on the use of mass spectrometry and therefore, the technical conditions can be optimised further. For example, the number of the proteins detected in the assay in siMYCN and siNCYM was smaller than that in untransfected negative control which might be due to a small fraction of cells transfected by siMYCN and siNCYM. Secondly, analysis of the proteins in nucleus would be ideal for our main interests, although the results in cytoplasm are also interesting. It will be necessary to confirm the mass spec by immunoblotting eventually.

a)

	UT ctrl	siMYCN	siNCYM	siNeg
Tubulin beta chain (TBB5)	0.000001	0.3544	0.2636	n.d.
Tubulin beta-2A chain (TBB2A)	0.0189	0.0096	n.d.	n.d.
Tubulin alpha-1A chain (TBA1A)	0.0276	0.0208	0.0064	0.7742
Tubulin beta-3 chain (TBB3)	0.0467	0.000001	n.d.	0.0505
Tubulin beta-4B chain (TBB2B)	0.1488	0.000001	0.0066	0.2013
Tubulin beta chain (Q5_JP53)	0.4881	0.000001	n.d.	0.571
Tubulin alpha-1B chain (TBA1B)	0.6253	0.5764	0.3521	0.0696

b)

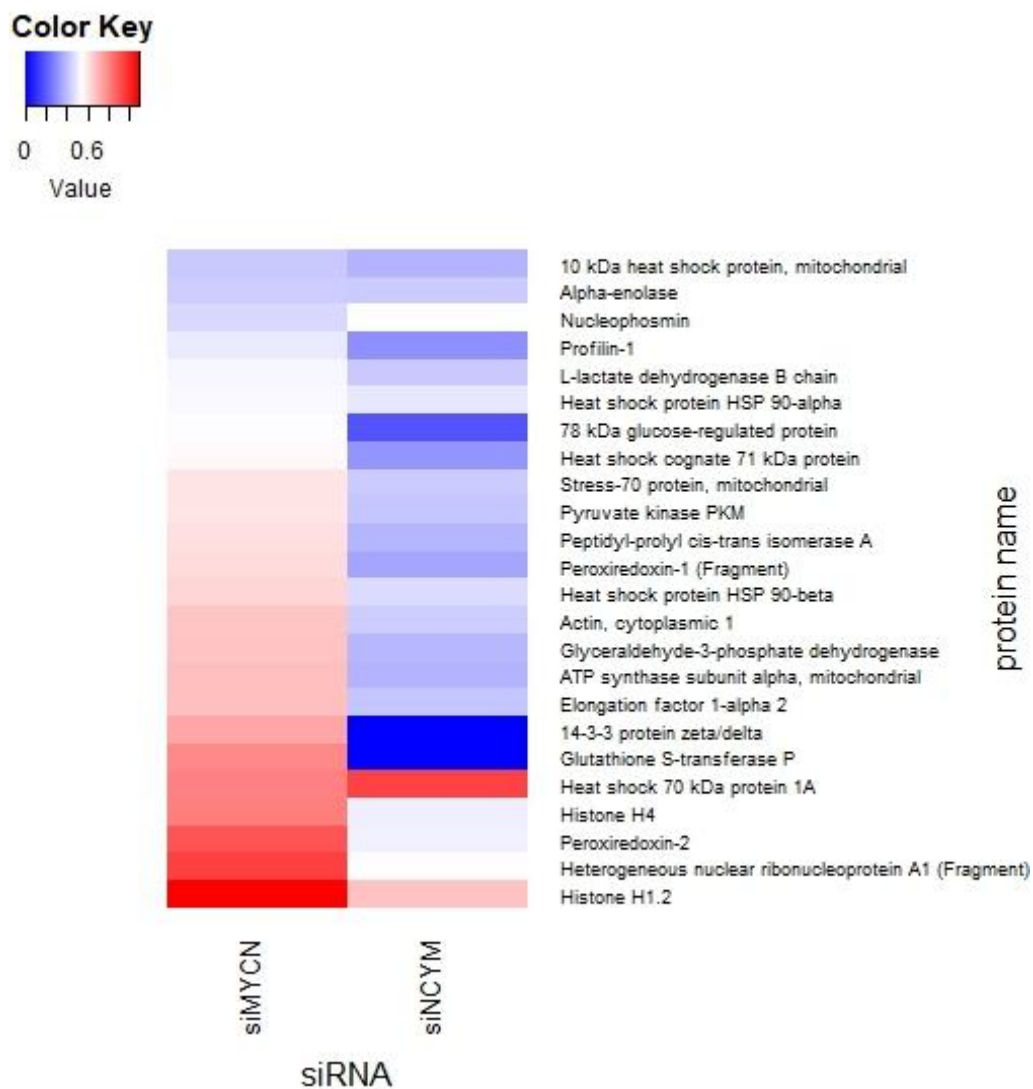


Fig. S1. The change of Tubulin expression and Heatmap representing up/downregulation of proteins by siMYCN/siNCYM transfection in SK-N-BE(2) cells a) The amount (ng) of each Tubulin by siMYCN, siNCYM, siNeg and Untransfected control. n.d. represents non-detectable. b) Proteins downregulated by siMYCN and siNCYM. All values were normalised by the value of siNeg. Red represents 1, while blue represents 0. (n=1)

Supplementary material

The raw data of the mass spectrometry analysis in SK-N-BE(2)

The unit of values is ng.

n.d. represents non-detectable.

All kinds of tubulin were marked with yellow.

Non-POU domain-containing octamer-binding protein is RNA binding protein NonO.

≥ 95%
≈ 50%
≤ 10%

Accession	Entry	Description	UT ctrl	siMYCN	siNCYM	siNeg
A0A087WVQ6	A0A087WVQ6_HUMAN	A0A087WVQ6 A0A087WVQ6_HUMAN Clathrin heavy chain OS=Homo sapiens GN=CLTC PE=1 SV=1	0	0.000001	n.d.	n.d.
A0A087WZV1	A0A087WZV1_HUMAN	A0A087WZV1 A0A087WZV1_HUMAN Heterogeneous nuclear ribonucleoprotein A/B OS=Homo sapiens GN=HNRNPAB PE=1 SV=1	0	0.000001	n.d.	0
A0A087X0X3	A0A087X0X3_HUMAN	A0A087X0X3 A0A087X0X3_HUMAN Heterogeneous nuclear ribonucleoprotein M OS=Homo sapiens GN=HNRNPM PE=1 SV=1	0	0.000001	n.d.	0
A0A0A0MTS2	A0A0A0MTS2_HUMAN	A0A0A0MTS2 A0A0A0MTS2_HUMAN Glucose-6-phosphate isomerase (Fragment) OS=Homo sapiens GN=GPI PE=1 SV=1	0	0.000001	n.d.	n.d.
A0A0C4DG17	A0A0C4DG17_HUMAN	A0A0C4DG17 A0A0C4DG17_HUMAN 40S ribosomal protein SA OS=Homo sapiens GN=RPSA PE=1 SV=1	0	0.000001	n.d.	0
A0A0C4DGL3	A0A0C4DGL3_HUMAN	A0A0C4DGL3 A0A0C4DGL3_HUMAN DUTP pyrophosphatase, isoform CRA_c OS=Homo sapiens GN=DUT PE=1 SV=1	0	0.000001	n.d.	n.d.
A0A0U1RR32	A0A0U1RR32_HUMAN	A0A0U1RR32 A0A0U1RR32_HUMAN HCG2039566, isoform CRA_b OS=Homo sapiens GN=hCG_2039566 PE=4 SV=1	0	0	0.000000	0
B2R4S9	B2R4S9_HUMAN	B2R4S9 B2R4S9_HUMAN Histone H2B OS=Homo sapiens GN=HIST1H2BC PE=2 SV=1	0	0	0.000000	0
B2R5W2	B2R5W2_HUMAN	B2R5W2 B2R5W2_HUMAN Heterogeneous nuclear ribonucleoproteins C1/C2 OS=Homo sapiens GN=HNRNPC PE=1 SV=1	0	0	0.000000	0
B4DNK4	B4DNK4_HUMAN	B4DNK4 B4DNK4_HUMAN Pyruvate kinase OS=Homo sapiens GN=PKM PE=1 SV=1	0	0.000001	n.d.	n.d.
B5MDF5	B5MDF5_HUMAN	B5MDF5 B5MDF5_HUMAN GTP-binding nuclear protein Ran OS=Homo sapiens GN=RAN PE=1 SV=1	0	0.000001	0.000000	0
C9IZL7	C9IZL7_HUMAN	C9IZL7 C9IZL7_HUMAN Non-POU domain-containing octamer-binding protein (Fragment) OS=Homo sapiens GN=NONO PE=1 SV=1	0	0.0205	n.d.	0.0336
C9JNW5	C9JNW5_HUMAN	C9JNW5 C9JNW5_HUMAN 60S ribosomal protein L24 OS=Homo sapiens GN=RPL24 PE=1 SV=1	0	0.000001	n.d.	n.d.
C9JW96	C9JW96_HUMAN	C9JW96 C9JW96_HUMAN Prohibitin (Fragment) OS=Homo sapiens GN=PHB PE=1 SV=2	0	0.000001	0.000000	0
D6RHH4	D6RHH4_HUMAN	D6RHH4 D6RHH4_HUMAN Guanine nucleotide-binding protein subunit beta-2-like 1 OS=Homo sapiens GN=GNB2L1 PE=1 SV=1	0	0.000001	n.d.	n.d.
F5GWF6	F5GWF6_HUMAN	F5GWF6 F5GWF6_HUMAN T-complex protein 1 subunit beta OS=Homo sapiens GN=CCT2 PE=1 SV=2	0	0.000001	n.d.	n.d.
H0Y6E7	H0Y6E7_HUMAN	H0Y6E7 H0Y6E7_HUMAN RNA-binding motif protein, X chromosome (Fragment) OS=Homo sapiens GN=RBMX PE=1 SV=2	0	0.000001	n.d.	n.d.
J3KPD9	J3KPD9_HUMAN	J3KPD9 J3KPD9_HUMAN Protein NME1-NME2 OS=Homo sapiens GN=NME1-NME2 PE=1 SV=1	0	0	0.000000	n.d.

Accession	Entry	Description	UT ctrl	siMYCN	siNCYM	siNeg
P14866	HNRPL_HUMAN	P14866 HNRPL_HUMAN Heterogeneous nuclear ribonucleoprotein L OS=Homo sapiens GN=HNRNPL PE=1 SV=2	0	0.000001	n.d.	0
P23528	COF1_HUMAN	P23528 COF1_HUMAN Cofilin-1 OS=Homo sapiens GN=CFL1 PE=1 SV=3	0	0	0.000000	0
P68104	EF1A1_HUMAN	P68104 EF1A1_HUMAN Elongation factor 1-alpha 1 OS=Homo sapiens GN=EEF1A1 PE=1 SV=1	0	0	0.000000	0
Q16695	H31T_HUMAN	Q16695 H31T_HUMAN Histone H3.1t OS=Homo sapiens GN=HIST3H3 PE=1 SV=3	0	0	0.000000	0
Q5VVC8	Q5VVC8_HUMAN	Q5VVC8 Q5VVC8_HUMAN 60S ribosomal protein L11 (Fragment) OS=Homo sapiens GN=RPL11 PE=1 SV=1	0	0.000001	n.d.	n.d.
A0A075B7A0	A0A075B7A0_HUMAN	A0A075B7A0 A0A075B7A0_HUMAN 60S ribosomal protein L18 OS=Homo sapiens GN=RPL18 PE=1 SV=1	0.000001	0.000001	0.000000	n.d.
A0A087WUI2	A0A087WUI2_HUMAN	A0A087WUI2 A0A087WUI2_HUMAN Heterogeneous nuclear ribonucleoproteins A2/B1 OS=Homo sapiens GN=HNRNPA2B1 PE=1 SV=1	0.000001	0.069	0.043200	n.d.
A0A087WUK2	A0A087WUK2_HUMAN	A0A087WUK2 A0A087WUK2_HUMAN Heterogeneous nuclear ribonucleoprotein D-like OS=Homo sapiens GN=HNRNPDL PE=1 SV=1	0.000001	0.000001	0.000000	n.d.
A0A087WYG8	A0A087WYG8_HUMAN	A0A087WYG8 A0A087WYG8_HUMAN Alpha-internexin OS=Homo sapiens GN=INA PE=1 SV=1	0.000001	0.1091	n.d.	n.d.
A0A087WZD7	A0A087WZD7_HUMAN	A0A087WZD7 A0A087WZD7_HUMAN F-box only protein 8 OS=Homo sapiens GN=FBXO8 PE=4 SV=1	0.000001	0	0.000000	n.d.
A0A0B4J213	A0A0B4J213_HUMAN	A0A0B4J213 A0A0B4J213_HUMAN 60S ribosomal protein L30 OS=Homo sapiens GN=RPL30 PE=1 SV=1	0.000001	0.000001	0.003500	n.d.
A8MUD9	A8MUD9_HUMAN	A8MUD9 A8MUD9_HUMAN 60S ribosomal protein L7 OS=Homo sapiens GN=RPL7 PE=1 SV=1	0.000001	0.000001	n.d.	0.0843
A8MX94	A8MX94_HUMAN	A8MX94 A8MX94_HUMAN Glutathione S-transferase P OS=Homo sapiens GN=GSTP1 PE=1 SV=1	0.000001	0.0572	n.d.	0.0712
B0YJC4	B0YJC4_HUMAN	B0YJC4 B0YJC4_HUMAN Vimentin OS=Homo sapiens GN=VIM PE=1 SV=1	0.000001	0.1043	n.d.	0.1361
B7Z645	B7Z645_HUMAN	B7Z645 B7Z645_HUMAN Heterogeneous nuclear ribonucleoprotein Q OS=Homo sapiens GN=SYNCRIP PE=1 SV=1	0.000001	0.000001	n.d.	0.0576
C9J0D1	C9J0D1_HUMAN	C9J0D1 C9J0D1_HUMAN Histone H2A OS=Homo sapiens GN=H2AFV PE=3 SV=1	0.000001	0.012	n.d.	n.d.
C9J386	C9J386_HUMAN	C9J386 C9J386_HUMAN Histone H2A OS=Homo sapiens GN=H2AFV PE=3 SV=1	0.000001	0.000001	n.d.	0.0178
D6R956	D6R956_HUMAN	D6R956 D6R956_HUMAN Ubiquitin carboxyl-terminal hydrolase OS=Homo sapiens GN=UCHL1 PE=1 SV=1	0.000001	0	0.000000	0
D6RAC2	D6RAC2_HUMAN	D6RAC2 D6RAC2_HUMAN Guanine nucleotide-binding protein subunit beta-2-like 1 OS=Homo sapiens GN=GNB2L1 PE=1 SV=1	0.000001	0.000001	n.d.	0
E7EQG2	E7EQG2_HUMAN	E7EQG2 E7EQG2_HUMAN Eukaryotic initiation factor 4A-II OS=Homo sapiens GN=EIF4A2 PE=1 SV=1	0.000001	0.000001	n.d.	0.1014

Accession	Entry	Description	UT ctrl	siMYCN	siNCYM	siNeg
E7ERL0	E7ERL0_HUMAN	E7ERL0 E7ERL0_HUMAN Nucleoside diphosphate kinase A OS=Homo sapiens GN=NME1 PE=1 SV=1	0.000001	0.000001	n.d.	0.1114
E9PL09	E9PL09_HUMAN	E9PL09 E9PL09_HUMAN 40S ribosomal protein S3 OS=Homo sapiens GN=RPS3 PE=1 SV=1	0.000001	0.000001	0.000000	0
E9PQD7	E9PQD7_HUMAN	E9PQD7 E9PQD7_HUMAN 40S ribosomal protein S2 OS=Homo sapiens GN=RPS2 PE=1 SV=1	0.000001	0.000001	n.d.	0
F5GWA7	F5GWA7_HUMAN	F5GWA7 F5GWA7_HUMAN Prohibitin-2 (Fragment) OS=Homo sapiens GN=PHB2 PE=1 SV=1	0.000001	0.000001	n.d.	0
F5H157	F5H157_HUMAN	F5H157 F5H157_HUMAN Ras-related protein Rab-35 (Fragment) OS=Homo sapiens GN=RAB35 PE=1 SV=1	0.000001	0.000001	n.d.	0.0466
F8VZJ2	F8VZJ2_HUMAN	F8VZJ2 F8VZJ2_HUMAN Nascent polypeptide-associated complex subunit alpha OS=Homo sapiens GN=NACA PE=1 SV=1	0.000001	0.000001	n.d.	0.0105
G3XAN0	G3XAN0_HUMAN	G3XAN0 G3XAN0_HUMAN 40S ribosomal protein S20 OS=Homo sapiens GN=RPS20 PE=1 SV=1	0.000001	0.000001	n.d.	0.0141
H0YA52	H0YA52_HUMAN	H0YA52 H0YA52_HUMAN Pterin-4-alpha-carbinolamine dehydratase 2 (Fragment) OS=Homo sapiens GN=PCBD2 PE=1 SV=1	0.000001	0.000001	0.257000	n.d.
P02545	LMNA_HUMAN	P02545 LMNA_HUMAN Prelamin-A/C OS=Homo sapiens GN=LMNA PE=1 SV=1	0.000001	0.000001	n.d.	0
P04264	K2C1_HUMAN	P04264 K2C1_HUMAN Keratin, type II cytoskeletal 1 OS=Homo sapiens GN=KRT1 PE=1 SV=6	0.000001	0.000001	0.000000	n.d.
P07355	ANXA2_HUMAN	P07355 ANXA2_HUMAN Annexin A2 OS=Homo sapiens GN=ANXA2 PE=1 SV=2	0.000001	0	n.d.	0
P07437	TBB5_HUMAN	P07437 TBB5_HUMAN Tubulin beta chain OS=Homo sapiens GN=TUBB PE=1 SV=2	0.000001	0.3544	0.263600	n.d.
P14618	KPYM_HUMAN	P14618 KPYM_HUMAN Pyruvate kinase PKM OS=Homo sapiens GN=PKM PE=1 SV=4	0.000001	0.3939	0.274300	0.6476
P17066	HSP76_HUMAN	P17066 HSP76_HUMAN Heat shock 70 kDa protein 6 OS=Homo sapiens GN=HSPA6 PE=1 SV=2	0.000001	0.000001	0.105900	n.d.
P27348	1433T_HUMAN	P27348 1433T_HUMAN 14-3-3 protein theta OS=Homo sapiens GN=YWHAQ PE=1 SV=1	0.000001	0.000001	0.000000	n.d.
P30050	RL12_HUMAN	P30050 RL12_HUMAN 60S ribosomal protein L12 OS=Homo sapiens GN=RPL12 PE=1 SV=1	0.000001	0.000001	n.d.	0.037
P34897	GLYM_HUMAN	P34897 GLYM_HUMAN Serine hydroxymethyltransferase, mitochondrial OS=Homo sapiens GN=SHMT2 PE=1 SV=3	0.000001	0.000001	n.d.	0.0598
P49411	EFTU_HUMAN	P49411 EFTU_HUMAN Elongation factor Tu, mitochondrial OS=Homo sapiens GN=TUFM PE=1 SV=2	0.000001	0.000001	n.d.	0.0686
P62258	1433E_HUMAN	P62258 1433E_HUMAN 14-3-3 protein epsilon OS=Homo sapiens GN=YWHAE PE=1 SV=1	0.000001	0.000001	n.d.	0.0697

Accession	Entry	Description	UT ctrl	siMYCN	siNCYM	siNeg
P62701	RS4X_HUMAN	P62701 RS4X_HUMAN 40S ribosomal protein S4, X isoform OS=Homo sapiens GN=RPS4X PE=1 SV=2	0.000001	0.000001	n.d.	0.0592
P62913	RL11_HUMAN	P62913 RL11_HUMAN 60S ribosomal protein L11 OS=Homo sapiens GN=RPL11 PE=1 SV=2	0.000001	0.000001	n.d.	0.0282
Q4VY20	Q4VY20_HUMAN	Q4VY20 Q4VY20_HUMAN 14-3-3 protein beta/alpha (Fragment) OS=Homo sapiens GN=YWHAB PE=1 SV=1	0.000001	0.000001	n.d.	0.0104
Q92841	DDX17_HUMAN	Q92841 DDX17_HUMAN Probable ATP-dependent RNA helicase DDX17 OS=Homo sapiens GN=DDX17 PE=1 SV=2	0.000001	0.000001	0.000000	0
P62318	SMD3_HUMAN	P62318 SMD3_HUMAN Small nuclear ribonucleoprotein Sm D3 OS=Homo sapiens GN=SNRPD3 PE=1 SV=1	0.0102	0.000001	n.d.	n.d.
P62857	RS28_HUMAN	P62857 RS28_HUMAN 40S ribosomal protein S28 OS=Homo sapiens GN=RPS28 PE=1 SV=1	0.0135	0.000001	n.d.	n.d.
E9PG15	E9PG15_HUMAN	E9PG15 E9PG15_HUMAN 14-3-3 protein theta (Fragment) OS=Homo sapiens GN=YWHAQ PE=1 SV=1	0.016	0.000001	n.d.	n.d.
B8ZZL8	B8ZZL8_HUMAN	B8ZZL8 B8ZZL8_HUMAN 10 kDa heat shock protein, mitochondrial OS=Homo sapiens GN=HSPE1 PE=1 SV=1	0.0166	0.0092	0.008200	0.0213
O75531	BAF_HUMAN	O75531 BAF_HUMAN Barrier-to-autointegration factor OS=Homo sapiens GN=BANF1 PE=1 SV=1	0.0166	0.000001	n.d.	n.d.
Q13885	TBB2A_HUMAN	Q13885 TBB2A_HUMAN Tubulin beta-2A chain OS=Homo sapiens GN=TUBB2A PE=1 SV=1	0.0189	0.0096	n.d.	n.d.
F2Z2S8	F2Z2S8_HUMAN	F2Z2S8 F2Z2S8_HUMAN 40S ribosomal protein S3 OS=Homo sapiens GN=RPS3 PE=1 SV=1	0.0213	0.0114	n.d.	n.d.
A2A2D0	A2A2D0_HUMAN	A2A2D0 A2A2D0_HUMAN Stathmin (Fragment) OS=Homo sapiens GN=STMN1 PE=1 SV=7	0.0242	0.000001	n.d.	0.0173
P0C0S5	H2AZ_HUMAN	P0C0S5 H2AZ_HUMAN Histone H2A.Z OS=Homo sapiens GN=H2AFZ PE=1 SV=2	0.0257	0.000001	0.012800	n.d.
P0DMV8	HS71A_HUMAN	P0DMV8 HS71A_HUMAN Heat shock 70 kDa protein 1A OS=Homo sapiens GN=HSPA1A PE=1 SV=1	0.0274	0.0185	0.021500	0.0225
Q71U36	TBA1A_HUMAN	Q71U36 TBA1A_HUMAN Tubulin alpha-1A chain OS=Homo sapiens GN=TUBA1A PE=1 SV=1	0.0276	0.0208	0.006400	0.7742
P17987	TCPA_HUMAN	P17987 TCPA_HUMAN T-complex protein 1 subunit alpha OS=Homo sapiens GN=TCP1 PE=1 SV=1	0.0315	0.000001	n.d.	n.d.
P24534	EF1B_HUMAN	P24534 EF1B_HUMAN Elongation factor 1-beta OS=Homo sapiens GN=EEF1B2 PE=1 SV=3	0.0317	0.000001	n.d.	n.d.
F8VUA6	F8VUA6_HUMAN	F8VUA6 F8VUA6_HUMAN 60S ribosomal protein L18 (Fragment) OS=Homo sapiens GN=RPL18 PE=1 SV=1	0.0326	0.019	n.d.	0.0387

Accession	Entry	Description	UT ctrl	siMYCN	siNCYM	siNeg
P51991	ROA3_HUMAN	P51991 ROA3_HUMAN Heterogeneous nuclear ribonucleoprotein A3 OS=Homo sapiens GN=HNRNPA3 PE=1 SV=2	0.0336	0.000001	n.d.	n.d.
A0A087WWU8	A0A087WWU8_HUMAN	A0A087WWU8 A0A087WWU8_HUMAN Tropomyosin alpha-3 chain OS=Homo sapiens GN=TPM3 PE=1 SV=1	0.039	0.0319	n.d.	0.0471
P23526	SAHH_HUMAN	P23526 SAHH_HUMAN Adenosylhomocysteinase OS=Homo sapiens GN=AHCY PE=1 SV=4	0.0392	0.000001	n.d.	0.0478
Q5JR95	Q5JR95_HUMAN	Q5JR95 Q5JR95_HUMAN 40S ribosomal protein S8 OS=Homo sapiens GN=RPS8 PE=1 SV=1	0.0408	0.000001	n.d.	0.0395
E7EPB3	E7EPB3_HUMAN	E7EPB3 E7EPB3_HUMAN 60S ribosomal protein L14 OS=Homo sapiens GN=RPL14 PE=1 SV=1	0.0425	0.0239	0.022200	0.046
Q13509	TBB3_HUMAN	Q13509 TBB3_HUMAN Tubulin beta-3 chain OS=Homo sapiens GN=TUBB3 PE=1 SV=2	0.0467	0.000001	n.d.	0.0505
P12004	PCNA_HUMAN	P12004 PCNA_HUMAN Proliferating cell nuclear antigen OS=Homo sapiens GN=PCNA PE=1 SV=1	0.0469	0.0393	0.022200	0.0694
P30048	PRDX3_HUMAN	P30048 PRDX3_HUMAN Thioredoxin-dependent peroxide reductase, mitochondrial OS=Homo sapiens GN=PRDX3 PE=1 SV=3	0.048	0.0424	0.021000	0.0371
P07737	PROF1_HUMAN	P07737 PROF1_HUMAN Profilin-1 OS=Homo sapiens GN=PFN1 PE=1 SV=2	0.0493	0.0313	0.019100	0.0623
A0A0G2JJZ9	A0A0G2JJZ9_HUMAN	A0A0G2JJZ9 A0A0G2JJZ9_HUMAN Spliceosome RNA helicase DDX39B (Fragment) OS=Homo sapiens GN=DDX39B PE=1 SV=1	0.0496	0.000001	n.d.	0.0524
P53396	ACLY_HUMAN	P53396 ACLY_HUMAN ATP-citrate synthase OS=Homo sapiens GN=ACLY PE=1 SV=3	0.0545	0.000001	n.d.	n.d.
P18669	PGAM1_HUMAN	P18669 PGAM1_HUMAN Phosphoglycerate mutase 1 OS=Homo sapiens GN=PGAM1 PE=1 SV=2	0.0566	0.000001	n.d.	n.d.
Q5SZU1	Q5SZU1_HUMAN	Q5SZU1 Q5SZU1_HUMAN D-3-phosphoglycerate dehydrogenase OS=Homo sapiens GN=PHGDH PE=1 SV=1	0.0584	0.000001	n.d.	0.0647
P12236	ADT3_HUMAN	P12236 ADT3_HUMAN ADP/ATP translocase 3 OS=Homo sapiens GN=SLC25A6 PE=1 SV=4	0.0603	0.000001	0.032100	0.0601
D6RE83	D6RE83_HUMAN	D6RE83 D6RE83_HUMAN Ubiquitin carboxyl-terminal hydrolase OS=Homo sapiens GN=UCHL1 PE=1 SV=1	0.0663	0.000001	n.d.	n.d.
P12956	XRCC6_HUMAN	P12956 XRCC6_HUMAN X-ray repair cross-complementing protein 6 OS=Homo sapiens GN=XRCC6 PE=1 SV=2	0.0694	0.000001	n.d.	n.d.
P23284	PPIB_HUMAN	P23284 PPIB_HUMAN Peptidyl-prolyl cis-trans isomerase B OS=Homo sapiens GN=PPIB PE=1 SV=2	0.0716	0.0608	0.027100	0.0852
F8VU65	F8VU65_HUMAN	F8VU65 F8VU65_HUMAN 60S acidic ribosomal protein P0 (Fragment) OS=Homo sapiens GN=RPLP0 PE=1 SV=1	0.0723	0.041	0.031600	0.0746

Accession	Entry	Description	UT ctrl	siMYCN	siNCYM	siNeg
A0A087WTT1	A0A087WTT1_HUMAN	A0A087WTT1 A0A087WTT1_HUMAN Polyadenylate-binding protein OS=Homo sapiens GN=PABPC1 PE=1 SV=1	0.0736	0.000001	n.d.	0
O60506	HNRPQ_HUMAN	O60506 HNRPQ_HUMAN Heterogeneous nuclear ribonucleoprotein Q OS=Homo sapiens GN=SYNCRIP PE=1 SV=2	0.0749	0.000001	n.d.	n.d.
P60174	TPIS_HUMAN	P60174 TPIS_HUMAN Triosephosphate isomerase OS=Homo sapiens GN=TPI1 PE=1 SV=3	0.0774	0.0543	0.045600	0.0967
P50990	TCPO_HUMAN	P50990 TCPO_HUMAN T-complex protein 1 subunit theta OS=Homo sapiens GN=CCT8 PE=1 SV=4	0.0786	0.000001	n.d.	n.d.
P55072	TERA_HUMAN	P55072 TERA_HUMAN Transitional endoplasmic reticulum ATPase OS=Homo sapiens GN=VCP PE=1 SV=4	0.0787	0.000001	n.d.	0.079
G3V4N7	G3V4N7_HUMAN	G3V4N7 G3V4N7_HUMAN Creatine kinase B-type (Fragment) OS=Homo sapiens GN=CKB PE=1 SV=1	0.0792	0.0519	0.050500	0.0577
P05141	ADT2_HUMAN	P05141 ADT2_HUMAN ADP/ATP translocase 2 OS=Homo sapiens GN=SLC25A5 PE=1 SV=7	0.0796	0.0875	0.044200	0.0866
P27797	CALR_HUMAN	P27797 CALR_HUMAN Calreticulin OS=Homo sapiens GN=CALR PE=1 SV=1	0.08	0.000001	n.d.	0
Q15084	PDIA6_HUMAN	Q15084 PDIA6_HUMAN Protein disulfide-isomerase A6 OS=Homo sapiens GN=PDIA6 PE=1 SV=1	0.0839	0.000001	n.d.	0.1254
P40926	MDHM_HUMAN	P40926 MDHM_HUMAN Malate dehydrogenase, mitochondrial OS=Homo sapiens GN=MDH2 PE=1 SV=3	0.0845	0.057	0.041800	0.0835
P17844	DDX5_HUMAN	P17844 DDX5_HUMAN Probable ATP-dependent RNA helicase DDX5 OS=Homo sapiens GN=DDX5 PE=1 SV=1	0.0889	0.000001	n.d.	n.d.
F8VTQ5	F8VTQ5_HUMAN	F8VTQ5 F8VTQ5_HUMAN Heterogeneous nuclear ribonucleoprotein A1 (Fragment) OS=Homo sapiens GN=HNRNPA1 PE=1 SV=1	0.0891	0.0811	0.047100	0.0846
E9PCY7	E9PCY7_HUMAN	E9PCY7 E9PCY7_HUMAN Heterogeneous nuclear ribonucleoprotein H OS=Homo sapiens GN=HNRNPH1 PE=1 SV=1	0.0913	0.000001	n.d.	0
Q13263	TIF1B_HUMAN	Q13263 TIF1B_HUMAN Transcription intermediary factor 1-beta OS=Homo sapiens GN=TRIM28 PE=1 SV=5	0.0947	0.000001	n.d.	n.d.
P32119	PRDX2_HUMAN	P32119 PRDX2_HUMAN Peroxiredoxin-2 OS=Homo sapiens GN=PRDX2 PE=1 SV=5	0.0949	0.0841	0.047700	0.0921
A0A0A0MSI0	A0A0A0MSI0_HUMAN	A0A0A0MSI0 A0A0A0MSI0_HUMAN Peroxiredoxin-1 (Fragment) OS=Homo sapiens GN=PRDX1 PE=1 SV=1	0.0966	0.0635	0.035600	0.0984
A0A0A0MR02	A0A0A0MR02_HUMAN	A0A0A0MR02 A0A0A0MR02_HUMAN Voltage-dependent anion-selective channel protein 2 (Fragment) OS=Homo sapiens GN=VDAC2 PE=1 SV=1	0.0999	0.0984	0.055900	0.1572
P61978	HNRPK_HUMAN	P61978 HNRPK_HUMAN Heterogeneous nuclear ribonucleoprotein K OS=Homo sapiens GN=HNRNPK PE=1 SV=1	0.1024	0.000001	0.000000	0.075

Accession	Entry	Description	UT ctrl	siMYCN	siNCYM	siNeg
Q16555	DPYL2_HUMAN	Q16555 DPYL2_HUMAN Dihydropyrimidinase-related protein 2 OS=Homo sapiens GN=DPYSL2 PE=1 SV=1	0.1031	0.0381	0.000000	0.1088
P63104	1433Z_HUMAN	P63104 1433Z_HUMAN 14-3-3 protein zeta/delta OS=Homo sapiens GN=YWHAZ PE=1 SV=1	0.1039	0.0723	n.d.	0.0979
P60842	IF4A1_HUMAN	P60842 IF4A1_HUMAN Eukaryotic initiation factor 4A-I OS=Homo sapiens GN=EIF4A1 PE=1 SV=1	0.1052	0.000001	n.d.	n.d.
P14174	MIF_HUMAN	P14174 MIF_HUMAN Macrophage migration inhibitory factor OS=Homo sapiens GN=MIF PE=1 SV=4	0.1091	0.072	0.054300	0.1026
P00558	PGK1_HUMAN	P00558 PGK1_HUMAN Phosphoglycerate kinase 1 OS=Homo sapiens GN=PGK1 PE=1 SV=3	0.1124	0	0.061900	0
P04075	ALDOA_HUMAN	P04075 ALDOA_HUMAN Fructose-bisphosphate aldolase A OS=Homo sapiens GN=ALDOA PE=1 SV=2	0.1149	0.0678	0.052300	0.1205
P08670	VIME_HUMAN	P08670 VIME_HUMAN Vimentin OS=Homo sapiens GN=VIM PE=1 SV=4	0.116	0.000001	0.066400	n.d.
P22626	ROA2_HUMAN	P22626 ROA2_HUMAN Heterogeneous nuclear ribonucleoproteins A2/B1 OS=Homo sapiens GN=HNRNPA2B1 PE=1 SV=2	0.1196	0.000001	n.d.	0.114
P09211	GSTP1_HUMAN	P09211 GSTP1_HUMAN Glutathione S-transferase P OS=Homo sapiens GN=GSTP1 PE=1 SV=2	0.1221	0.000001	0.044200	n.d.
P16401	H15_HUMAN	P16401 H15_HUMAN Histone H1.5 OS=Homo sapiens GN=HIST1H1B PE=1 SV=3	0.1242	0.0847	0.049200	0.1009
P30101	PDIA3_HUMAN	P30101 PDIA3_HUMAN Protein disulfide-isomerase A3 OS=Homo sapiens GN=PDIA3 PE=1 SV=4	0.1251	0.000001	0.052900	0.1284
P06576	ATPB_HUMAN	P06576 ATPB_HUMAN ATP synthase subunit beta, mitochondrial OS=Homo sapiens GN=ATP5B PE=1 SV=3	0.1319	0.0703	0.000000	0
P21796	VDAC1_HUMAN	P21796 VDAC1_HUMAN Voltage-dependent anion-selective channel protein 1 OS=Homo sapiens GN=VDAC1 PE=1 SV=2	0.1341	0.1106	0.064800	0.1297
Q00839	HNRPU_HUMAN	Q00839 HNRPU_HUMAN Heterogeneous nuclear ribonucleoprotein U OS=Homo sapiens GN=HNRNPU PE=1 SV=6	0.141	0.000001	n.d.	0.1495
P25705	ATPA_HUMAN	P25705 ATPA_HUMAN ATP synthase subunit alpha, mitochondrial OS=Homo sapiens GN=ATP5A1 PE=1 SV=1	0.1449	0.1217	0.067800	0.1772
P00761	TRYP_PIG	P00761 TRYP_PIG Trypsin OS=Sus scrofa PE=1 SV=1	0.1475	0.1921	0.122500	0.1727
P68371	TBB4B_HUMAN	P68371 TBB4B_HUMAN Tubulin beta-4B chain OS=Homo sapiens GN=TUBB4B PE=1 SV=1	0.1488	0.000001	0.006600	0.2013
P06733	ENOA_HUMAN	P06733 ENOA_HUMAN Alpha-enolase OS=Homo sapiens GN=ENO1 PE=1 SV=2	0.1493	0.0844	0.083900	0.1925
P16403	H12_HUMAN	P16403 H12_HUMAN Histone H1.2 OS=Homo sapiens GN=HIST1H1C PE=1 SV=2	0.1677	0.1341	0.082800	0.1222
P19338	NUCL_HUMAN	P19338 NUCL_HUMAN Nucleolin OS=Homo sapiens GN=NCL PE=1 SV=3	0.1813	0.099	0.091000	0.2411
P14625	ENPL_HUMAN	P14625 ENPL_HUMAN Endoplasmic reticulum protein OS=Homo sapiens GN=HSP90B1 PE=1 SV=1	0.1841	0.1293	0.048800	0.2073

Accession	Entry	Description	UT ctrl	siMYCN	siNCYM	siNeg
P07195	LDHB_HUMAN	P07195 LDHB_HUMAN L-lactate dehydrogenase B chain OS=Homo sapiens GN=LDHB PE=1 SV=2	0.2041	0.1335	0.108700	0.2519
A0A0U1RQF0	A0A0U1RQF0_HUMAN	A0A0U1RQF0 A0A0U1RQF0_HUMAN Fatty acid synthase OS=Homo sapiens GN=FASN PE=4 SV=1	0.2128	0.000001	n.d.	0.267
P10809	CH60_HUMAN	P10809 CH60_HUMAN 60 kDa heat shock protein, mitochondrial OS=Homo sapiens GN=HSPD1 PE=1 SV=2	0.218	0.1258	0.077300	0.2487
P06748	NPM_HUMAN	P06748 NPM_HUMAN Nucleophosmin OS=Homo sapiens GN=NPM1 PE=1 SV=2	0.221	0.1311	0.155800	0.2831
P62937	PPIA_HUMAN	P62937 PPIA_HUMAN Peptidyl-prolyl cis-trans isomerase A OS=Homo sapiens GN=PPIA PE=1 SV=2	0.2232	0.1287	0.080800	0.2072
I3L1N3	I3L1N3_HUMAN	I3L1N3 I3L1N3_HUMAN Phosphorylase b kinase regulatory subunit beta (Fragment) OS=Homo sapiens GN=PHKB PE=1 SV=1	0.2557	0.261	0.292800	0.1826
P13639	EF2_HUMAN	P13639 EF2_HUMAN Elongation factor 2 OS=Homo sapiens GN=EEF2 PE=1 SV=4	0.2958	0.2038	0.175100	0.4539
P38646	GRP75_HUMAN	P38646 GRP75_HUMAN Stress-70 protein, mitochondrial OS=Homo sapiens GN=HSPA9 PE=1 SV=2	0.3091	0.2204	0.157900	0.3638
P11021	GRP78_HUMAN	P11021 GRP78_HUMAN 78 kDa glucose-regulated protein OS=Homo sapiens GN=HSPA5 PE=1 SV=2	0.3266	0.2237	0.075500	0.4135
P62805	H4_HUMAN	P62805 H4_HUMAN Histone H4 OS=Homo sapiens GN=HIST1H4A PE=1 SV=2	0.3435	0.3658	0.226900	0.444
P07900	HS90A_HUMAN	P07900 HS90A_HUMAN Heat shock protein HSP 90-alpha OS=Homo sapiens GN=HSP90AA1 PE=1 SV=5	0.3703	0.2543	0.237100	0.4776
Q05639	EF1A2_HUMAN	Q05639 EF1A2_HUMAN Elongation factor 1-alpha 2 OS=Homo sapiens GN=EEF1A2 PE=1 SV=1	0.4248	0.356	0.218200	0.5163
P04406	G3P_HUMAN	P04406 G3P_HUMAN Glyceraldehyde-3-phosphate dehydrogenase OS=Homo sapiens GN=GAPDH PE=1 SV=3	0.4348	0.3906	0.225100	0.5767
P13929	ENOB_HUMAN	P13929 ENOB_HUMAN Beta-enolase OS=Homo sapiens GN=ENO3 PE=1 SV=5	0.4875	0.000001	n.d.	n.d.
Q5JP53	Q5JP53_HUMAN	Q5JP53 Q5JP53_HUMAN Tubulin beta chain OS=Homo sapiens GN=TUBB PE=1 SV=1	0.4881	0.000001	n.d.	0.571
P08238	HS90B_HUMAN	P08238 HS90B_HUMAN Heat shock protein HSP 90-beta OS=Homo sapiens GN=HSP90AB1 PE=1 SV=4	0.4891	0.3644	0.268400	0.57
E9PKE3	E9PKE3_HUMAN	E9PKE3 E9PKE3_HUMAN Heat shock cognate 71 kDa protein OS=Homo sapiens GN=HSPA8 PE=1 SV=1	0.5542	0.4158	0.234000	0.7359
P68363	TBA1B_HUMAN	P68363 TBA1B_HUMAN Tubulin alpha-1B chain OS=Homo sapiens GN=TUBA1B PE=1 SV=1	0.6253	0.5764	0.352100	0.0696
P60709	ACTB_HUMAN	P60709 ACTB_HUMAN Actin, cytoplasmic 1 OS=Homo sapiens GN=ACTB PE=1 SV=1	0.7829	0.653	0.424500	0.9676